UNIVERSITÄT ZU KÖLN

Olfactory Processing and Learning in *Drosophila*: Models Across Biological Scales & Computational Abstractions

Inaugural-Dissertation zur
Erlangung des Doktorgrades der
Mathematisch-Naturwissenschaftlichen Fakultät
der Universität zu Köln

vorgelegt von
Magdalena Anna Springer
aus Solingen

angenommen im Jahr 2025

Erster Gutachter:

Zweiter Gutachter:

There is no order in the world around us, we must adapt ourselves to the requirements of chaos instead.

– Kurt Vonnegut

Abstract

Olfaction is a fundamental and universal sensory modality across the animal kingdom. It enables animals to locate food sources, avoid danger, and identify mating partners. Moreover, odors can acquire predictive value through experience, allowing animals to infer and anticipate relevant aspects of their environment. Thus, olfactory perception and learning are critical for both survival and reproduction. Understanding how the brain processes and learns olfactory information provides a powerful window into the core principles of neural function. In this thesis, we investigate mechanisms of olfactory processing and learning in the compact yet sophisticated brain of the fruit fly, *Drosophila melanogaster*. Using computational modeling across multiple levels of abstraction, we aim to formalize and explore the biological principles that shape sensory representation, learning, and memory.

At the circuit level, we examine how specific network motifs support memory formation, updating, and extension, including mechanisms underlying second-order conditioning and extinction learning. At the cellular level, we investigate the role of inhibitory interactions in binary odor mixture processing in early olfactory circuits. Based on ultrastructural connectome data, we analyze how sensory information is integrated and develop computational models to explore how these circuits shape odor representations. At the molecular level, we develop a phenomenological model of synaptic transmission dynamics shaped by the differential expression of synaptic protein isoforms. This allows us to investigate how molecular composition tunes short-term plasticity and modulates information flow at synaptic resolution.

Through these interdisciplinary approaches, we aim to advance the understanding of olfactory computation and memory by bridging molecular mechanisms, circuit dynamics, and behavioral outcomes. Ultimately, this work seeks to uncover general principles of brain function that extend beyond the olfactory system and offer transferable insights into neural computation.

Zusammenfassung

Der Geruchssinn ist eine grundlegende und universelle Sinnesmodalität, die es Tieren ermöglicht, Nahrungsquellen zu lokalisieren, Gefahren zu meiden und Paarungspartner zu identifizieren. Darüber hinaus können Gerüche durch Erfahrung einen prädiktiven Wert erlangen, der es den Tieren ermöglicht, auf relevante Aspekte ihrer Umgebung zu schließen und diese vorauszusehen. Daher sind Geruchswahrnehmung und -lernen sowohl für das Überleben als auch für die Fortpflanzung entscheidend. Ein Verständnis darüber, wie das Gehirn Geruchsinformationen verarbeitet und erlernt, gibt Einblicke in die Grundprinzipien neuronalen Funktionen. In dieser Arbeit untersuchen wir die Mechanismen der Geruchsverarbeitung und des Lernens im kompakten, aber hoch entwickelten Gehirn der Fruchtfliege *Drosophila melanogaster*. Mit Hilfe von Computermodellierung auf mehreren Abstraktionsebenen wollen wir die biologischen Prinzipien, die sensorische Repräsentation, Lernen und Gedächtnis bestimmen, formalisieren und erforschen.

Auf der Ebene der Schaltkreise untersuchen wir, wie spezifische Netzwerkmotive die Gedächtnisbildung, -aktualisierung und -erweiterung unterstützen, einschließlich der Mechanismen, die Extinktionslernen und Lernen zweiter Ordnung zugrunde liegen. Auf zellulärer Ebene untersuchen wir die Rolle hemmender Interaktionen bei der Verarbeitung binärer Geruchsmischungen in frühen olfaktorischen Schaltkreisen. Auf der Grundlage von ultrastrukturellen Konnektomdaten analysieren wir, wie sensorische Informationen integriert werden, und entwickeln Computermodelle, um zu untersuchen, wie diese Schaltkreise Geruchsrepräsentationen formen. Auf molekularer Ebene entwickeln wir ein phänomenologisches Modell der synaptischen Übertragungsdynamik, die durch die unterschiedliche Expression synaptischer Proteinisoformen bestimmt wird. So können wir untersuchen, wie die molekulare Zusammensetzung die Kurzzeitplastizität steuert und den Informationsfluss bei der synaptischen Auflösung moduliert.

Mit diesen interdisziplinären Ansätzen wollen wir das Verständnis der olfaktorischen Berechnung und des Gedächtnisses verbessern, indem wir eine Brücke zwischen molekularen Mechanismen, Schaltkreisdynamik und Verhaltensergebnissen schlagen. Letztendlich zielt diese Arbeit darauf ab, allgemeine Prinzipien der Hirnfunktion aufzudecken, die über das olfaktorische System hinausgehen und übertragbare Einsichten zur neuronaler Berechnung bieten.

Contents

Abstract v
Zusammenfassung vii
List of Figures and Tables xi
1 Introduction 1
1.1 Modeling the Brain: Computational Approaches to Neural Function . 1
1.1.1 The Role of Computational Models in Understanding Neural Systems 1
1.1.2 Different Levels of Abstraction in Neuronal Modeling 2
1.2 *Drosophila* as a Model System in Neuroscience 5
1.2.1 The Organization of the Fly Olfactory Pathway 6
1.3 The Insect Olfactory Pathway as a Research Target in Computational Neuroscience 8
1.4 Organization of This Thesis 9
2 Results 11
2.1 Circuit Models of Associative Learning 11
2.1.1 A Mechanistic Model for Reward Prediction and Extinction Learning in the Fruit Fly 11
2.1.2 Functional Dissection of a Neuronal Brain Circuit Mediating Higher-Order Associative Learning 28
2.2 A Connectome-Based Approach for Investigating Neural Circuits of Odor Mixture Processing 57
2.3 A Model Investigation of Short-Term Synaptic Plasticity Tuned via Unc13 Isoforms 72
3 Discussion 83
3.1 Balancing Abstraction and Biological Detail in Computational Modeling 83
3.1.1 Point versus Compartmental Neuron Models 83
3.1.2 Benefits and Limitations of Connectome-Constrained Models . 86
3.1.3 Parameters and Computational Cost in Neural Networks . . . 87
3.2 Different Levels of Neural Plasticity 88
3.2.1 Linking Active Zone Composition to Plasticity and Behavior . . 89
3.2.2 Measuring Learned Behavior in Computational Models 90
3.2.3 Opposing Learning Principles in Extinction and Second-Order Learning 90
3.3 Comparative Insights and Generalizability of *Drosophila* 91
3.3.1 Comparison to Other Arthropods 92
3.3.2 Comparison to Mammals 95
3.4 Outlook: Towards Integrative Brain Models Across Abstraction Levels 97
Bibliography 99
Acknowledgements 119
List of Contributions 121
Eidesstattliche Erklärung 123

List of Figures

1.1 The role of computational modeling in neuroscience. 2
1.2 Different biological scales, their abstraction levels in computational models of the brain, and their applications in this thesis. 4
1.3 Schematic organization of the *Drosophila* olfactory pathway. 6

3.1 Functional interpretation of uPN autapses in a compartmentalized spiking model. 85
3.2 Statistical analysis of the connectome of the DL5 PN in *Drosophila*. . . . 93
3.3 Comparison of odor representations in canonical versus distributed olfactory network architectures. 94

List of Tables

3.1 Comparison of olfactory system components across different arthropod species 92

Note: This list includes only those figures and tables that are not part of the results chapter.

Chapter 1

Introduction

1.1 Modeling the Brain: Computational Approaches to Neural Function

Computational neuroscience is a multidisciplinary approach within the broad domain of neuroscience with the goal to investigate nervous systems through theoretical frameworks, mathematical models and neural simulations. Even though the term computational neuroscience is historically quite young, emerging in the mid to late 1980s (Sejnowski et al., 1988; Schwartz, 1990), the idea of understanding brain function in computational terms has roots going back more than a century. Some of these approaches, such as the integrate-and-fire model, of which the origins go back to concepts introduced by Lapicque in 1907, are still widely used today (Lacpique, 1907; Abbott, 1999; Brunel and Rossum, 2007; Yamazaki et al., 2022). In recent decades, the field of computational neuroscience has undergone rapid development, driven by advances in experimental tools and computational power, emergence of big data and growing impact of artificial intelligence (Summerfield and Miller, 2023; Dhiman et al., 2023; Verzelli et al., 2024).

1.1.1 The Role of Computational Models in Understanding Neural Systems

In neuroscience, different subdisciplines work hand in hand to address questions of how the brain functions – or fails to function. Computational models contribute by providing an isolated and controllable framework in which problems can be broken down into smaller, more abstract components while interference of external factors can be excluded. By integrating multi-scale data from experimental or clinical neuroscience and other concepts from disciplines such as physics and information theory, working hypotheses can be simulated and tested *in silico*. One advantage of modeling is that it can in some instances exceed the limitations of experimental approaches, for example by enabling large-scale simultaneous activity recordings across multiple brain areas. Moreover, models inherently represent a formalization of our understanding and can help to condense complex biological observations into coherent theoretical frameworks. If the working hypothesis based on experimental findings can be supported through the model, it can be used to perform further simulations that give rise to new model-based predictions and research questions (Figure 1.1). Thus, the contribution of computational modeling to neuroscience is to bridge experiment with theory, to validating or refining working models, and to rising new research questions (Trappenberg, 2009). In this way, it complements rather than competes with experimental and clinical neuroscience. Apart from classical neuroscience, computational neuroscience has also practical implications for fields

like neurotechnology and artificial intelligence. Computational neuroscience can inspire brain-inspired robotics and neuromorphic hardware, support the development of brain-machine interfaces for controlling prosthetics, and contribute to improving artificial neural networks, particularly in terms of energy efficiency and learning algorithms (Yamazaki et al., 2022).

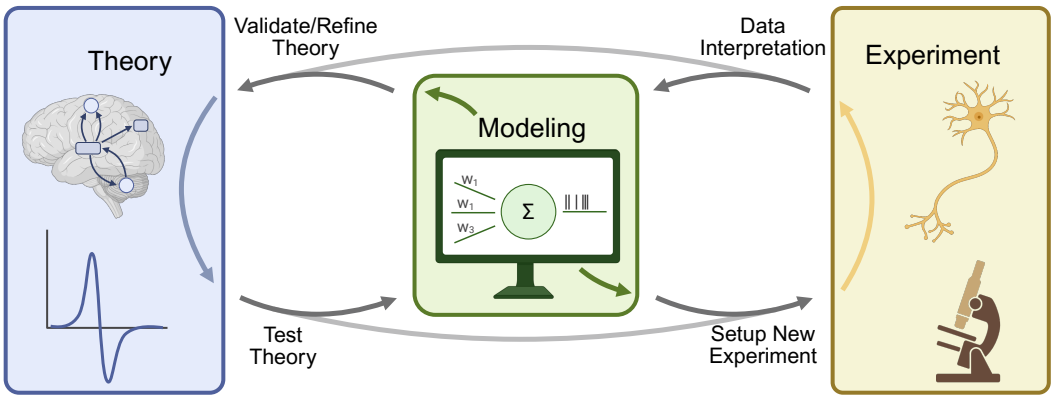

FIGURE 1.1: The role of computational modeling in neuroscience. Computational models provide a framework for integrating results across experiments, testing mechanistic hypotheses under controlled conditions, and generating predictions to guide future experiments. Ideally, models are grounded in theoretical principles and iteratively refined by empirical data, forming a mutually reinforcing loop between theory, experimentation, and interpretation. This interplay enables a deeper understanding of neural systems by linking observed phenomena to underlying mechanisms.

1.1.2 Different Levels of Abstraction in Neuronal Modeling

There are numerous established modeling approaches to formalize brain circuits and their function, differing in their level of abstraction (Herz et al., 2006; D'Angelo et al., 2013). In this thesis, the term level of abstraction refers to the corresponding biological scale at which a system is modeled, ranging from network-level rate models to detailed synapse-level models (Figure 2A-B). The choice of the specific modeling approach always depends on the specific research question, the availability of experimental data, and the available computational resources. A useful model should be as simple as possible, yet sufficiently complex to capture the key phenomena under investigation (Blohm et al., 2020). In the following, I will go through the different levels of abstraction, with a focus on the methods applied in this thesis.

To explore neural systems on the circuit or network level, rate-based models are commonly used as a powerful tool. In such models, neuronal activity is represented by firing rates, with neuron population connected via specific weights. These networks can operate in trial-based modes or as dynamical systems to capture temporal evolution. Further, key mechanisms found in the brain, such as recurrency, feedback, and convolution, can be implemented to explore their functional roles (Dayan and Abbott, 2001).

However, these models neglect some key characteristics of neurons, most importantly their spiking behavior. To capture neuronal dynamics on a cellular level and match them to observations from electrophysiological data, neurons can be

represented in different types of spiking neural networks (SNNs) (Gerstner and Kistler, 2012). One of the most prominent types of SNNs is the leaky integrate and fire (LIF) model, in which a neuron is described by a differential equation that integrates a leak term and other conductances that can either depolarize or hyperpolarize the membrane potential (Burkitt, 2006). Here, individual neuron properties like membrane capacitance or adaptation currents, as well as characteristic spiking patterns can be incorporated. Further, several extensions of the standard LIF, such as the generalized, exponential or quadratic integrate-and-fire (IF) models have been developed with the aim to capture neuronal dynamics more accurately. Connectivity between neurons is mediated by current- or conductance-based synapses, each modulating the postsynaptic neuron's state with a specific synaptic weight in response to presynaptic activity. Whenever the membrane potential of an IF neuron reaches a predefined threshold, spikes are registered as discrete events. In some use cases, however, it can be useful to explicitly simulate the full dynamics of action potentials. The Hodgkin Huxley (HH) model allows this by capturing the ion channel dynamics and the respective changes in membrane potential for each action potential (Hodgkin and Huxley, 1952). While the HH model provides increased biological realism, its greater complexity comes with higher parameter uncertainty and challenges in tuning. Hybrid models, such as the Izhikevich model, offer here a compromise to combine advantages of IF and Hodgkin–Huxley models (Izhikevich, 2003).

In standard SNNs, neurons commonly consist out of a single compartment, in which input and output is processed. However, simulation of neurons as single points neglects their often complex arborization. To capture compartment-specific dynamics, one can either simulate soma, axon and dendrites separately using a reduced compartmental model, or represent the complete morphology in a fully compartmentalized model (Herz et al., 2006). A pioneer of this approach was Wilfried Rall, who proposed the cable theory as basis for multi-compartment models enabling morphologically accurate simulations (Rall, 1964). Multi-compartment models can be especially useful when neurons do not operate in a strictly separated input-output manner, but instead also perform electrically isolated computations within their neurites, turning the neuron into a network-like structure (London and Häusser, 2005). In recent years, several large-scale connectome datasets have emerged and become publicly available, ranging from multiple brain areas in vertebrates to complete brain maps in invertebrates (Dorkenwald et al., 2024; Bae et al., 2025). These detailed brain maps provide new possibilities of incorporating compartmentalization and exact placements of synapses into neuronal models. Beyond the morphological aspect, connectome data also allows to constrain models using precise information on synaptic wiring within neural systems.

Neuronal and network dynamics emerge from multiple mechanisms across a broad range of timescales, including intrinsic neuron properties, neuromodulation, and synaptic transmission. To study how dynamical processes affect neural function, such as information decoding, learning and behavior, they can be incorporated at different sites of computational models (Abbott and Regehr, 2004; Magee and Grienberger, 2020). Intrinsic neuronal dynamics, such as spike-frequency adaptation, can be captured within dynamic neuron models that reflect time-dependent changes in excitability. Processes underlying learning and memory—often attributed to neuromodulation—are typically represented as activity-dependent changes in synaptic weights governed by specific learning rules (Gerstner and

Kistler, 2012). Synaptic transmission itself, shaped by both pre- and postsynaptic mechanisms, can be formalized with different models, describing these molecular processes functionally or aiming to represent the underlying biophysical processes, such as calcium signaling, vesicle release and recycling, the role of synaptic proteins, or cytoskeletal dynamics (Zucker and Regehr, 2002; Ferrante et al., 2008; Neher, 2015; Lee et al., 2024).

Over the past years, many platforms have been developed to perform model simulations with custom software in the form of neural network simulators, such as BRIAN, NEURON, GENESIS, NEST, Nengo or ANNarchy (Hines and Carnevale, 1997; Bower and Beeman, 1998; Gewaltig and Diesmann, 2007; Goodman and Brette, 2008; Bekolay et al., 2014; Vitay et al., 2015; Tikidji-Hamburyan et al., 2017). These simulators can be used for models of multiple scales, from simple rate models to detailed compartmental and biophysically realistic models.

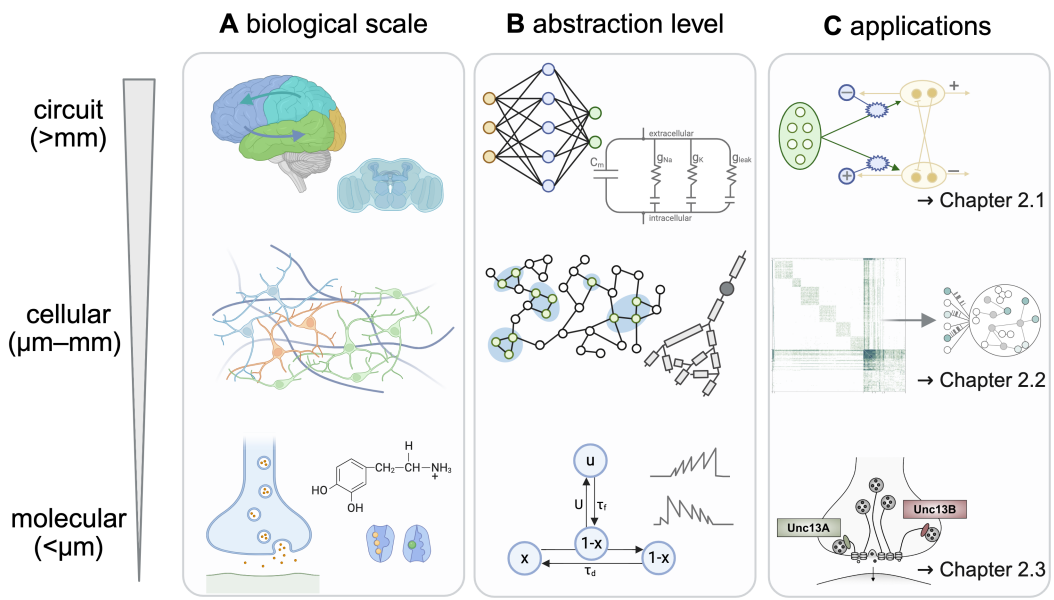

FIGURE 1.2: Different biological scales (A), their abstraction levels in computational models of the brain (B), and their applications in this thesis (C). On the circuit level, the interplay of different neuronal regions can be simulated in artificial neural networks (ANNs) to study general mechanisms and principles of neural computation. In this thesis, two circuit models are presented to illustrate how specific circuit motifs contribute to learning processes (Chapter 2.1). To consider mechanisms on the cellular level, spiking models allow modeling of individual neurons in greater detail. Constraining models with precise neural connectivity and compartmentalizing neurons can further refine these models. In Chapter 2.2, we utilize the fly connectome to investigate how structural wiring can shape information processing. Further, the relevance of model compartmentalization will be illustrated in the Discussion. Finally, to simulate elaborate processes on the molecular level, neuron and synapse models can be equipped with detailed formalizations of protein interactions, synaptic mechanisms and ion dynamics. Chapter 2.3 presents an example of a synapse model capturing protein-dependent synaptic dynamics. Note that transitions between the levels are continuous, and models usually integrate elements from multiple levels of abstraction.

1.2 *Drosophila* as a Model System in Neuroscience

When it comes to using animal models to investigate brain function, rodents such as mice and rats are the most heavily used animal models (Żakowski, 2020). However, in this thesis, we will focus on analyzing and modeling brain structures of *Drosophila melanogaster* (hereafter referred to as *Drosophila*), commonly known as the fruit fly. At first glance, a fruit fly does not share many similarities with us humans, does not come across as very smart and might therefore not be the most intuitive candidate to get insight on general brain function. However, it has been a successfully used model organism in neuroscience for more than 100 years and has even contributed to multiple Nobel Prize winning discoveries (Bellen et al., 2010). This is because the fruit fly as an animal model offers significant advantages alongside both the research on vertebrate and invertebrate species.

Despite the evolutionary distance, about 60 % of the genes in the fly that encode proteins are conserved in humans, and even 75% of the genes involved in causing diseases in humans have orthologue genes in *Drosophila* (Rubin et al., 2000; Reiter et al., 2001; Bellen and Yamamoto, 2015; Casas-Tintó, 2024). While more complex brain structures such as the cortex certainly have to be studied in mammalian brains and cannot be investigated in the small-sized fruit fly brain with about 140,000 neurons (Dorkenwald et al., 2024) – small compared to ~86 billion neurons in the human brain (Azevedo et al., 2009) or ~70 million neurons in the mouse brain (Herculano-Houzel et al., 2006). However, *Drosophila* can be a particularly valuable model when it comes to investigating conserved and fundamental neural principles of brain functionality and pathology in a simplified and reductionist framework (Kandel, 1979; Jeibmann and Paulus, 2009; Kazama, 2015; Atoki et al., 2025).

What especially sets *Drosophila* apart from other model organisms is its exceptional methodological accessibility. Many years of research have led to a broad range of techniques for obtaining structural, functional and behavioral data in the adult fly as well as the larva. The genome of *Drosophila* was not only one of the first ones to be fully sequenced (Adams et al., 2000), but is also very accessible through the availability of large sets of established mutant lines (e.g. the white eye mutant or the learning mutants dunce and rutabaga) and transgenic binary expression systems (e.g. the (Split-)Gal4/UAS system), which are used to manipulate or label neuron subsets of neurons (Bellen et al., 2010; Brand and Perrimon, 1993; Luan et al., 2020; Meissner et al., 2025). Temperature- or light-sensitive genetic tools enable precise, reversible inhibition or activation of specific neuron subsets, making it possible to determine whether their activation induces a specific behavior or whether they are essential during learning (Kazama, 2015; Riemensperger et al., 2016; Simpson and Looger, 2018; Kitamoto, 2001). Further, one can record activity in labeled neurons through or the whole-brain through functional imaging to get a local or global insight into brain functionality (Simpson and Looger, 2018; Aimon et al., 2019). Another major research focus in *Drosophila* in recent years has been the efforts to mapping and analyzing the full brain connectome of larval and adult fly brain which brings completely new possibilities to investigate the fly brain and its synaptic wiring on a single-cell level (Zheng et al., 2018; Scheffer et al., 2020; Winding et al., 2023; Dorkenwald et al., 2024). Further, there is a broad range of assays to study different types of behavior, from locomotion, chemo- or phototaxis, and behavioral choice to even social interactions (Neckameyer and Bhatt, 2016). Learning and memory can be studied as well, e.g. in Pavlovian paradigms in the

long-standing and well-established Tully machine to test classical aversive olfactory conditioning (Tully and Quinn, 1985; Tabone and Belle, 2014). This assay can also be extended to study appetitive conditioning or higher forms of learning, and even be automated (Tempel et al., 1983; Dwijesha et al., 2024; Jiang et al., 2016). Further, there are also assays focusing on other types of learning than associative learning, e.g. social learning paradigms (Battesti et al., 2012; Roemschied et al., 2024). Importantly, *Drosophila* behavior can be studied not only in group assays, but also in single-fly assays to test for individuality (Tsai and Chou, 2022).

Drosophila as a model organism further holds significant practical and economic benefits over vertebrate models. The maintenance of fruit flies in laboratory settings is remarkably simple, inexpensive, straightforward, and experiments with fruit flies are not subject to complex bureaucratic ethical regulations (Jennings, 2011). Further, their rapid reproduction cycle which spans about 10 days enables efficient crossing of genetic lines and thus facilitates timely establishment of experimental setups (Stocker and Gallant, 2008). Additionally, not only the adult fly is a well-studied model organism, but the larval stage, with its even simpler brain structures, is getting increasing attention, for example with regards to the investigation of chemosensation, locomotion, learning and memory (Aceves-Piña and Quinn, 1979; Gerber and Stocker, 2007; Weber et al., 2023; Yadav et al., 2024).

1.2.1 The Organization of the Fly Olfactory Pathway

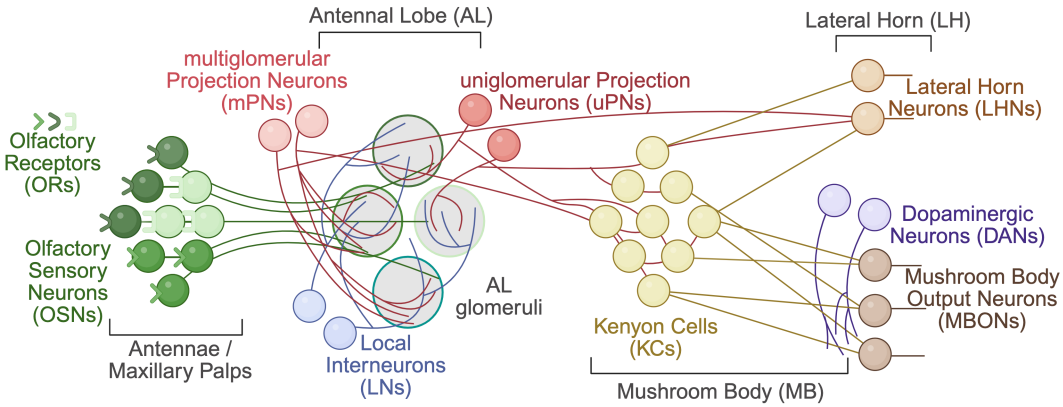

FIGURE 1.3: Schematic organization of the *Drosophila* olfactory pathway. OSNs detect odorants from the environment and converge to uPNs, mPNs and LNs within the AL. PNs then diverge to two higher brain centers, the LH and the MB. Within the MB, KCs relay information to MBONs, which mediate downstream processing and behavioral output. DANs innervate the MB and mediate neuromodulation.

One of the most studied structures in the adult *Drosophila*, as well as the main focus of this thesis, is the olfactory pathway. It represents a particularly relevant system for studying basic neuronal circuits underlying key functional aspects such as coding principles of stimuli and valences, stimulus discrimination, context learning, and navigation (Wilson, 2013; Benton, 2022; Davis, 2023). In the following, we will put a specific emphasis on sensory processing and plasticity mechanisms within two major computation hubs of the fruit fly, the antennal lobe (AL) and the mushroom body (MB). Importantly, the structural and functional organization of

the olfactory pathway and the MB share similarities with other insect species, such as the honeybee or the cockroach, which allows for gaining additional knowledge from other insects and comparing features between different insect species (Martin et al., 2011; Paoli and Galizia, 2021; Fuscà and Kloppenburg, 2021a; Watanabe and Tateishi, 2023; Arican et al., 2023).

Significant progress in understanding the olfactory pathway has been made in the past years, providing a solid basis for further exploration, which will be outlined in the following (Figure 1.3). Fruit flies sense odorants from their environment with their antennae and maxillary palps, housing ~1,200 olfactory sensory neurons (OSNs) per side, that express olfactory receptors (ORs) (Hallem and Carlson, 2004; Vosshall and Stocker, 2007). Each OSN type predominantly targets one specific glomerulus within the AL, which comprises ~300 projections neurons (PNs) (Stocker et al., 1990; Tanaka et al., 2012; Bates et al., 2020). PNs can be subdivided into two subtypes: uniglomerular PNs (uPNs), which innervate a single glomerulus in the AL and are predominantly excitatory, and multiglomerular PNs (mPNs), which connect to multiple glomeruli and include both excitatory and inhibitory neurons (Bates et al., 2020). Within the AL, odors are encoded as distinct activation patterns across one or multiple glomeruli with varying intensity, establishing the AL as the primary computation hub for olfactory processing (Wilson, 2013; Grabe et al., 2016). Mechanisms such as neural adaptation in OSNs and short-term plasticity at OSN–PN synapses refine the temporal and spatial profiles of glomerular activity, enabling efficient and robust sensory coding of complex odor stimulation patterns (De Bruyne et al., 2001; Kazama and Wilson, 2008; Wilson, 2013; Fulterer et al., 2018). A population of ~200 local interneurons (LNs) further shapes innervation within the AL, which exhibits high diversity in their neuronal properties, innervation patterns, synaptic characteristics, and neurotransmitter constitution (Wilson and Laurent, 2005; Husch et al., 2009b; Husch et al., 2009a; Chou et al., 2010; Seki et al., 2010; Schlegel et al., 2021; Fuscà and Kloppenburg, 2021b). These characteristics make LNs key players in the additional contribution to AL network dynamics by mediating important functional aspects such as gain control, contrast enhancement, and non-linear information integration across glomeruli (Sachse and Galizia, 2002; Wilson and Laurent, 2005; Olsen and Wilson, 2008; Mohamed et al., 2019; Barth-Maron et al., 2023).

From the antennal lobe, PNs diverge onto two higher olfactory centers, one of them being the lateral horn (LH), which consist of ~1,400 LH neurons (LHNs) and is commonly known for processing and integrating innate behavior (Marin et al., 2002; Wong et al., 2002; Tanaka et al., 2004; Frechter et al., 2019; Das Chakraborty and Sachse, 2021). The other one is the mushroom body (MB), composed of ~2,000-2,500 intrinsic Kenyon cells (KCs), which can be subdivided into the calyx, the peduncle and the lobes. The KCs receive diverging input from the PNs in the calyx and project their axons via the peduncle to form the α/β, α'/β', and γ lobes (Heisenberg, 2003; Lin et al., 2007; Aso et al., 2009; Takemura et al., 2017; Schlegel et al., 2024; Fiala and Kaun, 2024). From the KCs, the signal is further transmitted to the ~35 mushroom body output neurons (MBONs) (Ito et al., 1998; Tanaka et al., 2008; Aso et al., 2014b; Aso et al., 2014a). During olfactory conditioning, dopamine-mediated synaptic plasticity at KC–MBON synapses encodes learned associations that subsequently drive changes in the behavioral output (Davis, 2005; Davis, 2023). Therefore, the MB is often referred to as the center for learning and memory. However, recent advances point to a more comprehensive and integrative understanding of both higher-order

olfactory centers; the LH seems to play a role in memory formation and retrieval as well (Dolan et al., 2018; Zhao et al., 2019), whereas the role of the MB also comprises integration and learning of multimodal sensory inputs (Vogt et al., 2014; Yagi et al., 2016; Thiagarajan et al., 2022; Okray et al., 2023).

1.3 The Insect Olfactory Pathway as a Research Target in Computational Neuroscience

The olfactory pathway of *Drosophila* and other insects exhibits a high degree of complexity at the circuit, cellular, and molecular level, enabling it to perform efficient computations for sensory processing and adaptive behavior. Numerous scientific breakthroughs over the past decades in this research field, along with the increasing complexity of data, have driven computational neuroscientists to develop modeling frameworks to complement results from lab experiments through *in silico* approaches (Figure 1.2B) (Clemens and Murthy, 2017; Gupta et al., 2018). These computational models of the olfactory pathway and sensorimotor transformations allow us to explore the functionality of fundamental neural circuits in an isolated and mechanistic framework.

Models of olfactory sensory processing have focused on elucidating how odor identity, concentration, and valence are encoded in the olfactory pathway and the MB and how different information is integrated (e.g. Luo et al., 2010; Kao and Lo, 2020; Jürgensen et al., 2021). To explore how associative memories are formed, other models incorporate different forms of synaptic plasticity into their models. Thus, they enable reproduction of classical conditioning paradigms and provide valuable insight into the mechanisms underlying learning and memory (e.g. Wessnitzer et al., 2012; Faghihi et al., 2017; Nehrkorn et al., 2015; Jiang and Litwin-Kumar, 2021; Bennett et al., 2021; Jürgensen et al., 2024a). A third major focus of *Drosophila* modeling is the investigation of how sensory information is integrated in the network to generate behavioral output. For example, locomotion models simulating larva crawling or flight behavior in the adult can be used to generate hypotheses of how the fly responds towards stimuli and navigates in complex environments (e.g. Dickson et al., 2008; Shiu et al., 2024; Sakagiannis et al., 2025a; Wang-Chen et al., 2024).

Recent scientific advances during the past years have given rise to new opportunities on refining these neuronal modeling approaches. Beyond exploring the circuitry underlying classical associative learning, recent experimental studies have begun to elucidate the neuronal circuitry underlying more complex forms of learning, such as second order conditioning, latent inhibition, memory extinction (Cognigni et al., 2018; Yamada et al., 2023; Latshaw et al., 2023). At the same time, the growing availability of biologically detailed structural and functional data at both the cellular and molecular levels offer the potential to further extend modeling approaches and study how mechanisms at different biological scales shape brain function.

1.4 Organization of This Thesis

Building on these insights, this thesis aims to explore the olfactory system of the fruit fly to gain insight on the general mechanisms underlying sensory processing and learning. In the following chapters, different computational modeling approaches with varying levels of model abstraction will be presented, each tailored to address a specific research question. The chapters are organized by their biological scales and their levels of abstraction: beginning with circuit models exploring network motifs for associative learning, progressing to single-neuron and synapse-level models aiming to link structural data to sensory integration mechanisms, and concluding with the computational investigation of molecular mechanisms at the synapse (Figure 1.2C).

In Chapter 2.1, we present two examples of computational rate models capturing the circuitry underlying complex forms of associative learning in *Drosophila*. In the first example, we simulate reward prediction and extinction learning with a circuit model by forming a second memory trace within the MB circuit. The second project investigates the neuronal circuit underlying second-order conditioning in *Drosophila*. Here, the implementation of a computational rate model is used to test and refine the proposed circuit motifs. Both presented models integrate *in vivo* experimental findings from the fruit fly, including connectome data identifying connections between specific neuron subsets that are crucial for these learning processes.

In Chapter 2.2, we further extend the use of connectome data to explore the mechanisms behind odor mixture processing. We analyze the fly connectome regarding inhibitory network motifs that are crucial for processing conflicting odor information and implement a connectome-constrained model of the antennal lobe, tuning it to align the structural connectivity with functional data on odor processing.

Finally, in Chapter 2.3, we take an even closer look by zooming into the synapses between primary and secondary neurons of the *Drosophila* AL. Here, we modify a synapse model to capture a universal phenomenon of protein-dependent short-term plasticity. By examining our model, we aim to better understand molecular mechanisms underlying synaptic dynamics and enhance biological realism in neuronal models.

In total, this thesis comprises implementation and investigation of four comprehensive computational models of the fly olfactory and learning system on different biological scales and with different levels of abstraction. With these models, we aim to bridge circuit motifs, anatomical structure and molecular composition with functional aspects, such as neuromodulation, information integration and network dynamics. Overall, we hope to contribute to a more general understanding and formalization of sensory processing and learning in neural systems.

Chapter 2

Results

2.1 Circuit Models of Associative Learning

2.1.1 A Mechanistic Model for Reward Prediction and Extinction Learning in the Fruit Fly

Authors: Magdalena Springer, Martin P. Nawrot

Journal: ***eNeuro*** **(2021)**

DOI: 10.1523/ENEURO.0549-20.2021

Contribution: The study design was conceptualized by MPN and MS. All simulations and analyses were conducted by MS. The results were obtained in large part and analyzed in the master thesis of MS. The manuscript was written by MPN and MS. The complete manuscript preparation, submission and revision process was conducted during the PhD.

eNeuro

Research Article: New Research

Sensory and Motor Systems

A Mechanistic Model for Reward Prediction and Extinction Learning in the Fruit Fly

Magdalena Springer and Martin Paul Nawrot

https://doi.org/10.1523/ENEURO.0549-20.2021

Computational Systems Neuroscience, Institute of Zoology, University of Cologne, Biocenter, Cologne 50674, Germany

Visual Abstract

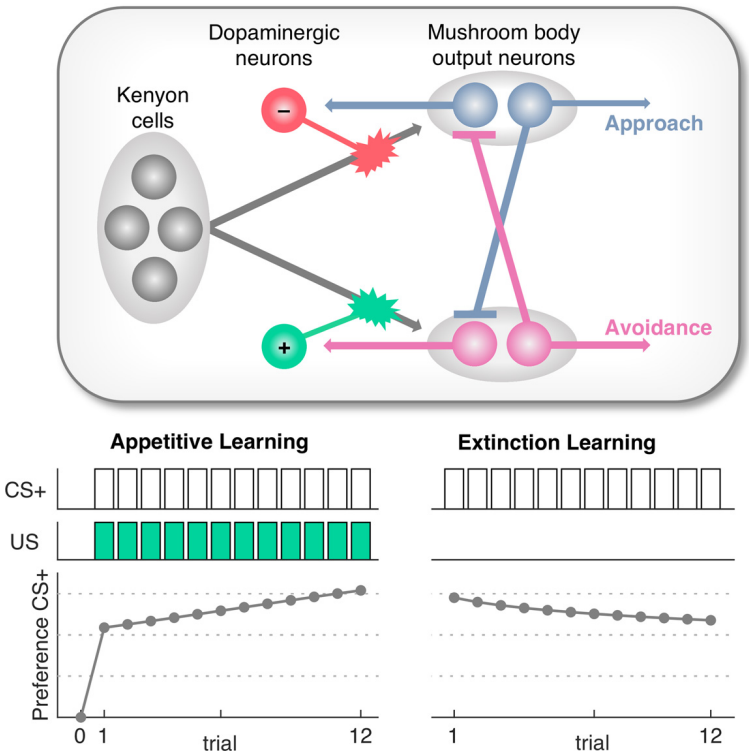

Significance Statement

A stressful experience can lead to a strong fear memory where a negative consequence has been associated with a certain stimulus or event. This can trigger fear whenever the same or similar event occurs. Extinction of such a maladaptive memory through extinction learning can thus be of high therapeutic value. Here, we present novel theoretical work on the formation and extinction of memories in the fruit fly that suggests an underlying neural circuit mechanism for reward prediction based on recently reported anatomic, physiological and behavioral data. Our findings propose how the theoretical concept of prediction error coding can be realized in a biologically realistic neuronal circuit motif to enable associative learning, saturation of learning, single-trial memory, and memory extinction.

Extinction learning, the ability to update previously learned information by integrating novel contradictory information, is of high clinical relevance for therapeutic approaches to the modulation of maladaptive memories. Insect models have been instrumental in uncovering fundamental processes of memory formation and memory update. Recent experimental results in *Drosophila melanogaster* suggest that, after the behavioral extinction of a memory, two parallel but opposing memory traces coexist, residing at different sites within the mushroom body (MB). Here, we propose a minimalistic circuit model of the *Drosophila* MB that supports classical appetitive and aversive conditioning and memory extinction. The model is tailored to the existing anatomic data and involves two circuit motives of central functional importance. It employs plastic synaptic connections between Kenyon cells (KCs) and MB output neurons (MBONs) in separate and mutually inhibiting appetitive and aversive learning pathways. Recurrent modulation of plasticity through projections from MBONs to reinforcement-mediating dopaminergic neurons (DAN) implements a simple reward prediction mechanism. A distinct set of four MBONs encodes odor valence and predicts behavioral model output. Subjecting our model to learning and extinction protocols reproduced experimental results from recent behavioral and imaging studies. Simulating the experimental blocking of synaptic output of individual neurons or neuron groups in the model circuit confirmed experimental results and allowed formulation of testable predictions. In the temporal domain, our model achieves rapid learning with a step-like increase in the encoded odor value after a single pairing of the conditioned stimulus (CS) with a reward or punishment, facilitating single-trial learning.

Key words: Drosophila melanogaster; memory extinction; reinforcement learning; reward prediction; single-trial learning

Introduction

Fruit flies can learn to associate an odor stimulus with a positive or negative consequence, e.g., food reward or electric shock punishment. In the training phase flies are typically exposed to two odors (differential conditioning) where one odor [conditioned stimulus minus (CS–)] is perceived alone whereas a second odor [CS plus (CS+)] is presented together with either reward or punishment [unconditioned stimulus (US)]. Once an association has formed between the CS+ and the respective US, the learned anticipation of the US can be observed in a memory test that enforces a binary choice behavior between the CS+ and the CS– (Tempel et al., 1983; Tully and Quinn, 1985). A single learning trial can be sufficient to form a stable memory in the fruit fly (Beck et al., 2000; Krashes and Waddell, 2008; Zhao et al., 2019) and other insect species (see Discussion).

The prediction error theory (Rescorla and Wagner, 1972) describes a basic theoretical concept of classical conditioning. It assumes that the efficacy of learning is determined by the momentary discrepancy (or error) between the expected and the received reinforcement (i.e., reward or punishment). In vertebrates, it has been shown that prediction error coding dopaminergic neurons (DANs) are involved in learning (Schultz et al., 1997; Schultz, 2016). Recent studies give rise to the assumption that DANs could play a similar role in *Drosophila melanogaster* (Hammer, 1997; Riemensperger et al., 2005; Ichinose et al., 2015; Eichler et al., 2017; Felsenberg et al., 2017, 2018; Zhao et al., 2021; Eschbach et al., 2020) and other insects (Terao and Mizunami, 2017), rejuvenating an earlier hypothesis based on experimental observations in the honeybee (Hammer, 1997).

Re-exposing the flies to the CS+ after successful training and in the absence of the US leads to a reduction of the previously learned behavior (Tempel et al., 1983; Schwaerzel et al., 2002; Felsenberg et al., 2017, 2018). This new learning is called extinction learning and has been observed across invertebrate (Eisenhardt and Menzel, 2007; Eisenhardt, 2014) and vertebrate species (Pavlov, 1927; Tully and Quinn, 1985; Myers and Davis, 2002; Bouton, 2004, 2017; Dudai, 2004). Following prediction error theory, extinction learning is caused by the mismatch between the expected outcome (predicted US) based on the initial learning and the actual outcome (no US). In humans, extinction learning is of high clinical relevance and is applied in the treatment of humans suffering from maladaptive memories (Quirk and Mueller, 2008; Chiamulera et al., 2014; Delamater and Westbrook, 2014; Bouton, 2017; Walsh et al., 2018). The majority of behavioral experiments in invertebrates and vertebrates suggest that extinction protocols, including the applied exposure therapy in humans, does not erase a memory

Received December 18, 2020; accepted March 18, 2021; First published March 30, 2021.

The authors declare no competing financial interests.

Author contributions: M.S. and M.P.N. designed research; M.S. and M.P.N. performed research; M.S. and M.P.N. analyzed data; M.S. and M.P.N. wrote the paper.

This work was funded by the German Research Foundation in parts within the Research Unit Structure, Plasticity and Behavioral Function of the Drosophila mushroom body (DFG-FOR 2705, Grant 403329959) and within the priority program Evolutionary Optimization of Neuronal Processing (DFG-SPP 2205, Grant 430592330).

Acknowledgements: We thank Johannes Felsenberg, who has been supporting this project throughout with his expertise and fruitful ideas. We also thank Anna-Maria Jürgensen for her contribution to the initial model implementation as well as Bertram Gerber and Anna-Maria Jürgensen for insightful comments on an earlier version of this manuscript.

Correspondence should be addressed to Magdalena Springer at magdalena.springer@uni-koeln.de or Martin Paul Nawrot at martin.nawrot@uni-koeln.de.

https://doi.org/10.1523/ENEURO.0549-20.2021

Copyright © 2021 Springer and Nawrot

This is an open-access article distributed under the terms of the Creative Commons Attribution 4.0 International license, which permits unrestricted use, distribution and reproduction in any medium provided that the original work is properly attributed.

but rather leads to the formation of a parallel but opposing memory, the extinction memory (Bouton, 2004; Eisenhardt and Menzel, 2007). Despite the relevance for clinical therapy, our understanding of the neural circuit mechanisms underlying extinction learning is still in its infancy.

We study a computational neural circuit model of the fruit fly mushroom body (MB) that captures the most recent anatomic and physiological facts. The model proposes detailed mechanisms for associative learning, extinction learning, prediction error coding, and single-trial learning. We compare the model outcomes quantitatively to the results of recent behavioral and physiological studies and we derive novel experimental predictions by mimicking neurogenetic manipulations of relevant neuron groups.

Materials and Methods

Circuit architecture

Our circuit model for olfactory coding and olfactory memory formation (Fig. 1) consists of three neuron layers [projection neurons (PNs), Kenyon cells (KCs), MB output neurons (MBONs)] representing the three major stages of the olfactory pathway in *Drosophila* and two reinforcement mediating DANs representing the PAM and PPL1 cluster. Each neuron in the circuit can assume an activation rate in the range of 0–1.

Olfactory model input was simulated through the activation of 50 out of the total 100 PNs. This matches experimental observations of ~40−60% of PNs being activated by a single odor stimulus (Krofczik et al., 2009; Brill et al., 2013; Wilson, 2013) and follows the model of Peng and Chittka (2017). Each PN is activated with a random rate drawn from a uniform distribution in the range between 0.2 and 0.8. To enhance variability between the networks that were set up, PN input patterns were further multiplied by a factor that was randomly distributed between 0.8 and 1. PNs are connected to 2000 KCs via the weight matrix W1 where each PN is connected to 5–15 KCs, each connection has a fixed synaptic weight of 0.2. Activation of the KC vector in the next layer resulted from the matrix product of the PN population vector and the respective weight matrix W1 according to

$$KC = PN \times W1. \tag{1}$$

Out of the total 2000 KCs only the subpopulation of 100 KCs (5%) with the highest activation rate kept its activation. All other KCs are set to zero to enforce population sparseness (Peng and Chittka, 2017). In a next step, KCs are fully connected to the four MBONs via the weight matrix W2, with all synaptic weights initially set to 0.01. The excitatory input to each MBON was calculated as the matrix products

$$M6^{+}, MV2 = KC \times W2_{av} \tag{2a}$$

$$MVP2, V2^{+} = KC \times W2_{app}. \tag{2b}$$

We further included lateral connectivity between the MBONs. The M6 MBON receives inhibitory input from

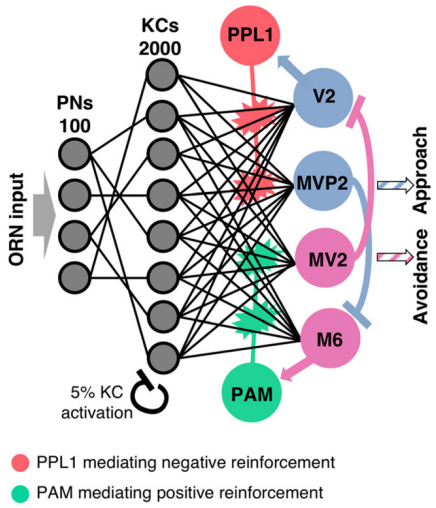

Figure 1. Circuit model. The olfactory pathway comprises three feedforward layers. Olfactory input activates an odor-specific combination of PNs. The connectivity matrix from PNs to the large population of KCs is divergent-convergent and sparse. The inhibitory feedback mechanism ensures population sparseness of 5% active cells in the KC layer. KCs are fully connected with four MBONs in the output layer. A positive or negative reinforcement stimulus directly excites the dopaminergic PAM or PPL1 neuron, respectively. Lateral inhibition between the MBONs and excitatory feedback from MBONs to DANs is crucial for the reward prediction and extinction mechanisms. Activation of the MVP2 output neuron mediates approach behavior, activation of MV2 mediates avoidance behavior. Behavioral preference toward an odor is calculated as the imbalance between the activations of MVP2 and MV2.

MVP2, whereas V2 gets inhibited by MV2. The respective inhibitory inputs are formalized according to

$$M6^{-} = \frac{-0.6}{(1+200 \times e^{(-MVP2 \times 15)})} \tag{3a}$$

$$V2^{-} = \frac{-0.6}{(1+200 \times e^{(-MV2 \times 15)})}. \tag{3b}$$

The activation rate of M6 and MV2 results from a summation of inhibitory and excitatory input as

$$M6 = M6^{+} + M6^{-} \tag{4a}$$

$$V2 = V2^{+} + V2^{-}, \tag{4b}$$

whereas for MVP2 and MV2, the activation rate is solely determined by the excitatory input.

The PAM and PPL1 DAN receive excitatory input by the M6 and V2 neurons, respectively. Additionally, reinforcing stimuli have an effect on both DANs. A rewarding US (US = +1, positive reinforcer) leads to an excitatory input to the PAM (Eq. 5a). At the same time, excitatory input from the V2 to the PPL1 is partially suppressed (represented by the factor ρ = 0.8 in Eq. 5b). Conversely, a punishing US (US = −1, negative reinforcer) results in excitation of the PPL1 (Eq. 5b) and in the suppression of excitatory input from M6 to the

PAM (Eq. 5a). The total DAN input was thus computed as

$$PAM_{In} = \begin{cases} R + M6, if\ US = +1(reward) \\ \rho \times M6, if\ US = -1(punishment) \\ M6, otherwise \end{cases} \quad (5a)$$

$$PPL1_{In} = \begin{cases} R + V2, if\ US = -1(punishment) \\ \rho \times V2, if\ US = +1(reward) \\ V2, otherwise \end{cases}. \quad (5b)$$

We fixed the US induced excitation to $R = 0.3$ for all our experiments. However, generally the parameter R allows for a modeling of variable reward magnitudes linked to the US such as, e.g., different levels of sugar concentration contained in a rewarding US.

The output activation rate of each DAN encoding the prediction error is calculated with a sigmoid transfer function

$$PAM = \frac{1}{(1 + 10000 \times e^{-PAM_{Input} \times 19})} \quad (6a)$$

$$PPL1 = \frac{1}{(1 + 10000 \times e^{-PPL1_{Input} \times 19})}. \quad (6b)$$

Plasticity rule at KC::MBON synapses

We implemented synaptic plasticity at the KC::MBON synapses. In the initial state of the model, the weights of all KC::MBON synapses are set to the same fixed value of 0.01. Each of the synaptic weights in W2 is subject to synaptic plasticity. At the end of a given trial t and for any synapse KC_i::$MBON_j$ a change of the synaptic weight w_{ij} occurs if both, the presynaptic KC and the respective DAN were active in trial t. If both conditions are met, the synaptic weight is reduced according to the two-factor learning rule

$$w_{app} = \begin{cases} w_{app} - (PPL1 \times \delta), if\ PPL1 > 0, KC > 0 \\ 0, if\ w_{app} < 0 \\ w_{app}, otherwise \end{cases} \quad (7a)$$

$$w_{av} = \begin{cases} w_{av} - (PAM \times \delta), if\ PAM > 0, KC > 0 \\ 0, if\ w_{av} < 0 \\ w_{av}, otherwise \end{cases}. \quad (7b)$$

where w_{app} refers to the weight of a synapse onto M6 or MV2 and w_{av} refers to the weight of a synapse onto MVP2 or V2. Note that the weight changes are proportional to the activation rate of the respective DAN. We fixed the learning rate as $\delta = 0.0045$ for all our experiments.

Experimental protocols

We subjected our model to a set of conditioning and extinction protocols. Further, it was operated and evaluated in a trial-resolved fashion where, in each trial, the excitatory and inhibitory synaptic input to each of the neurons and its output activation rate was computed. Within-trial neuronal dynamics were neglected.

Classical conditioning

The training procedure derives from a group assay developed by Tully and Quinn (1985) that is often used to study olfactory learning in flies. A group of flies are trained in a Tully-machine with a training arm and two testing arms. In the training arm, the animals are typically exposed to the CS+ in combination with either sugar (reward) or a train of electric shocks (punishment). In Felsenberg et al. (2018) the CS+ is presented for 1 min and combined with 12 electric shocks. Subsequently, animals are exposed to the CS– without reinforcer. After the training, the flies are transferred to the testing chamber in which they can choose between a CS+ and a CS– perfused arm.

Our classical conditioning protocol also consisted of a training phase and a subsequent memory retention test (Fig. 2*A*). An odor pattern (CS+) was paired with a positive or negative reinforcement (US) during each training trial. Subsequently, a second odor pattern (CS–) was presented without reinforcement. For our initial model analysis, we varied the number of training trials in the range of $n = 1, ..., 24$ to quantify the associative strength as a function of n (Fig. 2). Then, we fixed the number of training trials to $n = 12$ in our standard training procedure. The trial-based classical conditioning protocol is a standard procedure in other insect models for learning and memory, notably the honeybee (Bitterman et al., 1983; Pamir et al., 2011). Unlike in the experimental conditioning paradigm, paired and unpaired odors were presented alternately when the number of trials was >1. However, we expect no difference between continuous and alternating odor presentation, since CS– presentation does not induce synaptic plasticity. During retention, we presented the CS+ and CS– stimulus once. In contrast to the experimental paradigm, simultaneous presentation of both odors was not possible. However, effects on the behavioral outcome could be excluded by switching off learning during the retention test.

Extinction learning

The extinction protocol included an additional reactivation phase after training and before memory extinction (Figure 3*A*). During reactivation, the CS+ odor was presented alone, i.e., without reinforcement, during 12 reactivation trials. This procedure again mimics the experimental protocol used by Felsenberg et al. (2018), in which the authors presented the CS+ without shocks for the same duration (1 min) as in the training.

Neurogenetic manipulation experiments

To investigate the role of individual neurons in the memory extinction process we selectively suppressed their activation by setting their activation rate to zero during the reactivation phase. Thereby, we mimic neurogenetic manipulation experiments that suppress the activation of specific neurons. We specifically compare our model results to the experimental results performed in Felsenberg et al. (2018) based on the neurogenetic tool shibire^{ts1} and we generate experimentally testable hypotheses in novel model experiments.

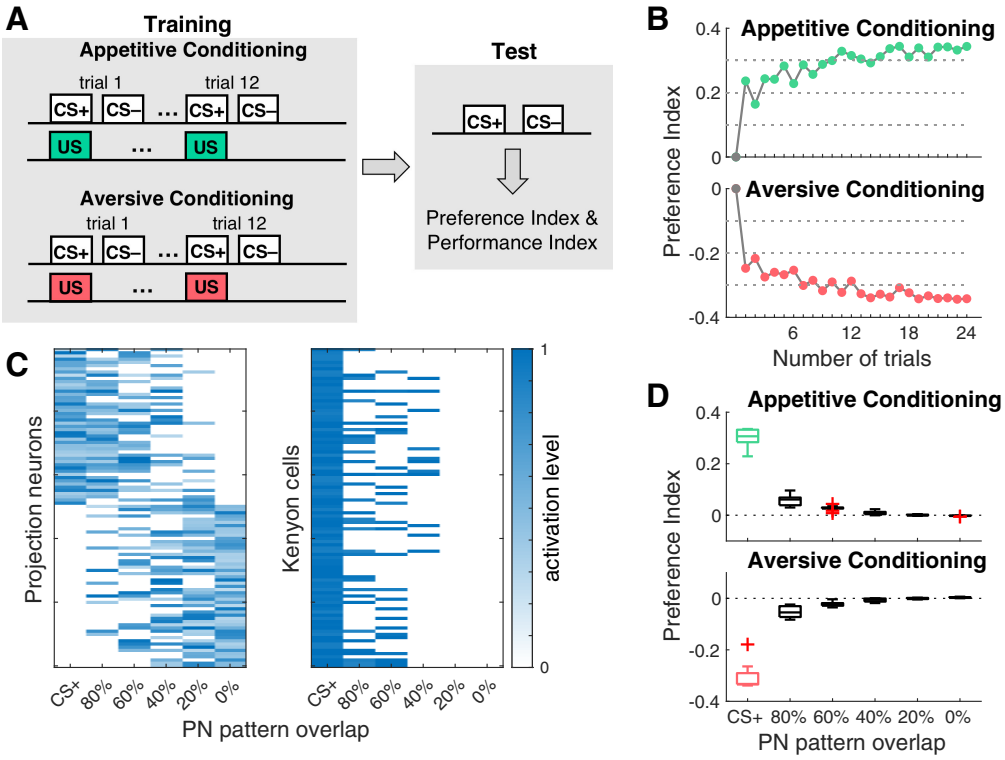

Figure 2. Differential conditioning leads to CS+-specific odor preference. ***A***, Experimental protocols for simulation of associative conditioning experiments. The model was trained in a classical conditioning paradigm, in which a conditioned odor stimulus (CS+) was paired with a reward (green) or punishment (red). Subsequently, a second unconditioned odor stimulus (CS–) was presented without reinforcement. The standard protocol comprises 12 training trials. During the retention test, both odor stimuli were presented alone without reinforcement. Preference index and performance index in the model were computed after each trial and during the retention test. ***B***, Dynamics of the odor preference index across 24 appetitive (top) and aversive (bottom) learning trials, respectively averaged across 10 networks. ***C***, left, Combinatorial response patterns in the PN population. Each odor stimulus activates 50% of all PNs. Similarities between the CS+ reference odor and five novel odors are defined by their overlap in the PN activation pattern (*x*-axis). Right, Activation patterns across the subpopulation of 100 KCs (5%) activated by the CS+ odor. Pattern overlap in the KC population reduces rapidly with decreasing odor similarity as expressed in the percentage of PN pattern overlap (*x*-axis). ***D***, Generalization to different odors after associative conditioning to the CS+ odor. The model shows a significant CS+ approach (green) or avoidance (red) after 12 training trials as expressed in the preference index ($n = 15$), which diminishes rapidly with decreasing odor similarity. Boxplots show the median and the lower and upper quartiles, whiskers indicate 1.5 times interquartile range, outliers are marked with + symbol.

Evaluation of model performance and quantitative model predictions

We evaluated model outcome by different measures that allow for a quantitative comparison with the outcome of animal experiments, both at the behavioral and at the physiological level. Applying these measures in untested experiments allowed us to formulate experimental predictions for novel experiments.

Behavioral output

To this end, we computed two quantities that can be interpreted as measures of approach or avoidance behavior. We used the activation rates of these MVP2 and MV2 to calculate the preference index as

$$preference\ index = \frac{(MBON_{MVP2} - MBON_{MV2})}{(MBON_{MVP2} + MBON_{MV2})}. \quad (8)$$

The innate preference index of our model is zero by construction.

In behavioral extinction learning experiments (Felsenberg et al., 2017, 2018), the number of animals that chose the CS– odor was then subtracted from the number of animals that chose the CS+, and the result was normalized by the total group size to compute the *performance index* (Tully and Quinn, 1985). In analogy, we calculated a model *performance index* computing the difference between the preference indices for CS+ and CS– as

$$performance\ index = preference\ index_{CS+} - preference\ index_{CS-}. \quad (9)$$

Dendritic input

We quantified activation rates of single neurons. Activation rates were measured in both DANs and MBONs. DAN activation rates were obtained during training trials, whereas the MBON activation rates were measured during the test trials (Fig. 4). Further, we compared the model to a recent study in which dendritic MBON activity was measured (Fig. 5; Felsenberg et al., 2018). KC::MBON synapses in M6 populate the dendritic tree while the MVP2::M6 are located proximal to the dendritic root (Felsenberg et al., 2018). Measuring the calcium activation across the dendritic field can thus be interpreted as the

overall excitatory KC input to the MBON. In analogy to the experimental approaches, not only the total synaptic input, but also the sum of excitatory synaptic input from KCs was measured.

Performance at the group level

Each new initialization of a network involved the random generation of the odor induced PN activation rates (ranging between 0.8 and 1, evenly distributed) and a random number of PN::KC connections (in the range 5–15, evenly distributed) for each KC to establish variability across individuals.

To test statistical significance of group differences in the performance index, the Wilcoxon rank-sum test was used. To test for differences of MBON activation rates in the same group before and after extinction learning, the Wilcoxon signed-rank test was used. Model results were compared with the experimental results obtained by Felsenberg et al. (2017, 2018). To extract single data points from the experimental studies, the GRABIT tool by MathWorks was applied. Model simulation and statistical analyses were performed with MATLAB_R2018b (MathWorks Inc). The full code for the (MB model is available on the GitHub account of the lab: https://github.com/nawrotlab.

Results

Circuit model of the *Drosophila* MB

We implemented a neural network model of the olfactory memory circuit of *D. melanogaster* (Fig. 1) where individual neurons exhibit trial-resolved activation dynamics (see Materials and Methods). Our network model integrates experimentally confirmed connections in the adult fruit fly. It involves three feed-forward layers of the antennal lobe PNs, the MB KCs, and four individual MBONs with specific lateral inhibitory connections. Reinforcing stimuli (US) of rewarding or punishing nature are mediated by two DANs. Each DAN receives specific feedback input from a single excitatory MBON and exerts a recurrent neuromodulatory effect on the plastic KC::MBON synapses.

Stimulation with a particular odor is modeled as one specific input pattern activating 50 out of total 100 PNs, each with a random activation rate (see Materials and Methods). Similarity between different odors was defined as the percentage of overlap between the PN activation patterns (Fig. 2*C*). This establishes a dense combinatorial odor code in the PN layer as reported experimentally for fruit flies (Wilson et al., 2004; Olsen et al., 2010) and other species, notably the honeybee (Joerges et al., 1997; Krofczik et al., 2009), the locust (Mazor and Laurent, 2005; Broome et al., 2006), and the moth (Namiki and Kanzaki, 2008).

The connectivity between the PNs and KCs is divergent-convergent and random (Caron et al., 2013) where each of the 2.000 KCs (Aso et al., 2009) connects to average 10 PNs (uniformly distributed, range of 5–15), matching the experimentally estimated numbers for *Drosophila* (Leiss et al., 2009; Turner et al., 2008) and establishing a sparse connectivity for each of the postsynaptic KCs. In a second step, a threshold criterion was implemented such that only the 5% of KCs with the highest activation rates retain their activation (Fig. 2*C*) while the activation rates of all other KCs was set to zero (Peng and Chittka, 2017). This enforces population sparse coding in the KC layer (Kloppenburg and Nawrot, 2014) as reported in physiological experiments in the fruit fly where, on average, ~5% of all KCs were activated by a single odor stimulus (Turner et al., 2008; Honegger et al., 2011; Lin et al., 2014).

In the MB output layer, we implemented four out of the 34 anatomically identified MBONs (Ito et al., 1998; Tanaka et al., 2008; Séjourné et al., 2011; Aso et al., 2014a). These are MV2 (MBON-$\beta 1 > \alpha$/MBON-06), M6 (MBON-$\gamma 5 \beta'$2a/MBON-01), MVP2 (MBON-γ1pedc $> \alpha/\beta$/MBON-11) and V2 (MBON-α'1, MBON-α'3ap, MBON-α'3m, MBON-α2sc and MBON-α2p3p/MBON-15 – MBON-19). The neuron cluster V2, consisting of five neurons, was modeled as a single neuron for simplicity. M6, MV2, MVP2, and V2 have been previously shown to be involved in odor valence coding with M6 and MV2 mediating odor driven avoidance behavior, and MVP2 and V2 promoting approach behavior toward an olfactory stimulus (Séjourné et al., 2011; Aso et al., 2014b; Bouzaiane et al., 2015; Owald et al., 2015; Perisse et al., 2016; Ueoka et al., 2017). All KCs connect to each of the four MBONs (full connectivity; Fig. 1). Our model includes two inhibitory lateral connections among MBONs. The inhibitory synapses between MVP2 and M6 (Perisse et al., 2016; Felsenberg et al., 2018) have been suggested to be functionally relevant for aversive memory extinction (Felsenberg et al., 2018). We additionally assume a symmetric lateral inhibitory connection from MV2 to the V2 neuron. It has been shown that the MV2 neuron projects onto MBON-α2sc and MBON-α2p3p, which are part of the V2 cluster and it was hypothesized that the glutamatergic MV2 acts inhibitory on both neurons (Aso et al., 2014a,b), as has been shown for glutamatergic neurons in the AL (Liu and Wilson, 2013).

Reinforcing pathways and synaptic plasticity

In our circuit model, the presence of the appetitive or the aversive US are signaled by two distinct neuromodulatory DANs, the PPL1 and PAM neuron, respectively (Fig. 1). The single PPL1 neuron is representative of the PPL1 neuron cluster activated by aversive sensory stimuli such as electric shock (Claridge-Chang et al., 2009; Mao and Davis, 2009; Aso et al., 2010, 2012), the PAM neuron represents the PAM cluster that is activated by appetitive sensory stimuli such as sucrose (Burke et al., 2012; Liu et al., 2012; Waddell, 2013; Yamagata et al., 2015). Both neurons receive additional excitatory input from either the M6 or the V2 MBON (Ichinose et al., 2015; Eichler et al., 2017; Felsenberg et al., 2017, 2018; Eschbach et al., 2020).

The presence of a reinforcing signal (US) has differential effects on the DAN activation. A rewarding US leads to an excitation of PAM and can reduce excitation of PPL1 input (Eq. 5a). Vice versa, a punishing reinforcer excites PPL1 and at the same time can modulate excitation of PAM input (Eq. 5b). This modulatory effect in our model is

based on an experimental study revealing that a negative reinforcement inhibits PAM-γ4 and PAM-γ5 neurons, whereas sugar feeding inhibits PPL1-γ2 and PAM-γ3 (Cohn et al., 2015).

Plasticity in our model exclusively resides in the KC::MBON synapses, reflecting the prevalent data-based hypothesis (see Discussion). These synapses are subject to plasticity according to the learning rule in Equations 7a, 7b. In the initial state of the model, the weights of all KC::MBON synapses are set to the same fixed value. In a given experimental trial, and for any synapse KC::MV2 or KC::M6, plasticity occurs when activation of the presynaptic KC coincides with activation of the reward-mediating PAM neuron. Likewise, any KC::V2 or KC::MVP2 synapse undergoes changes when the presynaptic KC and the punishment-mediating PPL1 neuron are active at the same time. The reduction of a synaptic weight is proportional to the DAN activation rate (for details, see Materials and Methods). This establishes two distinct parallel but interconnected neuromodulatory pathways, each involving feedback from MBONs to the DANs that, in turn, can modulate KC::MBON synapses (Fig. 1).

Appetitive and aversive conditioning establish a behavioral odor preference

In a first set of experiments, we subjected our model to a classical conditioning protocol. This protocol (Fig. 2*A*) mimics standard training procedures in the fruit fly (see Materials and Methods). In each trial the trained odor, CS+, was paired with either reward or punishment (US). Subsequently a second odor stimulus was presented without reinforcement (CS–).

After a predefined number of training trials, we performed a memory retention test by presenting the model with the CS+ alone (no reinforcement) and subsequently with the unpaired odor (CS). We computed a preference index (Eq. 8) based on the activation rates of approach and avoidance mediating MBONs for both odors, the CS+ and the CS– (see Materials and Methods). The model performance index (Eq. 9) mimics comparison with the behavioral performance index computed from experiments in the fruit fly.

Olfactory memories are established as a skew in the MBON network: aversive learning reduces CS+ driven responses in approach MBONs (MVP2-MBON and V2 cluster MBONs) resulting in a skew toward avoidance. In contrast, appetitive learning skews the network toward approach by reducing CS+ mediated input to avoidance coding M4 and M6 MBONs (Aso et al., 2014b; Owald et al., 2015; Owald and Waddell, 2015; Perisse et al., 2016; Zhang et al., 2019).

We explored the preference index during the retention test for a varying number of training trials (Fig. 2*B*). In the naive state, i.e., before the first training trial, the model did not reveal a preference. This is because of the balanced synaptic weight initialization of the model. A single appetitive training trial yielded a strong preference toward the rewarded odor, the CS+. With each additional training trial, the preference index further incremented by a small amount and thus additional training led to only a gradual increase of the preference index saturating after ~10–15 trials. Aversive conditioning revealed a negative preference index reaching a similar absolute level after a single training trial (Fig. 2*B*, lower panel). Both, single-trial learning and saturation of behavioral performance within few trials matches the experimental observations during associative learning in insects (see Discussion).

For all subsequent experiments, we chose 12 training trials, both for the training and the reactivation phase. This number mimics the standard experimental protocol for aversive conditioning in fruit flies, in which a group of animals is exposed to 12 subsequent electric shocks while constantly being exposed to the CS+ (Tully and Quinn, 1985; Scheunemann et al., 2013; Felsenberg et al., 2018).

Generalization to novel odors

We next analyzed how the learned preference to the CS+ odor generalizes to novel odors of varying similarity with the CS+ odor by comparing the preference indices toward CS+ and toward a novel odor during the retention test (Fig. 2*D*). We designed the pattern of activated PNs for each novel odor such that it has a defined overlap with the CS+ pattern, ranging from zero to 80% overlap (see Materials and Methods). Our results in Figure 2*D* predict that generalization to a novel odor is rather low even for the highest odor similarity and decays with decreasing odor similarity, effectively reaching zero generalization for odors that share 40% or less activated PNs with the CS+ odor. For the subsequent extinction learning experiments, we used CS– odors that had 60% pattern overlap with the CS+ odor.

Extinction learning significantly reduces the conditioned odor response

We analyzed extinction learning after appetitive and aversive conditioning according to the stimulation protocol in Figure 3*A*. The initial training phase was followed by a reactivation phase during which the model is repeatedly presented with the CS+ odor alone (no reinforcement). This matches the experimental protocols for appetitive (Felsenberg et al., 2017) and aversive (Felsenberg et al., 2018) conditioning and subsequent extinction learning and allows for a direct comparison of our simulation results with the experimental results, both at the behavioral and the physiological level (compare Extended Data Fig. 3-1).

Repeated reactivation of the CS+ odor alone after either appetitive or aversive conditioning resulted in memory extinction (Fig. 3*B*,*C*), i.e., in a significant reduction of the learned CS+ approach or avoidance. In addition, generalization to the CS– odor was abolished (Fig. 3*B*,*C*). The observation that learning is induced when the expected reward or punishment is omitted is in line with the idea of prediction error dependent learning (see Discussion). For a quantitative comparison with the behavioral results of the binary memory test in Felsenberg et al. (2017), we computed the performance index of the model by subtracting the preference index for CS– from the preference index for CS+ (see Materials and Methods). The appetitive conditioning protocol in the model and *in vivo* yielded similar performance indices (model: 0.30 ± 0.03 mean ±

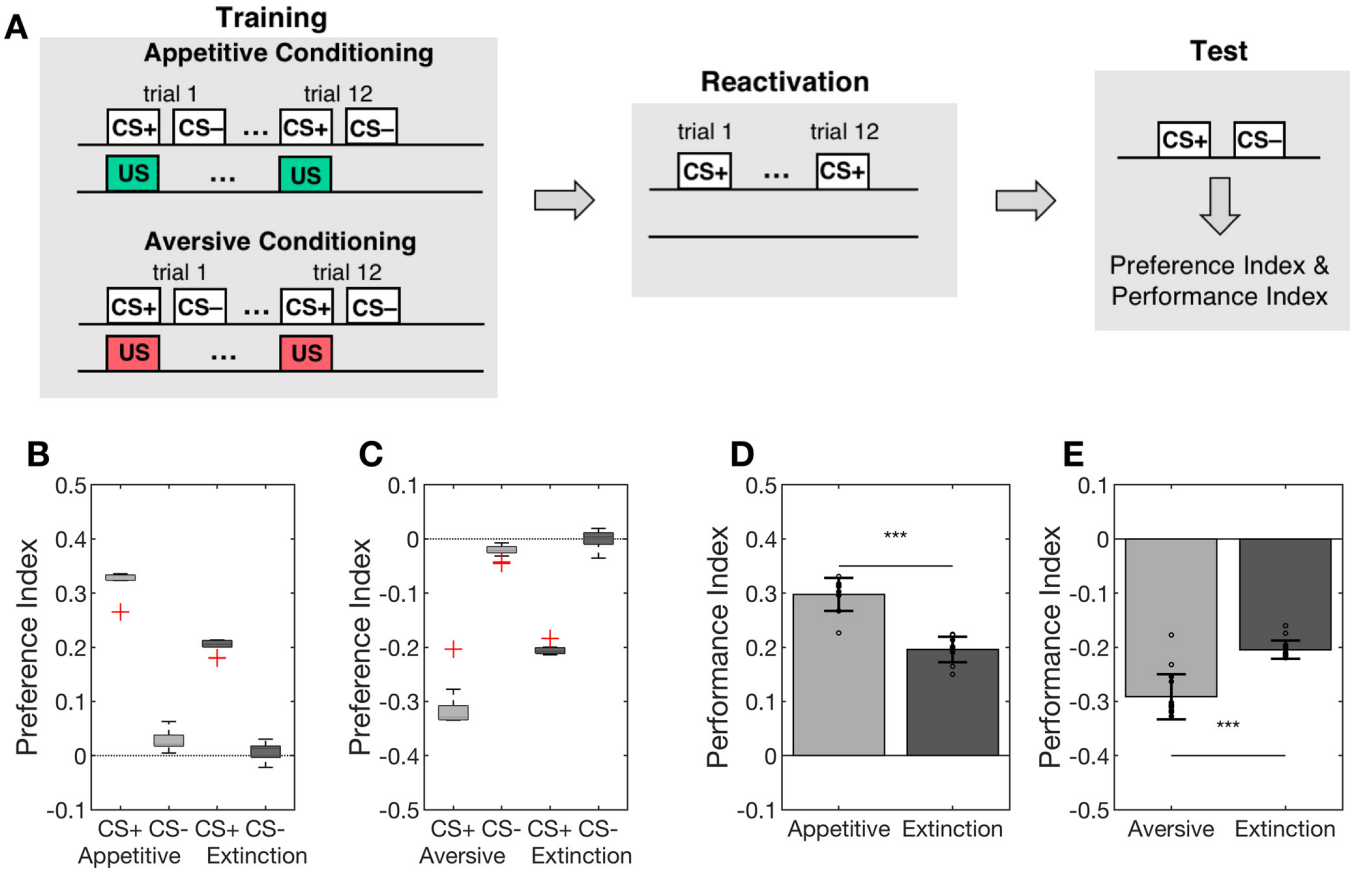

Figure 3. CS+ odor reactivation leads to memory extinction. ***A***, Training and test protocol as in Figure 2*A*. In the extinction protocol, the training phase is followed by an odor reactivation phase, in which the CS+ was presented alone for 12 consecutive trials before performing the retention test. ***B***, The appetitive conditioning protocol (light gray) induced a strong and significant preference for the CS+ odor and a weak and significant preference for the CS– odor. Extinction learning partly abolished the CS+ preference during the retention test (dark gray). The preference index for the CS+ odor was significantly lower than after initial appetitive conditioning, for the CS– odor no more significant preference was observed after extinction learning. ***C***, Symmetric results were observed for aversive conditioning. Again, extinction learning significantly reduced the learned preference for the CS+ odor. Boxplots show the median and the lower and upper quartiles, whiskers indicate 1.5 times interquartile range, outliers are marked with + symbol. ***D***, ***E***, The performance indices were significantly reduced after extinction compared with the initial appetitive and aversive memories. Data are presented mean ± SD; ***$p < 0.001$; $n = 15$ independent models. For preference and performance indices of the model tuned toward asymmetric appetitive and aversive learning pathways, see Extended Data Figure 3-2.

SD, experiment: 0.29 ± 0.05 mean ± SEM). Memory extinction led to a significantly reduced approach performance (0.20 ± 0.02; Fig. 2*B*). However, the effect of memory extinction in the behavioral experiment was considerably stronger, effectively erasing the initial behavioral memory expression (0.01 ± 0.03; Felsenberg et al., 2017). The aversive conditioning protocol led to a negative performance index of −0.29 ± 0.04 (mean ± SD) for the model, which in absolute terms was smaller than the experimental value of −0.39 ± 0.04 (mean ± SEM; Felsenberg et al., 2018). The reactivation of the CS+ odor after the aversive conditioning led to a significantly reduced avoidance behavior (−0.20 ± 0.02), very similar to the experimental results (−0.20 ± 0.03). A detailed quantitative comparison of experimental and model results is provided in Extended Data Extended Data Fig. 3-1.

Memory is rapidly established within a single trial

As a next step, we investigated the dynamics of plasticity during the course of learning and extinction. To this end, we monitored the activation rates of DANs and MBONs and the gross synaptic input to the MBONs across trials during single network simulations for appetitive (Fig. 4*A*,*B*) and aversive (Fig. 4*C*,*D*) conditioning and extinction.

In both, appetitive and aversive conditioning, the first pairing of CS+ and US induced a strong response in either the PAM or PPL1, respectively. This strong neuromodulatory signal resulted in a significant reduction of the respective KC::MBON synapses and led to a strongly reduced KC::MBON input to either MV2/M6 or MVP2/V2 during the second training trial. As a consequence, feedback excitation from M6 to PAM (V2 to PPL1) in appetitive (aversive) learning is abolished from the second trial onward, leading to further synaptic weight modulations that are weak compared with those in the very first training trial. The evolution of plasticity is reflected in the model performance index, indicating a switch-like increase after the first training trial and moderate but steady increase after subsequent trials. Saturation of the learning effect

becomes visible only after ~10–12 trials (compare Fig. 2*B*). In conclusion, the model learns within a single trial and more training leads to a stronger valence signal as encoded in the imbalance of MV2 and MVP2 activation.

Extinction learning follows a different and slower dynamics in our network model. While already a single presentation of the CS+ odor without reinforcer leads to the induction of the extinction memory and a significant reduction of the performance index (Fig. 4), we observe an only gradual extinction that saturates across the 12 extinction trials used here. No complete extinction is observed in our model.

Associative learning and extinction learning establish two separate memory traces

We tested the hypothesis that associative learning and subsequent extinction learning form two parallel and distinct memories at the physiological level. To this end, we mimicked experiments in Felsenberg et al. (2018), in which the authors measured KC input to individual MBONs by means of *in vivo* calcium-imaging from the dendritic field.

We first consider the case of aversive conditioning and subsequent extinction learning. After initial conditioning, the CS+-induced synaptic input to the MVP2 and V2 neurons is significantly lower than the CS–-induced input (Fig. 5*C*). The synaptic input to the M6 and MV2 neurons, however, is similar for both odors (Fig. 5*D*). The extinction protocol, i.e., the subsequent reactivation with CS+ alone (Fig. 3*A*), did not alter KC synaptic input to MVP2 and V2 (Fig. 5*C*). In contrast, CS+-induced synaptic input to M6 and MV2 was significantly reduced after extinction and in comparison to the CS–-induced input (Fig. 5*D*). These results are fully consistent with the *in vivo* calcium-imaging results by Felsenberg and colleagues (Felsenberg et al., 2018; compare Extended Data Fig. 3-1) who observed a significantly reduced dendritic calcium activation in MVP2 in response to the CS+ stimulus after aversive conditioning, while there was no significant change in M6 activation (Felsenberg et al., 2018; see their Fig. 3). After memory extinction, the decreased CS+ response in MVP2 remained while additional plasticity was observed as CS+-specific reduction in calcium levels in M6.

Our circuit model predicts a symmetric network behavior for the extinction of an appetitive memory. After appetitive conditioning, the CS+-induced excitatory input was lower than the CS–-mediated input to the avoidance-mediating M6 and MV2 (Fig. 5*B*). However, the input to the approach mediating MVP2 and MV2 remained unchanged (Fig. 5*A*). Reactivation of the memory by stimulation with the CS+ odor alone led to a reduction of the excitatory dendritic input into MVP2 and V2 (Fig. 5*A*). As a result, the CS+ preference and performance indices acquired during initial conditioning were significantly reduced after memory extinction (Fig. 3*B*,*D*).

Distinct pathways are crucial for appetitive and aversive memory extinction

To validate the idea of recurrent feedback as a teaching signal in our model we tested which neurons are necessary for extinction learning. To this end, we mimicked shibire^{ts1} experiments performed by Felsenberg et al. (2017, 2018), who selectively suppressed the activity of individual neurons or neuron clusters during CS+ odor reactivation (see Materials and Methods; Fig. 6).

We first tested extinction of appetitive memory. Selective blocking of PPL1-cluster or V2-cluster during the reactivation phase abolished the extinction of an appetitive memory. In contrast, blocking of PAM had no effect on extinction (Fig. 6*A*). These findings agree with the experimental results (Extended Data Fig. 3-1) in Felsenberg et al. (2017). Conversely, in the extinction of aversive memory, Felsenberg et al. (2018) showed that the behavioral effect of extinguishing the aversive memory was significantly diminished by either blocking the PAM cluster or the M6 neurons. However, blocking the vesicle release machinery of the PPL1 cluster had no effect on aversive memory extinction (Extended Data Fig. 3-1). Our model showed the same qualitative result where blocking of either the M6 or the PAM but not of the PPL1 neuron abolished the extinction of an aversive memory (Fig. 6*B*).

To formulate novel predictions for future experiments we further analyzed our model by silencing other MBONs during the reactivation phase (Fig. 6; Extended Data Fig. 3-1). Deactivating V2 during the reactivation phase did not significantly alter the aversive extinction memory. Conversely, a blockage of M6 during the extinction process had no effect on the appetitive extinction memory performance either. Blocking MVP2 or MV2 during odor reactivation had no effect on both, appetitive and aversive memory extinction. Thus, our model predicts that a single MBON, V2, or M6, is exclusively involved in the formation of the appetitive or aversive extinction memory, respectively.

KC activity is partly required for extinction learning

We additionally investigated the role of KCs in extinction learning in our model. To this end, we applied the shibire^{ts1} protocol to KCs. When we blocked all KCs during the training phase, neither appetitive nor extinction memory could be established. However, when we randomly chose and blocked 50% of all KCs during appetitive and aversive extinction training, we did not observe an effect on extinction memory acquisition (Fig. 6). Thus, partially blocking KC activity during odor reactivation might not or only mildly interfere with extinction learning while an almost complete block of all KCs should prevent extinction learning in the fly (Extended Data Fig. 6-1; see also Discussion).

Discussion

In the present study, we established a circuit model of the fruit fly based on confirmed anatomy and physiology. It can explain formation and extinction of an olfactory memory, and single-trial learning. We discuss the implications, limitations and predictions of our model.

Prediction error coding

The prediction error theory hypothesizes that learning takes place if there is an unexpected change in the

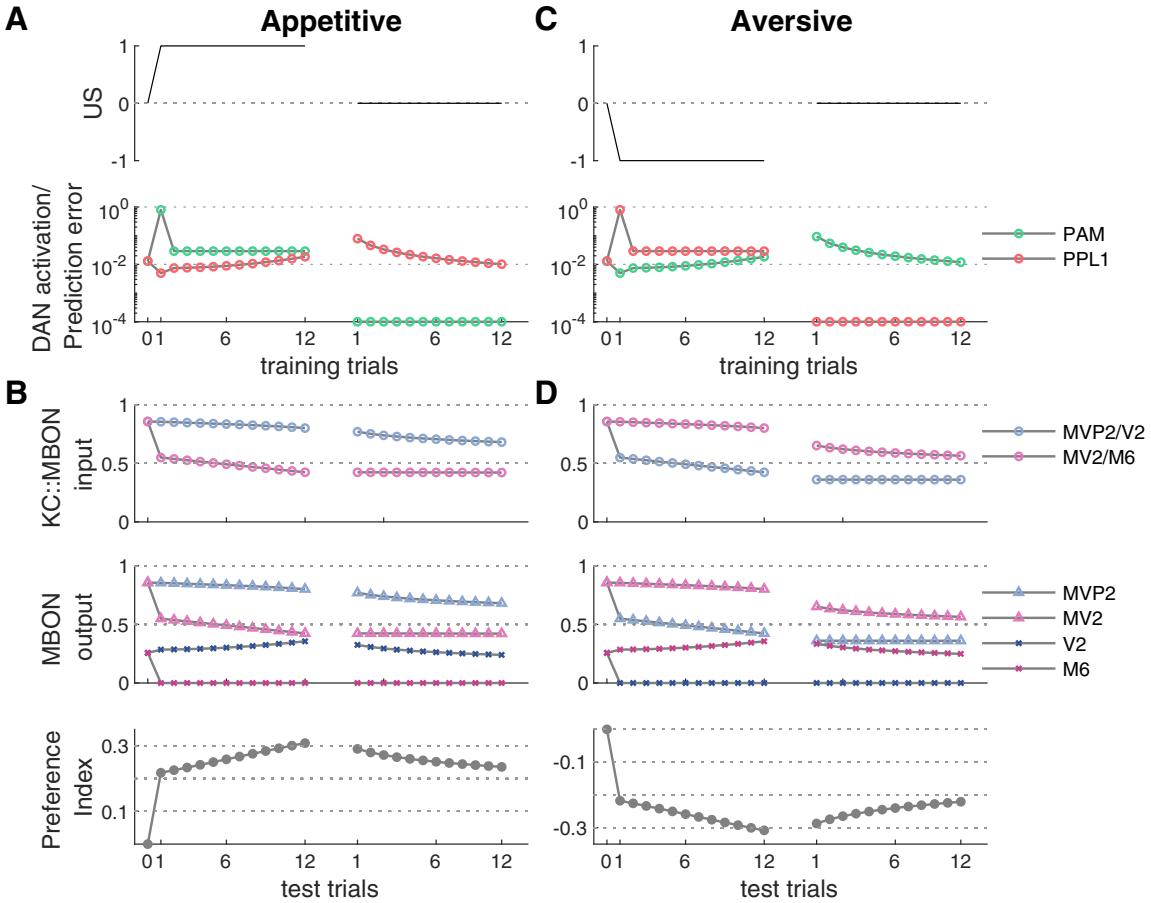

Figure 4. Neuron activation rates and behavioral performance across trials. ***A***, Reward value (US, top) and DAN activation rates (bottom) across 12 initial conditioning trials (left) and 12 extinction trials (right). Trial zero indicates neuron activation rates in the naive model before learning. Reward presentation resulted in a prominent peak activation of the PAM during the very first training trial, i.e., when the actual reward strongly deviates from the predicted reward. Omission of the reward during the first extinction trial (right) resulted in a step-like reduction of PAM activation the simultaneous increase in PPL1 activation, which is crucial for extinction learning. ***B***, Summed synaptic KC input to MBONs (top), MBON activation rates (middle), and model preference index (bottom) for each simulated test trial that followed the respective training trial (see Materials and Methods). The strong PAM activation during the first conditioning trial resulted in a strong change of the synaptic weights between KCs and MV2 and M6, and consequently in a step-like reduction of the synaptic input and the output activation rates. Consequently, the model preference index represents the imbalance between M6 and MV2 activation rates showed a step-like increase predicting a switch-like expression of a CR behavior after only a single conditioning trial. Additional training led to a further gradual reduction of gross synaptic input to and activation of MV2 and M6, paralleled by the gradual increase of the preference index. Extinction learning led to a gradual reduction of synaptic weights in the KC::MVP2 and KC::V2 pathway. This reduces the difference between M6 and MV2 activation and leads to a gradual extinction of the preference index. ***C***, ***D***, Same as ***A***, ***B*** for aversive conditioning (left) and subsequent extinction (right). Simulation results are shown for a single network. This was initiated identically before appetitive (***A***, ***B***) and aversive (***C***, ***D***) conditioning to enforce identical initial conditions stressing the symmetric mechanism of reward prediction.

valence of a stimulus (Rescorla and Wagner, 1972). The model performance index in Figure 4 computed after each training trial mimics behavioral performance across trials and fits the prediction error theory and experimental studies. The behavioral learning effect is reduced across trials and the learning curve saturates with increased training. The results match the well-known saturation in the conditioned response (CR) behavior in the honeybee (Pamir et al., 2011). This effect, typically observed across a group of animals, has been formalized in the Rescorla-Wagner model (Rescorla and Wagner, 1972). A recent rate-based model of the fly MB (Bennett et al., 2021) assumed that connections from MBONs to DANs are crucial for asymptotic learning based on reward prediction. Our model proposes that prediction error coding in *D. melanogaster* is achieved through a network mechanism supported by the specific circuit motif sketched in Figure 1. It is suggested that DANs receive relevant information not only from sensory neurons directly but also via odor activated MBONs (Felsenberg et al., 2017, 2018). It was implemented in the model through excitatory connections from laterally connected MBONs to DANs. Initial conditioning of the model leads to activation of the PAM (PPL1) DAN and therefore induces downregulation of the aversive (appetitive) MBONs. This learning effect declines after the first learning trial, since MBON

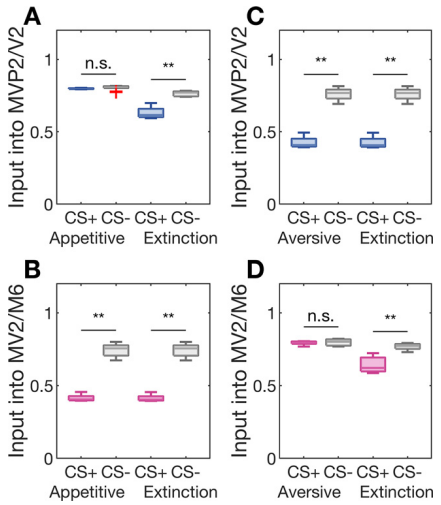

Figure 5. Two separate memories underlie initial and extinction learning. CS+ odor-induced activation rates of MBONs were measured before and after extinction training to locate associative and extinction memories. ***A***, ***B***, Appetitive learning led to a relative depression of CS+ odor-induced activation rates of MV2 and M6, but not MVP2 and V2 MBONs. The memory trace in MV2/M6 stayed intact even after appetitive memory was extinguished. Extinction decreased the CS+ response of MVP2/V2, establishing a parallel memory trace. ***C***, ***D***, Aversive conditioning led to a reduced CS+ input into MVP2/V2, but not into MV2/M6. After memory extinction, the memory trace in MVP2/V2 remained, and we observed an additional decrease in CS+ response in MV2/M6. Boxplots show the median and the lower and upper quartiles, whiskers indicate 1.5 times interquartile range, outliers are marked with + symbol; n.s. = not significant, $^{**}p < 0.01$. Results across simulation of $n = 10$ networks in all panels.

activity is not sufficient to activate DANs after being downregulated.

Single-trial learning

Learning within a single trial is a fundamental ability of vertebrates (Irwin et al., 1968; Cook and Fagot, 2009) and invertebrates, and the underlying mechanisms are at least partially conserved across phyla. In insects, single-trial learning has been intensely studied in classical and operant olfactory, tactile, and visual conditioning of the honeybee *Apis mellifera* (Menzel et al., 1974; Smith, 1991; Sandoz et al., 1995; Menzel, 1999; Pamir et al., 2014; Villar et al., 2020). Appetitive olfactory conditioning of the proboscis extension response allows the observation of the all-or-none CR behavior during successive training trials where the onset of US presentation is delayed with respect to the onset of the CS odor. Typically, 40–60% of bees show a CR after a single pairing of odor with reward (Pamir et al., 2014) and a single learning trial is sufficient to establish short-term and long-term memory, which can be recalled up to 3 d after training (Smith, 1991; Menzel, 1999; Pamir et al., 2014; Villar et al., 2020). Additional training trials lead to a saturation after approximately three to four trials with respect to the fraction of animals that express a CR.

In the fruit fly, single-trial learning has been established more recently. Aversive conditioning of adult flies with electric shock punishment showed that pairing of a single odor presentation (of 10–60 s in duration) with a single electric shock induces short term memory (Beck et al., 2000; Scheunemann et al., 2013) and long-term memory, retrievable for up to 14 d if the experimental context is kept strictly constant for training and memory test (Zhao et al., 2019). In appetitive conditioning, a single session of odor-reward pairing could establish long-term memory (Krashes and Waddell, 2008; Colomb et al., 2009). Weiglein et al. (2019) could show that also in the fruit fly larva a single session of appetitive conditioning of 5 min was sufficient to establish a short-term memory where the performance index in the memory test increased with increasing duration (in the order of minutes) of the training session.

In our circuit model, the very first training trial induces a switch-like change in the network response and in the behavioral memory expression. This parallels the switch-like behavioral dynamics observed in learner bees (Pamir et al., 2011) and provides an explanation for the single-trial induction of appetitive and aversive memories in the fruit fly (Krashes and Waddell, 2008; Colomb et al., 2009; Zhao et al., 2019). In contrast, during extinction learning we propose that an extinction memory builds up gradually in the opposing pathway.

Extinction learning

Experimental studies in the fruit fly have shown that extinction learning establishes distinct and opposing memory traces. The extinction of reward memory requires punishment coding dopamine neurons whereas extinction of aversive memory is mediated by reward coding neurons (Felsenberg et al., 2017, 2018). Recent findings in mice (Salinas-Hernández et al., 2018) and rats (Luo et al., 2018) suggest that this principle for extinction learning is conserved in mammals. The authors showed that DANs from the ventral tegmental area associated with reward signaling are required to extinguish fear memory.

The importance of MBON::DAN feedback to perform complex learning tasks such as extinction has been formalized recently in a rate-based model of the *Drosophila* larva (Eschbach et al., 2020). In our adult fly model, the MBON::MBON and MBON::DAN connections for the extinction of aversive and appetitive memories are strictly symmetrical. During extinction of an aversive memory the dopaminergic reward signal of the PAM neuron in extinction trials is driven by excitation from the M6 MBON, which receives reduced inhibition from the approach mediating MVP2 as a result of the initial aversive conditioning that reduced KC drive of MVP2. Thus, extinction learning establishes a reward-like extinction memory trace in parallel to the initial aversive memory trace. Intriguingly, the initial memory trace is not altered by extinction (Fig. 5). This matches the experimental results and the proposed mechanism in Felsenberg et al. (2018) supporting the long-standing hypothesis of two parallel memory traces after extinction (Bouton, 2004; Dudai, 2004; Eisenhardt and Menzel, 2007).

The strict symmetry of the recurrent pathways in our model has the consequence of symmetrical quantitative results for the performance index and neuron input activation rates (Extended Data Fig. 3-1). The experimental

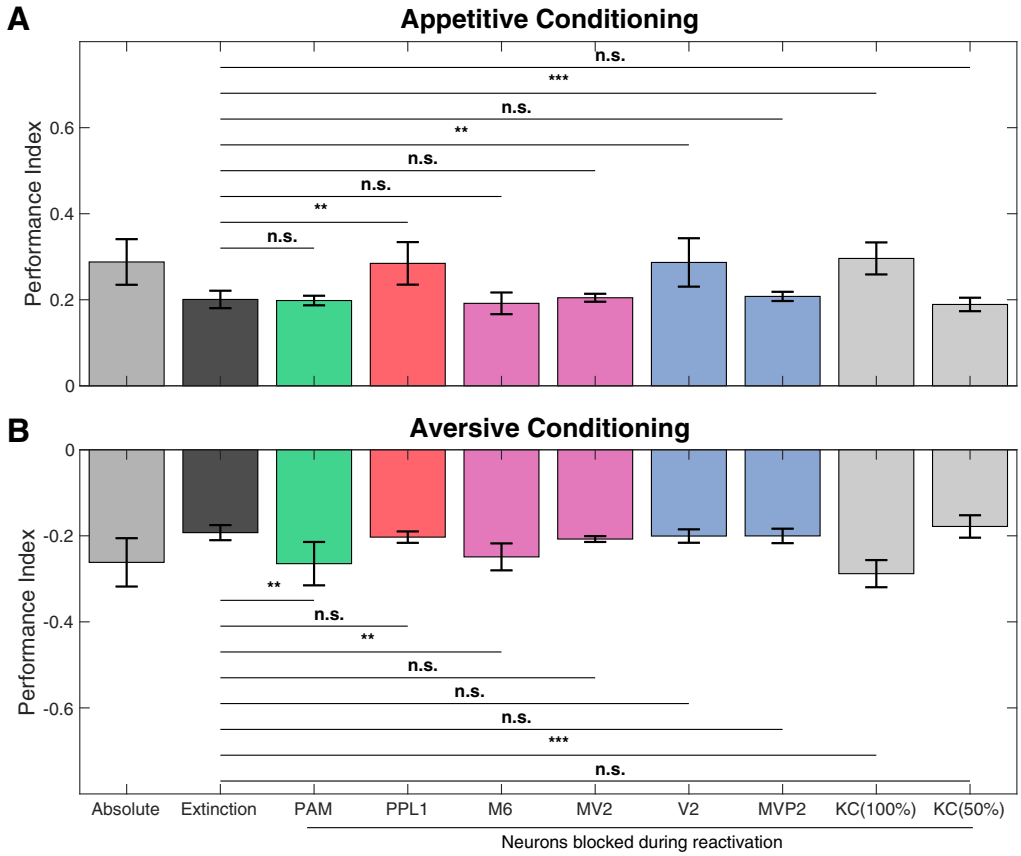

Figure 6. Blocking specific neuron groups can reverse memory extinction. The computational model was used to reproduce the neurogenetic manipulations with temperature-sensitive shibire^{ts1} mutant flies. The activation of individual neurons was suppressed during extinction training only. This allows to identify neurons that are crucial to the process of establishing the extinction memory in our model. ***A***, Knocking down PPL1 or V2 during extinction training led to a completely abolished the appetitive extinction memory. Blocking PAM, M6, MV2, or MVP2 neurons during odor re-exposure had no effect on the appetitive extinction memory. Blockage of all KCs (100%) prevented the model from extinction learning. However, when only 50% of the KC population was blocked during odor reactivation, extinction learning remained unaffected. Further effects of partial KC blocking on extinction learning are presented in Extended Data Figure 6-1. ***B***, Suppressing the activity of PAM DANs, M6 neurons, or KCs (100%) during CS+ odor re-exposure after aversive conditioning prevents the model from forming the aversive extinction memory. However, blocking PPL1 DANs, MV2, V2, MVP2, or KCs (50%) does not diminish the memory extinction. Data are presented as mean ± SD; n.s. = not significant, $^{**}p < 0.01$, $^{***}p < 0.001$; $n = 15$.

situation, however, does not provide fully symmetric behavioral results. Our model matches well in the aversive memory pathway, i.e., for appetitive conditioning and extinction of aversive memory. In aversive conditioning experiments, however, Felsenberg et al. (2017, 2018) obtained stronger performance indices than our model and extinction of the appetitive memory was complete (Extended Data Fig. 3-1). Independent tuning of model parameters for the two parallel pathways in our symmetric model allows for an improved quantitative match with the experimental results (Extended Data Fig. 3-2). However, a complete fit to the experimental data were not achievable. In particular, the complete extinction of the appetitive memory cannot be obtained. We thus conclude that the current model lacks at least on additional mechanism that introduces asymmetry in circuit and behavior. Our minimal model does not include all MBONs and DANs and their proven interconnections (Takemura et al., 2017), i.e., the inhibitory connection between MVP2 and the PPL1 cluster, might add functional asymmetry between the appetitive and the aversive memory pathway (Perisse et al., 2016; Pavlowsky et al., 2018).

Limitations of the model

Our network model (Fig. 1) can be viewed as a minimal circuit model of the MB sufficient to explain prediction error coding, single-trial conditioning and extinction learning. We focused on only four out of 34 MBONs and restricted MB connectivity to feedforward from KCs to four MBONs and feedback from MBONs to DANs but did not explore other synaptic contacts among KCs and between KCs, MBONs and DANs within the MB lobes as uncovered in the fly EM connectome (Takemura et al., 2017). Learning in our model is achieved through reinforcement-mediated plasticity at a single synaptic site, which has been shown to be involved in appetitive and aversive short-term olfactory memory (Zars et al., 2000; Pascual

and Préat, 2001; Owald and Waddell, 2015). Increasing experimental evidence indicates that olfactory learning can involve plasticity at multiple sites within the insect MB (Pascual and Préat, 2001; Kremer et al., 2010; Trannoy et al., 2011; Bouzaiane et al., 2015; Haenicke et al., 2018; Yamazaki et al., 2018). Also, it has been shown that memories can co-exist on different time scales representing short-term, mid-term, and long-term memories (Pascual and Préat, 2001; Davis, 2011; Trannoy et al., 2011; Yamagata et al., 2015). Our trial-based model approach does not accommodate explicit time scales that would allow to differentiate between simultaneous, delay and trace conditioning (Dylla et al., 2013), memory acquisition and consolidation (Felsenberg et al., 2017) or decay (Shuai et al., 2015). Future extensions may retain full temporal dynamics, e.g., by using spiking neural network models that have previously been used successfully to study classical conditioning in fruit flies (Smith et al., 2008; Wessnitzer et al., 2012; Faghihi et al., 2017; Gupta et al., 2018; Rapp and Nawrot, 2020).

In the present study, we aimed at reproducing the behavioral performance index that is measured in a group forced choice paradigm (Quinn et al., 1974) and thus represents a population measure across individuals, each performing either the correct or the incorrect behavioral choice. The long-held notion states that expression of the CR behavior in individual flies is stochastic and follows the group-averaged behavior (Quinn et al., 1974) has been questioned by Chabaud et al. (2010) and by studies in the honeybee (Pamir et al., 2011, 2014; Haenicke et al., 2018) and in the cockroach (Arican et al., 2020). They have shown that the average CR in a group of animals does not accurately reflect memory expression in individuals. Rather, it confounds two subgroups of learners and non-learners where learners showed a switch-like and stable expression of the CR behavior mostly after a single trial (average 1.7 trials) with high memory retention rates (>90%). Different parameters may account for individual learning abilities such as internal state, e.g., of hunger and satiety (Pamir et al., 2014; Sayin et al., 2018) that could influence perception or motivation. Establishing neural circuit models that take into account individuality of learning and individual parameters that influence memory formation is a challenge we aim to address in future model studies.

Model predictions

Our model makes several predictions that can be tested experimentally. First, we hypothesize that DANs in the PAM and PPL1 cluster compute a prediction error. Specifically, in naive animals and for the example of appetitive learning the PAM should show spontaneous baseline spiking activity and no stimulus response during the presentation of a novel odor. During a first pairing of the CS+ odor with a reward (US) the PAM cluster should show a clear odor response, which will be strongly reduced after the first learning trials (Fig. 4*A*). When reward is omitted during extinction trials or in the memory test, we predict a response in which the PAM reduces its spiking output below spontaneous level. This prediction matches the observation in DANs in the monkey (Schultz et al., 1997) and in the octopaminergic VUMmx1 neuron in the honeybee (Montague et al., 1995; Hammer, 1997), although the circuit mechanisms hypothesized here differs from that proposed by Schultz et al. (1997) and Hammer (1997).

Second, we hypothesize a switch-like induction of a memory trace during a single training trial, implying a step-like change in the MBON activation rates (Fig. 4). A second or third training trial should only induce gradual changes in cellular physiology. Likewise, the behavioral memory expression should be observable after a single learning trial.

Third, our systematic analysis of blocking experiments (Fig. 6) for all MBONs indicate that MV2, M6, and MVP2 do not play a role during appetitive memory extinction, whereas MVP2, MV2, and V2 are dispensable for aversive extinction learning. This could be experimentally tested by blocking these MBONs specifically during extinction trials only. While the co-existence of two memory traces after extinction of an aversive memory has been shown in calcium-imaging from MVP2 and M6 (Felsenberg et al., 2018; Fig. 5*D*) our model predicts parallel memory traces also for extinction of an appetitive memory (Fig. 5*A*,*B*).

Finally, in a study by Schwaerzel et al. (2002), in which KCs were blocked during aversive conditioning and odor reactivation, the authors argued that KC activity is dispensable for the acquisition of an extinction memory. However, the two GAL4 lines used in this study include <50% of all KCs (~700 and 850 cells). Our model analysis predicts that a sizable fraction of the KC population is required and sufficient to form an extinction memory (Fig. 6; Extended Data Fig. 6-1). A complete block of KCs however would interrupt the PN::KC::MBON::DAN signaling pathway and extinction memory could not be acquired. This could tested in a future blocking experiment using, e.g., the OK107-GAL4 line that has been reported to label practically all KCs (Aso et al., 2009).

References

Arican C, Bulk J, Deisig N, Nawrot MP (2020) Cockroaches Show Individuality in Learning and Memory During Classical and Operant Conditioning. Front Physiol 10:825265.

Aso Y, Grübel K, Busch S, Friedrich AB, Siwanowicz I, Tanimoto H (2009) The mushroom body of adult *Drosophila* characterized by GAL4 drivers. J Neurogenet 23:156–172.

Aso Y, Siwanowicz I, Bräcker L, Ito K, Kitamoto T, Tanimoto H (2010) Specific dopaminergic neurons for the formation of labile aversive memory. Curr Biol 20:1445–1451.

Aso Y, Herb A, Ogueta M, Siwanowicz I, Templier T, Friedrich AB, Ito K, Scholz H, Tanimoto H (2012) Three Dopamine pathways induce aversive odor memories with different stability. PLoS Genet 8: e1002768.

Aso Y, Hattori D, Yu Y, Johnston RM, Iyer NA, Ngo TTB, Dionne H, Abbott LF, Axel R, Tanimoto H, Rubin GM (2014a) The neuronal architecture of the mushroom body provides a logic for associative learning. Elife 3:e04577.

Aso Y, Sitaraman D, Ichinose T, Kaun KR, Vogt K, Belliart-Guérin G, Plaçais PY, Robie AA, Yamagata N, Schnaitmann C, Rowell WJ, Johnston RM, Ngo TT, Chen N, Korff W, Nitabach MN, Heberlein U, Preat T, Branson KM, Tanimoto H, et al. (2014b) Mushroom body output neurons encode valence and guide memory-based action selection in *Drosophila*. Elife 3:e04580.

Beck CDO, Schroeder B, Davis RL (2000) Learning performance of normal and mutant *Drosophila* after repeated conditioning trials with discrete stimuli. J Neurosci 20:2944–2953.
Bennett JEM, Philippides A, Nowotny T (2021) Learning with reward prediction errors in a model of the *Drosophila* mushroom body. Nat Commun 12:2569.
Bitterman ME, Menzel R, Fietz A, Schafer S (1983) Classical conditioning of proboscis extension in honeybees (*Apis mellifera*). J Comp Psychol 97:107–119.
Bouton ME (2004) Context and behavioral processes in extinction. Learn Mem 11:485–494.
Bouton ME (2017) Extinction: behavioral mechanisms and their implications. In: Learning and memory: a comprehensive reference, Ed 2. San Diego: Academic Press.
Bouzaiane E, Trannoy S, Scheunemann L, Plaçais PY, Preat T (2015) Two independent mushroom body output circuits retrieve the six discrete components of *Drosophila* aversive memory. Cell Rep 11:1280–1292.
Brill MF, Rosenbaum T, Reus I, Kleineidam CJ, Nawrot MP, Rössler W (2013) Parallel processing via a dual olfactory pathway in the honeybee. J Neurosci 33:2443–2456.
Broome BM, Jayaraman V, Laurent G (2006) Encoding and decoding of overlapping odor sequences. Neuron 51:467–482.
Burke CJ, Huetteroth W, Owald D, Perisse E, Krashes MJ, Das G, Gohl D, Silies M, Certel S, Waddell S (2012) Layered reward signalling through octopamine and dopamine in *Drosophila*. Nature 492:433–437.
Caron SJC, Ruta V, Abbott LF, Axel R (2013) Random convergence of olfactory inputs in the *Drosophila* mushroom body. Nature 497:113–117.
Chabaud MA, Preat T, Kaiser L (2010) Behavioral characterization of individual olfactory memory retrieval in *Drosophila melanogaster*. Front Behav Neurosci 4:192.
Chiamulera C, Hinnenthal I, Auber A, Cibin M (2014) Reconsolidation of maladaptive memories as a therapeutic target: pre-clinical data and clinical approaches. Front Psychiatry 5:107.
Claridge-Chang A, Roorda RD, Vrontou E, Sjulson L, Li H, Hirsh J, Miesenböck G (2009) Writing memories with light-addressable reinforcement circuitry. Cell 139:405–415.
Cohn R, Morantte I, Ruta V (2015) Coordinated and compartmentalized neuromodulation shapes sensory processing in *Drosophila*. Cell 163:1742–1755.
Colomb J, Kaiser L, Chabaud MA, Preat T (2009) Parametric and genetic analysis of *Drosophila* appetitive long-term memory and sugar motivation. Genes Brain Behav 8:407–415.
Cook R, Fagot J (2009) First trial rewards promote 1-trial learning and prolonged memory in pigeon and baboon. Proc Natl Acad Sci USA 106:9530–9533.
Davis RL (2011) Traces of *Drosophila* memory. Neuron 70:8–19.
Delamater AR, Westbrook RF (2014) Psychological and neural mechanisms of experimental extinction: a selective review. Neurobiol Learn Mem 108:38–51.
Dudai Y (2004) The neurobiology of consolidations, or, how stable is the engram? Annu Rev Psychol 55:51–86.
Dylla KV, Galili DS, Szyszka P, Lüdke A (2013) Trace conditioning in insects-keep the trace! Front Physiol 4:67.
Eichler K, Li F, Litwin-Kumar A, Park Y, Andrade I, Schneider-Mizell CM, Saumweber T, Huser A, Eschbach C, Gerber B, Fetter RD, Truman JW, Priebe CE, Abbott LF, Thum AS, Zlatic M, Cardona A (2017) The complete connectome of a learning and memory centre in an insect brain. Nature 548:175–182.
Eisenhardt D (2014) Molecular mechanisms underlying formation of long-term reward memories and extinction memories in the honeybee (*Apis mellifera*). Learn Mem 21:534–542.
Eisenhardt D, Menzel R (2007) Extinction learning, reconsolidation and the internal reinforcement hypothesis. Neurobiol Learn Mem 87:167–173.
Eschbach C, Fushiki A, Winding M, Schneider-Mizell CM, Shao M, Arruda R, Eichler K, Valdes-Aleman J, Ohyama T, Thum AS, Gerber B, Fetter RD, Truman JW, Litwin-Kumar A, Cardona A, Zlatic M (2020) Recurrent architecture for adaptive regulation of learning in the insect brain. Nat Neurosci 23:544–555.
Faghihi F, Moustafa AA, Heinrich R, Wörgötter F (2017) A computational model of conditioning inspired by *Drosophila* olfactory system. Neural Netw 87:96–108.
Felsenberg J, Barnstedt O, Cognigni P, Lin S, Waddell S (2017) Re-evaluation of learned information in *Drosophila*. Nature 544:240–244.
Felsenberg J, Jacob PF, Walker T, Barnstedt O, Edmondson-Stait AJ, Pleijzier MW, Otto N, Schlegel P, Sharifi N, Perisse E, Smith CS, Lauritzen JS, Costa M, Jefferis GSXE, Bock DD, Waddell S (2018) Integration of parallel opposing memories underlies memory extinction. Cell 175:709–722.e15.
Gupta A, Faghihi F, Moustafa AA (2018) Computational models of olfaction in fruit flies. In: Computational models of brain and behavior (Moustafa AA, ed), Ed 1, Vol 1, pp 199–213. Hoboken: Wiley.
Haenicke J, Yamagata N, Zwaka H, Nawrot MP, Menzel R (2018) Neural correlates of odor learning in the presynaptic microglomerular circuitry in the honeybee mushroom body. eNeuro 5: ENEURO.0128-18.2018–13.
Hammer M (1997) The neural basis of associative reward learning in honeybees. Trends Neurosci 20:245–252.
Honegger KS, Campbell RAA, Turner GC (2011) Cellular-resolution population imaging reveals robust sparse coding in the *Drosophila* mushroom body. J Neurosci 31:11772–11785.
Ichinose T, Aso Y, Yamagata N, Abe A, Rubin GM, Tanimoto H (2015) Reward signal in a recurrent circuit drives appetitive long-term memory formation. Elife 4:e10719.
Irwin S, Banuazizi A, Kalsner S, Curtis A (1968) One trial learning in the mouse. Psychopharmacologia 12:286–302.
Ito K, Suzuki K, Estes P, Ramaswami M, Yamamoto D, Strausfeld NJ (1998) The organization of extrinsic neurons and their implications in the functional roles of the mushroom bodies in *Drosophila melanogaster* Meigen. Learn Mem 5:52–77.
Joerges J, Küttner A, Galizia CG, Menzel R (1997) Representations of odours and odour mixtures visualized in the honeybee brain. Nature 387:285–288.
Kloppenburg P, Nawrot MP (2014) Neural coding: sparse but on time. Curr Biol 24:R957–R959.
Krashes MJ, Waddell S (2008) Rapid consolidation to a radish and protein synthesis-dependent long-term memory after single-session appetitive olfactory conditioning in *Drosophila*. J Neurosci 28:3103–3113.
Kremer MC, Christiansen F, Leiss F, Paehler M, Knapek S, Andlauer TFM, Förstner F, Kloppenburg P, Sigrist SJ, Tavosanis G (2010) Structural long-term changes at mushroom body input synapses. Curr Biol 20:1938–1944.
Krofczik S, Menzel R, Nawrot MP (2009) Rapid odor processing in the honeybee antennal lobe network. Front Comput Neurosci 2:9.
Leiss F, Groh C, Butcher NJ, Meinertzhagen IA, Tavosanis G (2009) Synaptic organization in the adult *Drosophila* mushroom body calyx. J Comp Neurol 517:808–824.
Lin AC, Bygrave A, de Calignon A, Lee T, Miesenböck G (2014) Sparse, decorrelated odor coding in the mushroom body enhances learned odor discrimination. Nat Neurosci 17:559–568.
Liu C, Plaçais PY, Yamagata N, Pfeiffer BD, Aso Y, Friedrich AB, Siwanowicz I, Rubin GM, Preat T, Tanimoto H (2012) A subset of dopamine neurons signals reward for odour memory in *Drosophila*. Nature 488:512–516.
Liu WW, Wilson RI (2013) Glutamate is an inhibitory neurotransmitter in the *Drosophila* olfactory system. Proc Natl Acad Sci USA 110:10294–10299.
Luo R, Uematsu A, Weitemier A, Aquili L, Koivumaa J, McHugh TJ, Johansen JP (2018) A dopaminergic switch for fear to safety transitions. Nat Commun 9:1–11.
Mao Z, Davis RL (2009) Eight different types of dopaminergic neurons innervate the *Drosophila* mushroom body neuropil: anatomical and physiological heterogeneity. Front Neural Circuits 3:5–17.

Mazor O, Laurent G (2005) Transient dynamics versus fixed points in odor representations by locust antennal lobe projection neurons. Neuron 48:661–673.
Menzel R (1999) Memory dynamics in the honeybee. J Comp Physiol A Neuroethol Sens Neural Behav Physiol 185:323–340.
Menzel R, Erber J, Masuhr T (1974) Learning and memory in the honeybee. In: Experimental analysis of insect behaviour (Barton Browne L, Ed), pp 195–217. New York: Springer.
Montague PR, Dayan P, Person C, Sejnowski TJ (1995) Bee foraging in uncertain environments using predictive Hebbian learning. Nature 377:725–728.
Myers KM, Davis M (2002) Behavioral and neural analysis of extinction. Neuron 36:567–584.
Namiki S, Kanzaki R (2008) Reconstructing the population activity of olfactory output neurons that innervate identifiable processing units. Front Neural Circuits 2:1–11.
Olsen SR, Bhandawat V, Wilson RI (2010) Divisive normalization in olfactory population codes. Neuron 66:287–299.
Owald D, Waddell S (2015) Olfactory learning skews mushroom body output pathways to steer behavioral choice in *Drosophila*. Curr Opin Neurobiol 35:178–184.
Owald D, Felsenberg J, Talbot CB, Das G, Perisse E, Huetteroth W, Waddell S (2015) Activity of defined mushroom body output neurons underlies learned olfactory behavior in *Drosophila*. Neuron 86:417–427.
Pamir E, Chakroborty NK, Stollhoff N, Gehring KB, Antemann V, Morgenstern L, Felsenberg J, Eisenhardt D, Menzel R, Nawrot MP (2011) Average group behavior does not represent individual behavior in classical conditioning of the honeybee. Learn Mem 18:733–741.
Pamir E, Szyszka P, Scheiner R, Nawrot MP (2014) Rapid learning dynamics in individual honeybees during classical conditioning. Front Behav Neurosci 8:313.
Pascual A, Préat T (2001) Localization of long-term memory within the *Drosophila* mushroom body. Science 294:1115–1117.
Pavlov IP (1927) Conditioned reflexes: an investigation of the physiological activity of the cerebral cortex. London: Oxford University Press.
Pavlowsky A, Schor J, Plaçais PY, Preat T (2018) A GABAergic feedback shapes dopaminergic input on the *Drosophila* mushroom body to promote appetitive long-term memory. Curr Biol 28:1783–1793.e4.
Peng F, Chittka L (2017) A simple computational model of the bee mushroom body can explain seemingly complex forms of olfactory learning and memory. Curr Biol 27:224–230.
Perisse E, Owald D, Barnstedt O, Talbot CBB, Huetteroth W, Waddell S (2016) Aversive learning and appetitive motivation toggle feed-forward inhibition in the *Drosophila* mushroom body. Neuron 90:1086–1099.
Quinn WG, Harris WA, Benzer S (1974) Conditioned behavior in *Drosophila melanogaster*. Proc Natl Acad Sci USA 71:708–712.
Quirk GJ, Mueller D (2008) Neural mechanisms of extinction learning and retrieval. Neuropsychopharmacology 33:56–72.
Rapp H, Nawrot MP (2020) A spiking neural program for sensorimotor control during foraging in flying insects. Proc Natl Acad Sci USA 117:28412–28421.
Rescorla RA, Wagner AR (1972) A theory of Pavlovian conditioning: variations in the effectiveness of reinforcement and nonreinforcement. In: Classical conditioning II: current research and theory (Black A and Prokasy WF, eds), pp 64–99. New York: Appleton-Century-Crofts.
Riemensperger T, Völler T, Stock P, Buchner E, Fiala A (2005) Punishment prediction by dopaminergic neurons in *Drosophila*. Curr Biol 15:1953–1960.
Salinas-Hernández XI, Vogel P, Betz S, Kalisch R, Sigurdsson T, Duvarci S (2018) Dopamine neurons drive fear extinction learning by signaling the omission of expected aversive outcomes. Elife 7:e38818.
Sandoz JC, Roger B, Pham-Delègue MH (1995) Olfactory learning and memory in the honeybee: comparison of different classical conditioning procedures of the proboscis extension response. C R Acad Sci III 318:749–755.
Sayin S, Boehm AC, Kobler JM, de Backer JF, Grunwald Kadow IC (2018) Internal state dependent odor processing and perception—The role of neuromodulation in the fly olfactory system. Front Cell Neurosci 12:11–17.
Scheunemann L, Skroblin P, Hundsrucker C, Klussmann E, Efetova M, Schwärzel M (2013) AKAPS act in a two-step mechanism of memory acquisition. J Neurosci 33:17422–17428.
Schmuker M, Pfeil T, Nawrot MP (2014) A neuromorphic network for generic multivariate data classification. Proc Natl Acad Sci USA 111:2081–2086.
Schultz W (2016) Dopamine reward prediction error coding. Dialogues Clin Neurosci 1:23–32.
Schultz W, Dayan P, Montague PR (1997) A neural substrate of prediction and reward. Science 275:1593–1599.
Schwaerzel M, Heisenberg M, Zars T (2002) Extinction antagonizes olfactory memory at the subcellular level. Neuron 35:951–960.
Séjourné J, Plaçais P-Y, Aso Y, Siwanowicz I, Trannoy S, Thoma V, Tedjakumala SR, Rubin GM, Tchénio P, Ito K, Isabel G, Tanimoto H, Preat T (2011) Mushroom body efferent neurons responsible for aversive olfactory memory retrieval in *Drosophila*. Nat Neurosci 14:903–910.
Shuai Y, Hirokawa A, Ai Y, Zhang M, Li W, Zhong Y (2015) Dissecting neural pathways for forgetting in *Drosophila* olfactory aversive memory. Proc Natl Acad Sci U S A 112:E6663–E6672.
Smith BH (1991) The olfactory memory of the honeybee *Apis mellifera*: I. Odorant modulation of short- and intermediate-term memory after single-trial conditioning. J Exp Biol 161:367–382.
Smith D, Wessnitzer J, Webb B (2008) A model of associative learning in the mushroom body. Biol Cybern 99:89–103.
Takemura SY, Aso Y, Hige T, Wong A, Lu Z, Xu CS, Rivlin PK, Hess H, Zhao T, Parag T, Berg S, Huang G, Katz W, Olbris DJ, Plaza S, Umayam L, Aniceto R, Chang LA, Lauchie S, Ogundeyi O, et al. (2017) A connectome of a learning and memory center in the adult *Drosophila* brain. Elife 6:e26975.
Tanaka NK, Tanimoto H, Ito K (2008) Neuronal assemblies of the *Drosophila* mushroom body. J Comp Neurol 508:711–755.
Tempel BL, Bonini N, Dawson DR, Quinn WG (1983) Reward learning in normal and mutant *Drosophila*. Proc Natl Acad Sci USA 80:1482–1486.
Terao K, Mizunami M (2017) Roles of dopamine neurons in mediating the prediction error in aversive learning in insects. Sci Rep 7:1–9.
Trannoy S, Redt-Clouet C, Dura JM, Preat T (2011) Parallel processing of appetitive short- and long-term memories in *Drosophila*. Curr Biol 21:1647–1653.
Tully T, Quinn WG (1985) Classical conditioning and retention in normal and mutant *Drosophila melanogaster*. J Comp Physiol A Neuroethol Sens Neural Behav Physiol 157:263–277.
Turner GC, Bazhenov M, Laurent G (2008) Olfactory representations by *Drosophila* mushroom body neurons. J Neurophysiol 99:734–746.
Ueoka Y, Hiroi M, Abe T, Tabata T (2017) Suppression of a single pair of mushroom body output neurons in *Drosophila* triggers aversive associations. FEBS Open Bio 7:562–576.
Villar ME, Marchal P, Viola H, Giurfa M (2020) Redefining single-trial memories in the honeybee. Cell Rep 30:2603–2613.e3.
Waddell S (2013) Reinforcement signalling in *Drosophila*; dopamine does it all after all. Curr Opin Neurobiol 23:324–329.
Walsh KH, Das RK, Saladin ME, Kamboj SK (2018) Modulation of naturalistic maladaptive memories using behavioural and pharmacological reconsolidation-interfering strategies: a systematic review and meta-analysis of clinical and 'sub-clinical' studies. Psychopharmacology 235:2507–2527.
Weiglein A, Gerstner F, Mancini N, Schleyer M, Gerber B (2019) One-trial learning in larval *Drosophila*. Learn Mem 26:109–120.
Wessnitzer J, Young JM, Armstrong JD, Webb B (2012) A model of non-elemental olfactory learning in *Drosophila*. J Comput Neurosci 32:197–212.

Wilson RI (2013) Early olfactory processing in *Drosophila*: mechanisms and principles. Annu Rev Neurosci 36:217–241.

Wilson RI, Turner GC, Laurent G (2004) Transformation of olfactory representations in the *Drosophila* antennal lobe. Science 303:366–370.

Yamagata N, Ichinose T, Aso Y, Plaçais PY, Friedrich AB, Sima RJ, Preat T, Rubin GM, Tanimoto H (2015) Distinct dopamine neurons mediate reward signals for short- and long-term memories. Proc Natl Acad Sci USA 112:578–583.

Yamazaki D, Hiroi M, Abe T, Shimizu K, Minami-Ohtsubo M, Maeyama Y, Horiuchi J, Tabata T (2018) Two parallel pathways assign opposing odor valences during *Drosophila* memory formation. Cell Rep 22:2346–2358.

Zars T, Fischer M, Schulz R, Heisenberg M (2000) Localization of a short-term memory in *Drosophila*. Science 288:672–675.

Zhang X, Noyes NC, Zeng J, Li Y, Davis RL (2019) Aversive training induces both presynaptic and postsynaptic suppression in *Drosophila*. J Neurosci 39:9164–9172.

Zhao B, Sun J, Zhang X, Mo H, Niu Y, Li Q, Wang L, Zhong Y (2019) Long-term memory is formed immediately without the need for protein synthesis-dependent consolidation in *Drosophila*. Nat Commun 10:4550.

Zhao C, Widmer YF, Diegelmann S, Petrovici M, Sprecher SG, Senn W (2021) Predictive olfactory learning in *Drosophila*. Sci Rep 11:6795.

2.1.2 Functional Dissection of a Neuronal Brain Circuit Mediating Higher-Order Associative Learning

Authors: El Yazid Rachad, Stephan H. Deimel, Lisa Epple, Yogesh V. Gadgil, Anna-Maria Jürgensen, **Magdalena Springer**, Chen-Han Lin, Martin P. Nawrot, Suewei Lin, and Andre Fiala

Journal: ***Cell Reports*** **(2025)**

DOI: 10.1016/j.celrep.2025.115593

Contribution: The conceptualization of the modeling was conducted by MPN, AMJ, and MS. All computational modeling and parts of the connectome analysis, along with the associated visualization and writing, were equally contributed by AMJ and MS.

Supplemental Information: Extended data and supplementary material for this study are available online at: https://doi.org/10.1016/j.celrep.2025.115593

Cell Reports

Article

Functional dissection of a neuronal brain circuit mediating higher-order associative learning

Graphical abstract

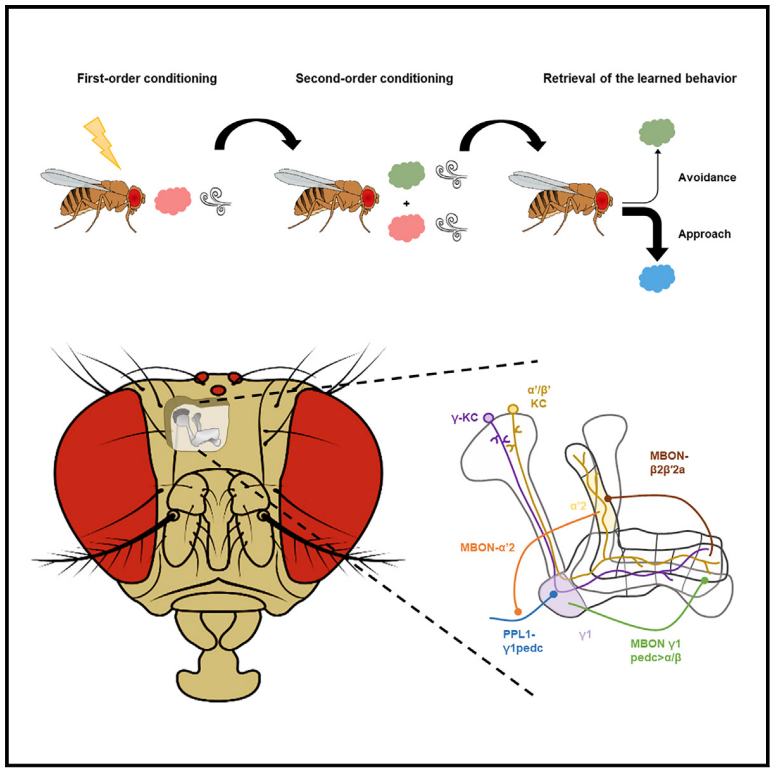

Highlights

- Neuronal circuits for aversive second-order conditioning are identified in *Drosophila*
- Flies can form associative chains through olfactory third-order conditioning
- Mushroom body circuits show recurrent feedback loops for higher-order conditioning
- Olfactory conditioning allows odors to control the dopaminergic valence-signaling system

Authors

El Yazid Rachad, Stephan Hubertus Deimel, Lisa Epple, ..., Martin Paul Nawrot, Suewei Lin, André Fiala

Correspondence

afiala@gwdg.de

In brief

Rachad et al.'s study elucidates how neuronal circuits enable the formation of associative chains through learning. They identify neuronal brain circuits and plasticity mechanisms that underlie aversive higher-order conditioning in the model organism *Drosophila melanogaster*. This work advances our understanding of processes underlying the acquisition of complex stimulus relationships.

Rachad et al., 2025, Cell Reports *44*, 115593
May 27, 2025 © 2025 The Author(s). Published by Elsevier Inc.
https://doi.org/10.1016/j.celrep.2025.115593

CellPress

Cell Reports

CellPress
OPEN ACCESS

Article

Functional dissection of a neuronal brain circuit mediating higher-order associative learning

El Yazid Rachad,[1] Stephan Hubertus Deimel,[1] Lisa Epple,[1] Yogesh Vasant Gadgil,[1] Anna-Maria Jürgensen,[2] Magdalena Springer,[2] Chen-Han Lin,[3] Martin Paul Nawrot,[2] Suewei Lin,[3] and André Fiala[1,4,*]
[1]Molecular Neurobiology of Behavior, University of Göttingen, 37077 Göttingen, Germany
[2]Computational Systems Neuroscience, University of Cologne, 50674 Cologne, Germany
[3]Institute of Molecular Biology, Academia Sinica, Taipei 115, Taiwan
[4]Lead contact
*Correspondence: afiala@gwdg.de
https://doi.org/10.1016/j.celrep.2025.115593

SUMMARY

A central feature characterizing the neural architecture of many species' brains is their capacity to form associative chains through learning. In elementary forms of associative learning, stimuli coinciding with reward or punishment become attractive or repulsive. Notably, stimuli previously learned as attractive or repulsive can themselves serve as reinforcers, establishing a cascading effect whereby they become associated with additional stimuli. When this iterative process is perpetuated, it results in higher-order associations. Here, we use odor conditioning in *Drosophila* and computational modeling to dissect the architecture of neuronal networks underlying higher-order associative learning. We show that the responsible circuit, situated in the mushroom bodies of the brain, is characterized by parallel processing of odor information and by recurrent excitatory and inhibitory feedback loops that empower odors to gain control over the dopaminergic valence-signaling system. Our findings establish a paradigmatic framework of a neuronal circuit diagram enabling the acquisition of associative chains.

INTRODUCTION

Detecting and learning associations between events in the world is a fundamental aspect of the cognitive abilities across species. At its most basic level, a stimulus that consistently coincides with a positive or negative outcome becomes ingrained as pleasant or unpleasant. Perhaps the most iconic illustration of this principle is found in Pavlov's dogs, who learned to salivate in response to a conditioned tone predicting a savory reward.[1] However, the learning of associations in the real world seldom follows a straightforward pattern of encountering direct rewards or punishments. Instead, intricate sequences and chains of multiple associations unfold, allowing for the acquisition of knowledge without the necessity of an immediate reward or punishment. Pavlov observed that his dogs could extend their associations by linking the conditioned tone with a black square—a phenomenon he termed second-order conditioning.[1] Consequently, a learned stimulus, having gained significance, can be linked to a second-order stimulus, and this second-order stimulus can, in turn, be associated with a third-order stimulus, creating a cascading chain. In essence, higher-order conditioning involves the development of chain-like, multi-step, sequential learning of causal relationships between stimuli and events, allowing for the generation of novel inferences. A crucial distinction lies in the fact that higher-order conditioning differs from first-order classical conditioning in that the reinforcing "teaching" signal does not inherently carry a positive or negative valence. Instead, it acquires its reinforcing valence through prior experiences. This dynamic process represents a fundamental aspect of the ongoing cognitive activities of brains across species.

The power of analyzing higher-order associations by employing a second-order learning regime lies in the ability to conduct controlled laboratory experiments. This approach allows for a precise determination of the associations formed and the timing of these associations. Additionally, the principles governing higher-order conditioning can be extrapolated across diverse animal species, given that it is a widespread phenomenon observed throughout the animal kingdom. Second-order conditioning has been documented not only in humans,[2,3] non-human primates,[4,5] and rodents,[6,7] but also in seemingly less complex organisms such as mollusks,[8,9] honeybees,[10,11] and fruit flies.[12–14]

Despite the fundamental nature of this brain function, the underpinning neuronal circuits and their modes of operation are not fully understood. Although brain regions implicated in higher-order learning have been identified in various species and behavioral contexts,[15] such as the basolateral amygdala or the hippocampus in rats,[7,16] detailed circuit diagrams explaining the synaptic changes underlying memory traces are lacking. In recent years, significant strides have been made in developing

This is an open access article under the CC BY license (http://creativecommons.org/licenses/by/4.0/).

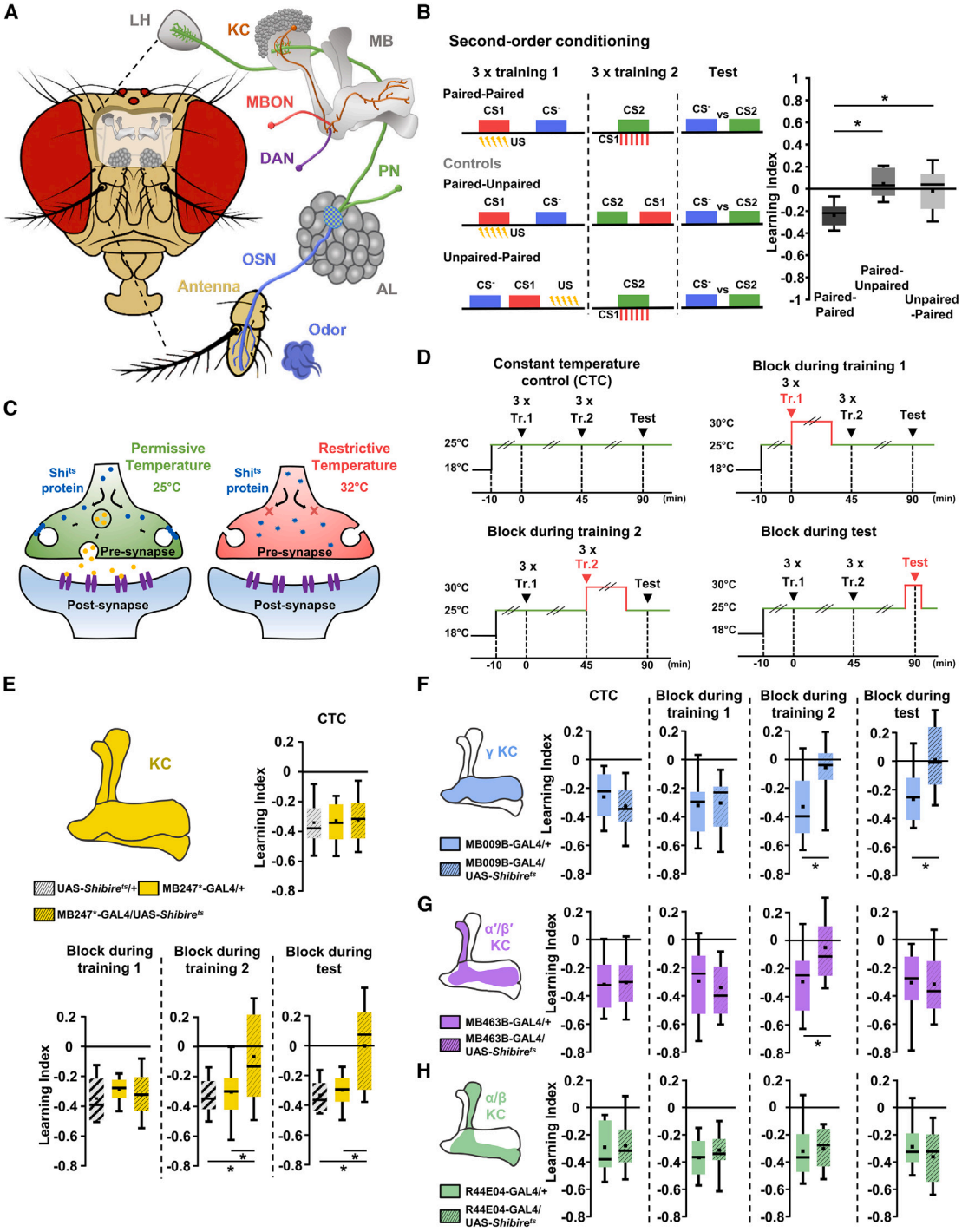

Figure 1. Synaptic transmission from distinct Kenyon cells is required for second-order conditioning

(A) The olfactory pathway of *Drosophila melanogaster*. AL, antennal lobe; DAN, dopaminergic neuron; KC, Kenyon cell; LH, lateral horn; MB, mushroom body; MBON, mushroom body output neuron; OSN, olfactory sensory neuron; PN, projection neuron.

(B) Left: second-order conditioning paradigm and controls. Colored rectangles represent conditioned odor stimuli (CS), flash symbols electric shocks (unconditioned stimuli [US]), and dashed red lines CS1 pulses as reinforcement in the second training phase. Right: learning indices. All groups, $n = 24$.

(C) Schematic illustration of thermo-genetic block of neurotransmission using *shibire*^{ts}.

(D) Thermo-genetic manipulation during the different training and test phases.

(legend continued on next page)

methods to express transgenes designed for the functional analysis of neuronal circuits, particularly in transgenic organisms such as mice, zebrafish, or *C. elegans*.[17] *Drosophila melanogaster*, with its extensive genetic toolkit,[18] is exceptionally suitable for dissecting the neuronal circuits involved in learning and memory formation. With approximately 100,000 neurons, its brain is numerically simpler than that of vertebrates, yet it exhibits a remarkably rich behavioral repertoire for functional comparisons with mammals. *Drosophila*'s intricate learning behavior, including higher-order conditioning, has been explored using various approaches and behavioral paradigms. A study employing olfactory reward learning has identified dopaminergic neurons (DANs) and mushroom body-associated neuronal circuits involved in appetitive second-order conditioning.[14] Previous investigations have observed aversive second-order learning using a flight simulator with visual stimuli as conditioned stimuli[12] and in a T-maze situation utilizing olfactory stimuli,[13] although the underlying neuronal substrates were not identified. The latter paradigm involving a T-maze and olfactory stimuli served as the foundation for our work. We selected this learning paradigm due to the well-characterized neuronal architecture that underlies simple aversive olfactory first-order conditioning.[19–21]

The most simplistic form of Pavlovian learning relies on the detection of odor stimuli that flies perceive by olfactory sensory neurons located on the third antennal segments and maxillary palps. These neurons target the glomeruli of the antennal lobes,[22] considered the structural and functional analog of the olfactory bulb of mammals.[23] Olfactory projection neurons, akin to the mitral/tufted cells of vertebrates, then convey the odor information to higher brain centers, specifically the lateral horn and the calyx of the mushroom body in insects.[24,25] Within the mushroom body, olfactory projection neurons synapse onto intrinsic mushroom body neurons known as Kenyon cells. These cells encode odor identity through sparsely distributed activity,[26–28] mirroring the situation in the anterior piriform cortex of mammals.[29] The axons of Kenyon cells collectively form the mushroom body lobes, with α/β and α'/β' Kenyon cell axons bifurcating to create the α-, β-, α'-, and β'-lobes. In contrast, the axons of γ Kenyon cells of adult flies do not bifurcate, constituting the γ-lobes. The convergence of odor signals and punishment signals occurs specifically in the axons of Kenyon cells, where the reinforcing valence is established[20,30] (Figure 1A). DANs mediate the reinforcing valence,[31] akin to midbrain DANs in vertebrates.[32] Those DANs signaling punishment originate from the protocerebral posterior lateral 1 (PPL1) cluster, innervating spatially restricted areas, termed lobe compartments, within the mushroom body lobes.[31,33,34] During classical conditioning, the coincident activation of Kenyon cells by odor stimulation and punishment-induced dopamine release leads to presynaptic depression of synaptic transmission between Kenyon cells and mushroom body output neurons (MBONs).[35,36] Ultimately, these changes instruct the animal's approach or avoidance behavior.[37] While substantial evidence supports this concept, the mechanism through which higher-order associative chains are formed remains less well understood. A hint comes from studies showing that if an odor stimulus is presented together with the artificial suppression of one inhibitory MBON (MBON-γ1pedc>α/β), that projects to a punishment-mediating DAN (PPL1-γ1pedc), induces aversive learning of that odor.[38,39] This has led to the hypothesis of a simple disinhibition mechanism that might mediate second-order conditioning,[39] which has not been experimentally validated as yet. Three critical areas of unknown persist: first, it is unclear whether reinforcing DANs that inherently respond to punishments really mediate the valence of learned secondary reinforcers. Second, the precise location of odor representations within lobe compartments that become subject to modification during higher-order learning remains uncertain. Third, the synaptic changes constituting the learned behavioral modification, essentially the engram in a strict sense, have yet to be identified. This report addresses these points and characterize the neuronal circuit responsible for the formation of associative chains as a paradigmatic case.

RESULTS

Aversive second-order conditioning requires mushroom body Kenyon cells of the γ-lobes and the α'/β'-lobes

To validate the capability of *Drosophila* for higher-order associative odor learning, as previously demonstrated,[13] we devised a computer-controlled training apparatus (Figures S1A and S1B) to expose wild-type flies to an aversive second-order conditioning regimen (Figure 1B). In the initial training phase, an odor (conditioned stimulus 1 [CS1]) was temporally paired with a series of pulsed, punishing electric shocks (unconditioned stimulus [US]). A different odor (CS–) was presented without electric shocks. In a second training phase, a novel odor (CS2) was then temporally paired with pulsed presentations of the previously conditioned odor CS1. In a subsequent T-maze test, flies exhibited significant avoidance of CS2 compared with CS− (Figure 1B). Control experiments, in which either the temporal coincidence of CS+ and US was disrupted in the first, but not second, training phase ("Unpaired-Paired"), or in which the two odors in the second training phase were presented with a temporal gap ("Paired-Unpaired"), yielded no learning (Figure 1B). These standard control experiments[40] demonstrated that the temporal coincidence of trained stimuli in the two training phases caused the learned avoidance.[13] Additionally, these experiments ascertained that the learned avoidance was not predicated on the potential attractiveness of the CS− acquired during the first training phase—an occurrence known as conditioned inhibition, which can manifest in flies.[41] Three different chemical compounds (3-octanol, 4-methylcyclohexanol, and benzaldehyde) were used as odorants, and their concentrations were carefully

(E) Learning indices resulting from second-order conditioning when synaptic output from all Kenyon cells (KCs) was blocked during different training or test phases. All groups, $n = 16$.

(F–H) Learning indices resulting from second-order conditioning when synaptic output from γ-lobe KCs (F), α'/β'-lobe KCs (G), or α/β-lobe KCs (H) was blocked during different training or test phases. All groups, $n = 16$. $^*p < 0.05$. Boxplots show interquartile ranges, means (squares), medians (lines), and 10/90 percentiles (whiskers). Statistical tests: Table S1.

chosen such that their innate repulsive valences were balanced (Figure S1C). All three odorants were used as CS1, CS2, or CS–, and the flies exhibited second-order conditioning in all odorant combinations, independent of their chemical identity (Figure S1E). Since the chemical identity of odorants did not influence second-order conditioning, we followed the protocol established by Tabone et al.[13] and used 3-octanol and 4-methylcyclohexanol as CS1 and CS− in a balanced manner, with benzaldehyde as CS2. Second-order conditioning resulted in a weaker learning index compared with first-order conditioning (Figure S1D). Since it is well described that additional CS-US trials in regular first-order conditioning, as it is part of our learning paradigm with three CS-US trials, lead even to a gradual increase in memory retrieval shortly after training,[42] we conclude that second-order conditioning is less efficient at inducing short-term memory. However, we must take into account that the longer training phase in the learning paradigm according to Tabone et al.[13] with three CS-US trials and 10 min gaps in between cannot be regarded as short-term memory by definition. It is well-established that, in *Drosophila*, olfactory memories generally weaken over time from training.[43] Given the longer-lasting training procedure in second-order conditioning (42.75 min for the first-order training phase and 40.1 min for the second-order training phase) compared with the more commonly used first-order conditioning regime, followed by a short-term memory test lasting only several minutes,[44] we explored whether the lower learning indices might be also affected by the extended training. Indeed, when a standard first-order conditioning procedure was conducted, but the second training phase was replaced by a temporal gap, the first-order memory score significantly diminished compared with a memory test conducted 3 min after training. The score remained slightly, but not significantly, higher than that from second-order conditioning (Figure S1D). Thus, the lower learning index in second-order conditioning is due to both lower training efficiency and the extended training duration.

Having successfully replicated aversive olfactory second-order conditioning, we aimed to identify the neuronal circuits underlying this learning. While the mushroom body circuitry was a plausible candidate, formal confirmation was needed. To investigate, we ectopically expressed the dominant-negative, temperature-sensitive dynamin mutant shibire^{ts} in Kenyon cells, a widely used method for reversibly blocking synaptic transmission at restrictive temperatures.[45–47] This allowed selective inhibition during specific training or testing phases (Figures 1C and 1D). Initially, we blocked synaptic output in all Kenyon cells using a novel MB247-Gal4 driver (Figures S1F and S1G). Blocking during the first training phase had no effect on memory scores, but blocking during the test phase abolished learned avoidance (Figure 1E), confirming that Kenyon cell output is required for memory retrieval but not acquisition.[48–50] Interestingly, blocking synaptic output from Kenyon cells during the second training phase disrupted learning and memory formation (Figure 1E). This suggests that synaptic output from Kenyon cells is crucial for initiating higher-order learning, either in brain regions downstream of the mushroom body or within the mushroom body circuit through feedback loops. To pinpoint the required output, we selectively blocked synaptic transmission in α/β-lobe, α′/β′-lobe, or γ-lobe Kenyon cells using specific Gal4-driver lines (Figures S1F and S1G). Blocking γ-lobe output mirrored the effect of blocking all Kenyon cells (Figures 1E and 1F), indicating its necessity during the second training phase and memory retrieval—consistent with first-order odor-shock learning and short-term memory localization in γ-lobes,[51,52] particularly γ1.[36] Surprisingly, α′/β′-lobe Kenyon cell output was required only during the second training phase when CS1 and CS2 were paired, not during retrieval (Figure 1G). In contrast, α/β-lobe Kenyon cell output was completely dispensable at all stages (Figure 1H).

Specific MBONs required for aversive second-order conditioning

Having identified the necessity of two mushroom body output pathways for enabling second-order conditioning, we further investigated the specific MBONs mediating this process. Employing highly specific split-Gal4 lines[34,53] (Figures S2A and S2B), we selectively expressed shibire^{ts} in each MBON type, targeting specific compartments of the γ-lobes (Figure S2A) or α′/β′-lobes (Figure S2B). In the case of the γ-lobes, we found that synaptic transmission from a specific MBON, MBON-γ1pedc>α/β (also known as MBON11 or MB-MVP2), receiving input from γ-lobe Kenyon cells, was required during the second-order training phase and the memory retrieval test (Figure 2A). Interestingly, synaptic output from all other MBONs receiving input in the γ2 to γ5 compartments was dispensable for this specific task (Figures S4A–S4D). In the context of the α′/β′-lobes, synaptic output from MBON-α′2 (also known as MBON13 or MB-V4), which targets the α′2 compartment (Figure 2B), was found to be the only MBON required for second-order conditioning, specifically during the second training phase when the already-conditioned odor CS1 was paired with the novel odor CS2 (Figures 2B and S4E–S4H). We conducted additional tests to determine whether the requirement for MBON-α′2 was specifically tied to second-order associative learning or potentially associated with the maintenance of information during the protracted training procedure. Given that the second-order training protocol involves repeated CS1-US associations and CS2-CS1 associations before memory recall testing, we explored whether the role of MBON-α′2 extended beyond short-term memory mechanisms. We selectively blocked the output of MBON-α′2 during a regular first-order odor-shock learning and subsequent short-term memory test 3 min after training (Figure S2D). Our results indicated that synaptic transmission from MBON-α′2 was not required for short-term memory recall in this context (Figures S2E and S2F). As previously reported,[36] synaptic transmission from MBON-γ1pedc>α/β and MBONs γ5β′2α/β′2mp is required for short-term memory recall (Figures S2E and S2F), the latter presumably through disinhibition by MBON-γ1pedc>α/β.[36] Comparatively, when a first-order conditioning protocol mimicking the structure of second-order training (i.e., repeating CS-US associations in three blocks) was used (Figure S2C), with an introduced temporal gap equivalent to the second-order training phase, MBON-γ1pedc>α/β was required for memory recall, but the output of MBON-α′2 remained unnecessary (Figures S2E and S2F). In conclusion, the evidence thus far does not support the notion that the

CellPress
OPEN ACCESS

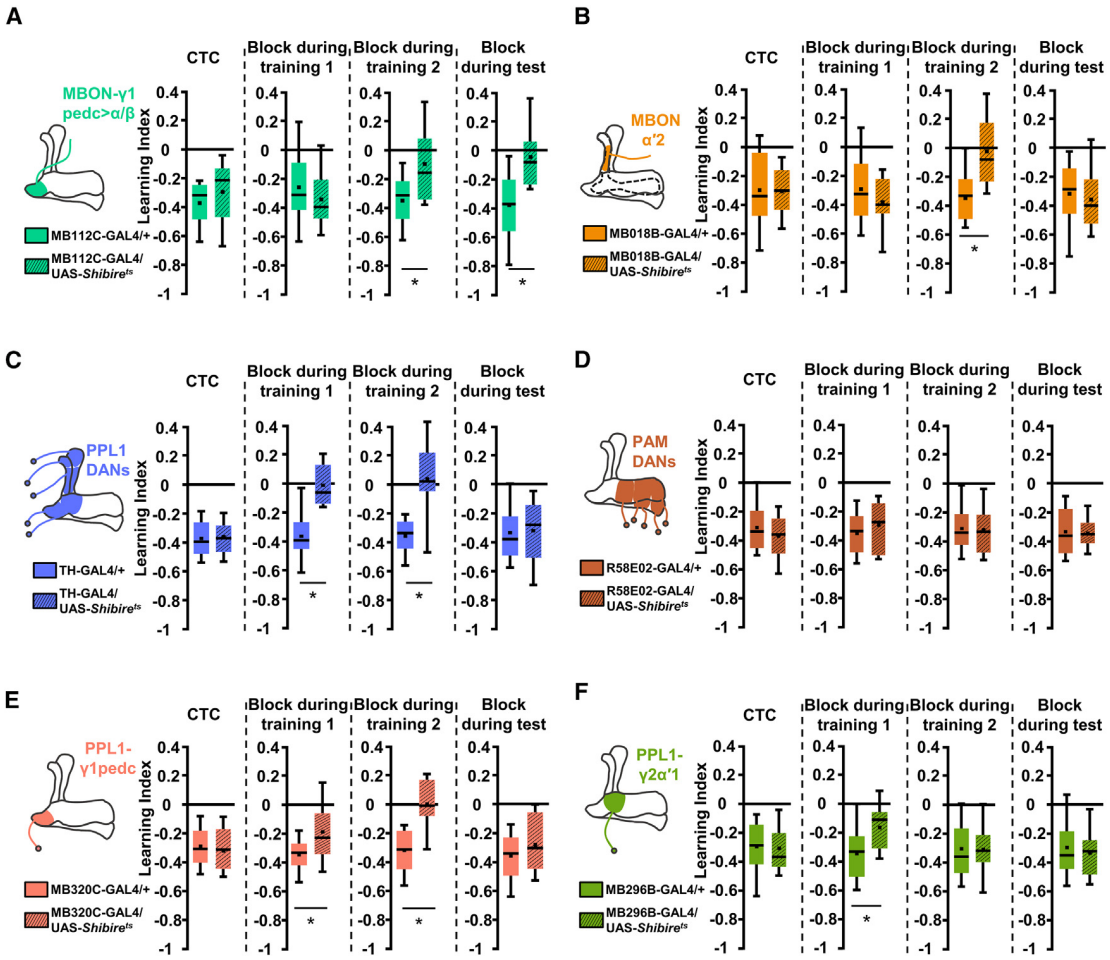

Figure 2. Synaptic transmission from distinct mushroom body output neurons and dopaminergic neurons is required for second-order conditioning

(A–F) Learning indices resulting from second-order conditioning when synaptic output from individual output from MBON-γ1pedc>α/β (A), MBON-α′2 (B), punishment-mediating PPL1-cluster DANs (C), reward-mediating PAM cluster DANs (D), PPL1-γ1pedc DANs (E), and PPL1-γ2α′1 DANs (F) was blocked. All groups, $n = 16$. $^*p < 0.05$. Boxplots show interquartile ranges, means (squares), medians (lines), and 10/90 percentiles (whiskers). Statistical tests: Table S1.

requirement of MBON-α′2 for second-order conditioning is linked to a potential role in memory consolidation.

Distinct DANs mediate punishment signals and synaptic plasticity in second-order conditioning

Associative learning involves at least three types of signals or neuronal representations. The first signal encodes the conditioned odor stimuli, which is accomplished in *Drosophila* by the array of Kenyon cells. The learned, conditioned response is signaled through neurons instructing behavior-modulating circuits, which is achieved in *Drosophila* through distinct MBONs.[37] The third signal conveys the reinforcing valence, which in this case is a punishment; in *Drosophila*, electric shock punishment during aversive conditioning is mediated by dopaminergic neurons (DANs).[31] To discern which DANs mediate the reinforcing information in second-order conditioning, two Gal4-driver lines targeting the two main populations of DANs, the PPL1 and the PAM cluster of neurons,[54] were employed. When synaptic output was blocked through the expression of shibire^{ts}, only DANs of the PPL1 cluster were found to be required for inducing learning during both the first and second conditioning phases, but not during memory retrieval in the test phase (Figure 2C). The synaptic output from DANs of the PAM cluster was dispensable for any phase of aversive second-order conditioning (Figure 2D). To further refine which exact PPL1 cluster DANs were necessary for second-order conditioning, specific split-Gal4 driver lines were utilized[34] (Figure S3A). During the first conditioning phase, in which the CS1 odor was associated with the electric shock, dopamine release from neurons innervating the γ1 compartment (PPL1-γ1pedc DAN, also termed PPL101 or MB-MP1) and DANs innervating the γ2 compartment that also innervate the α′1 compartment (PPL1-γ2α′1 DAN, PPL103 or MB-MV1) were found to be necessary. Blocking their output resulted in a significant, but not complete,

reduction in second-order learning (Figures 2E and 2F). Importantly, in the second training phase, where CS1 and CS2 were associated, only PPL1-γ1pedc DANs were required (Figure 2E). Synaptic output from all other DANs was dispensable (Figures 2F, S4I, and S4J). The identities of the DANs that mediate the reinforcing properties of the punishment were equivalent for the odor-shock association in regular first-order conditioning and in the first training phase of the second-order conditioning protocol. In both cases, PPL1-γ1pedc and PPL1-γ2α′1 DANs were required (Figures 2E, 2F, and S3B–S3E). This is independent of the duration of the training protocol, although the contribution of PPL1-γ2α′1 DAN was smaller in the longer-lasting learning and memory protocol (Figures S3B–S3E).

The investigation brought to light a perplexing scenario wherein the mushroom body inputs and outputs crucial for second-order conditioning exhibited compartment-specific disparities. In the case of the γ1 compartment, the requirement for both dopaminergic input and the output through its associated MBON was logically consistent, involving valence-signaling dopamine release during the two training phases and the behavior-instructive MBON during memory retrieval. However, for the γ2 compartment, although dopaminergic input was necessary only during the first conditioning phase, its corresponding MBON-γ2α′1 (MBON12) was seemingly dispensable. Similarly, for the α′2 compartment, the relevant MBON was essential only during the second conditioning phase, whereas its corresponding dopaminergic input neuron was not required. To unravel this enigma, an initial step involved confirming which DANs could effectively signal electric shock information. Employing *in vivo* two-photon imaging with the combination of a pre-synaptically localized green fluorescent calcium (Ca^{2+}) sensor (Synaptophysin-GCaMP) and a red fluorescent pH-sensitive sensor to monitor synaptic exocytosis (Synaptophysin-pHTomato),[55] our experiments demonstrated that both PPL1-γ1pedc and PPL1-γ2α′1 DANs exhibited robust responses to electric shock pulses (Figures 3A and 3B). By contrast, DANs innervating the α′2 compartment (PPL1-α′2α2 DAN, PPL105, or MB-V1) did not show any response to the electric shocks, similar to the PAM cluster DAN that innervates the γ5 compartment (PAM-γ5 DAN, PAM01, or MB-M1) (Figures 3A and 3B), which served as a negative control due to its role in mediating reward signals.[56] Because MBON-α′2 is required for the second training phase, during which the novel odor CS2 is associated with the previously trained odor CS1, we concluded that this compartment should encode and store information about the "punished" odor CS1 to be able to further transmit information about it. Conclusively, it should receive a thus far unknown input teaching signal of the punishment. To clarify whether such a functional connection exists, we asked whether the two types of DANs that respond to electric shocks (Figures 3A and 3B) and that are required for second-order conditioning (Figures 2E and 2F), might contact the α′2 compartment as well. Indeed, split-GFP-reconstitution across synaptic partners (GRASP)[57] revealed that the PPL1-γ2α′1 DAN also innervates a small fraction of the α′2 compartment (Figure 3C). The PPL1-γ1pedc or the PAM-γ5 DANs used as a negative control did not deviate in their innervation from their concomitant compartment that they were assigned to (Figure 3C). We quantified the volume of the GRASP fluorescence between the PPL1-γ2α′1 DAN and the Kenyon cells, and compared it with the volume occupied by the fluorescence of presynaptically localized Synaptotagmin-GFP[58] expressed in PPL1-γ2α′1 DAN (Figures S5D and S5E). This comparison, which showed equivalent volumes occupied by the fluorescent markers, ruled out that the covalent bonds formed by the complementary splitGFP molecules affect and alter the innervation of DANs onto Kenyon cells. The mushroom body compartments were identified using anti-Bruchpilot immunostaining (Video S1). To further confirm the finding, we made use of the electron microscopy-based connectome[59] and its web-based user interface NeuPrint to reconstruct the morphology of the PPL1-γ2α′1 DAN (Figure 3D). This neuron innervates the mushroom body lobes very densely in the adjacent γ2 and α′1 compartments (Figure 3Di). However, if one compares the exact areas of innervation with the dendritic tree of the reconstructed MBON-α′2, one can identify a small region of overlap at the posterior end of the α′2 lobe (Figure 3Dii). A quantification of identified synaptic connections corroborates this finding; the Kenyon cells' synapses within the α′2 compartment predominantly target MBON-α′2. But, in addition, reciprocal synaptic connections exist between these Kenyon cells and DANs,[60] including the PPL1-γ2α′1 DAN. Very few reciprocal synaptic connections were also identified between PPL1-γ2α′1 DAN and MBON-α′2 (Figure 3Diii).

The connectome database confirmed synaptic connectivity between the PPL1-γ2α′1 DAN and the α′2 compartment, primarily at Kenyon cells and, to a lesser extent, MBONs. The number of direct synapses in the α′2 compartment is small, but synapse count alone does not determine functional relevance. If all existing synapses are functionally significant, then the γ1 compartment receives punishment information via PPL1-γ1pedc DAN, while the α′2 compartment does so via PPL1-γ2α′1 DAN. Dopamine can influence synaptic transmission beyond the synaptic cleft through volume transmission.[61] We analyzed the spatial organization of dopaminergic inputs relative to KC-MBON synapses in the α′2 compartment, assessing synaptic release sites of PPL1-γ2α′1 and PPL1-α′2α2 DANs (Figure S7A). Almost all (96.7%) KC-MBON synapses in α′2 lie within 2 μm of PPL1-α′2α2 release sites, while only 2.25% are within 2 μm of PPL1-γ2α′1 sites. To reach 90% of KC-MBON synapses, dopamine from PPL1-γ2α′1 would need to diffuse 24.7 μm, compared with just 1.71 μm for PPL1-α′2α2. Despite the limited direct connectivity of PPL1-γ2α′1 DAN, we conclude that it achieves functional significance due to its responsiveness to electric shocks, unlike PPL1-α′2α2. A spatial randomization analysis (10 million iterations) confirmed a non-random organization of DAN synapses ($p < 0.001$), as the observed PPL1-γ2α′1 connectivity was significantly different from random expectation ($p < 0.001$; Monte Carlo permutation test). PPL1-γ2α′1 synapses were within 2 μm of 2.25% of MBON-KC synapses (vs. 1.17% expected by chance), while PPL1-α′2α2 synapses were within 2 μm of 96.7% (vs. 61.55% expected) (Figure S7B). Interestingly, although PPL1-α′2α2 exhibits higher anatomical connectivity, it does not modulate the α′2 compartment in response to electric shocks. In contrast, PPL1-γ2α′1 demonstrates robust physiological responses to electric shocks. Other potential pathways

CellPress
OPEN ACCESS

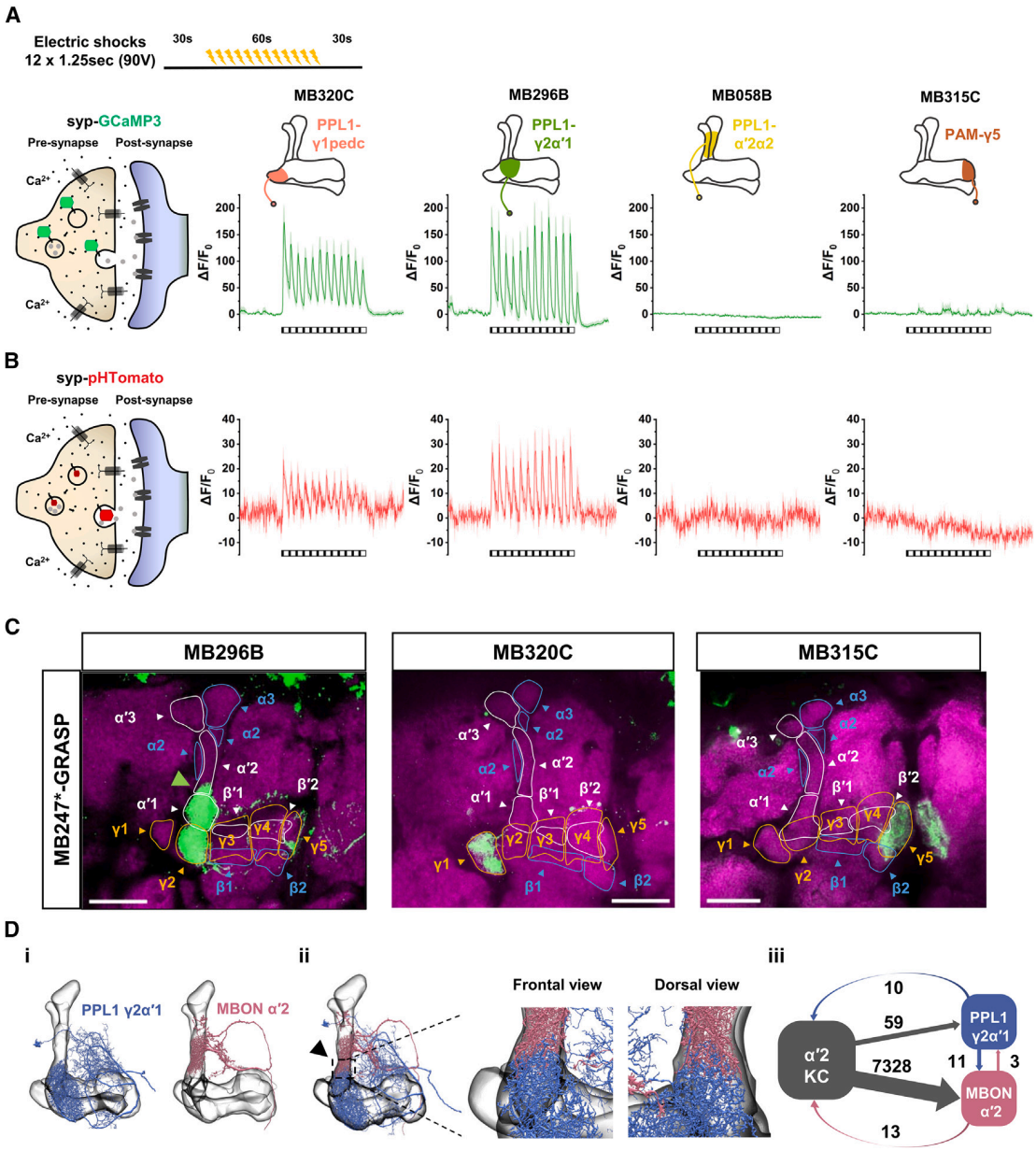

Figure 3. Collateral arborizations from γ2-α′1 dopaminergic neurons innervate the α′2 compartment of the mushroom body to convey electric shock signals

(A) Top: optical imaging protocol. Flies were subjected to pulses of electric shocks. Bottom: illustration of the pre-synaptic Ca^{2+} sensor syp-GCaMP3 and electric shock-induced fluorescence changes in individual PPL1- and PAM-cluster DANs (mean ± SEM). Electric pulses are indicated by horizontal rectangle with black lines.

(B) Illustration of the pre-synaptic vesicle release sensor syp-pHTomato and electric shock-induced fluorescence changes in individual PPL1- and PAM-cluster DANs (mean ± SEM). All groups, $n = 8$.

(C) Confocal microscopy images of split-GFP reconstitution between PPL1-γ1pedc (MB320C), PPL1-γ2α′1 (MB296B), and PAM-γ5 (MB315C), and KCs. Green: reconstituted split-GFP fluorescence; magenta: anti-N-cadherin immunoreactivity. Scale bars, 30 μm.

(D) Reconstruction (i and ii) and quantification of synaptic connections (iii) in the α′2 compartment of the mushroom body between the PPL1-γ2α′1 DAN (id no. 5813022424), MBON-α′2 (id no. 1139667240) and KCs using neuPrint:; analysis tools for EM Connectomics by Janelia. Arrows indicate directions and magnitudes of synaptic transmission, numbers indicate the numbers of synapses.

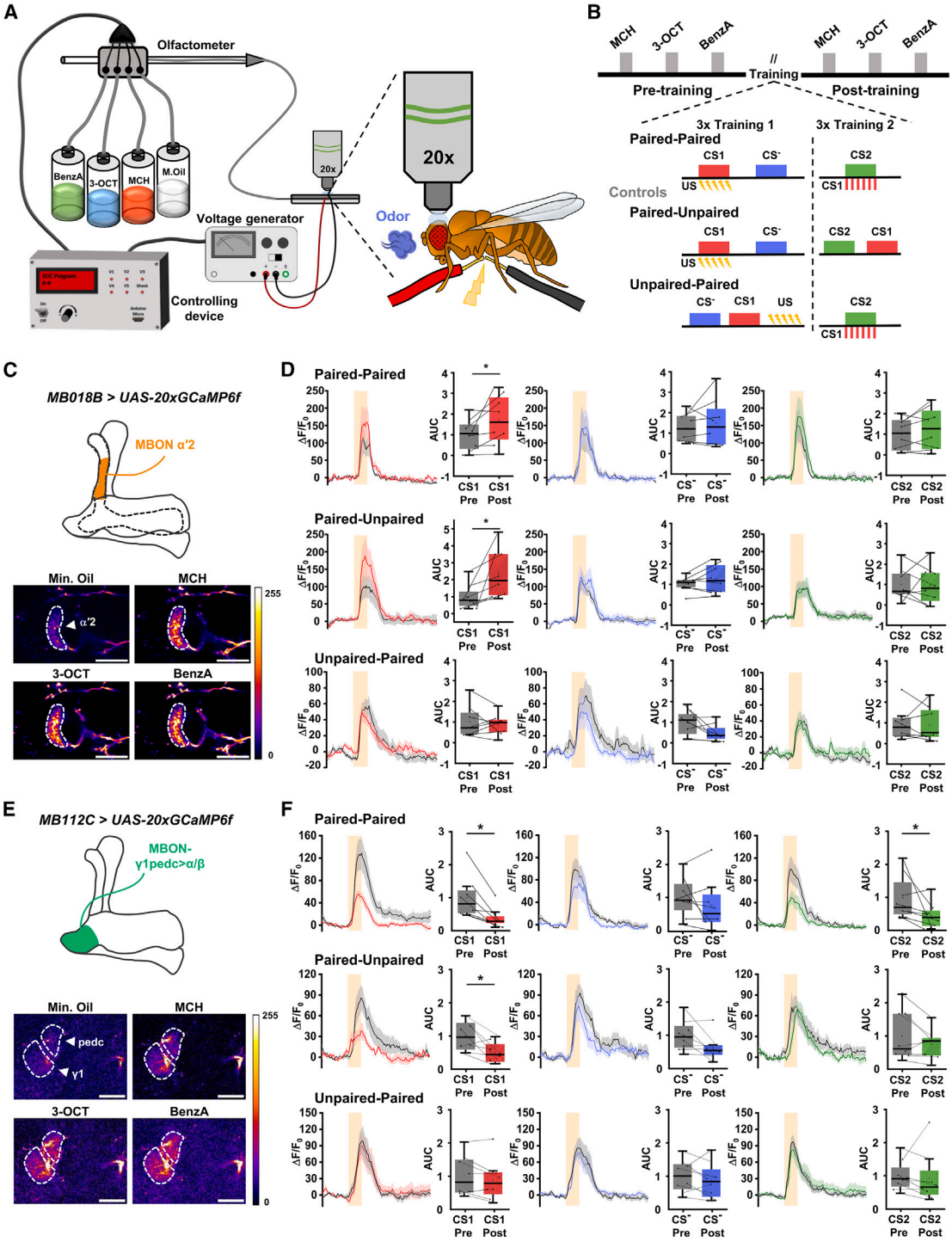

Figure 4. Functional optical calcium imaging of synaptic plasticity induced by second-order conditioning

(A) Experimental imaging set-up using two-photon microscopy.

(B) Imaging protocol of flies subjected to second-order conditioning. Each second-order conditioning experiment was preceded (pre-training) and followed (post-training) by a sequence of odor stimulations with the odorants used for conditioning.

(C and E) Pseudo-colored images of odor-evoked Ca^{2+} responses in MBON-α′2, using MB018B-Gal4 (C) and MBON-γ1pedc>α/β (E) to the trained odors and mineral oil. Scale bars, 10 μm.

(legend continued on next page)

conveying punishment signals to α′2 cannot be excluded, but how these distinct dopaminergic signals affect Kenyon cell-MBON synapses remains to be clarified. We reasoned that a reinforcing, punishment-mediating teaching signal through DANs might cause synaptic plasticity in Kenyon cell-to-MBON connections.

Bi-directional synaptic plasticity in distinct mushroom body compartments underlies second-order conditioning

To investigate learning-induced plasticity, we performed functional Ca^{2+} imaging before, during, and after olfactory conditioning. Flies were placed under a two-photon microscope with their brains exposed and subjected to odor stimuli and electric shocks (Figure 4A). As in freely behaving flies (Figure 1B), they underwent first- and second-order conditioning, with control groups receiving temporally separated stimuli (Unpaired-Paired and Paired-Unpaired) (Figure 4B). Using MB018B-Gal4, we expressed the Ca^{2+} sensor GCaMP6f[62] in MBON-α′2 and monitored odor-evoked neuronal activity. The odorants 4-methylcyclohexanol and 3-octanol were used as CS1 and CS–, and benzaldehyde as CS2. Odor stimulation caused a robust Ca^{2+} influx (Figure 4C). After training, response intensity significantly increased only for CS1, confirming potentiation due to odor-shock pairing (Figure 4D). This effect was present in Paired-Unpaired but not in Unpaired-Paired controls.

Next, expressing GCaMP6f in MBON-γ1pedc>α/β with MB112C-Gal4 revealed strong depression of Ca^{2+} signals for CS1 post-training (Figures 4E and 4F), as previously reported.[36] Interestingly, CS2 also induced synaptic depression after second-order training, dependent on temporal pairing of CS1-US in phase one and CS2-CS1 in phase two (Figure 4F). Thus, two memory traces emerged: MBON-α′2 showed potentiation (required only in second-order training, Figure 2B), while MBON-γ1pedc>α/β exhibited depression for both CS1 and CS2 (required for both training phases, Figure 2A). Notably, after simple first-order conditioning, MBON-α′2 activity was depressed (Figures S6A–S6C), as previously shown.[63] This suggests that potentiation after second-order conditioning results from subsequent non-reinforced odor stimulation rather than first-order conditioning alone.

To determine if MBON-α′2 potentiation arises from presynaptic plasticity, we used a GRAB acetylcholine sensor[64] expressed in Kenyon cells. The borders of the mushroom body compartments could be unambiguously recognized by the differential fluorescence intensity at compartment boundaries (Video S2). Potentiation in MBON-α′2 correlated with increased Kenyon cell output (Figures S5A–S5C), unlike the depression seen after first-order conditioning alone (Figures S6C and S6G). This suggests synaptic potentiation involves presynaptic plasticity, akin to odor-shock-induced presynaptic depression.[35] The potentiation strengthened with odor stimulation trials and became statistically significant after three second-order conditioning trials (Figures S5A–S5C). However, acetylcholine release differed from postsynaptic Ca^{2+} signals, showing potentiation for both CS1 and CS2. This discrepancy may result from differing sensor properties, with the GRAB sensor potentially detecting smaller plastic changes than the cytosolic Ca^{2+} sensor.

Importantly, the finding that the MBON-γ1pedc>α/β shows lower activity for both the CS1 and the CS2 demonstrates that the synaptic depression, which is typically induced by an innate reinforcer such as punitive electric shocks,[36] can be induced by a learned odor as reinforcement as well. This in turn implies that learned odor representation can take control over the reinforcing dopamine system, i.e., the PPL1-γ1pedc DAN, and it implies that the odor associated with punishment through classical odor-shock conditioning can drive the PPL1-γ1pedc DAN stronger. In fact, a potentiation of odor-evoked activity in the PPL1-γ1pedc DAN after aversive conditioning has been well-documented,[65] confirming a previous report in which a single-cell resolution could not be achieved yet.[31]

Identification of feedback loops from MBONs to a valence-signaling DAN

To test this concept more directly, we investigated the effects that the activities of the inhibitory, GABAergic MBON-γ1pedc>α/β, and the excitatory, cholinergic MBON-α′2 actually exert on the PPL1-γ1pedc DAN, either via mono- or polysynaptic connections. The red-shifted, light-sensitive channelrhodopsin variant Cs-Chrimson[66] was used to optogenetically drive the excitation of both MBONs. Simultaneously, the activity of the PPL1-γ1pedc DAN was monitored under a two-photon microscope using the Ca^{2+} sensor GCaMP6m.[62] In comparison with a control that carried only the UAS construct, clear effects were observed; MBON-α′2 induced an increase in the activity of the PPL1-γ1pedc DAN (Figures 5A and 5B). By contrast, MBON-γ1pedc>α/β inhibited it (Figures 5B and 5C), in accordance with previous reports.[34,38] This finding leads to a circuit model that encompasses two feedback loops, one that inhibits the reinforcing PPL1-γ1pedc DAN and one that activates it. During the first training phase, the electric shock activates both PPL1-γ1pedc and PPL1-γ2α′1 DANs. Kenyon cells-to-MBON synapses are depressed in the α′2 compartment and in the γ1 compartment (Figure 5E). In the course of the second-order conditioning phase, the previously depressed synapses in the α′2 compartment undergo a switch to potentiation resulting from non-reinforced odor stimulation. This enables the trained odor CS1 in the second training phase to drive the PPL1-γ1pedc DAN through an activation by the potentiated and excitatory MBON-α′2, and by the depressed and thereby disinhibiting MBON-γ1pedc>α/β. Through the coincident activation of the CS2 with the CS1-induced dopamine release,

(D and F) Odor-evoked Ca^{2+} responses in MBON-α′2 (D) and MBON-γ1pedc>α/β (F) before (Pre) and after (Post) second-order conditioning ("Paired-Paired") and control ("Paired-Unpaired" and "Unpaired-Paired") protocols. Lines indicate mean Ca^{2+} transients, shaded areas represent SEMs, black lines represent pre-training responses, and colored lines represent post-training responses. Shaded orange rectangles indicate the 3-s odor presentations. All groups, $n = 8$. $^{*}p < 0.05$. Boxplots show integral values (areas under the curve [AUC] as interquartile ranges, means [squares], medians [lines], and 10/90 percentiles [whiskers]). Statistical tests: Table S1.

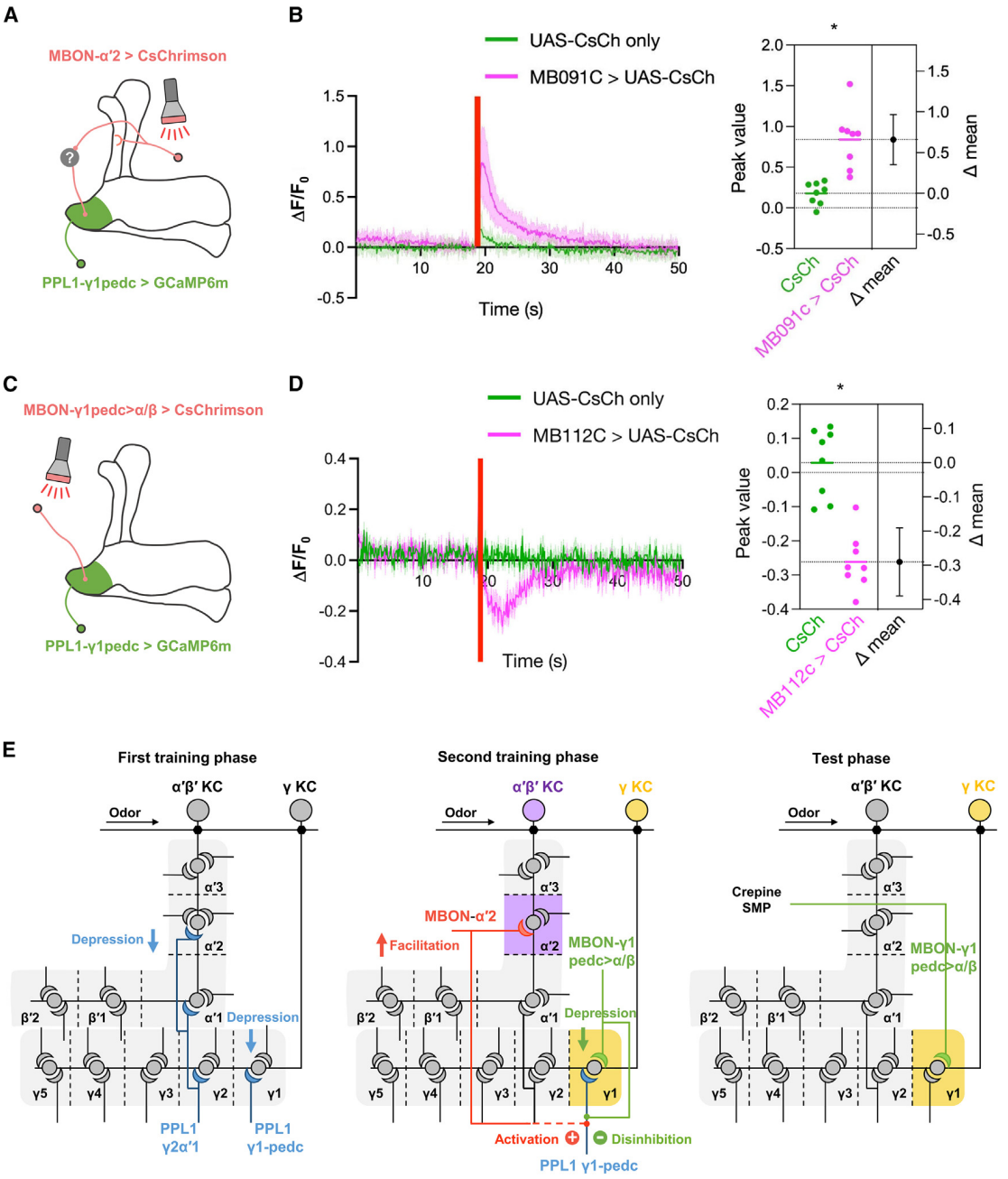

Figure 5. Parallel excitatory and inhibitory feedback loops enable second-order reinforcement

(A and C) Optogenetic activation of MBON-α′2 (A) and MBON-γ1pedc>α/β (C) using CsChrimson and simultaneous Ca^{2+} calcium imaging in PPL1-γ1pedc DAN. TH-LexA drove LexAop-GCaMP6m expression in all PPL1 DANs, and Ca^{2+} in the γ1 compartment was monitored.

(B and D) Left: Ca^{2+} dynamics in PPL-γ1pedc DAN in response to optogenetic activation of MBON-α′2 using MB091C-Gal4 (B), and to MBON-γ1pedc>α/β using MB112C-Gal4 (D). The red bar indicates a 0.5-s train of 20 red light pulses. Green traces show GCaMP6m fluorescence in control brains without CsChrimson expression. Traces show means ± SEM. Right: Estimation plot shows peak values (left) and the mean difference with a 95% confidence interval (right).

(E) Circuit diagram of identified neuronal circuits underlying first-order, second-order, and test phases.

All groups, $n = 8$. *$p < 0.05$. Statistical tests: Table S1.

the Kenyon cell-to-MBON-γ1pedc>α/β synapses become inhibited as well. The memory readout (i.e., avoidance of the learned odor through higher-order conditioning) relies on the inhibition of the approach-inducing MBON-γ1pedc>α/β (Figure 5E). The multiple targeted brain regions of this neuron, such as the crepine or the superior medial protocerebrum,

CellPress
OPEN ACCESS

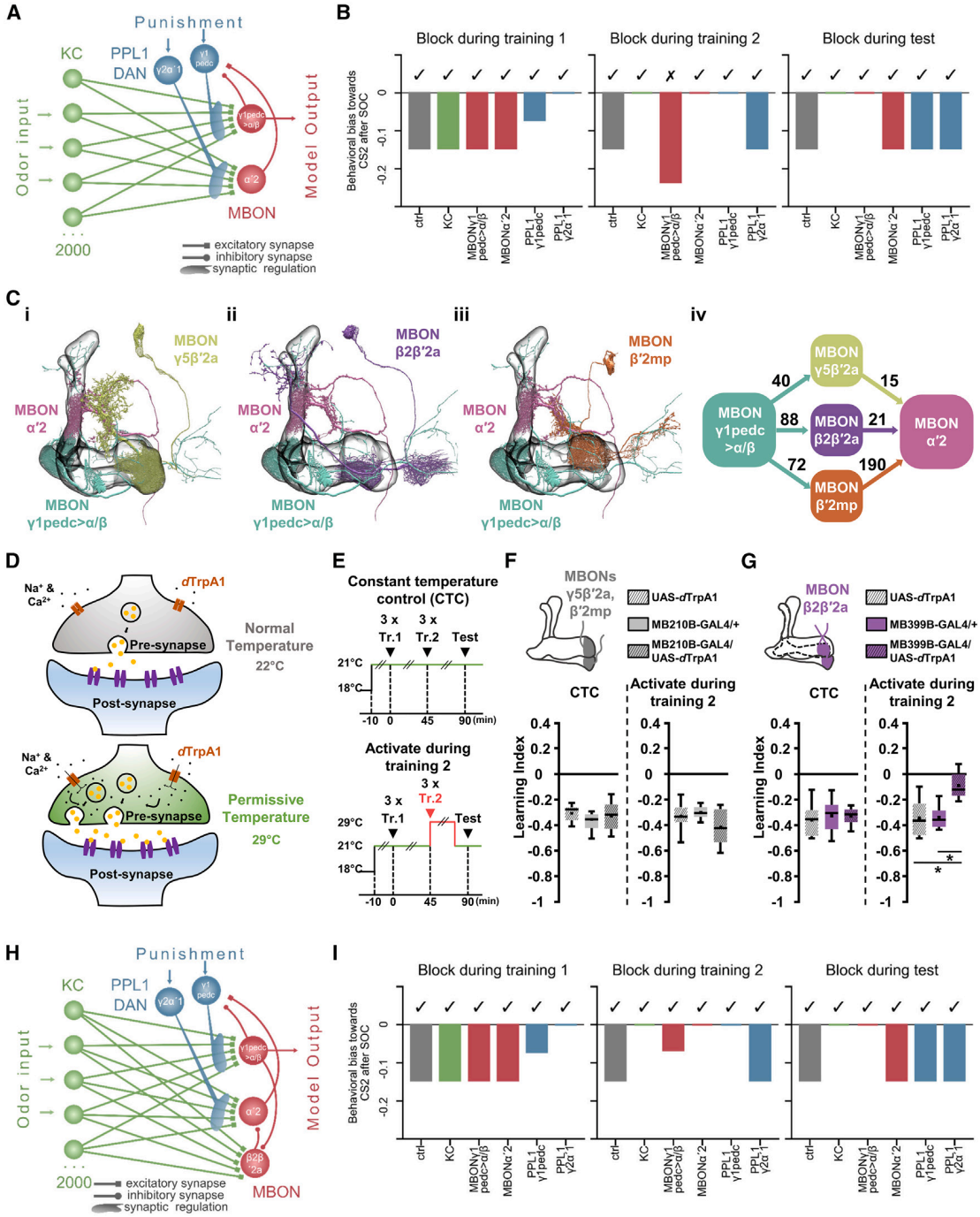

Figure 6. Computational modeling reveals an additional inhibitory interneuron involved in second-order conditioning

(A) Connectivity network overview underlying a computational rate model simulating second-order conditioning.

(B) Calculated behavioral response to the trained odor after second-order conditioning (SOC), quantified as learned avoidance (relative negative values), using a computational rate model. In the control condition, all neurons remained intact. Blocking output from individual neurons or neuronal population during the first-order training (left), second-order training (middle), or test (right) disrupted second-order conditioning selectively.

(C) Reconstruction (i–iii) and quantification of synaptic connections (iv) of MBON-γ1pedc>α/β (id no. 424767514), MBON-γ5β′2a (id no. 612371421), MBON-β2β′2a (id no. 424789697), MBON-β′2mp (id no. 12738462), and MBON-α′2 (id no. 1139667240) using neuPrint: analysis tools for EM Connectomics by Janelia. Arrows indicate directions and magnitudes of synaptic transmission, numbers indicate numbers of synapses.

(legend continued on next page)

might act as pre-motor centers to guide learned avoidance behavior.

Computational modeling reveals a missing inhibitory pathway in second-order conditioning

Complex neuronal circuits—like the one described here—are difficult to understand, characterize and test without computational approaches. Therefore, we used a computational rate model to isolate the circuit motif of interest (Figure 6A). This allowed us to further scrutinize our understanding of the circuit, test its ability to produce second-order conditioning under various simulated conditions, and compare it with behavioral experiments (Figure 2). First, we tested whether the model could support learning of CS1 and CS2 in a combined first- and second-order conditioning protocol with three trials each. We measured MBON-γ1pedc>α/β output to assess the extent of synaptic depression at the KC-MBON-γ1pedc>α/β synapses. Compared with the untrained state, modeled MBON-γ1pedc>α/β activation for both CS1 and CS2 was reduced, with a stronger effect for CS1 than for CS2 (Figure S7C). After verifying the model's ability to perform first- and second-order learning, we conducted simulations (Figure 6B) in which we selectively suppressed the output of different neuron types to replicate the behavioral experiments with blocked synaptic transmission (Figure 2). Suppression of PPL1-γ1pedc DAN or PPL1-γ2α′1 DAN during first-order conditioning impaired learning of the CS2 valence. During second-order conditioning, the output of KCs, MBON-α′2, and PPL1-γ1pedc DAN was necessary. During memory testing, suppressing KCs or MBON-γ1pedc>α/β prevented CS2 valence retrieval. Overall, *in silico* synaptic blocking experiments conducted in the computational model largely replicated behavioral knockout experiments.

However, there was one discrepancy between modeling and behavioral results: in the computational model, MBON-γ1pedc>α/β output was not required during the second-order conditioning phase (Figure 6B), whereas in behavioral experiments blocking its output impaired second-order learning (Figure 2A). MBON-γ1pedc>α/β is a GABAergic, inhibitory neuron[34,37] whose KC input synapses are depressed during conditioning, reducing inhibition on the PPL1-γ1pedc DAN and thus promoting its activity (Figure 5E). Given the proposed circuit (Figure 6A), blocking the output of MBON-γ1pedc>α/β should not prevent second-order conditioning, in contrast to the behavioral results (Figure 2A). To resolve this mismatch (Figure 6B vs. Figure 2A), we explored possible missing circuit elements. We hypothesized the involvement of an additional MBON with inhibitory connections to MBON-α′2, whose inhibitory effect would decrease during first-order conditioning. Using the fly brain connectome,[59] we investigated whether such inhibitory connections to MBON-α′2 exist. In fact, three MBONs (γ5β′2a, β2β′2a, and β′2mp) were identified as potential candidates to mediate this function (Figure 6C). These MBONs are glutamatergic and, in flies, glutamate often has an inhibitory effect.[67] We reasoned that, when these presumably inhibitory neurons are strongly activated, they would in turn inhibit MBON-α′2, and only their inhibition through MBON-γ1pedc>α/β would allow second-order reinforcement. We tested this idea in behavioral experiments by artificially activating the respective MBONs during second-order conditioning using *d*TRPA1[68] (Figure 6D). No effect on learning was observed when MBON-γ5β′2a and MBON-β′2mp were activated together (Figures 6E and 6F). However, driving MBON-β2β′2a activity during second-order conditioning substantially impaired learning (Figure 6G). Implementing the additional inhibitory connection in the computational model and repeating all simulations now abolished CS2 learning when MBON-γ1pedc>α/β output was suppressed during second-order conditioning (Figures 6H and 6I). With this modification, the computational model fully matched the behavioral results (Figure 2A). Thus, it helped to guide behavioral experiments and refine the circuit model by identifying a missing inhibitory pathway essential for replicating all experimental results.

Flies exhibit higher-order associative learning extending to third-order conditioning

We continued by turning to a critical and well-documented distinction between first-order and second-order associative learning. Typically, first-order learning results in an asymptotically increasing, saturating memory over repeated trials of CS-US pairings,[69] and this has also been shown for aversive conditioning in *Drosophila*.[42] However, repeated second-order conditioning trials often lead to an initial increase in memory scores followed by a subsequent decline, resembling an inverted U-shaped function. This decline is attributed to the absence of the primary reinforcer during the second-order conditioning phase, where the presentation of CS1 without punishment leads to extinction.[70] Consequently, the temporal pairing of CS1 with CS2 becomes either ineffective or even indicative of the absence of punishment (i.e., conditioned inhibition). We experimentally tested if such an effect occurs in flies. Indeed, while one second-order conditioning trial was ineffective, three trials produced robust second-order learning. However, with six or nine CS1-CS2 pairings, a subsequent decline in memory scores occurred (Figures 7B and 7C), aligning with theoretical concepts.[69]

As robust as the experimental data and the refined circuit model (Figure 7A) are, evidence of higher-order learning beyond second-order conditioning is essential to assert that flies can genuinely form associative chains. Therefore, we investigated whether associative learning could extend by at least one more chain link—that is, whether flies could perform a third-order conditioning task. Notably, pairing an odor with an electric shock punishment, followed by second-order conditioning of a novel odor with the trained one, and third-order conditioning of another novel odor with the previously trained odor as a reinforcer

(D) Thermo-genetic neuronal activation using *d*TrpA1.
(E) Thermo-genetic activation of distinct mushroom body output neurons during the second-order training phase.
(F and G) Learning indices when MBON-γ5β′2a (F) and MBON-β′2mp (G) were activated only during second-order training.
(H) Modified connectivity network overview underlying the computational rate model, now including MBON-β2β′2a.
(I) Calculated behavioral responses with modified computational rate model.
All groups, $n = 8$. $^*p < 0.05$. Boxplots show interquartile ranges, means (squares), medians (lines), and 10/90 percentiles (whiskers). Statistical tests: Table S1.

CellPress
OPEN ACCESS

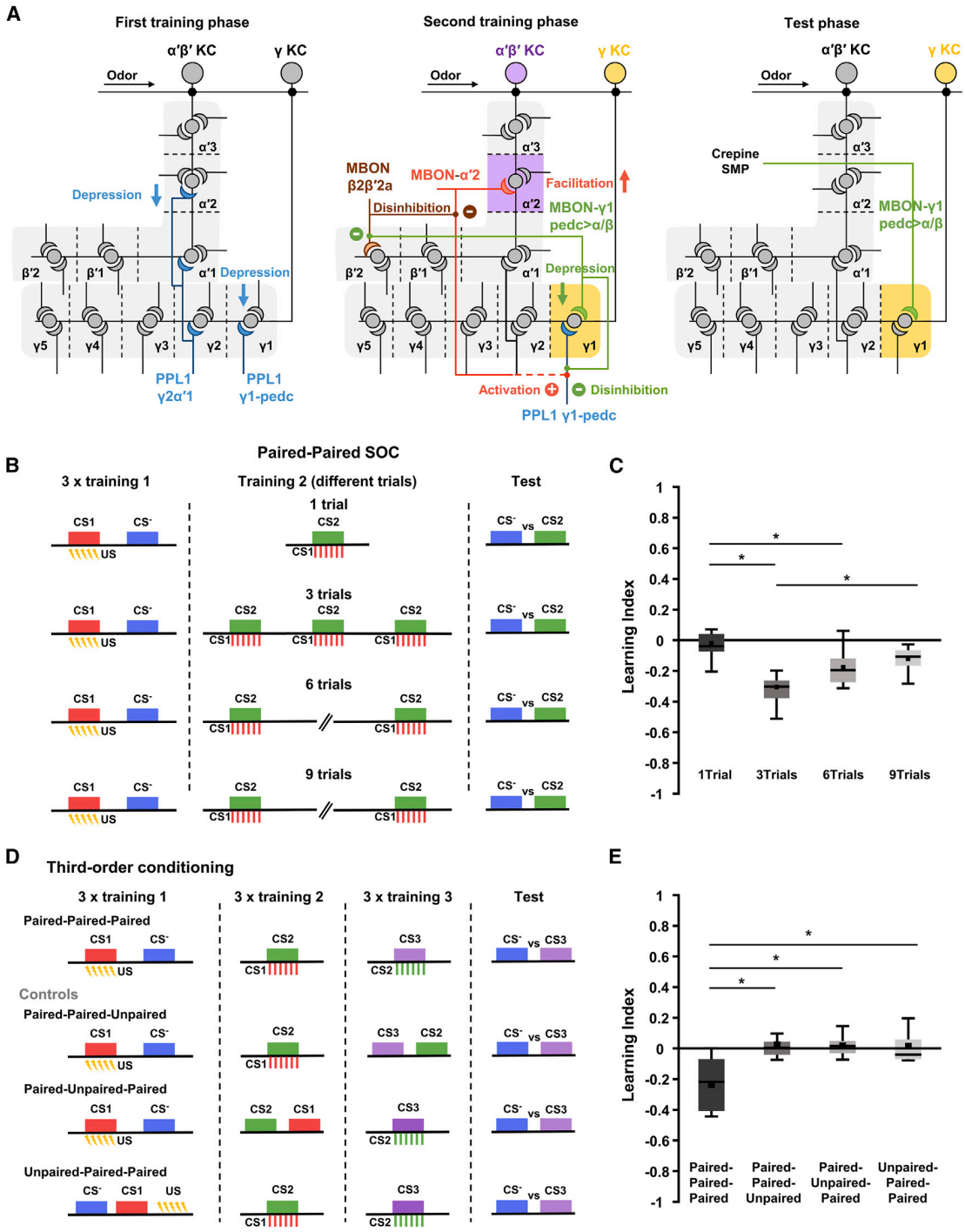

Figure 7. Higher-order associative learning beyond second-order conditioning

(A) Updated neuronal circuit diagram after computational model validation.

(B) Schematic illustration of the second-order conditioning (SOC) paradigm with one, three, six, and nine training trials in the second-order training phase. Colored rectangles indicate the conditioned stimuli, the sequence of aligned lightning bolts represents the electric shocks (unconditioned stimulus), and the dashed red lines represent the pulses of the CS1 acting as reinforcement in the second-order training phase.

(C) Learning indices after one, three, six, and nine second-order conditioning trials.

(legend continued on next page)

resulted in clear and statistically significant learned avoidance in wild-type Canton-S flies (Figures 7D and 7E). Control experiments demonstrated the necessity of temporal coincidence between the conditioned stimuli and their respective reinforcements in each training phase, excluding potential non-associative effects or conditioned inhibition of the CS–. In conclusion, flies exhibit the capacity to learn associative chains beyond second-order associations.

DISCUSSION

Various computational neural network models of associative learning, ranging in complexity, have successfully performed second-order conditioning tasks. Several models explicitly based on *Drosophila* mushroom body circuitry have also been developed.[71–74] While multiple theoretical solutions exist for higher-order learning, their validation requires empirical data. In this context, we identified a *Drosophila* neuronal circuit underlying higher-order associative learning, revealing novel mechanisms mediating this process.

A first unexpected aspect of the identified neuronal circuit is the separation of the reinforcement signal into two additive dopamine channels: the punishment-activated PPL1-γ1pedc and PPL1-γ2α′1 DANs. This separation may stem from differences in learning-induced plasticity between these neurons. Predictive learning models suggest that reinforcing neuron responsiveness to a US, such as electric shock, changes over CS-US associations to encode prediction errors.[75–77] However, no empirical evidence for prediction error coding in *Drosophila* DANs exists,[31,78] unlike, for example, in the midbrain DANs of monkeys.[79] In reward prediction error coding in monkeys, the reinforcing neurons cease responding to the US once it is already predicted by the learned conditioned stimulus. In flies, reinforcing neurons instead strengthen or prolong their response to the conditioned stimulus alongside the electric shock,[31,78] a plasticity observed only in PPL1-γ1pedc DAN, and not in PPL1-γ2α′1 DAN.[65] In this context, it is important to consider that, in second-order conditioning, CS1 is presented without shock in the second training phase, potentially leading to extinction.[10,11,70,80] Initially, CS2 may serve as a second-order predictor of punishment (conditioned excitation), but as CS1 undergoes extinction, CS2 may predict the omission of punishment (conditioned inhibition), a process demonstrated in flies.[41] Given the complex learning-dependent modification of the responsiveness of PPL1-γ1pedc DAN, an independent, stable, unmodified responsiveness to the US in the PPL1-γ2α′1 DAN could help to associate novel, unpredicted conditioned stimuli independent of previous learning history. This aligns with the idea that that the US-like, reinforcing properties of an acquired conditioned stimulus should be independent of the original reinforcement by the innate US to avoid constant conditioned inhibition.[81]

A second unexpected finding concerns across-compartment signaling by DANs. A previous report that the PPL1-α′2α2, which directly innervates the α′2 compartment of the mushroom body, responds to punishing electric shocks[60] could not be confirmed, in accordance with a recent study using voltage-dependent imaging.[82] The discrepancy between studies might be due to a more specific split-Gal4 line used in our study (MB058B-Gal4) compared with a less cell-specific transgenic LexA-line (R82C10-LexA) that includes other PPL1 DANs.[60] We found that PPL1-γ2α′1 DAN is not strictly confined to its assigned γ2 and α′1 compartments. This challenges the conventional view of lobe compartments as isolated functional units. While previous studies suggested that DANs typically innervate only their designated compartments and remain within ∼2 μm of KC-MBON synapses,[61] PPL1-γ2α′1 DAN forms synaptic connections in α′2, identifying it as an α′2-innervating DAN rather than merely influencing this region via volume transmission. Interestingly, two Kenyon cell populations—γ-lobe and α′/β′-lobe Kenyon cells—are involved in higher-order associative learning. Whereas the synaptic odor representation in the γ1 compartment is permanently subject to modification through the acquisition of associative chains, the α′2 compartment appears to be only transiently tagged as relevant to facilitate odor-odor associations. Our discovery that PPL1-γ2α′1 DAN innervates α′2 provides a potential explanation for mismatches between input and output neurons in the identified circuits. However, as the number of synapses between PPL1-γ2α′1 DAN and Kenyon cells or dopaminergic release sites near KC-MBON synapses in α′2 is relatively low, we do not rule out alternative circuit motifs in punishment signaling.

A third unexpected finding is the discovery of learning-induced synaptic depression in the Kenyon cell-to-MBON-γ1pedc>α/β compartment and a switch from depression during first-order conditioning to potentiation during second-order conditioning in the Kenyon cell-to-MBON-α′2 compartment. How is this transition mediated? Differential involvement of DANs in distinct temporal learning regimes ("learning rules") has been described.[83] Antagonistic synaptic depression and potentiation have been observed depending on CS-US timing: forward conditioning (odor preceding punishment) induces avoidance, while relief learning (punishment preceding odor) has the opposite effect.[84] Temporally precise optogenetic activation of punishing DANs elicits synaptic depression via DopR1 receptors and potentiation via DopR2 receptors.[85] Moreover, a time-dependent switch from depression to potentiation has also been linked to NO accumulation, possibly a co-transmitter released by DANs.[86,87] Notably, PPL1-γ2α′1 DAN, central to our analysis, responds to diverse aversive stimuli, including bitter gustatory inputs, showing activity at both stimulus onset and offset.[88] During classical first-order odor conditioning, KC-MBON synapses undergo bidirectional modulation, depending on the precise timing of odor presentation and DAN activity, i.e., with a coincidence of the odor at stimulus on- or offset.[88] Future research should explore whether similar temporally precise interactions underlie bidirectional plasticity during second-order conditioning. However, the

(D) Schematic timeline of third-order conditioning and controls. Colored rectangles indicate the conditioned stimuli (CS), flash symbols indicate electric shocks (unconditioned stimulus [US]), and dashed red and green lines show CS1 and CS2 pulses acting as reinforcement in second- and third-order training.
(E) Learning indices after third-order conditioning and controls.
All groups, $n = 8$. $^*p < 0.05$. Boxplots show interquartile ranges, means (squares), medians (lines), and 10/90 percentiles (whiskers). Statistical tests: Table S1.

CellPress
OPEN ACCESS

observed bidirectional activity at KC-to-MBON-α′2 synapses differs from prior reports, as only previously depressed synapses undergo potentiation.

The distinct plasticity patterns align with the opposing effects of the two MBONs involved in second-order conditioning on PPL1-γ1pedc DAN—one inhibitory, the other excitatory. This architecture, where an excitatory connection is potentiated while an inhibitory connection is depressed (disinhibition), may help stabilize the system. Potentiating excitatory input can rapidly enhance postsynaptic reinforcing neuron responses, while a graded inhibition/disinhibition balance maintains functional stability. Artificially inhibiting MBON-γ1pedc>α/β during odor presentation has been shown to induce aversive memory,[38,39] supporting our finding that its inhibition is not only required for second-order conditioning, but is also sufficient. Future studies could explore whether optogenetic activation of MBON-α′2 also induces reinforcement signals. The identified circuit for aversive second-order conditioning shares similarities with *Drosophila* circuits for appetitive learning, including involvement of multiple mushroom body compartments, inter-compartmental connections, and diverse dopaminergic reinforcers.[14] However, there are also differences. A key difference is that, in both aversive first- and second-order conditioning, plastic modifications converge onto the same behavior-instructing MBON-γ1pedc>α/β.

Limitations of the study

Focusing on aversive higher-order olfactory classical Pavlovian conditioning limits discoveries to specific neuronal circuit properties. How this circuitry interacts with networks governing other learning processes, such as reward-based higher-order learning,[14] sensory pre-conditioning,[89,90] extinction learning,[50,91] or state-dependent modulation of learning[92] remains unclear. The recent characterization of the entire *Drosophila* brain connectome[93,94] may offer a broader framework for deconstructing neural circuits and explaining multiple such phenomena. Additionally, our study has limitations in elucidating the molecular mechanisms underlying the bidirectional plasticity that mediates higher-order learning. Future research on these molecular foundations will be crucial for a deeper understanding of these processes.

RESOURCE AVAILABILITY

Lead contact

Further information and requests for resources and reagents should be directed to the lead contact, André Fiala (afiala@gwdg.de).

Materials availability

All reagents, strains and experimental apparatus' design generated in this study are available from the lead contact.

Data and code availability

- Data: all processed data (without raw large imaging files) can be obtained at https://data.mendeley.com/datasets/55cfd3km5c/1, and all raw and processed data at https://for2705.de/archive/5/110.
- Code: all original code for the fly learning apparatus can be obtained at https://for2705.de/archive/5/110. The code for the circuit implementation can be obtained in addition at https://github.com/nawrotlab/higher_order_learning_circuit (https://doi.org/10.5281/zenodo.14932132).

ACKNOWLEDGMENTS

We are grateful to Betty Hong for providing the novel MB247-Gal4 strain; to the Janelia Research Campus and their FlyLight Project for providing numerous fly strains; to Amrita Paul Nishu, Eva Küsters, Marie Eileen Wiesenhavern, and Julia Kniep for help with experiments; to Jan Hoffmann and Tobias Mühmer for constructing electronic devices; to Muhammad Afaque Khan for help with programming, to Sabyasachi Chakrabarty and Elhanan Buchsbaum for assistance with data analysis. This work was funded by the German Research Council (DFG) through the Research Unit FOR 2705 (project no. 365082554) to A.F. and M.P.N., through the SFB 889/B04 (project no. 154113120) to A.F., through the Priority Program SPP 2205 (project no. 430592330) to M.P.N., by the Ministry for Science and Culture of Lower Saxony (project no. ZN 3014) to A.F., by the German Federal Ministry of Education and Research (BMBF) within the project DrosExpect (project no. 01GQ2103A) to M.P.N., by the Taiwan Ministry of Science and Technology (grant no. 111-2326-B-001-005-MY3) to S.L., and the Academia Sinica Career Development Award (grant no. AS-CDA-110-L06) to S.L.

AUTHOR CONTRIBUTIONS

A.F. conceptualized and supervised the overall project. E.Y.R., S.H.D., L.E., Y.V.G., and C.-H.L. designed and performed the experiments, and analyzed the data. A.-M.J., M.S., and M.P.N. designed and performed a computational analysis. A.F., M.P.N., and S.L. supervised parts of the project. A.F. and E.Y.R. wrote the manuscript with input from all authors.

DECLARATION OF INTERESTS

The authors declare no competing interests.

STAR★METHODS

Detailed methods are provided in the online version of this paper and include the following:

- KEY RESOURCES TABLE
- EXPERIMENTAL MODEL AND STUDY PARTICIPANT DETAILS
  - *Drosophila* strains and genotypes
- METHOD DETAILS
  - Aversive olfactory conditioning
  - *In vivo* functional imaging
  - Optogenetic stimulation and calcium imaging
  - Immunohistochemistry
  - Confocal microscopy
  - Reconstruction of neuronal connections with the neuPrint database
  - Second-order conditioning circuit computational modeling
- QUANTIFICATION AND STATISTICAL ANALYSIS
  - Two-photon image processing
  - Behavioral statistical analysis
  - Confocal microscopy image processing
  - Analysis of synaptic distances with NeuPrint phyton code

SUPPLEMENTAL INFORMATION

Supplemental information can be found online at https://doi.org/10.1016/j.celrep.2025.115593.

Received: January 3, 2024
Revised: January 28, 2025
Accepted: March 30, 2025
Published: April 17, 2025

REFERENCES

1. Pavlov, I. (1927). Conditioned Reflexes: An Investigation of the Physiological Activity of the Cerebral Cortex (Oxford University Press).
2. Craddock, P., Wasserman, J.S., Polack, C.W., Kosinski, T., Renaux, C., and Miller, R.R. (2018). Associative structure of second-order conditioning in humans. Learn. Behav. *46*, 171–181. https://doi.org/10.3758/s13420-017-0299-5.
3. Lee, J.C. (2021). Second-order conditioning in humans. Front. Behav. Neurosci. *15*, 672628. https://doi.org/10.3389/fnbeh.2021.672628.
4. Murphy, J.V., and Miller, R.E. (1957). Higher-order conditioning in the monkey. J. Gen. Psychol. *56*, 67–72. https://doi.org/10.1080/00221309.1957.9918363.
5. Cook, M., and Mineka, S. (1987). Second-order conditioning and overshadowing in the observational conditioning of fear in monkeys. Behav. Res. Ther. *25*, 349–364. https://doi.org/10.1016/0005-7967(87)90013-1.
6. Rizley, R.C., and Rescorla, R.A. (1972). Associations in second-order conditioning and sensory preconditioning. J. Comp. Physiol. Psychol. *81*, 1–11. https://doi.org/10.1037/h0033333.
7. Gostolupce, D., Iordanova, M.D., and Lay, B.P.P. (2021). Mechanisms of higher-order learning in the amygdala. Behav. Brain Res. *414*, 113435. https://doi.org/10.1016/j.bbr.2021.113435.
8. Hawkins, R.D., Greene, W., and Kandel, E.R. (1998). Classical conditioning, differential conditioning, and second-order conditioning of the *Aplysia* gill-withdrawal reflex in a simplified mantle organ preparation. Behav. Neurosci. *112*, 636–645. https://doi.org/10.1037//0735-7044.112.3.636.
9. Loy, I., Fernández, V., and Acebes, F. (2006). Conditioning of tentacle lowering in the snail (*Helix aspersa*): acquisition, latent inhibition, overshadowing, second-order conditioning, and sensory preconditioning. Learn. Beyond Behav. *34*, 305–314. https://doi.org/10.3758/bf03192885.
10. Bitterman, M.E., Menzel, R., Fietz, A., and Schäfer, S. (1983). Classical conditioning of proboscis extension in honeybees (*Apis mellifera*). J. Comp. Psychol. *97*, 107–119. https://doi.org/10.1037/0735-7036.97.2.107.
11. Hussaini, S.A., Komischke, B., Menzel, R., and Lachnit, H. (2007). Forward and backward second-order Pavlovian conditioning in honeybees. Learn. Mem. *14*, 678–683. https://doi.org/10.1101/lm.471307.
12. Brembs, B., and Heisenberg, M. (2001). Conditioning with compound stimuli in *Drosophila melanogaster* in the flight simulator. J. Exp. Biol. *204*, 2849–2859. https://doi.org/10.1242/jeb.204.16.2849.
13. Tabone, C.J., and de Belle, J.S. (2011). Second-order conditioning in *Drosophila*. Learn. Mem. *18*, 250–253. https://doi.org/10.1101/lm.2035411.
14. Yamada, D., Bushey, D., Li, F., Hibbard, K.L., Sammons, M., Funke, J., Litwin-Kumar, A., Hige, T., and Aso, Y. (2023). Hierarchical architecture of dopaminergic circuits enables second-order conditioning in *Drosophila*. Elife *12*, e79042. https://doi.org/10.7554/eLife.79042.
15. Holmes, N.M., Fam, J.P., Clemens, K.J., Laurent, V., and Westbrook, R.F. (2022). The neural substrates of higher-order conditioning: A review. Neurosci. Biobehav. Rev. *138*, 104687. https://doi.org/10.1016/j.neubiorev.2022.104687.
16. Gilboa, A., Sekeres, M., Moscovitch, M., and Winocur, G. (2014). Higher-order conditioning is impaired by hippocampal lesions. Curr. Biol. *24*, 2202–2207. https://doi.org/10.1016/j.cub.2014.07.078.
17. Luo, L., Callaway, E.M., and Svoboda, K. (2018). Genetic dissection of neural circuits: a decade of progress. Neuron *98*, 256–281. https://doi.org/10.1016/j.neuron.2018.03.040.
18. Venken, K.J.T., Simpson, J.H., and Bellen, H.J. (2011). Genetic manipulation of genes and cells in the nervous system of the fruit fly. Neuron *72*, 202–230. https://doi.org/10.1016/j.neuron.2011.09.021.
19. Busto, G.U., Cervantes-Sandoval, I., and Davis, R.L. (2010). Olfactory learning in *Drosophila*. Physiology *25*, 338–346. https://doi.org/10.1152/physiol.00026.2010.
20. Fiala, A., and Riemensperger, T. (2017). Localization of a memory trace: Aversive associative olfactory learning and short-term memory in *Drosophila*. In Learning and Memory: A Comprehensive Reference, Vol.1, Learning Theory and Behavior, R. Menzel and J.H. Byrne, eds. (Academic Press), pp. 475–482.
21. Boto, T., Stahl, A., and Tomchik, S.M. (2020). Cellular and circuit mechanisms of olfactory associative learning in *Drosophila*. J. Neurogenet. *34*, 36–46. https://doi.org/10.1080/01677063.2020.1715971.
22. Vosshall, L.B., and Stocker, R.F. (2007). Molecular architecture of smell and taste in *Drosophila*. Annu. Rev. Neurosci. *30*, 505–533. https://doi.org/10.1146/annurev.neuro.30.051606.094306.
23. Hildebrand, J.G., and Shepherd, G.M. (1997). Mechanisms of olfactory discrimination: converging evidence for common principles across phyla. Annu. Rev. Neurosci. *20*, 595–631. https://doi.org/10.1146/annurev.neuro.20.1.595.
24. Marin, E.C., Jefferis, G.S.X.E., Komiyama, T., Zhu, H., and Luo, L. (2002). Representation of the glomerular olfactory map in the *Drosophila* brain. Cell *109*, 243–255. https://doi.org/10.1016/s0092-8674(02)00700-6.
25. Wong, A.M., Wang, J.W., and Axel, R. (2002). Spatial representation of the glomerular map in the *Drosophila* protocerebrum. Cell *109*, 229–241. https://doi.org/10.1016/s0092-8674(02)00707-9.
26. Turner, G.C., Bazhenov, M., and Laurent, G. (2008). Olfactory representations by *Drosophila* mushroom body neurons. J. Neurophysiol. *99*, 734–746. https://doi.org/10.1152/jn.01283.2007.
27. Honegger, K.S., Campbell, R.A.A., and Turner, G.C. (2011). Cellular-resolution population imaging reveals robust sparse coding in the *Drosophila* mushroom body. J. Neurosci. *31*, 11772–11785. https://doi.org/10.1523/JNEUROSCI.1099-11.2011.
28. Bilz, F., Geurten, B.R.H., Hancock, C.E., Widmann, A., and Fiala, A. (2020). Visualization of a distributed synaptic memory code in the *Drosophila* brain. Neuron *106*, 963–976.e4. https://doi.org/10.1016/j.neuron.2020.03.010.
29. Stettler, D.D., and Axel, R. (2009). Representations of odor in the piriform cortex. Neuron *63*, 854–864. https://doi.org/10.1016/j.neuron.2009.09.005.
30. Heisenberg, M. (2003). Mushroom body memoir: from maps to models. Nat. Rev. Neurosci. *4*, 266–275. https://doi.org/10.1038/nrn1074.
31. Riemensperger, T., Völler, T., Stock, P., Buchner, E., and Fiala, A. (2005). Punishment prediction by dopaminergic neurons in *Drosophila*. Curr. Biol. *15*, 1953–1960. https://doi.org/10.1016/j.cub.2005.09.042.
32. Schultz, W. (2007). Multiple dopamine functions at different time courses. Annu. Rev. Neurosci. *30*, 259–288. https://doi.org/10.1146/annurev.neuro.28.061604.135722.
33. Aso, Y., Herb, A., Ogueta, M., Siwanowicz, I., Templier, T., Friedrich, A.B., Ito, K., Scholz, H., and Tanimoto, H. (2012). Three dopamine pathways induce aversive odor memories with different stability. PLoS Genet. *8*, e1002768. https://doi.org/10.1371/journal.pgen.1002768.
34. Aso, Y., Hattori, D., Yu, Y., Johnston, R.M., Iyer, N.A., Ngo, T.T.B., Dionne, H., Abbott, L.F., Axel, R., Tanimoto, H., and Rubin, G.M. (2014). The neuronal architecture of the mushroom body provides a logic for associative learning. Elife *3*, e04577. https://doi.org/10.7554/eLife.04577.
35. Hige, T., Aso, Y., Modi, M.N., Rubin, G.M., and Turner, G.C. (2015). Heterosynaptic plasticity underlies aversive olfactory learning in Drosophila. Neuron *88*, 985–998. https://doi.org/10.1016/j.neuron.2015.11.003.
36. Hancock, C.E., Rostami, V., Rachad, E.Y., Deimel, S.H., Nawrot, M.P., and Fiala, A. (2022). Visualization of learning-induced synaptic plasticity in output neurons of the *Drosophila* mushroom body γ-lobe. Sci. Rep. *12*, 10421. https://doi.org/10.1038/s41598-022-14413-5.

37. Aso, Y., Sitaraman, D., Ichinose, T., Kaun, K.R., Vogt, K., Belliart-Guérin, G., Plaçais, P.Y., Robie, A.A., Yamagata, N., Schnaitmann, C., et al. (2014). Mushroom body output neurons encode valence and guide memory-based action selection in *Drosophila*. Elife *3*, e04580. https://doi.org/10.7554/eLife.04580.

38. Ueoka, Y., Hiroi, M., Abe, T., and Tabata, T. (2017). Suppression of a single pair of mushroom body output neurons in *Drosophila* triggers aversive associations. FEBS Open Bio. *7*, 562–576. https://doi.org/10.1002/2211-5463.12203.

39. König, C., Khalili, A., Niewalda, T., Gao, S., and Gerber, B. (2019). An optogenetic analogue of second-order reinforcement in *Drosophila*. Biol. Lett. *15*, 20190084. https://doi.org/10.1098/rsbl.2019.0084.

40. Rescorla, R.A. (1980). Pavlovian Second-Order Conditioning: Studies in Associative Learning (Psychology Press), p. 2014.

41. Barth, J., Dipt, S., Pech, U., Hermann, M., Riemensperger, T., and Fiala, A. (2014). Differential associative training enhances olfactory acuity in *Drosophila melanogaster*. J. Neurosci. *34*, 1819–1837. https://doi.org/10.1523/JNEUROSCI.2598-13.2014.

42. Beck, C.D., Schroeder, B., and Davis, R.L. (2000). Learning performance of normal and mutant Drosophila after repeated conditioning trials with discrete stimuli. J. Neurosci. *20*, 2944–2953. https://doi.org/10.1523/JNEUROSCI.20-08-02944.2000.

43. Margulies, C., Tully, T., and Dubnau, J. (2005). Deconstructing memory in *Drosophila*. Curr. Biol. *15*, R700–R713. https://doi.org/10.1016/j.cub.2005.08.024.

44. Tully, T., and Quinn, W.G. (1985). Classical conditioning and retention in normal and mutant Drosophila melanogaster. J. Comp. Physiol. *157*, 263–277. https://doi.org/10.1007/BF01350033.

45. Kitamoto, T. (2001). Conditional modification of behavior in *Drosophila* by targeted expression of a temperature-sensitive shibire allele in defined neurons. J. Neurobiol. *47*, 81–92. https://doi.org/10.1002/neu.1018.

46. Kitamoto, T. (2002). Targeted expression of temperature-sensitive dynamin to study neural mechanisms of complex behavior in *Drosophila*. J. Neurogenet. *16*, 205–228. https://doi.org/10.1080/01677060216295.

47. Kasuya, J., Ishimoto, H., and Kitamoto, T. (2009). Neuronal mechanisms of learning and memory revealed by spatial and temporal suppression of neurotransmission using shibire, a temperature-sensitive dynamin mutant gene in *Drosophila* melanogaster. Front. Mol. Neurosci. *2*, 11. https://doi.org/10.3389/neuro.02.011.2009.

48. Dubnau, J., Grady, L., Kitamoto, T., and Tully, T. (2001). Disruption of neurotransmission in *Drosophila* mushroom body blocks retrieval but not acquisition of memory. Nature *411*, 476–480. https://doi.org/10.1038/35078077.

49. McGuire, S.E., Le, P.T., and Davis, R.L. (2001). The role of *Drosophila* mushroom body signaling in olfactory memory. Science *293*, 1330–1333. https://doi.org/10.1126/science.1062622.

50. Schwaerzel, M., Heisenberg, M., and Zars, T. (2002). Extinction antagonizes olfactory memory at the subcellular level. Neuron *35*, 951–960. https://doi.org/10.1016/s0896-6273(02)00832-2.

51. Zars, T., Fischer, M., Schulz, R., and Heisenberg, M. (2000). Localization of a short-term memory in *Drosophila*. Science *288*, 672–675. https://doi.org/10.1126/science.288.5466.672.

52. Qin, H., Cressy, M., Li, W., Coravos, J.S., Izzi, S.A., and Dubnau, J. (2012). Gamma neurons mediate dopaminergic input during aversive olfactory memory formation in *Drosophila*. Curr. Biol. *22*, 608–614. https://doi.org/10.1016/j.cub.2012.02.014.

53. Pfeiffer, B.D., Ngo, T.T.B., Hibbard, K.L., Murphy, C., Jenett, A., Truman, J.W., and Rubin, G.M. (2010). Refinement of tools for targeted gene expression in *Drosophila*. Genetics *186*, 735–755. https://doi.org/10.1534/genetics.110.119917.

54. Pech, U., Pooryasin, A., Birman, S., and Fiala, A. (2013). Localization of the contacts between Kenyon cells and aminergic neurons in the *Drosophila melanogaster* brain using SplitGFP reconstitution. J. Comp. Neurol. *521*, 3992–4026. https://doi.org/10.1002/cne.23388.

55. Pech, U., Revelo, N.H., Seitz, K.J., Rizzoli, S.O., and Fiala, A. (2015). Optical dissection of experience-dependent pre- and postsynaptic plasticity in the *Drosophila* brain. Cell Rep. *10*, 2083–2095. https://doi.org/10.1016/j.celrep.2015.02.065.

56. Yamagata, N., Ichinose, T., Aso, Y., Plaçais, P.Y., Friedrich, A.B., Sima, R.J., Preat, T., Rubin, G.M., and Tanimoto, H. (2015). Distinct dopamine neurons mediate reward signals for short- and long-term memories. Proc. Natl. Acad. Sci. USA *112*, 578–583. https://doi.org/10.1073/pnas.1421930112.

57. Feinberg, E.H., Vanhoven, M.K., Bendesky, A., Wang, G., Fetter, R.D., Shen, K., and Bargmann, C.I. (2008). GFP Reconstitution Across Synaptic Partners (GRASP) defines cell contacts and synapses in living nervous systems. Neuron *57*, 353–363. https://doi.org/10.1016/j.neuron.2007.11.030.

58. Zhang, Y.Q., Rodesch, C.K., and Broadie, K. (2002). Living synaptic vesicle marker: Synaptotagmin-GFP. Genesis *34*, 142–145. https://doi.org/10.1002/gene.10144.

59. Scheffer, L.K., Xu, C.S., Januszewski, M., Lu, Z., Takemura, S.Y., Hayworth, K.J., Huang, G.B., Shinomiya, K., Maitlin-Shepard, J., Berg, S., et al. (2020). A connectome and analysis of the adult *Drosophila* central brain. Elife *9*, e57443. https://doi.org/10.7554/eLife.57443.

60. Cervantes-Sandoval, I., Phan, A., Chakraborty, M., and Davis, R.L. (2017). Reciprocal synapses between mushroom body and dopamine neurons form a positive feedback loop required for learning. Elife *6*, e23789. https://doi.org/10.7554/eLife.23789.

61. Takemura, S.Y., Aso, Y., Hige, T., Wong, A., Lu, Z., Xu, C.S., Rivlin, P.K., Hess, H., Zhao, T., Parag, T., et al. (2017). A connectome of a learning and memory center in the adult Drosophila brain. Elife *6*, e26975. https://doi.org/10.7554/eLife.26975.

62. Chen, T.W., Wardill, T.J., Sun, Y., Pulver, S.R., Renninger, S.L., Baohan, A., Schreiter, E.R., Kerr, R.A., Orger, M.B., Jayaraman, V., et al. (2013). Ultrasensitive fluorescent proteins for imaging neuronal activity. Nature *499*, 295–300. https://doi.org/10.1038/nature12354.

63. Zhang, X., Noyes, N.C., Zeng, J., Li, Y., and Davis, R.L. (2019). Aversive training induces both presynaptic and postsynaptic suppression in Drosophila. J. Neurosci. *39*, 9164–9172. https://doi.org/10.1523/JNEUROSCI.1420-19.2019.

64. Jing, M., Li, Y., Zeng, J., Huang, P., Skirzewski, M., Kljakic, O., Peng, W., Qian, T., Tan, K., Zou, J., et al. (2020). An optimized acetylcholine sensor for monitoring *in vivo* cholinergic activity. Nat. Methods *17*, 1139–1146. https://doi.org/10.1038/s41592-020-0953-2.

65. Vrontou, E., Groschner, L.N., Szydlowski, S., Brain, R., Krebbers, A., and Miesenböck, G. (2021). Response competition between neurons and antineurons in the mushroom body. Curr. Biol. *31*, 4911–4922.e4. https://doi.org/10.1016/j.cub.2021.09.008.

66. Klapoetke, N.C., Murata, Y., Kim, S.S., Pulver, S.R., Birdsey-Benson, A., Cho, Y.K., Morimoto, T.K., Chuong, A.S., Carpenter, E.J., Tian, Z., et al. (2014). Independent optical excitation of distinct neural populations. Nat. Methods *11*, 338–346. https://doi.org/10.1038/nmeth.2836.

67. Liu, W.W., and Wilson, R.I. (2013). Glutamate is an inhibitory neurotransmitter in the *Drosophila* olfactory system. Proc. Natl. Acad. Sci. USA *110*, 10294–10299. https://doi.org/10.1073/pnas.1220560110.

68. Hamada, F.N., Rosenzweig, M., Kang, K., Pulver, S.R., Ghezzi, A., Jegla, T.J., and Garrity, P.A. (2008). An internal thermal sensor controlling temperature preference in *Drosophila*. Nature *454*, 217–220. https://doi.org/10.1038/nature07001.

69. Rescorla, R.A., and Wagner, A.R. (1972). A theory of Pavlovian conditioning: Variations in the effectiveness of reinforcement and nonreinforcement. In Classical Conditioning II: Current Research and Theory, A.H. Black and W.F. Prokasy, eds. (Appleton-Century-Crofts), pp. 64–99.

70. Rescorla, R.A. (1973). Second-order conditioning: Implications for theories of learning. In Contemporary Approaches to Conditioning and Learning, F.J. McGuigan and D.B. Lumsden, eds. (V. H. Winston).

71. Faghihi, F., Moustafa, A.A., Heinrich, R., and Wörgötter, F. (2017). A computational model of conditioning inspired by *Drosophila* olfactory system. Neural Netw. *87*, 96–108. https://doi.org/10.1016/j.neunet.2016.11.002.

72. Eschbach, C., Fushiki, A., Winding, M., Schneider-Mizell, C.M., Shao, M., Arruda, R., Eichler, K., Valdes-Aleman, J., Ohyama, T., Thum, A.S., et al. (2020). Recurrent architecture for adaptive regulation of learning in the insect brain. Nat. Neurosci. *23*, 544–555. https://doi.org/10.1038/s41593-020-0607-9.

73. Jiang, L., and Litwin-Kumar, A. (2021). Models of heterogeneous dopamine signaling in an insect learning and memory center. PLoS Comput. Biol. *17*, e1009205. https://doi.org/10.1371/journal.pcbi.1009205.

74. Jürgensen, A., Schmitt, F.J., and Nawrot, M.P. (2024). Minimal circuit motifs for second-order conditioning in the insect mushroom body. Front. Physiol. *14*, 1326307. https://doi.org/10.3389/fphys.2023.132630.

75. Springer, M., and Nawrot, M.P. (2021). A mechanistic model for reward prediction and extinction learning in the fruit fly. eNeuro *8*, ENEURO.0549-20.2021. https://doi.org/10.1523/ENEURO.0549-20.2021.

76. Bennett, J.E.M., Philippides, A., and Nowotny, T. (2021). Learning with reinforcement prediction errors in a model of the *Drosophila* mushroom body. Nat. Commun. *12*, 2569. https://doi.org/10.1038/s41467-021-22592-4.

77. Zhao, C., Widmer, Y.F., Diegelmann, S., Petrovici, M.A., Sprecher, S.G., and Senn, W. (2021). Predictive olfactory learning in *Drosophila*. Sci. Rep. *11*, 6795. https://doi.org/10.1038/s41598-021-85841-y.

78. Dylla, K.V., Raiser, G., Galizia, C.G., and Szyszka, P. (2017). Trace conditioning in *Drosophila* induces associative plasticity in mushroom body Kenyon cells and dopaminergic neurons. Front. Neural Circ. *11*, 42. https://doi.org/10.3389/fncir.2017.00042.

79. Schultz, W., Dayan, P., and Montague, P.R. (1997). A neural substrate of prediction and reward. Science *275*, 1593–1599. https://doi.org/10.1126/science.275.5306.1593.

80. Holland, P.C., and Rescorla, R.A. (1975). Second-order conditioning with food unconditioned stimulus. J. Comp. Physiol. Psychol. *88*, 459–467. https://doi.org/10.1037/h0076219.

81. Miller, R.R., Barnet, R.C., and Grahame, N.J. (1995). Assessment of the Rescorla-Wagner model. Psychol. Bull. *117*, 363–386. https://doi.org/10.1037/0033-2909.117.3.363.

82. Huang, C., Luo, J., Woo, S.J., Roitman, L.A., Li, J., Pieribone, V.A., Kannan, M., Vasan, G., and Schnitzer, M.J. (2024). Dopamine-mediated interactions between short- and long-term memory dynamics. Nature *634*, 1141–1149. https://doi.org/10.1038/s41586-024-07819-w.

83. Aso, Y., and Rubin, G.M. (2016). Dopaminergic neurons write and update memories with cell-type-specific rules. Elife *5*, e16135. https://doi.org/10.7554/eLife.16135.

84. Tanimoto, H., Heisenberg, M., and Gerber, B. (2004). Experimental psychology: event timing turns punishment to reward. Nature *430*, 983. https://doi.org/10.1038/430983a.

85. Handler, A., Graham, T.G.W., Cohn, R., Morantte, I., Siliciano, A.F., Zeng, J., Li, Y., and Ruta, V. (2019). Distinct dopamine receptor pathways underlie the temporal sensitivity of associative learning. Cell *178*, 60–75.e19. https://doi.org/10.1016/j.cell.2019.05.040.

86. Aso, Y., Ray, R.P., Long, X., Bushey, D., Cichewicz, K., Ngo, T.T., Sharp, B., Christoforou, C., Hu, A., Lemire, A.L., et al. (2019). Nitric oxide acts as a cotransmitter in a subset of dopaminergic neurons to diversify memory dynamics. Elife *8*, e49257.

87. Yamada, D., Davidson, A.M., and Hige, T. (2024). Cyclic nucleotide-induced bidirectional long-term synaptic plasticity in Drosophila mushroom body. J. Physiol. *602*, 2019–2045. https://doi.org/10.1113/JP285745.

88. Devineni, A.V., Deere, J.U., Sun, B., and Axel, R. (2021). Individual bitter-sensing neurons in *Drosophila* exhibit both ON and OFF responses that influence synaptic plasticity. Curr. Biol. *31*, 5533–5546.e7. https://doi.org/10.1016/j.cub.2021.10.020.

89. Martinez-Cervantes, J., Shah, P., Phan, A., and Cervantes-Sandoval, I. (2022). Higher-order unimodal olfactory sensory preconditioning in Drosophila. Elife *11*, e79107. https://doi.org/10.7554/eLife.79107.

90. Guo, J., and Guo, A. (2005). Crossmodal interactions between olfactory and visual learning in Drosophila. Science *309*, 307–310. https://doi.org/10.1126/science.1111280.

91. Felsenberg, J., Barnstedt, O., Cognigni, P., Lin, S., and Waddell, S. (2017). Re-evaluation of learned information in Drosophila. Nature *544*, 240–244.

92. Çoban, B., Poppinga, H., Rachad, E.Y., Geurten, B., Vasmer, D., Rodriguez Jimenez, F.J., Gadgil, Y., Deimel, S.H., Alyagor, I., Schuldiner, O., et al. (2024). The caloric value of food intake structurally adjusts a neuronal mushroom body circuit mediating olfactory learning in Drosophila. Learn. Mem. *31*, a053997.

93. Dorkenwald, S., Matsliah, A., Sterling, A.R., Schlegel, P., Yu, S.C., McKellar, C.E., Lin, A., Costa, M., Eichler, K., Yin, Y., et al. (2024). Neuronal wiring diagram of an adult brain. Nature *634*, 124–138.

94. Schlegel, P., Yin, Y., Bates, A.S., Dorkenwald, S., Eichler, K., Brooks, P., Han, D.S., Gkantia, M., Dos Santos, M., Munnelly, E.J., et al. (2024). Whole-brain annotation and multi-connectome cell typing of Drosophila. Nature *634*, 139–152.

95. Jenett, A., Rubin, G.M., Ngo, T.T.B., Shepherd, D., Murphy, C., Dionne, H., Pfeiffer, B.D., Cavallaro, A., Hall, D., Jeter, J., et al. (2012). A GAL4-driver line resource for *Drosophila* neurobiology. Cell Rep. *2*, 991–1001. https://doi.org/10.1016/j.celrep.2012.09.011.

96. Friggi-Grelin, F., Coulom, H., Meller, M., Gomez, D., Hirsh, J., and Birman, S. (2003). Targeted gene expression in Drosophila dopaminergic cells using regulatory sequences from tyrosine hydroxylase. J. Neurobiol. *54*, 618–627. https://doi.org/10.1002/neu.10185.

97. Yuan, Q., Lin, F., Zheng, X., and Sehgal, A. (2005). Serotonin modulates circadian entrainment in Drosophila. Neuron *47*, 115–127. https://doi.org/10.1016/j.neuron.2005.05.027.

98. Berry, J.A., Cervantes-Sandoval, I., Chakraborty, M., and Davis, R.L. (2015). Sleep facilitates memory by blocking dopamine neuron-mediated forgetting. Cell *161*, 1656–1667. https://doi.org/10.1016/j.cell.2015.05.027.

99. Riemensperger, T., Issa, A.R., Pech, U., Coulom, H., Nguyễn, M.V., Cassar, M., Jacquet, M., Fiala, A., and Birman, S. (2013). A single dopamine pathway underlies progressive locomotor deficits in a *Drosophila* model of Parkinson disease. Cell Rep. *5*, 952–960. https://doi.org/10.1016/j.celrep.2013.10.032.

100. Connolly, J.B., Roberts, I.J., Armstrong, J.D., Kaiser, K., Forte, M., Tully, T., and O'Kane, C.J. (1996). Associative learning disrupted by impaired Gs signaling in Drosophila mushroom bodies. Science *274*, 2104–2107. https://doi.org/10.1126/science.274.5295.2104.

101. Jovanic, T., Schneider-Mizell, C.M., Shao, M., Masson, J.B., Denisov, G., Fetter, R.D., Mensh, B.D., Truman, J.W., Cardona, A., and Zlatic, M. (2016). Competitive disinhibition mediates behavioral choice and sequences in *Drosophila*. Cell *167*, 858–870.e19. https://doi.org/10.1016/j.cell.2016.09.009.

102. Strother, J.A., Wu, S.T., Wong, A.M., Nern, A., Rogers, E.M., Le, J.Q., Rubin, G.M., and Reiser, M.B. (2017). The emergence of directional selectivity in the visual motion pathway of *Drosophila*. Neuron *94*, 168–182.e10. https://doi.org/10.1016/j.neuron.2017.03.010.

103. Hancock, C.E., Bilz, F., and Fiala, A. (2019). *In vivo* optical calcium imaging of learning-induced synaptic plasticity in *Drosophila melanogaster*. JoVE J. *152*, e60288. https://doi.org/10.3791/60288.

104. Hancock, C.E., Geurten, B.R.H., and Fiala, A. (2020). Visualization of naive and learned odor representations using in vivo calcium imaging

and immunohistochemical bouton mapping of single *Drosophila* mushroom body neurons. STAR Protoc. *1*, 100210. https://doi.org/10.1016/j.xpro.2020.100210.

105. Luo, L., Hina, B.W., McFarland, B.W., Saunders, J.C., Smolin, N., and von Reyn, C.R. (2022). An optogenetics device with smartphone video capture to introduce neurotechnology and systems neuroscience to high school students. PLoS One *17*, e0267834. https://doi.org/10.1371/journal.pone.0267834.

106. Thévenaz, P., Ruttimann, U.E., and Unser, M. (1998). A pyramid approach to subpixel registration based on intensity. IEEE Trans. Image Process. *7*, 27–41. https://doi.org/10.1109/83.650848.

STAR★METHODS

KEY RESOURCES TABLE

REAGENT or RESOURCE	SOURCE	IDENTIFIER
Antibodies		
Mouse anti-discs large (DLG)	Developmental Studies Hybridoma Bank	Cat#4F3; RRID: AB_528203
Rabbit anti-GFP	Invitrogen	Cat#A-6455; RRID: AB_221570
Mouse anti-IgG (Alexa Fluor 633)	Invitrogen	Cat#A-21050; RRID: AB_2535718
Rabbit anti-IgG (Alexa Fluor 488)	Invitrogen	Cat#A-11034; RRID: AB_2576217
Rat anti-Cadherin, DN- (extracellular domain)	Developmental Studies Hybridoma Bank	Cat# DN-Ex #8; RRID: AB_528121
Mouse monoclonal anti-green fluorescent protein (GFP) – clone GFP-20	Sigma-Aldrich	Cat#G6539; RRID:AB_ 259941
Chemicals, peptides, and recombinant proteins		
Triton™ X-100	Sigma-Aldrich	Cat# X100; CAS: 9036-19-5
Bovine Serum Albumin (BSA)	Carl Roth GmbH + Co. KG	Cat#0163; CAS: 90604-29-8
Normal goat serum (NGS)	Invitrogen - Thermo Fisher Scientific	Cat#31873; RRID AB_2532167
Paraformaldehyde (PFA)	Carl Roth GmbH + Co. KG	Cat#0335; CAS: 30525-89-4
Mineral Oil	Sigma-Aldrich	Cat#M8410; CAS: 8042-47-5
4-Methycyclohexanol	Sigma-Aldrich	Cat#153095; CAS: 589-91-3
3-Octanol	Sigma-Aldrich	Cat#218405; CAS: 589-98-0
Benzaldehyde	Sigma-Aldrich	Cat#12010; CAS: 100-52-7
Pentylacetate	Sigma-Aldrich	Cat#109584; CAS: 628-63-7
VECTASHIELD® Antifade Mounting Medium	Vector Laboratories Inc	Cat#H-1000; CAS: Trade Secret
All-trans-retinal	Sigma, MO, USA	Cat# R2500; CAS: 116-31-4
Deposited data		
All processed data (without large raw imaging files)	https://data.mendeley.com/datasets/55cfd3km5c/1	N/A
All raw and processed data	https://for2705.de/archive/5/110	N/A
Code for the fly learning apparatus	https://for2705.de/archive/5/110	N/A
Code for the circuit implementation	https://github.com/nawrotlab/higher_order_learning_circuit	https://doi.org/10.5281/zenodo.14932132
Experimental models: Organisms/strains		
D. melanogaster: Canton-S	Bloomington Drosophila Stock Center	BDSC: 64349; FlyBase: FBst0064349
D. melanogaster: w[1118]	Bloomington Drosophila Stock Center	BDSC: 6326; FlyBase: FBst0006326
D. melanogaster: UAS-Shibire^{ts}	Bloomington Drosophila Stock Center; Kitamoto et al.[45]	BDSC: 44222; FlyBase: FBst0044222
D. melanogaster: MB247BH-GAL4	Elizabeth J. Hong	Generated by Elizabeth J. Hong. (The Hong lab) California Institute of Technology. Department of Biology and Bioengineering. 1200 E. California Blvd M/C 216-76. Pasadena, CA 91125
D. melanogaster: MB009B-splitGAL4	Bloomington Drosophila Stock Center; Aso et al.[34]	BDSC: 68292; FlyBase: FBst0068292
D. melanogaster: MB463B-splitGAL4	Bloomington Drosophila Stock Center; Aso et al.[34]	BDSC: 68370; FlyBase: FBst0068370
D. melanogaster: R44E04-GAL4	Bloomington Drosophila Stock Center; Jenett et al.[95]	BDSC: 50210; FlyBase: FBst0050210
D. melanogaster: TH-GAL4	Bloomington Drosophila Stock Center, Friggi-Grelin et al.[96]	BDSC: 8848; FlyBase: FBst0008848

(*Continued on next page*)

Continued

REAGENT or RESOURCE	SOURCE	IDENTIFIER
D. melanogaster: R58E02-GAL4	Bloomington Drosophila Stock Center; Jenett et al.[95]	BDSC: 41347; FlyBase: FBst0041347
D. melanogaster: MB320C-splitGAL4	Bloomington Drosophila Stock Center; Aso et al.[34]	BDSC: 68253; FlyBase: FBst0068253
D. melanogaster: MB296B-splitGAL4	Bloomington Drosophila Stock Center; Aso et al.[34]	BDSC: 68308; FlyBase: FBst0068308
D. melanogaster: MB058B-splitGAL4	Bloomington Drosophila Stock Center; Aso et al.[34]	BDSC: 68278; FlyBase: FBst0068278
D. melanogaster: MB304B-splitGAL4	Bloomington Drosophila Stock Center; Aso et al.[34]	BDSC: 68367; FlyBase: FBst0068367
D. melanogaster: MB112C-splitGAL4	Bloomington Drosophila Stock Center; Aso et al.[34]	BDSC: 68263; FlyBase: FBst0068263
D. melanogaster: MB077B-splitGAL4	Bloomington Drosophila Stock Center; Aso et al.[34]	BDSC: 68283; FlyBase: FBst0068283
D. melanogaster: MB083C-splitGAL4	Bloomington Drosophila Stock Center; Aso et al.[34]	BDSC: 68287; FlyBase: FBst0068287
D. melanogaster: MB434B-splitGAL4	Bloomington Drosophila Stock Center; Aso et al.[34]	BDSC: 68325; FlyBase: FBst0068325
D. melanogaster: MB210B-splitGAL4	Bloomington Drosophila Stock Center; Aso et al.[34]	BDSC: 68272; FlyBase: FBst0068272
D. melanogaster: MB027B-splitGAL4	Bloomington Drosophila Stock Center; Aso et al.[34]	BDSC: 68301; FlyBase: FBst0068301
D. melanogaster: MB018B-splitGAL4	Bloomington Drosophila Stock Center; Aso et al.[34]	BDSC: 68296; FlyBase: FBst0068296
D. melanogaster: MB543B-splitGAL4	Bloomington Drosophila Stock Center; Aso et al.[34]	BDSC: 68335; FlyBase: FBst0068335
D. melanogaster: MB057B-splitGAL4	Bloomington Drosophila Stock Center; Aso et al.[34]	BDSC: 68277; FlyBase: FBst0068277
D. melanogaster: MB399B-splitGAL4	Bloomington Drosophila Stock Center; Aso et al.[34]	BDSC: 68369; FlyBase: FBst0068369
D. melanogaster: MB091C-SplitGal4	Aso et al.,[34] Gift from Aso, Y	N/A
D. melanogaster: 5HT1B-GAL4	Bloomington Drosophila Stock Center; Yuan et al.[97]	BDSC: 27637; FlyBase: FBst0027637
D. melanogaster: UAS-GCaMP6f	Bloomington Drosophila Stock Center; Chen et al.[62]	BDSC: 52869; FlyBase: FBst0052869
D. melanogaster: 20XUAS-CsChrimson-mCherry (VK00005)	Bloomington Drosophila Stock Center; Klapoetke et al.[66]	BDSC: 82180; FlyBase: FBst0082180
D. melanogaster: 13XLexAop2-IVS-GCaMP6m-p10 (attp1)	Bloomington Drosophila Stock Center; Strother et al.[98]	BDSC: 44275; FlyBase: FBst0044275
D. melanogaster: TH-LexA (2rd)	Berry et al.,[98] Gift from Davis, R	N/A
D. melanogaster: UAS-mCD8::GFP, UAS-n-syb::GFP	Riemensperger et al.[99]	N/A
D. melanogaster: UAS:sypGCaMP3; syp3xpHTomato	Pech et al.[55]	N/A
D. melanogaster: GRASP recombination: Mb247-GFP11; UAS-GFP1-10	Pech et al.[54]	N/A
D. melanogaster: UAS-dTrpA1	Hamada et al.[68]	BDSC: 26263 FlyBase: FBst0026263
D. melanogaster: 10xUAS-GRAB(Ach3.0)	Jing et al.[64]	BDSC: 86550 FlyBase: FBst0086550
D. melanogaster: UAS-syt.eGFP	Zhang et al.[58]	BDSC: 6925 FlyBase: FBst0006925

(*Continued on next page*)

Continued

REAGENT or RESOURCE	SOURCE	IDENTIFIER
D. melanogaster: OK107-GAL4	Connolly et al.[100]	BDSC: 854 FlyBase: FBst0027637
Software and algorithms		
ImageJ	N/A	https://imagej.nih.gov/ij/
Zen 2011 SP4 (black edition)	Carl Zeiss AG	https://www.micro-shop.zeiss.com/de/de/softwarefinder/software-categories/zen-black/
Leica Application Suite X (LASX; software)	Leica Microsystems GmbH	https://www.leica-microsystems.com/products/microscope-software/p/leica-las-x-ls/
Ethovision XT15	Noldus	https://www.noldus.com/ethovision-xt
Pylon Viewer 64-Bit	Basler AG	https://www.baslerweb.com/en/downloads/software-downloads/
OriginPro 2020	OriginLab Corp.	https://www.originlab.com/index.aspx?go=Products/Origin
GraphPad Prism 9	GraphPad Software, San Diego, California USA	https://www.graphpad.com
Arduino	Arduino	https://www.arduino.cc
Other		
Two-photon microscope	Carl Zeiss AG	LSM 7MP
Two-photon microscope	Carl Zeiss AG	LSM880
Chameleon laser	Coherent Inc.	Chameleon Ultra Ti:Sapphire Laser
Ti-Sapphire laser	Spectra-Physics, CA, USA	Mai Tai HP 1040S
Water Immersion Objective W Plan-Apochromat 20×	Carl Zeiss AG	Cat# 421452-9800-000
High-power LED driver	Doric Lens	N/A
Confocal laser scanning microscope	Leica Microsystems GmbH	SP8 LIGHTNING confocal microscope
Microscope slides	Carl Roth GmbH + Co. KG	Cat#0656
Blue light curing glue	NorDenta - Kent Dental	Cat#953683
Blue light lamp (Starlight pro)	Mectron Deutschland GmbH	Cat#05100083
Fine forceps - mirror finish	Fine Science Tools GmbH	Cat#11412-11
Surgical scalpel blade no.11	Swann-Morton	Cat#0303
Surgical scalpel handle no. 7	Swann-Morton	Cat#0907
Insect Minutien pins	Fine Science Tools GmbH	Cat#26002-10
Blade holders & breakers -Concave-convex jaws	Fine Science Tools GmbH	Cat#10053-09
Microknife	Fine Science Tools GmbH	Cat#10315-12

EXPERIMENTAL MODEL AND STUDY PARTICIPANT DETAILS

Drosophila strains and genotypes

Flies were reared on standard cornmeal food medium in incubators maintained at 25°C and 60% relative humidity with a 12hr/12hr light/dark cycle. The lines that were used throughout this study are: For the behavioral study, wild-type Canton-S flies were used to establish the learning paradigm. In addition, different specific GAL4 driver lines were crossed to UAS-*Shibire*^{ts} (BDSC #44222), UAS-*d*TrpA1 (BDSC #26263), and to W[1118] (BDSC #6326) flies to obtain the experimental lines in the filial generations. The following driver lines were used: Mushroom body: All Kenyon cells (MB247*-GAL4/CyO, generated by Elizabeth Hong and published in this study), α/β Kenyon cells (R44E04-GAL4, BDSC #50210), α′/β′ Kenyon cells (MB463B, BDSC #30829), and γ Kenyon cells (MB009B, BDSC #68292). Split-GAL4 driver lines used to drive expression in MBONs were obtained from the Bloomington Drosophila Stock Center: MBON-γ1pedc>α/β (MB112C, BDSC #68263), MBON-γ2α′1 (MB077B, BDSC #68283), MBON-γ3 and MBON-γ3β′1 (MB083C, BDSC #68287), MBON-γ4>γ1γ2 (MB434B, BDSC #68325), MBON-γ5β′2a, MBON-β′2mp (MB210B, BDSC #68272), MBON-α′1 (MB543B, BDSC #68335), MBON-α′2 (MB018B, BDSC #68296), MBON-α′3ap and MBON-α′3m

(MB027B, BDSC #68301), MBON-β′1 (MB057B, BDSC #68301), and MBON-β2β′2a (MB399B, BDSC #68369). PPL1 cluster: All PPL1-DANs (TH-GAL4, BDSC #8848), PPL1-γ1pedc (MB320C, BDSC #68253), PPL1-γ2α′1 (MB296B, BDSC #68308), PPL1-α′2α2 (MB058B, BDSC #68278), and PPL1-α′3 (MB304B, BDSC #68367). PAM cluster: All PAM-DANs (R58E02-GAL4, BDSC #41347). The resulting offspring was reared at 18°C and 60% relative humidity.

For two-photon imaging, the reporter lines that were used to evaluate pre- and post-calcium activity and during second-order training are 10xUAS-GRAB(Ach3.0),[64] UAS-GCaMP6f (BDSC #52869) crossed to MB112C (MBON-γ1pedc>α/β) and MB018B (MBON-α′2). For the electric shock imaging protocol syp-GCaMP3; syp3x-pHTomato[55] was crossed to MB320C (PPL1-γ1pedc), MB296B (PPL1-γ2α′1), MB058B (PPL1- α′2α2) and MB315C (PPL1-γ5, BDSC #68316). For optogenetic activation and simultaneous optical imaging, 20XUAS-CsChrimson-mCherry[101] and 13XLexAop2-IVS-GCaMP6m-p10[102] were crossed to MB091C (MBON-α′2), MB112C (MBON-γ1pedc>α/β) and TH-LexA.[98] For confocal imaging of the IHC, GAL4 driver lines were crossed to UAS-mCD8:GFP-nsyb:GFP[99] and GRASP recombination: MB247-GFP11; UAS-GFP1-10.[54]

METHOD DETAILS

Aversive olfactory conditioning

The flies were trained and tested in a custom-built conditioning apparatus (Figures S1A and S1B). All experiments were performed at a humidity of 65–85% and a temperature ranging from either 21°C–25°C for normal conditions or 29°C–30°C for *shibire*^{ts} restrictive conditions and *d*TrpA1 permissive conditions. To achieve this, two separate set-ups were designated in different boxes to maintain the desired temperature. Each set-up contained a training and a testing apparatus. For the training phase, the flies were placed in double-wired copper electric tubes that were connected to a voltage generator and a vacuum. A custom-built and Arduino programmed shock/odor-delivery controlling device was connected and provided input to the different components of the machine (see Arduino code for training and testing machine). The input from this device delivered a precise and automatic spatiotemporal modulation to the voltage generator and the valves of the olfactometer. To present the odors in the training tubes, air flowed through the odor bottles at a rate of 0.20–0.25 L per minute.

For first-order conditioning, around 30 flies aged 3 to 7days were loaded into four separate training tubes that were trained and then tested. During training, the flies received the shock and the odors according to the classical conditioning paradigm.[44] CS1 was presented for 60 s together with 12 × 1.25-s pulses of 90V shocks every 5 s, followed by 60 s of blank odor, and then finally CS^{-} was introduced in the tubes for 60 s. Reciprocal training was accounted for. For second-order conditioning experiments, the flies received the shock and the odors according to the protocol described.[13] The second-order conditioning paradigm was comprised of three phases: a first training phase, a second training phase, and testing (Figure 1B). The reinforcer and the stimuli were temporally paired in the standard second-order conditioning paradigm, also referred to as 'Paired-Paired' (Figure 1B). In the first training phase, 3- to 7-day-old flies were placed into double-wired copper electric tubes that were connected to electric wires and the vacuum. During training, they were first exposed to a blank odor (mineral oil) for 90 s. Next, CS1 was presented for 60 s together with 12 × 1.25-s pulses of 90V shocks every 5 s, followed by another 45 s of the blank odor. In the end, CS^{-} was presented in the tubes for 60 s. This training cycle was repeated three times with 10 min intervals in between. In the second training phase, the flies received another presentation of a blank odor for 90 s followed by 7 s of CS2. For the next 60 s, CS2 was dispensed in a continuous airflow paired with 12 x 4-s pulses of CS1 alternating with the blank odor every 5 s. The blank odor was then presented alone for 45 s to flush any odor contamination during this phase. This cycle was also repeated three times at 10 min intervals. Control experiments were conducted such as the reinforcer and the stimuli were either unpaired during the first or the second training phases. The first control experiment "paired-unpaired" (Figure 1B) consisted of unpairing the CS1 and CS2 odors during the second training phase, which resulted in 60 s of CS2 presented alone, followed by 45 s of blank odor, then 60 s of CS1. In the second control experiment "unpaired-paired" (Figure 1B), the electric shocks and the CS1 odor were presented separately during the first training phase (60 s of CS^{-}, followed by 45 s of blank and 60 s of CS1, then another 45-s blank followed by 12 × 1.25-s pulses of 90V shocks every 5 s). Third-order conditioning experiments consisted of adding one more training phase (training phase 3) to the second-order conditioning paradigm. In this phase, a blank odor was presented for 90 s followed by 7 s of CS2, then followed by a continuous airflow of CS3 paired with 12 x 4-s pulses of CS2 alternating with the blank odor every 5 s. Control experiments were conducted where the reinforcer and the stimulus were unpaired during the first, second, or third training phases (Figure 7B). For the testing phase, the flies were transferred after the training from the electric tubes to the central carrier of the testing arena. Composed of four lanes, this arena matched the training tubes in number. A second controlling device was connected to the testing arena along with its respective olfactometers (one for each side) so that, according to the program, the two selected odors were presented from either the left or the right side of the arena. The air pressure was maintained to be the same in comparison to the training tubes (0.20–0.25 LPM). When the lever of the central carrier was pushed down, the flies had 2 min to choose one of the two sides of the arena. This phase was recorded by a high-speed camera (Basler GigE camera acA 1300–60gc/CS – mount) with an objective (Lens Kowa 4.4–11mm zoom lens) that was equipped with an IR filter. During the testing phase, multiple IR-LED bulbs are switched on from under the arena for video acquisition. We used four different odorants, benzaldehyde (1:100), 3-octanol (1:10), 4-methylcyclohexanol (1:10), and pentyl acetate (1:10). While 4-methylcyclohexanol and 3-octanol were reciprocally used as CS1 and CS^{-} to account for odor bias, benzaldehyde remained as CS2 and pentyl acetate remained as CS3 in all experiments. Control experiments demonstrated that all other possible odor

combinations showed no significant difference (Figure S1E). The positions of the odors in the testing phase were also reversed to account for side bias by switching the odor presentations from the left and right olfactometer.

In vivo functional imaging

Fly brains were prepared for *in vivo* imaging as described in Hancock et al.,[103,104] and this procedure was used in all imaging experiments performed with a two-photon microscope. Single flies were cold anesthetized by putting them on a previously cooled-down steel plate on ice. Once immobilized, the fly was then moved to a custom-built chamber, in which the head was placed on a small pedestal to ensure contact with the tape. A small window was carefully cut into the tape to expose the head capsule while the antennae and the thorax remain covered. Moreover, the head was hindered from further movement by applying UV-hardening glue around the sides of the cut window and setting it with a special UV-emitting lamp to limit movement of the sample, and thus disruption of the imaging experiments. The head capsule was then covered with 2–3 drops of RT Ringer's solution to ensure adequate physiological conditions during the dissection and avoid dryness of the brain. A micro blade was used to open the head capsule by making a first incision into the ocelli, followed by two perpendicular cuts along the left and right sides of the of the head capsule. After removing the cuticle and the excess fat tissue with fine forceps, the Ringer's solution was refreshed and the chamber was allocated to the mechanical stage of the microscope to start image acquisition. Prepared flies were placed under the microscope objective lens and connected to a custom-built odor delivery device. Excitation wavelengths of 920 nm (for GCaMP6f, GRAB Ach3.0 and G-Flamp1) and 950 nm (for syp-GCaMP3 and syp-pHTomato) were used for image acquisition, which was controlled using Zeiss Zen (2011 SP4 black edition) software. Images were captured at a frame rate of 4 Hz and with a frame size of 512 × 512 pixels. Simultaneous odor delivery, shock pulses, and image acquisition were controlled via a custom-built controlling device. Three odorants were used in all experiments, as follows: 4-methylcyclohexanol, 3-octanol, and benzaldehyde, at concentrations of 1:10, 1:10, and 1:100, respectively, and were diluted in mineral oil. To monitor the effects of second-order conditioning, a three-step imaging protocol was used. First, flies were sequentially presented with the three odors to assess naive odor-evoked responses by monitoring the changes in fluorescence (pre-training). The second step immediately followed the first and consisted of exposing the flies to any of the three second-order conditioning protocols (Paired-Paired, Paired-Unpaired, or Unpaired-Paired). Third, the flies were again presented with the three odorants and their responses were measured (post-training). This final imaging step was carried out 3–4 min after the end of the respective conditioning protocol. In the first and third steps, all odor presentations lasted for 3 s and were separated by an interval of approximately 40 s. For the shock-imaging protocol, image acquisition started 30 s before the first electric pulse. The imaged shock protocol consisted of 90V x 12 pulses of 1.25 s presented every 5 s for a total duration of 1 min, followed by 30 s of imaging after the shock protocol.

Optogenetic stimulation and calcium imaging

1- to 3-day-old flies were fed with regular fly food containing 0.4 mM all-trans-retinal for 48–72 h in the dark at 23°C and 60% humidity. The fly brain was then dissected in imaging buffer (103 mM NaCl, 3 mM KCl, 26 mM $NaHCO_3$, 1 mM NaH_2PO_4, 1.5 mM $CaCl_2$, 4 mM $MgCl_2$, 8 mM trehalose, 10 mM glucose, 5mM TES, osmolarity 275 mOsm, pH 7.3) and placed in a recording chamber (PH-5 & RC-20, Wanner Instrument). The brain was perfused with imaging buffer mixed with 95% O_2 and 5% CO_2 for 5 min before being imaged under a two-photon microscope with a 20× water-immersion objective lens (Zeiss LSM880). The fluorescence signal of GCamp6m expressed in PPL1-γ1pedc DANs was excited by a 910-nm, two-photon laser (Spectra-Physics, CA, USA; Mai Tai HP 1040S). The GCaMP6m signals were captured at 9.63 frames per sec with an 80 × 100 pixel resolution. Each brain was recorded twice, for 500 frames each, and the interval between the two recordings was 10 s. During each recording, the baseline GCaMP6m signals were collected for 20 s (∼185 frames), followed by the stimulation of CsChrimson-expressing MBONs with a 633-mm LED light for 0.5 s (40 Hz, 20 pulses with a 10 msec pulse duration). The GCaMP6m signals from the two recordings were averaged to generate a mean signal trace for subsequent data analysis. In the experiments where we activated MBON-γ1pedc>αβ and recorded responses in PPL1-γ1pedc DAN axonal terminals in the γ1 compartment, the baseline GCaMP6m signals were barely detectable. This subdued baseline signal was not observed in the UAS-CsChrimson-only control flies. We reasoned that this low baseline was due to the activation of the GABAergic MBON-γ1pedc>αβ by the two-photon laser. Consequently, we did not feed the flies retinal in this set of experiments, as CsChrimson has been shown to retain a reduced level of efficacy in neurons with low activation thresholds.[105] This approach restored the baseline signal and maintained the response of MBON-γ1pedc>αβ to the red LED stimulation.

Immunohistochemistry

Flies first had to be immobilized by placing them on ice in empty vials for about 5 min. A single fly was then fixed on a dissection plate, dorsal side down, with two pins placed into the thorax and then covered with Ringer's solution. Brains were extracted in Ringer's solution (5 mM KCl, 130 nM NaCl, 2 mM $MgCl_2$, 2 mM $CaCl_2$, 5 mM HEPES, 36 mM sucrose, pH 7.3) by swiftly removing the proboscis and detaching the brain from the head capsule. Brains were then fixed in 4% paraformaldehyde at room temperature for 45 min, and then washed three times for 30 min each in PBS with 0.6% Triton X-. Brains were then incubated at 4°C overnight in blocking solution containing 2% bovine serum albumin and 2% normal goat serum. Subsequently, brains were incubated with anti-GFP primary antibody (rabbit anti-GFP, Invitrogen A6455) at a concentration of 1:2000 and, an anti-discs large (DLG) primary antibody (mouse anti-DLG, Developmental Studies Hybridoma Bank 4F3) was used at a concentration of 1:200 to visualize brain structures. For the GRASP

experiments, anti-splitGFP (mouse monoclonal anti-green fluorescent protein (GFP) – clone GFP-20, Sigma-Aldrich G6539) was used at a concentration of 1:2000, and anti-Cadherin (Rat anti-Cadherin DN-extracellular domain, Developmental Studies Hybridoma Bank DN-Ex #8) at a concentration of 1:50 was used for background staining. Brains were incubated in primary antibody solution for 1 day at 4°C, and washed again three times in PBS with Triton X- before incubation in secondary antibody. Secondary antibodies anti-rabbit Alexa Fluor 488, anti-mouse Alexa 633, and anti-rat Alexa 633 were used at a concentration of 1:300 for 1 day at 4°C. Brains were washed again three times in PBS with Triton X-, and then mounted in VectaShield for confocal scanning.

Confocal microscopy

A Leica SP8 line-scanning confocal microscope was used to image the stained brains. An argon laser of wavelength 488 nm and a HeNe-laser of 633 nm were used to excite the corresponding secondary antibodies. Scanning and image acquisition were performed using Leica LSAX software. Laser intensity and hybrid detector gains were optimized to ensure minimal noise and bleaching. The brains were then scanned using a 20× objective and 1024×1024 resolutions with a 2 frame averaging, and Z-stacks were acquired as LIF files for processing.

Reconstruction of neuronal connections with the neuPrint database

Reconstruction and synaptic quantification of the connectivity of the PPL1-γ2α′1 DAN and MBON-α′2 in the α′2 compartment of the mushroom body, along with connectivity between MBON-γ1pedc>α/β, MBON-γ5β′2a, MBON-β2β′2a, MBON-β′2mp, and MBON-α′2, was performed using the neuPrint database: Analysis Tools for EM Connectomics by Janelia (link in key resource table). Identification numbers for the used neurons are as follows: PPL1-γ2α′1 DAN (id #5813022424), MBON-α′2 (id #1139667240), MBON-γ1pedc>α/β (id #424767514), MBON-γ5β′2a (id #612371421), MBON-β2β′2a (id #424789697), and MBON-β′2mp (id #612738462). The reconstruction images were obtained in 'skeleton view' mode along with allowing only the mushroom body lobes to show using the scroll bar and selecting the regions of interest. The synaptic connectivity quantification was gained by adding input/output from α′2 compartment of the mushroom body by allowing all brain regions and selecting a′2(R) in the scroll down menu 'output brain regions' of 'find neurons'.

Second-order conditioning circuit computational modeling

We implemented a simple mechanistic model in Python to explore the performance of the proposed circuit (Figure 6A) in simulated second-order conditioning experiments. In the computational model, the activation of each neuron is denoted by the spike rate. The network consists of 2000 KCs, each innervating MBON-γ1pedc>α/β and MBON-α′2, with initially uniform synaptic weights (KC-MBON-γ1pedc>α/β = 0.035nS and KC-MBON-α′2 = 0.035nS). Two DANs (PPL1-γ1pedc and PPL1-γ2α′1) modulate the weights at the KC-MBON-γ1pedc>α/β and KC-MBON-α′2 synapses, respectively. MBON-γ1pedc>α/β provides inhibitory and MBON-α′2 excitatory feedback onto PPL1-γ1pedc DAN.

Odor and punishment signals are provided via input to the KCs and the DANs. Each odor exclusively activates 10% of the KCs with a rate of 10Hz. Odor 1 (CS1) and odor 2 (CS2) activate fully independent sets of KCs. The compound odor, consisting of both components, activates 50% of the KCs activated by each individual odor to maintain an overall 10% active KCs.[27] PPL1-γ1pedc DAN and PPL1-γ2α′1 DAN are each activated by punishment with a spike rate of 20Hz, and PPL1-γ1pedc DAN receives additional input from both MBONs. The sum of activation of PPL1-γ1pedc DAN is then transformed via a sigmoid transfer function with a scaling factor (Equation 1). All equations use abbreviated versions of neuron names.

$$DAN\gamma 1 = \frac{1}{1+2000 \times e^{DAN\gamma_1 \times 2}} \times 10 \qquad \text{(Equation 1)}$$

Trial-based co-occurrence of odor-driven KC activation and DAN activation by punishment triggers plasticity at the KC-MBON synapses. For each odor-activated KC, the respective KC-MBON-γ1pedc>α/β weight is decreased by applying a multiplicative learning rule (Equation 2) depending on the spike rate of the PPL1-γ1pedc DAN and the learning rate (α_1 = 0.0009).

The KC-MBON-α′2 synapses (Equation 3) are initially depressed and then facilitated, similar to previous experimental observation.[87,88] However, the exact mechanism differs in that only previously depressed synapses undergo facilitation. We hypothesize that the dopamine released by PPL1-γ2α′1 DAN is causing the synaptic depression. The exact cellular mechanism that induces a bidirectional switch from depression to potentiation due to non-reinforced odor stimulation is not known. However, previous studies have shown that co-transmitters (CT) released by DANs can have opposing effects on synaptic weights.[88] This simultaneous release of dopamine and a CT could potentially explain the experimentally observed flip from depression to facilitation after first-order conditioning (Figure 4D), and we have implemented a hypothetical CT factor as a potential signaling mechanism in the absence of electric shock. In the model, the direction and magnitude of the synaptic weight change depend on the difference between the activity of PPL1-γ2α′1 DAN and the CT, multiplied by the learning rate (α_2 = 0.0009). Depression of the KC-MBON-α′2 synapses is the primary effect of the PPL1-γ2α′1 DAN activity. It represents the effect of the released dopamine when the neuron is activated by external punishment during first-order conditioning. While PPL1-γ2α′1 DAN is active, the term CT increases, depending on the activity of PPL1-γ2α′1 DAN and a scaling factor (Equation 4) and is transformed via a sigmoid transfer function with a scaling factor (Equation 5). Once the value of CT exceeds the activity value of PPL1-γ2α′1 DAN (Equation 3), the direction of the synaptic plasticity flips from depression to facilitation.

Weight change for all KC-MBON synapses is bound. In the case of depression, a single KC-MBON-γ1pedc>α/β cannot become negative, and the growth of KC-MBON-α′2 weights is limited to a value of 2. The initial synaptic weights and learning rates were optimized to reproduce the data (Figure S5), showing that the effect of first-order conditioning tends to be stronger than that of second-order conditioning in *Drosophila.*[14]

$$w_{KC-MBON\gamma1} = \begin{cases} w_{KC-MBON\gamma1} - (DAN\gamma_1 \times \alpha_1), if\ KC > 0,\ w_{KC-MBON\gamma1} > (\alpha_1 \times DAN\gamma_1) \\ 0, if\ KC > 0, w_{KC-MBON\gamma1} \leq (\alpha_1 \times DAN\gamma_1) \\ w_{KC-MBON\gamma1}, otherwise \end{cases} \quad \text{(Equation 2)}$$

$$w_{KC-MBON\alpha'2} = \begin{cases} w_{KC-MBON\alpha'2} - ((DAN\gamma_2\alpha'_1 - CT) \times \alpha_2), if\ KC > 0,\ w_{KC-MBON\alpha'2}\langle(2 - \alpha_2 \times (DAN\gamma_2\alpha'_1 - CT)) \\ 0, if\ KC > 0, w_{KC-MBON\alpha'2} \leq (\alpha_2 \times (DAN\gamma_2\alpha'_1 - CT)) \\ 2, if\ KC > 0, w_{KC-MBON\alpha'2} - (\alpha_2 \times (DAN\gamma_2\alpha'_1 - CT)) \geq 2 \\ w_{KC-MBON\alpha'2}, otherwise \end{cases} \quad \text{(Equation 3)}$$

$$CT = CT + DAN\gamma_2\alpha'_1 \times 0.7 \quad \text{(Equation 4)}$$

$$CT = \frac{1}{1+10000000 \times e^{-CT \times 0.5}} \times 40 \quad \text{(Equation 5)}$$

A second version of the circuit model (Figure 6H) is based entirely on the circuit described above, and all shared parameters are kept at the same values to allow a comparison between the mechanisms in both circuit models. It includes the additional MBON-β2β′2a that receives input from the KCs with a fixed weight for each synapse (0.035ns) and inhibits MBON-α′2 via a single synapse (2.0nS). MBON-β2β′2a receives inhibitory input from MBON-γ1pedc>α/β via a single synapse (2.0nS). None of these additionally introduced synapses are plastic.

Both versions of the model are trained in a simulated associative learning experiment with three first-order conditioning trials followed by three second-order conditioning trials. CS1 is paired with punishment during first-order conditioning trials, while second-order conditioning trials combine the presentation of CS1 and CS2. The behavioral bias (Equation 6) is computed based on the MBON-γ1pedc>α/β rate, which serves as an approximation of the preference index reported in behavioral animal experiments and is assessed before the first first-order conditioning trial and following the last second-order conditioning trial:

$$Behavioural\ Bias = \frac{\text{MBON}\gamma1_{CS1/CS2} - \text{MBON}\gamma1_{CS-}}{\text{MBON}\gamma1_{CS1/CS2} + \text{MBON}\gamma1_{CS-}} \quad \text{(Equation 6)}$$

To test whether each model reproduces the results of the behavioral animal experiments, additional simulation experiments were conducted that suppressed the output of different types of neurons during first-order conditioning, second-order conditioning, or retrieval.

The code for the circuit implementation can be obtained at https://github.com/nawrotlab/higher_order_learning_circuit.

QUANTIFICATION AND STATISTICAL ANALYSIS

Two-photon image processing

Images were processed using *ImageJ* (https://imagej.nih.gov/ij/). Small movements on the X and Y axes were corrected using the TurboReg plugin.[106] The desired structures of the mushroom body were manually drawn to encircle the entire dendritic arborization, thus highlighting the regions of interest (ROIs). In the case of imaging Kenyon cells, the borders of the mushroom body compartments that were to be analyzed can be unambiguously recognized by the differential fluorescence intensity at compartment boundaries[28] (see Video S2). The fluorescent intensity throughout the recording period was then multi-measured from these ROIs and used to calculate the normalized relative change in fluorescence over time (ΔF/F0) for each recording. This normalized relative fluorescence was calculated by obtaining the average fluorescence intensity over the 2 s preceding odor delivery (baseline or F0), and ΔF was calculated by subtracting this value at each time point of the measurement. In order to statistically compare responses pre- and post-training, the area under the curve (AUC) of each ΔF/F0 of these responses was quantified. The AUC was integrated from odor onset to 2 s after its offset. Before pooling the data together by arranging those in their respective CS1, CS^-, or CS2 slot, the large variability in odor responses between the odors was accounted for, and the AUC values were normalized within each experimental group (all responses to each odor were normalized to the mean pre-training response to that odor). Statistical analyses consisted of comparing pre and post values using paired sample *t* tests in case of normally distributed datasets, and Paired Sample Wilcoxon Signed Rank Test in the opposite case. For multiple comparisons to control the Type I error rate between groups, we performed a Bonferroni Correction.

CellPress
OPEN ACCESS

Behavioral statistical analysis

To analyze the flies' learned behavior, an endpoint calculation was made at the end of the 2-min time window of the testing phase. Flies were counted on each lane for both sides of the testing arena. Preference index 1 was calculated (PI_1) according to Equation 7, wherein **A** stands for the number of flies that chose the CS1 odor (for classical conditioning) or CS2 (for second-order conditioning), and **B** represents the number of flies that chose the CS^- odor. The performance index 2 (PI_2) corresponded to the reciprocal training and was similarly calculated.

$$PI_1 = \frac{A - B}{A+B} \quad \text{(Equation 7)}$$

As stated in Equation 8, the mean value of the performance indices was then calculated to obtain the flies' learning index (LI).

$$LI = \frac{PI_1 + PI_2}{2} \quad \text{(Equation 8)}$$

Analysis of raw data was performed with OriginPro2020. First, a Shapiro-Wilk test was performed to verify the normal distributions of the groups. If the groups exhibited a normal distribution, Bonferroni-corrected, two-tailed one-sample *t* tests were performed with to test the hypothesis of means against 0, and two-tailed, two-sample *t* tests were performed to test the difference in between the experimental and genetic control groups. A one-way ANOVA with a Tukey post-hoc test was used to assess differences among 3 or more groups. For data that did not follow a normal distribution, a Wilcoxon signed-rank test with a Bonferroni correction was performed to test the hypothesis of medians against 0, and Mann–Whitney U tests were executed to assess differences among the groups. A Kruskal-Wallis ANOVA with a Dunn's post-hoc test was carried out to test the difference between 3 or more groups.

Confocal microscopy image processing

All confocal image processing was conducted using ImageJ (NIH). The stacks were separated by channel; the slices of interest in the z stack were transformed into a single Z-projection for each channel and the brightness and contrast adjusted to minimize background noise. The two channels were then merged to obtain an overlay picture showing the structures of interest. For the GRASP experiments, the stacks stained with the brain structure antibody (N-cadherin) were meticulously screened to draw the different compartments of the mushroom body. The borders of the mushroom body compartments that were to be analyzed can be unambiguously recognized by the differential fluorescence intensity at compartment boundaries (see Video S1). The annotations in Video S1 were added using the ImageJ plugins SPIM_DrawArrowInMovie_-14.0.0 and TimeStamper2. For comparison of GRASP volumes, the channels were separated. The 3D volume covered by the GFP signal was segmented using the 3D Objects Counter plug-in with equal thresholds for all samples. Representatives were generated using the same method as in the main figure.

Analysis of synaptic distances with NeuPrint phyton code

To analyze the spatial relationship between dopaminergic and KC-MBON synapses, we used Neuprint-Python API to extract the relevant information for this study. We calculated pairwise Euclidean distances between all PPL1-$\gamma 2\alpha'1$ or PPL1-$\alpha'2\alpha 2$ pre-synapses and KC-to-MBON-$\alpha'2$ synapses. Distances were initially computed in voxel units (8 nm per voxel) and converted to micrometers. Based on previous studies of dopamine diffusion in *Drosophila*,[61] we used a threshold of 2 μm as the maximum effective distance for dopaminergic modulation.

To determine whether the observed spatial relationships were significantly different from random arrangement, we implemented a spatial randomization analysis (Monte Carlo analysis). For each neuron type (PPL1-$\gamma 2\alpha'1$, PPL1-$\alpha'2\alpha 2$, and MBON-$\alpha'2$), we preserved their spatial bounds by identifying the minimum and maximum coordinates in each dimension (x, y, z) from the original data. We then generated random distributions by repositioning each neuron's synapses uniformly within their respective spatial bounds while maintaining the original number of synapses. This approach preserves the basic spatial constraints of the $\alpha'2$ compartment while disrupting any specific spatial organization between dopaminergic and MBON synapses. For each randomization iteration (n = 10 million), we calculated the percentage of KC-MBON synapses within the 2 μm diffusion threshold of dopaminergic synapses. This generated null distributions representing the expected percentage of synapses within range if spatial positioning was random. We compared our observed percentages to these null distributions to calculate p-values, defined as the proportion of random iterations that produced percentages equal to or more extreme than the observed values. Additionally, we computed 95% confidence intervals from the null distributions to estimate the range of percentages expected under random spatial organization. This analysis allowed us to test whether the observed spatial proximity between dopaminergic and KC-MBON synapses represents specific organizational principles rather than random chance while accounting for the physical constraints of the neural compartment. A significantly higher percentage of proximate synapses compared to the null distribution suggests selective positioning of dopaminergic inputs near KC-MBON synapses, while a significantly lower percentage suggests spatial segregation.

2.2 A Connectome-Based Approach for Investigating Neural Circuits of Odor Mixture Processing

– manuscript in preparation–

Contribution: The study was conceptualized by Martin P. Nawrot, Silke Sachse, Pramit Bandyopadhyay and Magdalena Springer (MS). The physiological data shown in Fig. 4A,B were obtained from Mohamed et al. (2019). All data analysis and modeling, visualization, and writing were performed by MS.

A Connectome-Based Approach for Investigating Neural Circuits of Odor Mixture Processing.

Animals can suppress their response to attractive stimuli when these are mixed with aversive ones. This behavioral phenomenon is central to understanding how the brain integrates conflicting sensory valences. Recent studies in the fruit fly have focused on exploring the underlying neuronal circuit in the antennal lobe, which serves as the primary station for odor processing. It has been observed that local interneurons within selected regions of the antennal lobe establish inhibitory synapses from aversive to appetitive glomeruli, that effectively suppress their output during presentation of mixtures containing both aversive and appetitive odors. In this project, our objective is to establish a connection between the observed functionality and the structural organization of the fly antennal lobe. For this purpose, we conduct a comprehensive analysis of the connectome data available for the antennal lobe. Our findings reveal a highly innervated structure with distinct lateralization between aversive and appetitive glomeruli. However, the connectome data alone does not provide sufficient evidence to support a significant directed pattern from aversive to appetitive units. To bridge this gap, we construct a computational spiking model that comprises the neural circuitry of the fly antennal lobe. By fine-tuning the model, we want to accurately reproduce the experimental results obtained from our experimental collaborators. To this end, we aim to make predictions on how the synapses within the antennal lobe network are weighted and which neural circuits shape sensory processing and information integration in the fly olfactory system.

Fly Connectome | Information Integration | Spiking Neural Network

In complex natural environments, animals are often confronted with combinations of different sensory stimuli and must integrate this information to make appropriate decisions (1, 2). One instance of information integration is mixture inhibition, where animals need to evaluate whether to approach mixture of appetitive and aversive stimuli, and may avoid the mixture if the aversive component outweighs the appetitive one (3–5). This behavioral strategy can be ecologically highly relevant, for example to help the animal to avoid a potentially contaminated food source. In the fruit fly *Drosophila melanogaster* and other insects, the neuronal basis of odor mixture inhibition has been linked to computations in the antennal lobe (AL), the primary olfactory processing center (2, 6–9). The AL is organized in a glomerular structure, with each glomerulus responding to specific olfactory stimuli (10–12). In each glomerulus, incoming axons from olfactory sensory neurons (OSNs) target projection neurons (PNs), which then convey the information to higher brain regions (13–15). Local interneurons (LNs) form dense networks within the AL, shaping response properties of PNs and OSNs. They are characterized by their high diversity in terms of their morphology, their activation and innervation patterns, and their neurotransmitter constitution (16–24). LNs contribute to multiple aspects of odor processing, such as gain control, odor discrimination, and habituation (25–29). A study by Mohamed *et al.* (9) has demonstrated how these local circuits in the AL also contribute to odor mixture inhibition. Behavioral experiments showed that when a low concentration of an appetitive odor presented together with an aversive odor, the aversive odor partially suppresses the attraction towards the appetitive odor. Using two-photon imaging, the authors could demonstrate that a subpopulation of LNs mediate cross-talk between glomeruli during processing of odor mixtures of opposing valence. More specifically, inhibitory LNs get activated by repellent-responsive glomeruli and in turn suppress activation in attractant-responsive glomeruli. This directed inhibition then drives the suppressed behavioral attraction. The recent emergence of large-

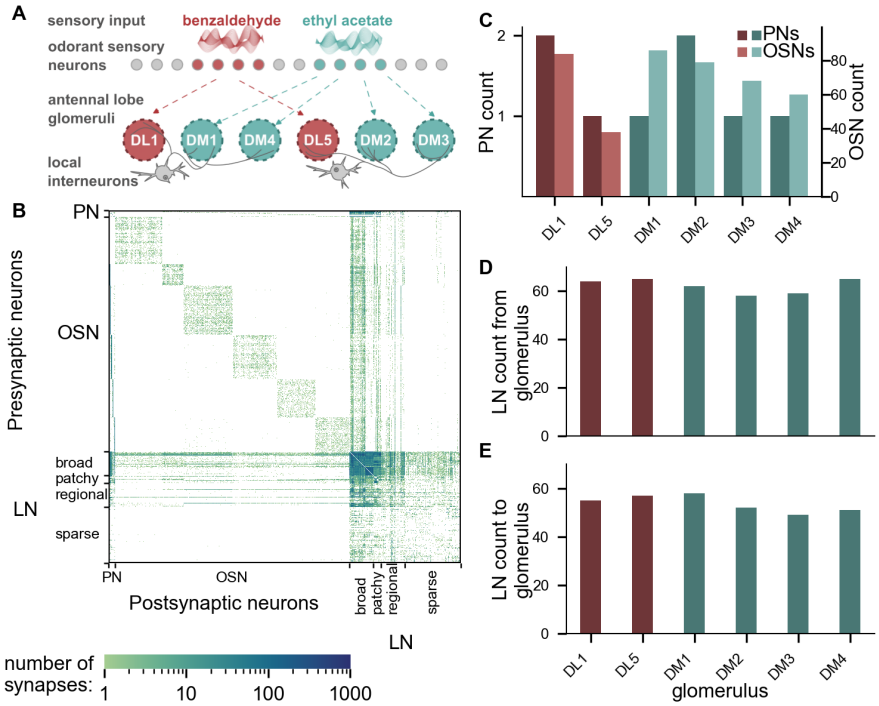

Fig. 1. Wiring patterns in selected antennal lobe glomeruli of the fly connectome. (A) Schematic of the circuit model illustrating the components of the neural pathway involved in odor mixture processing, as investigated in (9). The aversive odor benzaldehyde and the appetitive odor ethyl acetate activate distinct sets of olfactory sensory neurons (OSNs). Benzaldehyde-responsive OSNs target PNs in the AL glomeruli DL1 and DL5, while ethyl acetate-responsive OSNs target glomeruli DM1-4. Local interneurons (LNs) mediate crosstalk between glomeruli. **(B)** Connectivity matrix of PNs and OSNs in the six glomeruli DL1, DL5, DM1, DM2, DM3, and DM4 within the right hemisphere of the AL, along with LNs from all four morphological classes. Color indicates the number of synapses between neurons. **(C)** Number of OSNs and PNs innervating each of the six glomeruli. Aversive glomeruli are marked in red, appetitive glomeruli are marked in green. **(D)** Number of LNs receiving input from each glomerulus. A neuron is counted if it is connected via > 10 synapses with any OSN or PN within that glomerulus **(E)** As in **D**, but showing the number of LNs which provide output to each glomerulus.

scale connectome datasets of the fly brain now provides highly detailed insight into the structural organization of the AL, including the complex LN innervation patterns (21, 30–32). In the hemibrain dataset, 197 LNs have been segmented, identified, and classified into one of four morphological categories: broad, patchy, regional, or sparse (18, 21). The connectome data further specifies exact synaptic numbers among LNs and between LNs and other neurons.

In this study, we aim to investigate how the structural connectome data supports the functional insights into information processing circuits. First, we performed a comprehensive analysis of LN innervation patterns within the AL to identify any potential directed connectivity between glomeruli. In a second step, we then integrate the structural data into a spiking neural network model, to investigate whether and under which conditions the connectome-constrained model can reproduce the functional key features of odor mixture inhibition.

Results

Structural connectivity across AL glomeruli. Building on the insights into the mechanism underlying odor mixture inhibition described by Mohamed *et al.* (9), we analyzed the hemibrain connectome dataset, which reconstructs the right hemisphere of a single female fruit fly. In particular, we focused on the structural representation of two odors with opposing valences: the aversive odor benzaldehyde and the appetitive odor ethyl acetate. We analyzed the six AL glomeruli that have been previously shown to be involved in odor mixture inhibition: DL1 and DL5, which respond to benzaldehyde ('bea'), and DM1–4, which respond to ethyl acetate ('eta', Figure 1A). We identified 38-86 OSNs and 1–2 uniglomerular PNs innervating each of the six glomeruli, which is consistent with previous studies (Figure 1B,C) (14). While neuron numbers varied across glomeruli, no substantial differences were observed between appetitive and aversive glomeruli (Figure 1C). To investigate LN connectivity, we retrieved neuron IDs and morphological classifications from Schlegel *et al.* (21), resulting in a total of 197 LNs from four morphological classes. We counted 42 broadly, 14 patchy, 42 regional and 99 sparsely innervating LNs (Figure 1B). The number of LNs providing input to or receiving output from a given glomerulus was relatively consistent across all six glomeruli, ranging

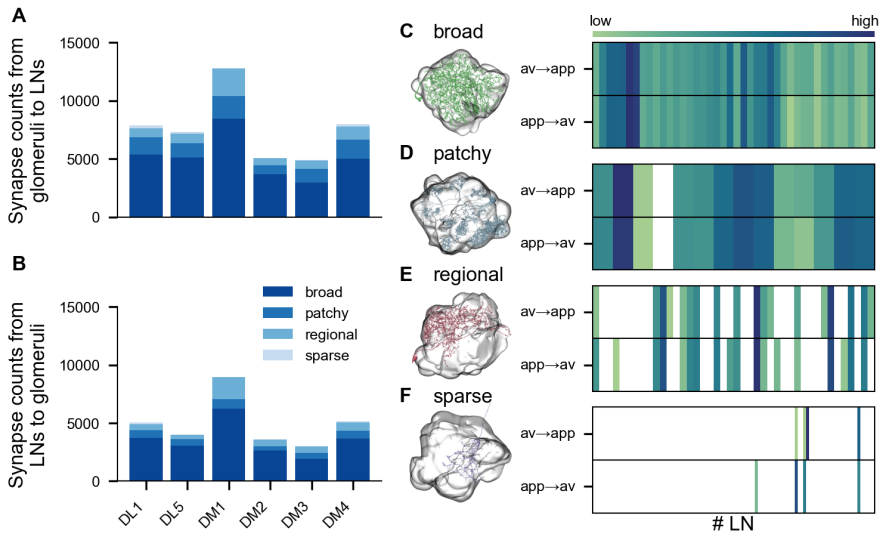

Fig. 2. Direction of glomerular crosstalk via LNs across all morphological classes (A) Total number of synapses from glomeruli DL1, DL5, and DM1–DM4 (presynaptic) onto LNs (postsynaptic), summed across all neurons. Different shades of blue indicate different LN morphological classes. **(B)** As in **A**, but synapse counts from LNs to each glomerulus. **(C-F)** Left: Example morphologies of LNs from each morphological class. The gray shading illustrates the volume of the right AL. Right: Heatmaps showing the directionality of glomerular crosstalk mediated via LNs. Each heatmap shows innervation pattern for one LN class, with columns corresponding to individual LNs, and rows corresponding to valence-specific directions from aversive to appetitive glomeruli (upper row) or vice versa (lower row). The directionality metric is computed as the product of total input from glomeruli of one valence to each LN and total output from the same LN to glomeruli of the opposite valence. A value of 0 for input or output results in a white field; increasing values are represented by darker shades.

from 49–65, with a large fraction of broadly innervating LNs (Figure 1D,E). Given the total LN counts were similar, we next turned to analyzing synapse numbers, separately for each morphological LN class.

Directionality of LN innervation patterns. We next examined whether synapse counts in LN innervation pattern support a directed flow of information between glomeruli. We primarily focused on two of the four LN morphological classes: patchy LNs, which have been identified as key players in mixture inhibition based on prior functional data (9), and regional LNs, which display a clear segregation between dendritic and axonal compartments (21), making them suitable candidates to potentially mediate directed inhibition. Our working hypothesis was that LNs receive more synaptic input from aversive glomeruli DL1 and DL5 and project preferentially onto appetitive glomeruli DM1–4. However, while absolute synapse counts indicated extensive input and output connectivity for LNs (Figure 2A,B), we found no evidence of consistent directional innervation. This remained true also after normalization by neuron number (Figure S1A). Interestingly, we observed a strong correlation between LN input and output for each glomerulus. This observation can be at least partly linked to the glomerulus size (Figure S1B) (14). For instance, LNs show both high input from and output to DM1, a glomerulus which is substantially larger in volume than others. Normalizing synaptic counts to glomerular volume erased this difference. To rule out potential non-linear effects due to varying synapse counts between neuron pairs, we analyzed the distribution of synapse counts among LNs across glomerular pairs and found no significant differences (Figure S2). We next aimed to correlate input to and output from LNs, with the idea that each LN would be only a potential candidate for mediating mixture inhibition if it gets both a lot of input and makes a lot of output from appetitive and to aversive glomeruli, respectively. To quantify potential directionality, we calculated the product of synaptic input and output per LN between glomerulus groups. This metric serves as a proxy for potential directional communication. While patchy and broad LNs showed high connectivity across both directions (Figure 2C,D), several regional LNs appeared to selectively project from aversive to appetitive glomeruli (Figure 2E). However, an equal number of neurons exhibited the opposite pattern, suggesting no clear asymmetry. In conclusion, our connectome analysis did not provide clear evidence for directed LN crosstalk from aversive to appetitive glomeruli.

Building a connectome-constrained model. In the next step, we wanted to explore potential mechanisms that might explain how mixture inhibition could nonetheless arise

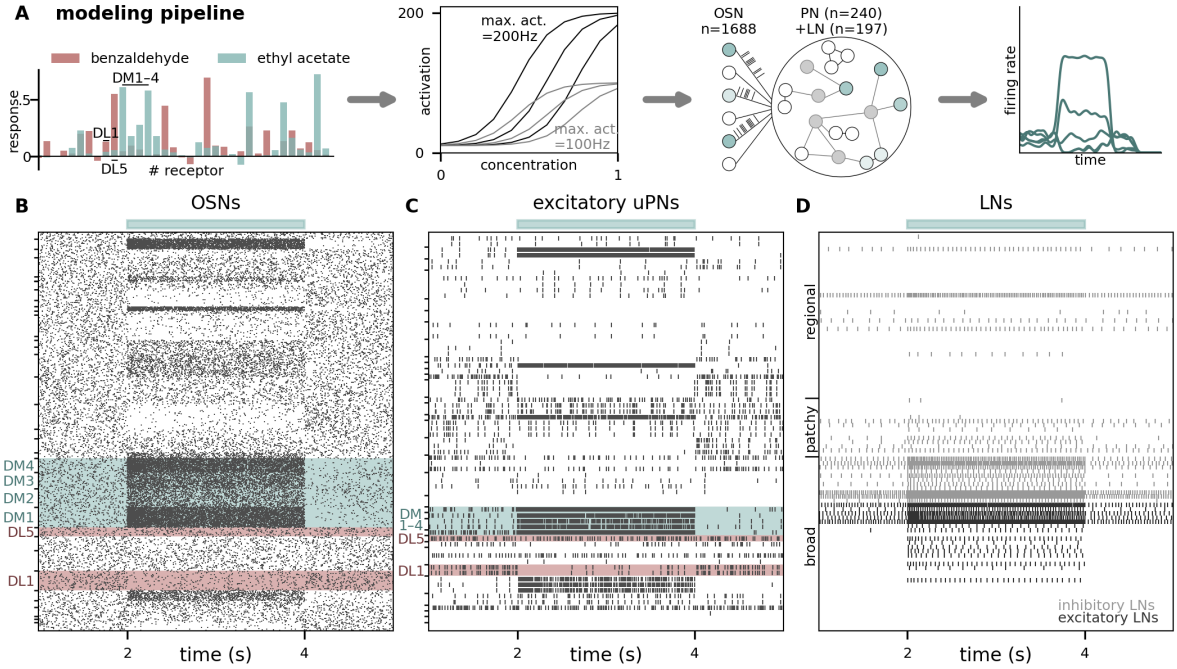

Fig. 3. Computational model of the fly AL. (A) Overview of the model implementation pipeline. Receptor responses for the odors benzaldehyde and ethyl acetate were obtained from the DoOR database (33) and mapped to corresponding glomeruli. Odor concentration was translated into OSN activation using a sigmoid transfer function, whose horizontal offset introduced variability across individual OSNs. Receptor responses scaled the maximal activation rate per OSN type. The resulting OSN activation patterns served as Poisson input to a connectome-constrained spiking network model of OSNs, PNs, and LNs in the AL. All neurons were modeled as leaky integrate-and-fire neurons and connected via conductance-based synapses. The output of each neuron was recorded to quantify odor-specific activation in all neurons. **(B)** Spike raster plot for responses of all modeled OSNs to a 2-second ethyl acetate stimulus. OSNs projecting to glomeruli DL1 and DL5 (aversive) are highlighted in red, OSNs projecting to DM1–DM4 (appetitive) in green. **(C)** As in **B**, but for excitatory uniglomerular projection neurons (uPNs). Inhibitory uPNs and multiglomerular PNs are not shown. **(D)** As in **B** and **C**, but for broad, patchy, and regional LNs. Odors evoked only minimal responses in sparse LNs, therefore they are not shown. Excitatory LNs are shown in dark gray, inhibitory LNs in light gray.

from the known connectivity. To this end, we integrated the connectome data into a spiking neural network model of the *Drosophila* AL (Figure 3A), enabling direct comparison between simulation results and imaging experiments. Given that both odor representation and LN arborization are distributed across the entire AL, we covered a large portion of the AL in our model, rather than restricting it to the six glomeruli analyzed previously. Ultimately, the network model included 35 of the 51 annotated glomeruli in the hemibrain dataset and comprised 2,125 leaky integrate-and-fire (LIF) neurons connected by over 194,000 synapses. Odor stimulation patterns were modeled based on the DoOR database (Figure 3A, 33–35), with 2 second odor stimulation with benzaldehyde, ethyl acetate, and their binary mixture. Receptor-to-glomerulus mapping followed canonical coding rules, with each receptor corresponding to a specific glomerulus (14). Firing rates for each OSN during odor stimulation was calculated from odor concentration via a transfer function, with maximal activation scaled to receptor response described in the DoOR database. Synaptic weights between neurons were scaled according to the number of synapses with group-specific scaling factors, since it is known that for example PNs are particularly sensitive to OSN input. Neurotransmitters were assigned as following: all OSNs were assigned excitatory; uniglomerular and multiglomerular PNs were classified based on their neuron-level prediction in Eckstein *et al.* (36), while LNs were generally assigned inhibitory, with the exception of a subset of broad excitatory LNs. Further details on the model implementation are provided in the Materials and Methods section.

Tuning odor concentration and synaptic weighting. We tuned both input patterns and synaptic parameters of the model to align its output with the functional imaging results on mixture inhibition described by Mohamed *et al.* (9). A key finding from the previous study was that suppression in response to odor mixtures occurred only when ethyl acetate was presented at a lower concentration than

benzaldehyde. To replicate this nonlinear concentration effect, we systematically decreased the modeled ethyl acetate concentration from its default value. Importantly, the same study demonstrated how a mixture of low benzaldehyde and high ethyl acetate concentrations did in turn not lead to suppressed responses in aversive glomeruli. We therefore hypothesized that reduction in odor concentration alone would not be sufficient to explain the experimental data. One idea was that functional synaptic weights may not be fully determined by synapse counts alone, but other factors such as synapse size, vesicle pool size, or release probability may contribute as well. This idea is supported by immunostaining results in Mohamed *et al.* (9), which revealed asymmetries in presynaptic marker intensity between glomeruli. To incorporate such asymmetries, we introduced an imbalanced scaling of synaptic weights in the model. Specifically, we gradually increased the synaptic weights from regional and patchy LNs to appetitive glomeruli, while decreasing the weights from those LNs to aversive glomeruli and vice versa. To test the impact of these two model manipulations — odor concentration and synaptic weighting — we performed a grid search, with differing levels of ethyl acetate concentrations ranging from 0.2 to 1 (default) and synaptic scaling factors ranging from 1 (default) to 40. Model performance was evaluated based on four criteria: (1) robust responses to benzaldehyde and ethyl acetate in the respective aversive and appetitive glomeruli; (2) no or low activation in unrelated glomeruli; (3) similar activation between benzaldehyde and the binary mixture in aversive glomeruli; and (4) reduced responses to the binary mixture compared to ethyl acetate alone in appetitive glomeruli. For each parameter combination, we quantified PN firing rates in response to each odor and visualized the results as a heatmap (Figure S3). Results of the grid-search showed that lowering ethyl acetate concentration alone was not sufficient to reproduce mixture inhibition. Although very low ethyl acetate concentrations reduced activation in appetitive glomeruli, they also failed to elicit substantial responses to ethyl acetate itself. In contrast, when combined with imbalanced synaptic weight scaling, we indeed observed the characteristic suppression in appetitive glomeruli in response to the odor mixture. At very high weight scaling, suppression was also very prominent at equal benzaldehyde and ethyl acetate concentrations. For further simulations and analysis, we selected a synaptic scaling factor of 20.

Tuned model aligns with functional data. Figure 3B,C shows the recorded spiking activity across all neuron populations in our tuned model. As expected, stimulation with the appetitive odor ethyl acetate led to an increased firing rates in OSNs and PNs innervating the appetitive glomeruli DM1, DM2, DM3, and DM4 . This activation also recruited LNs via OSN and PN input (Figure 3D). Similarly, stimulation with the aversive odor benzaldehyde resulted in strong responses in DL1 and DL5, whereas presentation of the binary mixture elicited increased firing rates all six key glomeruli (Figure S4). We estimated the mean instantaneous firing rates of PNs innervating each glomerulus across ten model runs, allowing a direct comparison to the mean calcium imaging responses reported by Mohamed *et al.* (9) (Figure 4). The experimental results had shown that at high concentrations of ethyl acetate, there was no effect of mixture inhibition (Figure 4A). Consistent with these findings, our model showed only a subtle reduction in DM2 and DM3 responses at high ethyl acetate concentrations (Figure 4C). However, when ethyl acetate concentration was decreased, PN responses to the mixture were completely abolished in DM2 and DM3, and strongly reduced in DM1 and DM4 (Figure 4C). These patterns closely match the *in vivo* imaging results for a low ethyl acetate concentration (Figure 4B), showing odor mixture inhibition in all four appetitive glomeruli. As a control, we reset synaptic scaling to a balanced state and repeated the same simulation (Figure S5). As expected, the model with balanced weighting showed no significant odor mixture inhibition in appetitive glomeruli. This additionally supports the hypothesis that the suppression effect in the tuned model arises from the imbalanced synaptic weighting and is further facilitated by reduced ethyl acetate concentrations. Overall, the tuned model qualitatively reproduces

the experimental findings and supports the hypothesis that circuit-level asymmetries in the AL contribute to odor mixture processing.

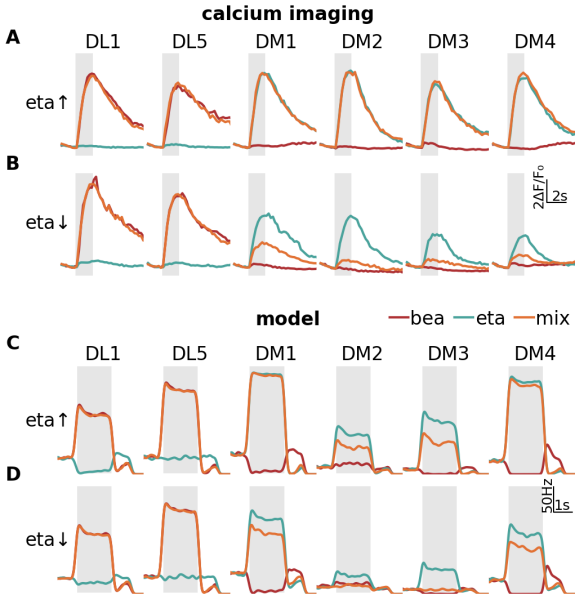

Fig. 4. Tuned model reproduces functional recordings from the antennal lobe during odor mixture processing. (A) Mean time-resolved calcium signals in PNs of aversive (DL1, DL5) and appetitive (DM1–4) glomeruli during 2 second odor stimulation (highlighted in gray) with ethyl acetate (eta, 10^{-2}, green), benzaldehyde (bea, 10^{-1}, red), and their binary mixture (orange), n=11. **(B)** As in **A**, but using a lower concentration of ethyl acetate (10^{-3}) for the single odor and in the binary mixture. Experimental imaging data is obtained from (9). **(C)** Mean simulated time-resolved firing rates in the tuned model in response to 2 second odor stimulation (highlighted in gray) with benzaldehyde and ethyl acetate at maximal concentration (1), and their binary mixture, n=10. **(D)** As in **C**, but with a lower ethyl acetate concentration (0.6) and corresponding lower concentration in the binary mixture.

Discussion

In this study, we aimed to investigate how functional mechanisms of information integration can be linked to structural connectivity. Our analysis of the connectome data revealed dense innervation and substantial crosstalk between regions of interest. However, structural data alone could not support the directionality of innervation observed in (9). We therefore propose that, in addition to structural connectivity, functional connectivity might play a role in shaping the integration of opposing odor information. Specifically, we hypothesize that the synaptic pathway via LNs from aversive to appetitive glomeruli might be stronger than the pathway from appetitive to aversive glomeruli. Using a connectome-constrained network model, we demonstrate that introducing an imbalance in synaptic weights can reproduce functional mechanisms underlying odor mixture inhibition.

Inferring function from fly connectome structural data. Previous studies have shown how connectome data can be used to infer functional properties of neural systems in the fruit fly (37–41). These studies — ranging in complexity from connectivity analyses to compartmental models of single neurons — demonstrate that *Drosophila* circuit models can predict neural activity and even behavior. A recent study by Shiu *et al.* further advanced this approach by showing that whole-brain modeling based solely on synapse-level connectivity and neurotransmitter identity can reproduce functional properties at the circuit level without any parameter tuning (42). Their model generated testable predictions that were subsequently confirmed in *in vivo* experiments. However, other studies have cautioned against inferring function from structure alone, by demonstrating that even when a model is constrained by the connectome, it may still yield multiple solutions regarding the biophysical parameter space capable of reproducing the same functional output (43, 44). This degeneracy highlights the importance of combining both structural and functional data to constrain network models.

Limitations of connectome-constrained modeling. In this study, we propose an imbalance in synaptic weighting as a potential mechanism to link structure to function. The connectome alone cannot fully explain circuit function, and additional layers of complexity involving LNs may contribute to the observed effects (45).

First, our analysis is based on a single brain hemisphere from one individual, without accounting for inter-individual variability. The early olfactory system of the fly is generally highly stereotyped, and analysis of the Flywire connectome revealed largely similar LN–glomerulus innervation patterns (Figure S1C). However, a comparative study showed occasional variability in neuron numbers and connectivity patterns between the two available fly connectomes (46). Other studies have similarly shown that specifically LN innervation patterns in the AL can differ

between animals, suggesting that they are not entirely stereotyped (18, 21, 47).

Second, synaptic plasticity may also play a role, since the brain is constantly shaped by development and experience, such as odor exposure. LNs have been shown to be targets of such plasticity, for example during odor habituation or differential conditioning(29, 48, 49). This may be particularly relevant when analyzing neuron counts without considering synapse sizes, which might undergo more changes during plasticity (50).

Third, our ability to draw conclusions about the neurotransmitter identity of LNs is very limited. In previous studies, it has been shown that LNs express a range of excitatory and inhibitory neurotransmitters, including acetylcholine, GABA, glutamate, and various neuropeptides (51–55). While GABA and glutamate both act as inhibitory neurotransmitters in LNs, they appear to serve distinct functional roles within the AL circuit (55). In the use case of odor mixture inhibition, Mohamed *et al.* (9) suggested that the glomerular crosstalk is mediated specifically by GABAergic interneurons. Recently, the fly connectomes have been complemented with neurotransmitter predictions at the neuron and synapse level using machine learning-based classification (36). However, transmitter classification for LNs remained particularly challenging, since neurotransmitter constitution of LNs appears to be highly complex. The trained network predicted the existence of GABAergic, cholinergic, dopaminergic, glutamatergic, and serotonergic LNs, but potential misclassifications are acknowledged. There are indications to assume that LNs may break both Lacin's law — which states that all neurons within a hemilineage express the same transmitter — (56) and Dale's law, which asserts that a neuron releases the same transmitter at all its synapses (57, 58). Local molecular mechanisms of diversification at the presynaptic site may potentially underlie such variability between different synapses of one neuron (59). Taking these aspects into consideration, it remains conceivable that a single LN could make synapses with different neurotransmitters onto different postsynaptic targets. One possible implication for odor mixture inhibition is that synapses from LNs to OSNs and PNs in appetitive glomeruli might release more inhibitory neurotransmitters, whereas synapses from the same LNs to aversive glomeruli might be more excitatory.

Complementary mechanisms for odor mixture inhibition. We studied odor mixture processing specifically at the at the level of the lateral inhibitory pathway in the AL. However, previous studies have shown that mixture processing, including mixture inhibition, occurs at multiple peripheral and central sites within the olfactory pathway in *Drosophila* and other species (1, 2, 60). Importantly, evidence suggests integration of odor information already begins at the level of OSNs, which make non-synaptic ephaptic interactions among each other (61–63). Specific inhibitory ephaptic interactions have been shown to mediate lateral inhibition between OSN in the same sensillum during processing of a mixture of two odors with opposing valence (64). In addition to ephaptic coupling, OSNs projecting to the same glomerulus are highly connected via axo-axonal synapses (Figure 1B) (21, 65). Such connections among OSNs can facilitate nonlinear amplification of high-concentration odor responses (66) and could potentially intensify to the observed effects during mixture inhibition. Taken together, these findings highlight that odor mixture inhibition is likely shaped by complementary mechanisms acting across different stages of the olfactory pathway.

Outlook. In future investigations, it would be interesting to quantify the size of synapses in EM reconstructions to explore differences beyond synapse count. Previous studies have demonstrated a linear relationship between synapse size and synapse strength (67), and while synapse counts are generally a suitable approximation for synaptic strength (68), it would be interesting to investigate any potential differences in synapse size from LNs to appetitive versus aversive glomeruli. Such analyses could provide a structural correlate to the asymmetries observed in synaptic marker immunostainings (Figure 8 in (9)). Additionally, imaging and electrophysiological recordings from LNs during odor mixture stimulation would give further insight into

their functional roles. From the modeling perspective, future work could aim to integrate additional layers of complexity. For example, it would be interesting to include compartmentalization to capture differential synapse placement along dendrites (40, 69), or expand towards full-brain simulations that also account for behavioral output (42). Moreover, incorporating competing mechanisms, such as mixture synergism and studying their interplay with mixture inhibition, could provide a more comprehensive understanding of information integration in the olfactory system.

Materials and Methods

Calcium imaging data. All imaging data shown in Figure 4A,B have been previously published in (9). Refer to this publication for details on the experimental setup, data analysis and interpretation.

Fly connectome. We analyzed the *Drosophila* connectome hemibrain dataset published by Scheffer *et al.* (30), accessible via the Neuprint platform (70). Neuron IDs for OSNs, PNs, and LNs were obtained from the data files provided in Schlegel *et al.* (21), and neurons and their connectivity were retrieved using the neuprint-python API. For exemplary LN morphologies shown in Figure 2C-F, we selected the following neuron IDs using the Neuprint web interface: #5813062199 (broad), #2041621893 (patchy), #5813034531 (regional) and #1915155348 (sparse). To normalize synapse counts to glomerular volume, we used the mean glomerular volumes from a female fly as reported by Grabe *et al.* (14). For the product calculations in Figure 2C-F, we computed the total number of synapses between each LN and all glomeruli (both input and output). The product of these two values was calculated per LN. For the comparative analysis shown in Figure S1C, we additionally included data from the whole-brain connectome published by Dorkenwald *et al.* (31).

Modeling. We implemented a spiking neural network of the fly AL including OSNs, PNs and LNs. All neurons were implemented as leaky-integrate-and-fire (LIF) neurons described by

Table 1. Neuronal parameters used in the spiking computational model of the fly AL.

Parameter	Symbol	Value
Membrane capacitance OSN	C_{osn}	73 pF
Membrane capacitance PN	C_{pn}	73 pF
Membrane capacitance LN	C_{ln}	64 pF
Leak conductance OSN	$g_{L,\mathrm{OSN}}$	0.56 nS
Leak conductance PN	$g_{L,\mathrm{PN}}$	3.33 nS
Leak conductance LN	$g_{L,\mathrm{LN}}$	1.00 nS
Leak reversal potential OSN	$E_{L,\mathrm{OSN}}$	−70 mV
Leak reversal potential PN	$E_{L,\mathrm{PN}}$	−55 mV
Leak reversal potential LN	$E_{L,\mathrm{LN}}$	−50 mV
Reset potential OSN	$V_{\mathrm{reset,OSN}}$	−70 mV
Reset potential PN	$V_{\mathrm{reset,PN}}$	−55 mV
Reset potential LN	$V_{\mathrm{reset,LN}}$	−60 mV
Refractory period OSN	$\tau_{\mathrm{ref,OSN}}$	2 ms
Refractory period PN	$\tau_{\mathrm{ref,PN}}$	5 ms
Refractory period LN	$\tau_{\mathrm{ref,LN}}$	4 ms
Spike threshold OSN	$V_{\mathrm{thresh,OSN}}$	−50 mV
Spike threshold PN	$V_{\mathrm{thresh,PN}}$	−30 mV
Spike threshold LN	$V_{\mathrm{thresh,LN}}$	−40 mV
Increase of OSN adaptation conductance	g_{adap}	0.5 nS
Adaptation time constant OSN	τ_{adap}	500 ms
Excitatory reversal potential	E_e	0 mV
Inhibitory reversal potential	E_i	−90 mV
Exc. synapse time constant	τ_{syn}	2 ms
Inh. synapse time constant	$\tau_{\mathrm{syn,i}}$	20 ms

$$C\frac{dV_m}{dt} = g_L(E_L - V_m) + g_{\mathrm{syn,e}}(E_{\mathrm{e}} - V_m) - g_{\mathrm{syn,i}}(E_{\mathrm{i}} - V_m) \quad [1]$$

where C is the membrane capacitance, V_m the membrane potential, g_L the leak conductance, E_L the leak reversal potential, $g_{\mathrm{syn,e}}$ and $g_{\mathrm{syn,i}}$ the excitatory and inhibitory synaptic conductances, and E_{e}, E_{i} the corresponding synaptic reversal potentials. Synaptic conductances evolved according to

$$\frac{dg_{\mathrm{syn,e}}}{dt} = -\frac{g_{\mathrm{syn,e}}}{\tau_{\mathrm{e}}} \qquad \frac{dg_{\mathrm{syn,i}}}{dt} = -\frac{g_{\mathrm{syn,i}}}{\tau_{\mathrm{i}}} \quad [2]$$

with τ_{e} and τ_{i} as time constants for the excitatory and inhibitory conductances, respectively. Neuron parameters for each neuron group are listed in Table 1. OSNs were additionally driven by a spontaneous Poisson firing rate of 10 Hz and an adaptation current (12), implemented as an increase in the adaptation conductance g_{adap} upon each spike, which evolved according to

$$\frac{g_{\mathrm{adap}}}{dt} = -\frac{g_{\mathrm{adap}}}{\tau_{\mathrm{adap}}} \quad [3]$$

Neurotransmitter were assigned as follows: all OSNs were assigned excitatory. For PNs, transmitter identity was based on assignments in Eckstein *et al.* (36), resulting in 69 excitatory and 6 inhibitory uniglomerular PNs (uPNs), and 85 excitatory and 80 inhibitory multiglomerular PNs (mPNs). Neurotransmitter assignment for LNs was challenging and partly ambiguous in the analysis performed by Eckstein *et al.* (see Discussion). Therefore, we chose to assign 31 out of 197 LNs excitatory, following previous estimations that around 16% of LNs are excitatory (71). Since excitatory LNs have rather broad innervation patterns (36, 51), we chose cholinergic LNs from the broad class with the highest cholinergic assignment confidence. All other LNs were modeled as inhibitory neurons.

Odor input was derived from the DoOR database (33–35), providing receptor responses between –1 and 1 for benzaldehyde and ethyl acetate. Maximal OSN activation rates max_{act} were computed as:

$$\max_{\text{act}} = \begin{cases} 200 \cdot r & \text{if } r > 0 \\ \text{spont} & \text{if } r = 0 \\ \text{spont} \cdot (1 + r) & \text{if } r < 0 \end{cases} \quad [4]$$

where r is the receptor response. For zero receptor response, the spontaneous rate of 10 Hz was used; for positive receptor response, the rate was scaled linearly up to 200 Hz; and for negative odor strengths, the spontaneous rate was downscaled proportionally (72). Then, OSN firing rate OSN_{FR} was calculated via a sigmoid transfer function as

$$\text{OSN}_{\text{FR}}(c) = s + \left(\frac{1}{1 + 3^v \cdot e^{-10c}} \right) \cdot (max_{\text{act}} - s) \quad [5]$$

where c denotes odor concentration, s denotes the spontaneous firing rate and v (drawn randomly between 4 and 7) defines the variability between OSNs. For the binary mixture, we then selected the higher receptor response per glomerulus. OSNs were activated based on which glomerulus they innervate. In total, we included those 35 out of 51 glomeruli for which receptor response for both odors were available in the DoOR database. Connectivity was established via a connectivity matrix capped at 500 synapses per connection to avoid overrepresentation of intraglomerular contacts among broad LNs (Figure 1B). Synaptic weights were assigned based on synapse counts and individually scaled between neuron types as listed in Table 2.

Table 2. Synaptic conductance scales used in the model, depending on presynaptic and postsynaptic neuron type.

Connection	Symbol	Value
OSN → PN	$g_{\text{osn_pn}}$	200 pS
OSN → LN	$g_{\text{osn_ln}}$	25 pS
OSN → OSN	$g_{\text{osn_osn}}$	1 pS
PN_e → OSN	$g_{\text{pn}_\text{e}\text{_osn}}$	1 pS
PN_e → PN	$g_{\text{pn}_\text{e}\text{_pn}}$	1 pS
PN_e → LN	$g_{\text{pn}_\text{e}\text{_ln}}$	1 pS
PN_i → OSN	$g_{\text{pn}_\text{i}\text{_osn}}$	2 pS
PN_i → PN	$g_{\text{pn}_\text{i}\text{_pn}}$	2 pS
PN_i → LN	$g_{\text{pn}_\text{i}\text{_ln}}$	0.1 pS
LN_e → OSN	$g_{\text{ln}_\text{e}\text{_osn}}$	1 pS
LN_e → PN	$g_{\text{ln}_\text{e}\text{_pn}}$	1 pS
LN_e → LN	$g_{\text{ln}_\text{e}\text{_ln}}$	1 pS
LN_i → OSN	$g_{\text{ln}_\text{i}\text{_osn}}$	2 pS
LN_i → PN	$g_{\text{ln}_\text{i}\text{_pn}}$	2 pS
LN_i → LN	$g_{\text{ln}_\text{i}\text{_ln}}$	0.1 pS

For introducing imbalance in the weights between patchy and regional LNs with aversive and appetitive glomeruli, synaptic weights from OSNs and PNs in the aversive glomeruli DL1 and DL5 to LNs from LNs to appetitive glomeruli DM1-4 were multiplied with a weight factor w. Synapses in the reverse direction were accordingly multiplied with the reciprocal factor $(1/w)$. Parameter tuning was conducted via a grid search over odor concentration c (0.2–1) and synaptic weight factor w (1–40). All analyses and modeling was performed in Python3, models were simulated with the neuron simulator Brian2 (73). The programming code and data is stored on internal lab servers and available upon request.

ACKNOWLEDGMENTS. We thank Silke Sachse for providing us with the two-photon imaging data set as analyzed in (9). We further thank Silke Sachse and Pramit Bandyopadhyay for helpful discussions on LN crosstalk. This research was funded by the German Research Foundation (DFG) through the priority program "Evolutionary Optimization of Neuronal Processing" (DFG-SPP 2205, ID 430592330).

1. T Thomas-Danguin, C Sinding, S Romagny, F El Mountassir, B Atanasova, E Le Berre, AM Le Bon, G Coureaud, The perception of odor objects in everyday life: a review on the processing of odor mixtures. *Front. Psychol.* **5** (2014).
2. P Bandyopadhyay, S Sachse, Mixing things up! — how odor blends are processed in Drosophila. *Curr. Opin. Insect Sci.* **59**, 101099 (2023).
3. PG Becher, M Bengtsson, BS Hansson, P Witzgall, Flying the Fly: Long-range Flight Behavior of Drosophila melanogaster to Attractive Odors. *J. Chem. Ecol.* **36**, 599–607 (2010).
4. LR Saraiva, K Kondoh, X Ye, Kh Yoon, M Hernandez, LB Buck, Combinatorial effects of odorants on mouse behavior. *Proc. Natl. Acad. Sci.* **113**, E3300–E3306 (2016).
5. Q Qiu, Y Wu, L Ma, CR Yu, Encoding innately recognized odors via a generalized population code. *Curr. Biol.* **31**, 1813–1825.e4 (2021).
6. N Deisig, M Giurfa, H Lachnit, JC Sandoz, Neural representation of olfactory mixtures in the honeybee antennal lobe. *Eur. J. Neurosci.* **24**, 1161–1174 (2006).
7. AF Silbering, CG Galizia, Processing of Odor Mixtures in the Drosophila Antennal Lobe Reveals both Global Inhibition and Glomerulus-Specific Interactions. *J. Neurosci.* **27**, 11966–11977 (2007).
8. JA Riffell, H Lei, TA Christensen, JG Hildebrand, Characterization and Coding of Behaviorally Significant Odor Mixtures. *Curr. Biol.* **19**, 335–340 (2009).
9. AA Mohamed, T Retzke, S Das Chakraborty, B Fabian, BS Hansson, M Knaden, S Sachse, Odor mixtures of opposing valence unveil inter-glomerular crosstalk in the Drosophila antennal lobe. *Nat. Commun.* **10**, 1–17 (2019).
10. RF Stocker, MC Lienhard, A Borst, KF Fischbach, Neuronal architecture of the antennal lobe in Drosophila melanogaster. *Cell Tissue Res.* **262**, 9–34 (1990).
11. A Couto, M Alenius, BJ Dickson, Molecular, Anatomical, and Functional Organization of the Drosophila Olfactory System. *Curr. Biol.* **15**, 1535–1547 (2005).
12. RI Wilson, Early olfactory processing in drosophila: Mechanisms and principles. *Annu. Rev. Neurosci.* **36**, 217–241 (2013).
13. NY Masse, GC Turner, GSXE Jefferis, Olfactory Information Processing in *Drosophila*. *Curr. Biol.* **19**, R700–R713 (2009).
14. V Grabe, A Baschwitz, HK Dweck, S Lavista-Llanos, BS Hansson, S Sachse, Elucidating the Neuronal Architecture of Olfactory Glomeruli in the Drosophila Antennal Lobe. *Cell Reports* **16**, 3401–3413 (2016).
15. AS Bates, et al., Complete Connectomic Reconstruction of Olfactory Projection Neurons in the Fly Brain. *Curr. Biol.* **30**, 3183–3199. (2020).
16. A Husch, M Paehler, D Fusca, L Paeger, P Kloppenburg, Distinct Electrophysiological Properties in Subtypes of Nonspiking Olfactory Local Interneurons Correlate With Their Cell Type–Specific Ca2+ Current Profiles. *J. Neurophysiol.* **102**, 2834–2845 (2009).
17. A Husch, M Paehler, D Fusca, L Paeger, P Kloppenburg, Calcium Current Diversity in Physiologically Different Local Interneuron Types of the Antennal Lobe. *J. Neurosci.* **29**, 716–726 (2009).
18. YH Chou, ML Spletter, E Yaksi, JC Leong, RI Wilson, L Luo, Diversity and wiring variability of olfactory local interneurons in the Drosophila antennal lobe. *Nat. Neurosci.* **13**, 439–449 (2010).
19. Y Seki, J Rybak, D Wicher, S Sachse, BS Hansson, Physiological and morphological characterization of local interneurons in the Drosophila antennal lobe. *J. Neurophysiol.* **104**, 1007–1019 (2010).
20. KI Nagel, RI Wilson, Mechanisms underlying population response dynamics in inhibitory interneurons of the Drosophila antennal lobe. *J. Neurosci.* **36**, 4325–4338 (2016).
21. P Schlegel, et al., Information flow, cell types and stereotypy in a full olfactory connectome. *eLife* **10**, e66018 (2021).
22. D Fuscà, P Kloppenburg, Task-specific roles of local interneurons for inter- and intraglomerular signaling in the insect antennal lobe. *eLife* **10**, e65217 (2021).
23. P Singh, S Goyal, S Gupta, S Garg, A Tiwari, V Rajput, AS Bates, AK Gupta, N Gupta, Combinatorial encoding of odors in the mosquito antennal lobe. *Nat. Commun.* **14**, 3539 (2023).
24. A Barth-Maron, I D'Alessandro, RI Wilson, Interactions between specialized gain control mechanisms in olfactory processing. *Curr. Biol.* **33**, 5109–5120.e7 (2023).
25. S Sachse, CG Galizia, Role of Inhibition for Temporal and Spatial Odor Representation in Olfactory Output Neurons: A Calcium Imaging Study. *J. Neurophysiol.* **87**, 1106–1117 (2002).
26. SR Olsen, RI Wilson, Lateral presynaptic inhibition mediates gain control in an olfactory circuit. *Nature* **452**, 956–960 (2008).
27. SR Olsen, V Bhandawat, RI Wilson, Divisive normalization in olfactory population codes. *Neuron* **66**, 287–299 (2010).
28. CM Root, K Masuyama, DS Green, LE Enell, DR Nässel, CH Lee, JW Wang, A Presynaptic Gain Control Mechanism Fine-Tunes Olfactory Behavior. *Neuron* **59**, 311–321 (2008).
29. S Das, et al., Plasticity of local GABAergic interneurons drives olfactory habituation. *Proc. Natl. Acad. Sci.* **108**, E646–E654 (2011).
30. LK Scheffer, et al., A connectome and analysis of the adult Drosophila central brain. *eLife* **9**, e57443 (2020).
31. S Dorkenwald, et al., Neuronal wiring diagram of an adult brain. *Nature* **634**, 124–138 (2024).
32. Z Zheng, et al., A Complete Electron Microscopy Volume of the Brain of Adult Drosophila melanogaster. *Cell* **174**, 730–743.e22 (2018).
33. CG Galizia, D Münch, M Strauch, A Nissler, S Ma, Integrating Heterogeneous Odor Response Data into a Common Response Model: A DoOR to the Complete Olfactome. *Chem. Senses* **35**, 551–563 (2010).
34. D Münch, GC Galizia, DoOR - The Database of Odorant Responses. *Chem. Senses* **13**, 1–6 (2011).
35. D Münch, CG Galizia, DoOR 2.0 - Comprehensive Mapping of Drosophila melanogaster Odorant Responses. *Sci. Reports* **6**, 21841 (2016).
36. N Eckstein, et al., Neurotransmitter classification from electron microscopy images at synaptic sites in Drosophila melanogaster. *Cell* **187**, 2574–2594.e23 (2024).
37. K Eichler, et al., The complete connectome of a learning and memory centre in an insect brain. *Nature* **548**, 175–182 (2017).
38. C Eschbach, et al., Recurrent architecture for adaptive regulation of learning in the insect brain. *Nat. Neurosci.* **23**, 544–555 (2020).
39. MH Turner, K Mann, TR Clandinin, The connectome predicts resting-state functional connectivity across the *Drosophila* brain. *Curr. Biol.* **31**, 2386–2394.e3 (2021).
40. TX Liu, PA Davoudian, KM Lizbinski, JM Jeanne, Connectomic features underlying diverse synaptic connection strengths and subcellular computation. *Curr. Biol.* **32**, 559–569.e5 (2022).
41. JK Lappalainen, FD Tschopp, S Prakhya, M McGill, A Nern, K Shinomiya, Sy Takemura, E Gruntman, JH Macke, SC Turaga, Connectome-constrained networks predict neural activity across the fly visual system. *Nature* **634**, 1132–1140 (2024).
42. PK Shiu, et al., A Drosophila computational brain model reveals sensorimotor processing. *Nature* **634**, 210–219 (2024).
43. CI Bargmann, E Marder, From the connectome to brain function. *Nat. Methods* **10**, 483–490 (2013).
44. M Beiran, A Litwin-Kumar, Prediction of neural activity in connectome-constrained recurrent networks (2024) Pages: 2024.02.22.581667 Section: New Results.
45. LK Scheffer, IA Meinertzhagen, A connectome is not enough – what is still needed to understand the brain of Drosophila? *J. Exp. Biol.* **224**, jeb242740 (2021).
46. P Schlegel, et al., Whole-brain annotation and multi-connectome cell typing of Drosophila. *Nature* **634**, 139–152 (2024).
47. K Rihani, S Sachse, Shedding Light on Inter-Individual Variability of Olfactory Circuits in Drosophila. *Front. Behav. Neurosci.* **16** (2022).
48. IP Sudhakaran, EE Holohan, S Osman, V Rodrigues, K VijayRaghavan, M Ramaswami, Plasticity of Recurrent Inhibition in the Drosophila Antennal Lobe. *J. Neurosci.* **32**, 7225–7231 (2012).
49. S Joshi, S Haney, Z Wang, F Locatelli, H Lei, Y Cao, B Smith, M Bazhenov, Plasticity in inhibitory networks improves pattern separation in early olfactory processing. *Commun. Biol.* **8**, 1–17 (2025).
50. IA Meinertzhagen, Of what use is connectomics? A personal perspective on the Drosophila connectome. *J. Exp. Biol.* **221**, jeb164954 (2018).
51. Y Shang, A Claridge-Chang, L Sjulson, M Pypaert, G Miesenböck, Excitatory Local Circuits and Their Implications for Olfactory Processing in the Fly Antennal Lobe. *Cell* **128**, 601–612 (2007).

52. R Okada, T Awasaki, K Ito, Gamma-aminobutyric acid (GABA)-mediated neural connections in the *Drosophila* antennal lobe. *J. Comp. Neurol.* **514**, 74–91 (2009).
53. MA Carlsson, M Diesner, J Schachtner, DR Nässel, Multiple neuropeptides in the Drosophila antennal lobe suggest complex modulatory circuits. *J. Comp. Neurol.* **518**, 3359–3380 (2010).
54. A Das, A Chiang, S Davla, R Priya, H Reichert, K VijayRaghavan, V Rodrigues, Identification and analysis of a glutamatergic local interneuron lineage in the adult Drosophila olfactory system. *Neural Syst. & Circuits* **1**, 4 (2011).
55. WW Liu, RI Wilson, Glutamate is an inhibitory neurotransmitter in the Drosophila olfactory system. *Proc. Natl. Acad. Sci. United States Am.* **110**, 10294–10299 (2013).
56. H Lacin, HM Chen, X Long, RH Singer, T Lee, JW Truman, Neurotransmitter identity is acquired in a lineage-restricted manner in the Drosophila CNS. *eLife* **8**, e43701 (2019).
57. H Dale, Pharmacology and Nerve-endings (Walter Ernest Dixon Memorial Lecture). *Proc. Royal Soc. Medicine* **28**, 319–330 (1934).
58. P Strata, R Harvey, Dale's principle. *Brain Res. Bull.* **50**, 349–350 (1999).
59. M van Oostrum, EM Schuman, Understanding the molecular diversity of synapses. *Nat. Rev. Neurosci.* (2024).
60. CD Derby, BW Ache, EW Kennel, Mixture suppression in olfaction: electrophysiological evaluation of the contribution of peripheral and central neural components. *Chem. Senses* **10**, 301–316 (1985).
61. CY Su, C Martelli, T Emonet, JR Carlson, Temporal coding of odor mixtures in an olfactory receptor neuron. *Proc. Natl. Acad. Sci.* **108**, 5075–5080 (2011).
62. CY Su, K Menuz, J Reisert, JR Carlson, Non-synaptic inhibition between grouped neurons in an olfactory circuit. *Nature* **492**, 66–71 (2012).
63. M Pannunzi, T Nowotny, Non-synaptic interactions between olfactory receptor neurons, a possible key feature of odor processing in flies. *PLOS Comput. Biol.* **17**, e1009583 (2021).
64. ST Wu, JY Chen, V Martin, R Ng, Y Zhang, D Grover, RJ Greenspan, J Aljadeff, CY Su, Valence opponency in peripheral olfactory processing. *Proc. Natl. Acad. Sci.* **119**, e2120134119 (2022).
65. WF Tobin, RI Wilson, WCA Lee, Wiring variations that enable and constrain neural computation in a sensory microcircuit. *eLife* **6**, e24838 (2017).
66. JE Manoim-Wolkovitz, T Camchy, E Rozenfeld, HH Chang, H Lerner, YH Chou, R Darshan, M Parnas, Nonlinear high-activity neuronal excitation enhances odor discrimination. *Curr. Biol.* **35**, 1521–1538.e5 (2025).
67. S Holler, G Köstinger, KAC Martin, GFP Schuhknecht, KJ Stratford, Structure and function of a neocortical synapse. *Nature* **591**, 111–116 (2021).
68. CL Barnes, D Bonnéry, A Cardona, Synaptic counts approximate synaptic contact area in Drosophila. *PLOS ONE* **17**, e0266064 (2022).
69. I Ganguly, A Litwin-Kumar, Connectomics: Relating synaptic connectivity to physiology. *Curr. Biol.* **32**, R118–R120 (2022).
70. SM Plaza, J Clements, T Dolafi, L Umayam, NN Neubarth, LK Scheffer, S Berg, neuPrint: An open access tool for EM connectomics. *Front. Neuroinformatics* **16**, 896292 (2022).
71. KT Tsai, CK Hu, KW Li, WL Hwang, YH Chou, Circuit variability interacts with excitatory-inhibitory diversity of interneurons to regulate network encoding capacity. *Sci. Reports* **8**, 1–15 (2018).
72. G Si, JK Kanwal, Y Hu, CJ Tabone, J Baron, M Berck, G Vignoud, AD Samuel, Structured Odorant Response Patterns across a Complete Olfactory Receptor Neuron Population. *Neuron* **101**, 950–962.e7 (2019).
73. DFM Goodman, R Brette, Brian: a simulator for spiking neural networks in Python. *Front. Neuroinformatics* **2**, 5 (2008).

Supplemental Figures

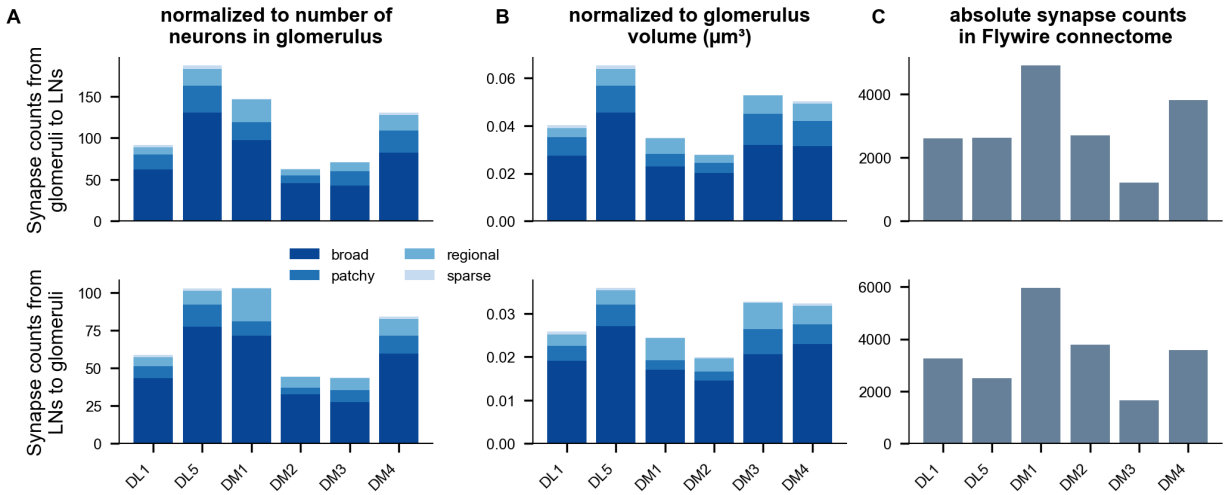

Fig. S1. Alternative analysis methods to compare synapse numbers across glomeruli. (A) Synapse numbers between glomeruli and LNs of all morphological classes, normalized to the total number of OSNs and PNs innervating each glomerulus. **(B)** As in **A**, but normalized to total volume of each glomerulus. Glomerular volumes were obtained from Grabe *et al.* (14). **(C)** Analysis of the Flywire connectome dataset (31), showing the total number of synapses from glomeruli onto LNs and from LNs to each glomerulus in the right hemisphere. Each bar represents the entire LN population, without subdivision into single morphological classes as in **A** and **B**.

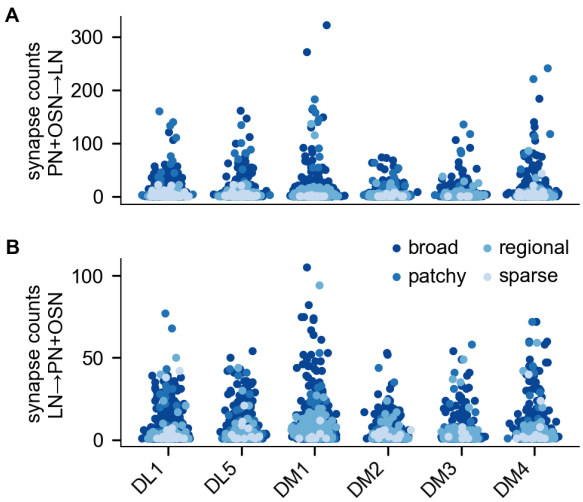

Fig. S2. Distribution of synapse counts. (A) Synapse counts between individual LNs and OSNs or PNs within each glomerulus. Each marker represents the number of synapses from a single OSN or PN in the respective glomerulus to a single LN. Different colors represent the four morphological classes. **(B)** As in **A**, but with the number of synapses from a single LN to each OSN or PN in the respective glomerulus.

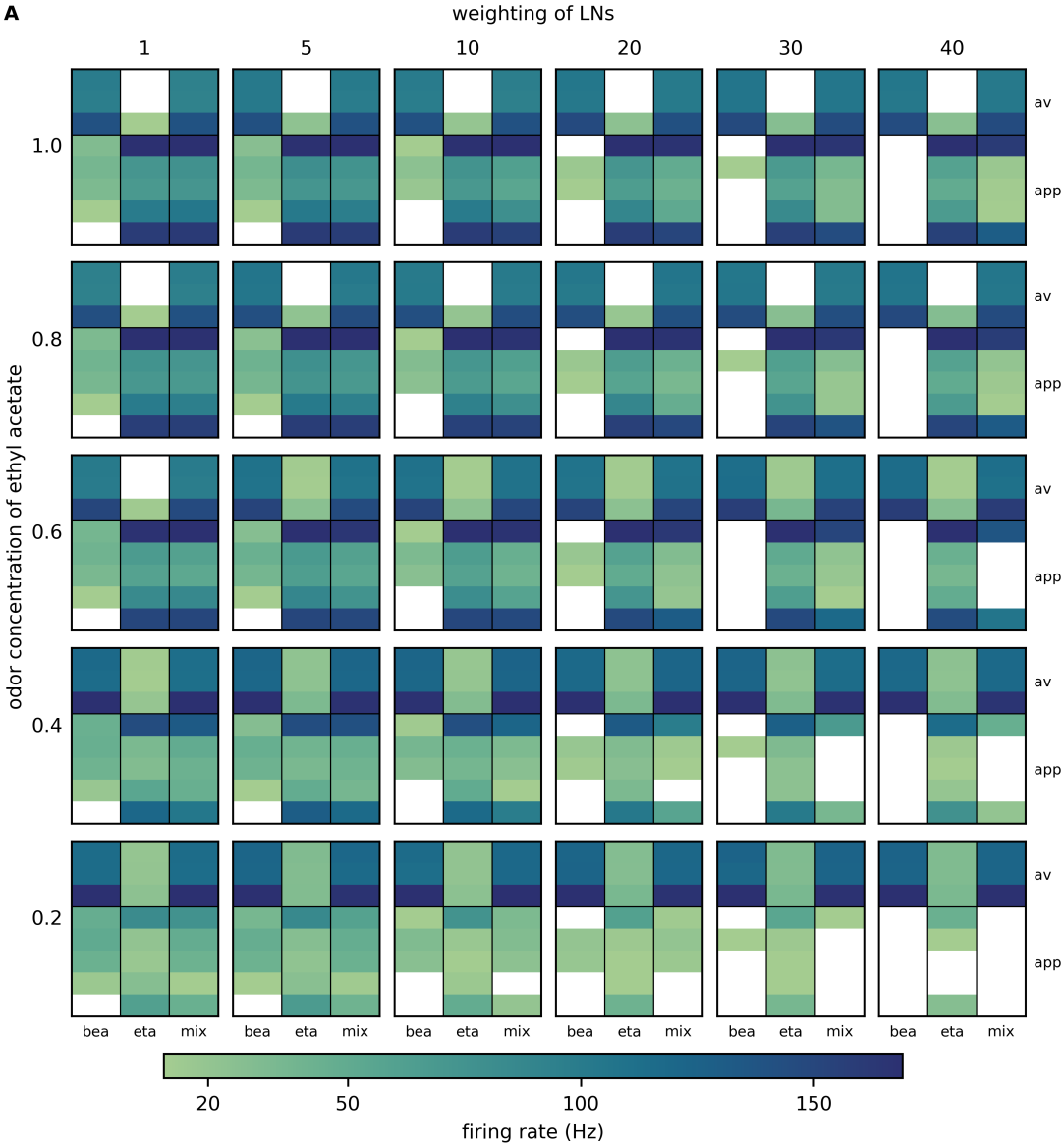

Fig. S3. Tuning of odor concentration and LN weight imbalance in the spiking network model. A grid search was used to tune the two key model parameters, which are the odor concentration and the imbalance in weighting of LNs. The y-axis indicates different ethyl acetate concentrations ranging from 0.2 (low concentration) to 1 (high concentration), while the x-axis shows increasing levels of synaptic weight imbalance in LNs. Each heatmap shows the PN responses to benzaldehyde, ethyl acetate and their binary mixture for aversive (DL1, DL5) and appetitive (DM1-4) glomeruli. The color indicates the mean PN firing rate during odor stimulation.

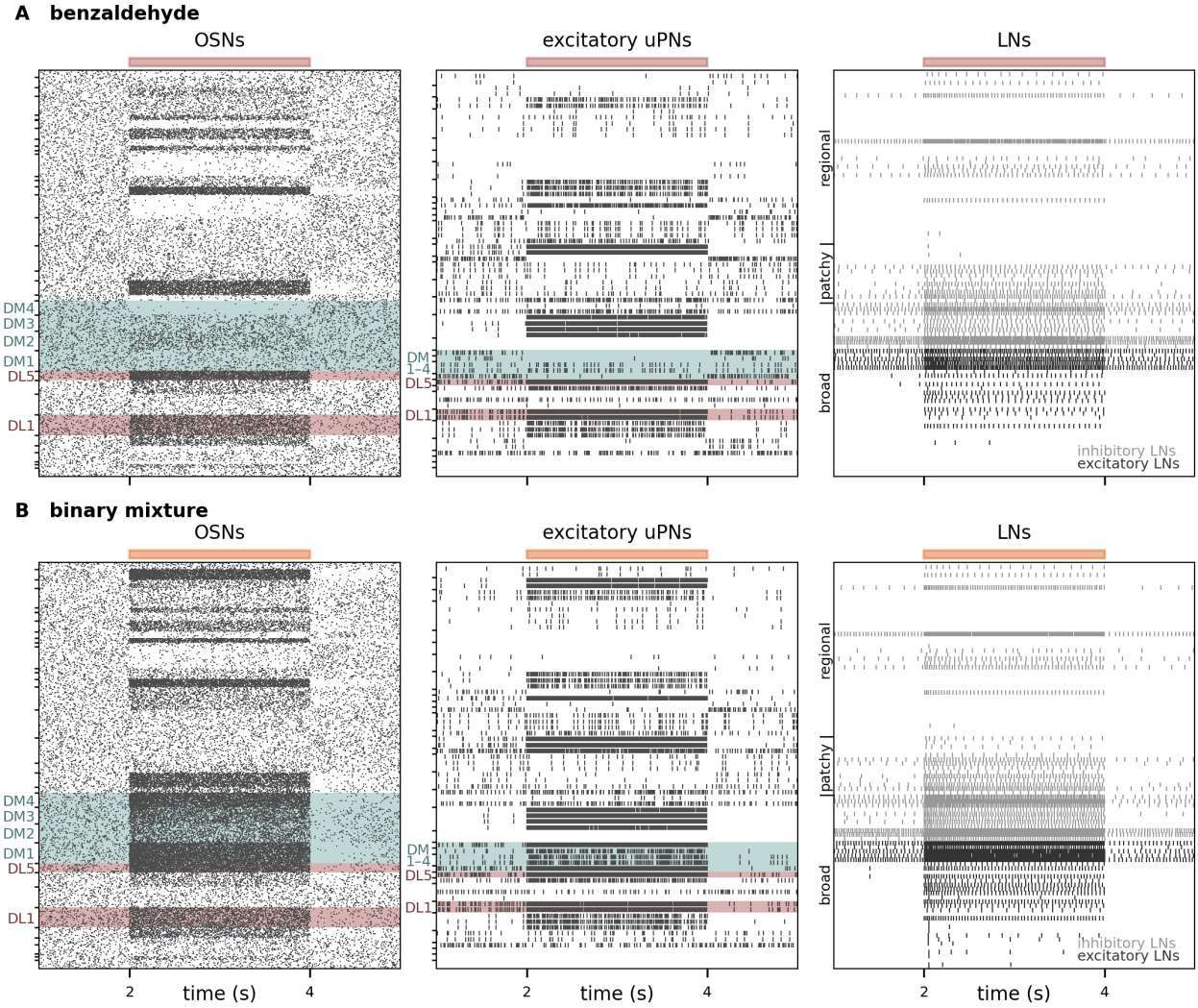

Fig. S4. Spike raster plots of network activity in response to odor stimulation. (A) As in Figure 3B-D, but showing network response to odor stimulation with benzaldehyde. **(B)** As in **A**, but for odor stimulation with a binary mixture of benzaldehyde and ethyl acetate. The ethyl acetate concentration in this simulation was set to 1.

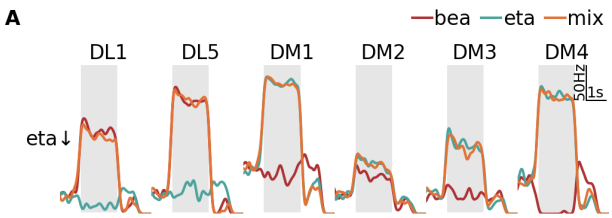

Fig. S5. Balanced model fails to reproduce functional recordings during odor mixture processing. Mean simulated time-resolved firing rates in the balanced model in response to 2 second odor stimulation (highlighted in gray) with benzaldehyde (bea) and ethyl acetate (eta) at low concentration (0.6), and their binary mixture (n=10). Note that the response towards the binary mixture in glomeruli DM1-4 is not reduced compared to the response to the pure ethyl acetate.

2.3 A Model Investigation of Short-Term Synaptic Plasticity Tuned via Unc13 Isoforms

Authors: Magdalena Springer, Stephan J. Sigrist, Martin P. Nawrot

Repository: ***bioRxiv*** **(2025)**

DOI: 10.1101/2025.06.18.660326

Contribution: The study was conceptualized by MPN, SJS, and MS. The physiological data were obtained from Fulterer et al. (2018). All modeling, data analysis and visualization were conducted by MS. The manuscript was written by MPN, SJS, and MS.

bioRxiv preprint doi: https://doi.org/10.1101/2025.06.18.660326; this version posted June 19, 2025. The copyright holder for this preprint (which was not certified by peer review) is the author/funder, who has granted bioRxiv a license to display the preprint in perpetuity. It is made available under aCC-BY-NC 4.0 International license.

A model investigation of short-term synaptic plasticity tuned via Unc13 isoforms.

Magdalena Springer[1], Stephan Sigrist[2] and Martin Paul Nawrot[1]

[1]Computational Systems Neuroscience, Institute of Zoology, University of Cologne, 50674 Cologne, Germany
[2]Institute for Biology and Genetics, Free University Berlin, 14195 Berlin, Germany

Short-term synaptic plasticity (STP) is a fundamental mechanism of neural computation supporting a variety of nervous system functions from sensory adaptation and gain control to working memory and decision making. At the presynaptic release site, an interplay between distinct (M)Unc13 protein isoforms is suggested to orchestrate depressing and facilitating components of STP. In this study, we introduce a modification of the well-established Tsodyks-Markram Model (TMM) for STP. We constrain our model by *in vivo* intracellular recordings in the olfactory system of the fruit fly, where previous work suggested Unc13A to provide a phasic, depressing and Unc13B a tonic, facilitating release component. A combination of a facilitating and a depressing model component indeed allowed for accurate model fits. Differential knock-down experiments of the Unc13A and Unc13B gene variants provide biological model interpretation, linking the protein-specific molecular mechanisms to synaptic function and STP. Our mathematical formulation of protein-dependent STP can be readily and efficiently used to design biologically realistic spiking neural network models that feature different genetically defined synapse types.

Keywords: Synaptic transmission | Short-term plasticity | Unc13 | Tsodyks-Markram Model

STP is an ubiquitous phenomenon in excitatory and inhibitory synapses of the invertebrate and vertebrate peripheral and central nervous systems (1–4). It describes the modulation of synaptic efficacy in response to the temporal pattern of presynaptic action potential (AP) firing and takes effect on the time scales of sensory-motor transformation, communication and working memory (3, 5–9).

Synaptic computations form fundamental building blocks for network- and systems-level functions. At the synaptic level, STP enables synaptic filtering (10–13), while at the circuit level it supports input-specific sensory adaptation and gain control mechanisms (3, 14–16). Network-level implementations demonstrate its role in shaping attractor dynamics for state transitions (17), maintaining working memory representations (8, 18–20), and facilitating action selection and decision-making processes (8, 20).

New insights into the molecular and cellular mechanisms underlying STP (21, 22) highlight the role of the two protein isoforms Unc13A and Unc13B in *Drosophila melanogaster*. They are enriched at the active zones (AZs) of most chemical synapses and are critical for synaptic vesicle fusion and neurotransmitter release (23). While Unc13A is localized close ($\approx$ 70 nm) to the voltage-gated calcium channels by the AZ scaffold protein Bruchpilot, Unc13B is positioned more distantly ($\approx$ 120 nm) by the Syd-1 AZ scaffold protein (24). It has been suggested that Unc13A promotes phasic vesicle release and short-term depression, whereas Unc13B dominated synapses show more tonic vesicle release and dominant short-term facilitation (24–26). The relative expression of the two isoforms varies across different synapse types and thus regulates the short-term dynamics of synaptic transmission and determines the functional synapse type (2, 25, 26).

In mammals, a homologous protein family with distinct Munc13 isoforms has been shown to play a highly similar role in presynaptically regulating synaptic transmission dynamics and STP (2, 27).

Results

Application of the TMM to OSN–PN synapses. The TMM (1, 28) is a phenomenological model of STP and finds wide application in local circuit and large scale spiking

bioRxiv preprint doi: https://doi.org/10.1101/2025.06.18.660326; this version posted June 19, 2025. The copyright holder for this preprint (which was not certified by peer review) is the author/funder, who has granted bioRxiv a license to display the preprint in perpetuity. It is made available under aCC-BY-NC 4.0 International license.

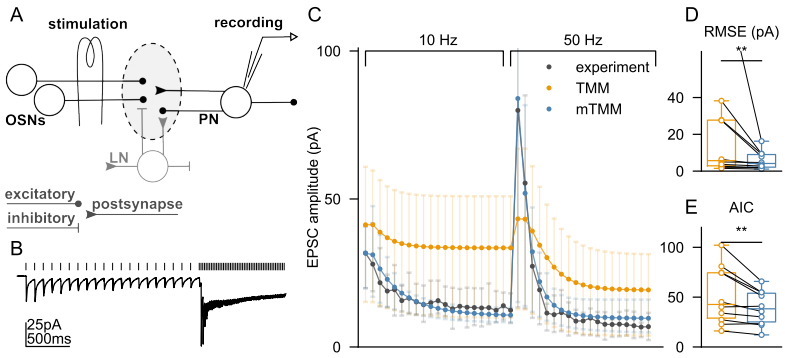

Fig. 1. Models of short-term plasticity evaluated at the OSN-PN wild-type synapse. (A) Schematic of the experimental setup. Electrical stimulation of the antennal nerve activates OSN axons, postsynaptic EPSCs are monitored in single PNs using whole-cell patch clamp recording. Adapted from (32). (B) Top: The stimulation protocol assembles a 10 Hz pulse train (100ms inter-stimulus interval), immediately followed by a 50 Hz pulse train (20ms inter-stimulus interval). Bottom: Mean postsynaptic current trace in PNs. Adapted from (25). (C) Analysis of successive EPSC amplitudes (mean ± 25th and 75th percentiles across 10 PNs) in response to the stimulus protocol for experimental recordings (black), original TMM (orange), and the modified TMM (blue). (D) Root Mean Squared Error (RMSE) of the model fit to experimental EPSC amplitudes for TMM and mTMM. (E) Akaike Information Criterion (AIC) comparing TMM with mTMM.

neural network models (8, 29–31). In its original form (eqns. 1a-1c) it describes a short-term depressing (STD) component governed by the variable x ($0 \leq x \leq 1, x_0 = 1$) that represents the fraction of available neurotransmitter resources, and a short-term facilitating (STF) component that is modeled by the variable u ($0 \leq u \leq 1, u_0 = 0$), representing the AP induced accumulation of calcium in the presynaptic terminal. With each AP of the presynaptic neuron, the facilitation variable u increases while the depression variable x decreases. The synaptic current I_S is then defined according to

$$\frac{du}{dt} = -\frac{u}{\tau_f} + U * (1 - u^-)\delta(t - t_{sp}), \quad [1a]$$

$$\frac{dx}{dt} = \frac{1 - x}{\tau_d} - u^+ * x^-\delta(t - t_{sp}), \quad [1b]$$

$$I_S = A * u^+ * x^-, \quad [1c]$$

where t_{s_p} denotes the AP times, U is the increment of u induced by each AP, τ_d and τ_f represent the time constants with which variables u and x approach their initial values, and A defines the maximum synaptic efficacy. The superscripts $^-$ and $^+$ indicate the time point right before and right after t_{s_p}, respectively. The parameter set (A, U, τ_d, τ_f) determines the extend to which facilitation and depression are expressed in the model synapse.

We applied the TMM to electrophysiological data recorded at the synapse between Olfactory Sensory Neurons (OSNs) and Projection Neurons (PNs) in the antennal lobe of the wild-type fruit fly *D. melanogaster* (25). As sketched in Fig. 1 A, whole-cell voltage clamp recordings were performed from individual postsynaptic PNs during electrical stimulation of presynaptic OSN axons in the antennal nerve. The stimulation protocol (Fig. 1 B) included a step change from a regular 10 Hz stimulation to a regular 50 Hz stimulation. The excitatory postsynaptic current (EPSC) amplitude decays over repeated stimulation, indicating a clear depressing component (black curve in Fig. 1 C). At the same time, a high increase in EPSC amplitude after the first short-latency stimulus indicates a component of paired-pulse facilitation at this synapse type. We then fitted the TMM to our experimental data, identifying the best-matching parameter set for each individual neuron (Tab. 1, Material and Methods). The resulting model performance remained poor, despite an extensive parameter search. It particularly could not accurately reproduce the temporal pattern of EPSC amplitudes, failing to simultaneously capture both, the clear depression of high amplitudes and the paired-pulse facilitation in response to the first short inter-stimulus interval (Fig. 1 C).

Modifications improve model performance. Out of this reason, we introduced two modifications to the original model. In the modified TMM (mTMM), the amount of decrease in x is defined by $(u^-)^X$. The introduction of the exponent $X < 1$ implies a convex dependence of depression on the release probability u, meaning that the amount of depression increases with the availability of ready-releasable vesicles in a sublinear manner and approaches a plateau as release probability nears its maximum. Additionally, u increases from its initial value $u_0 > 0$ and is incremented immediately after the occurrence of an AP, allowing for the decoupling of the baseline

bioRxiv preprint doi: https://doi.org/10.1101/2025.06.18.660326; this version posted June 19, 2025. The copyright holder for this preprint (which was not certified by peer review) is the author/funder, who has granted bioRxiv a license to display the preprint in perpetuity. It is made available under aCC-BY-NC 4.0 International license.

release probability from the activity-dependent increase in release probability (33, 34). The EPSC amplitude is then defined as

$$\frac{du}{dt} = \frac{u_0 - u}{\tau_f} + U * (1 - u^-)\delta(t - t_{sp}), \quad [2a]$$

$$\frac{dx}{dt} = \frac{1 - x}{\tau_d} - (u^-)^X * x^- \delta(t - t_{sp}), \quad [2b]$$

$$I_S = \frac{A}{u_0} * u^- * x^-. \quad [2c]$$

Importantly, the proposed model adjustments in the tuned mTMM allowed to accurately reproduce EPSC amplitudes throughout the stimulation protocol (Tab. 1, Fig. 1 C). The RMSE is strongly and significantly decreased in the mTMM compared to the original model (Fig. 1 D). The Akaike Information Criterion (AIC) is also reduced (Fig. 1 E), indicating that the performance gain by the mTMM is not caused by overfitting. We conclude that the mTMM outperforms the original TMM.

Table 1. Optimized model parameters for the TMM and the mTMM.

TMM				mTMM			
	min	max	optimal		min	max	optimal
A	2	1024	330±295	**X**	0.01	0.99	0.37±0.12
U	0.01	0.99	0.17±0.13	**U**	0.01	0.99	0.31±0.29
tau_f	12	2380	46.5±16.2	**tau_f**	12	2380	15.8±4.7
tau_d	12	2380	510±323	**tau_d**	12	2380	1490±653

Model parameters were optimized using an exponential grid search with 10 values per parameter to identify the best-performing parameter sets. Optimal values (mean±standard deviation across 10 PNs) correspond to the parameter set that yielded the lowest weighted error relative to the experimental data. The time constants tau_f and tau_d are reported in ms.

Model investigation of Unc13A and Unc13B isoforms. In the previous study by Fulterer and colleagues (25), the roles of Unc13A and Unc13B isoforms in synaptic transmission at the OSN–PN synapse were investigated in separate knock-down (KD) experiments of both isoforms (Fig. 2). We re-analyzed these data with the objective to reveal the change of model parameters when one isoform predominates. For parameter optimization we employed a Bayesian method that resulted in a four-dimensional likelihood distribution across the four adjustable model parameters (33). We then used the parameter set with the highest likelihood for the optimal model, which accurately replicated the experimentally observed EPSC amplitudes in all three experimental conditions (Fig. 2 B,E,H).

Data and model clearly show a strong effect of Unc13A KD in comparison to the WT synapse and only a weak effect of the Unc13B KD, confirming the result that the OSN-PN synapse is Unc13A dominated. The Unc13A KD is expressed in a strong reduction of the paired-pulse facilitation at the transition from 10Hz to 50Hz stimulation. In our model, this finds expression in a strong reduction of the parameter U in Fig. 2J, while the marginal distribution for the facilitation time constant τ_f is now flattened. The depression time constant τ_d assumes smaller values, indicating a faster recovery of x and thus clear depression takes effect only for short inter-pulse intervals. Together, the model parameters allow us to infer that Unc13A supports the phasic and Unc13B the tonic component of synaptic transmission.

Discussion

This study presents a tailored model of STP that captures the functional diversity introduced by Unc13 isoforms at central synapses in the fly olfactory system.

Functional implications. Previous studies have shown that the distinct roles of Unc13 isoforms in shaping synaptic transmission have important functional consequences across multiple levels of neural processing, as evidenced in *D. melanogaster* (22). These isoform-specific differences extend beyond synaptic physiology to influence sensory processing and behavior. For instance, Unc13A and Unc13B differentially shape sensory coding and innate behavior towards appetitive and aversive cues, including food odors (35–37). In the context of learned behavior, Unc13A plays a particularly critical role in the formation of short- and mid-term aversive memories (38–40). Our phenomenological model of Unc13A or Unc13B-dominated synaptic transmission can serve as a modular component for integration into existing circuit models of the fly olfactory system. This offers a framework for investigating the functional implications of molecular properties of synaptic release.

Comparison to other models. Several previous studies have proposed modified versions of the widely applied TMM, tailored to specific

bioRxiv preprint doi: https://doi.org/10.1101/2025.06.18.660326; this version posted June 19, 2025. The copyright holder for this preprint (which was not certified by peer review) is the author/funder, who has granted bioRxiv a license to display the preprint in perpetuity. It is made available under aCC-BY-NC 4.0 International license.

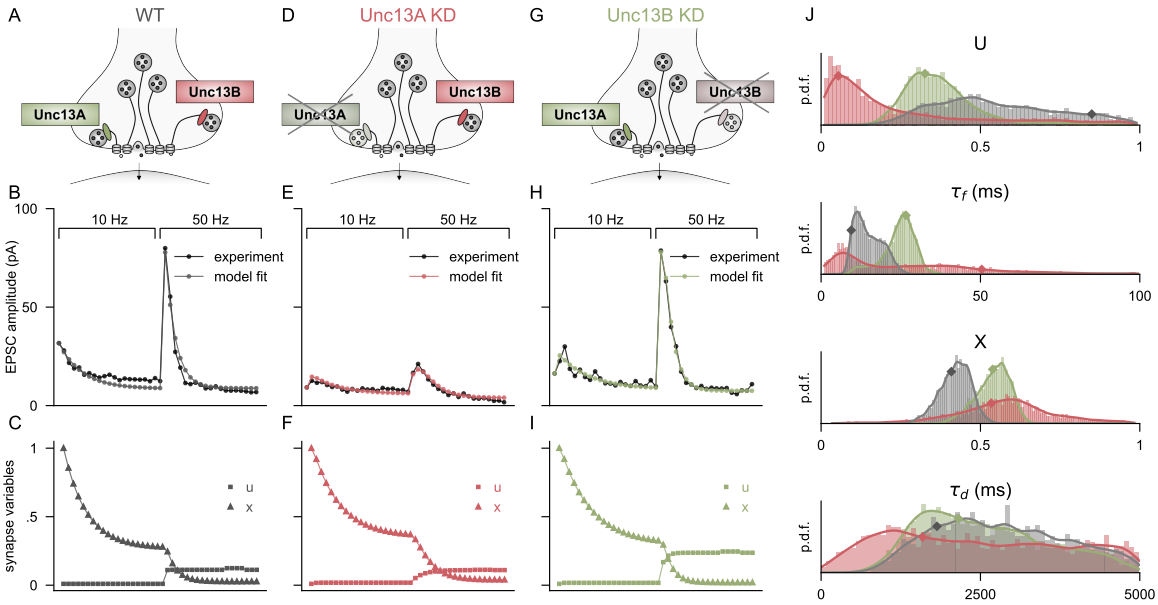

Fig. 2. Tuning the extended mTMM to Unc13 KD conditions. (A) Schematic of vesicle release mediated by the Unc13A and Unc13B isoforms. (B) Model fit of the extended mTMM to the mean EPSC amplitudes under wild-type (WT) conditions. Experimental data adapted from (25). (C) Dynamics of short-term plasticity variables x and u in the WT condition. (D–F) Corresponding panels for the Unc13A KD condition, showing (D) vesicle release via Unc13A, (E) model fit to EPSC amplitudes, and (F) short-term plasticity dynamics. (G–I) As in panels D–F, but for the Unc13B KD condition. (J) Histograms and kernel density estimates of posterior distributions of synaptic parameters for WT (grey), Unc13A KD (red), and Unc13B KD (green). Diamonds indicate the maximum *a posteriori* estimates, corresponding to the highest log-likelihood values that were used for fits in B,E,H.

use cases (18, 33, 34). For instance, (34) introduced a version of the TMM in which the equilibrium release fraction u_0 is decoupled from the spike-triggered increment U. This modification allows independent tuning of both model parameters, similar to the approach used in this study. In contrast to the phenomenological TMM, other models of synaptic transmission have taken a more mechanistic perspective. For example, several studies have explored parallel or sequential vesicle priming mechanisms, incorporating distinct vesicle states and transitions between loosely and tightly docked vesicles, as well as their replenishment from a reserve pool (41–45). These distinct vesicle pools align with the separate roles of Unc13 isoforms, offering a potential alternative framework for modeling the dual release mechanisms. Another study has highlighted how vesicle-Ca^{2+} channel distances shape STP through activity-dependent modulation of the readily releasable pool (46). In this work, we present a phenomenological model capturing Unc13-specific diversity in short-term synaptic dynamics. The key advantage of this model lies in its small parameter set, providing a biologically realistic yet computationally efficient mathematical abstraction of the underlying molecular mechanism.

Limitations. While our proposed model effectively captures the transmission dynamics of the studied synapse type and offers insight into Unc13 isoform function, certain limitations should be considered. First, our study focuses on synapses between OSNs and PNs in the fly olfactory pathway, which are dominated by the phasic Unc13A isoform (Fig. 2,(25)). This allows us to infer properties of Unc13A-specific transmission but does not directly inform us on the transmission properties of the tonic Unc13B isoform. Future work could explore whether our model captures well Unc13B-dominated transmission, such as at the synapse between local interneurons (LNs) in the fly antennal lobe or between PNs and specific classes of lateral horn neurons (LHNs) (25, 36). While (36) provide initial electrophysiological recordings from PN-LHN synapses, detailed transmission data for Unc13B-rich sites remain limited, highlighting an important area for future experimental and modeling efforts. Second, the experimental data used to fit our model, particularly in the Unc13 KD conditions (Fig. 2), is limited in sample size. Given this constraint and the variability

bioRxiv preprint doi: https://doi.org/10.1101/2025.06.18.660326; this version posted June 19, 2025. The copyright holder for this preprint (which was not certified by peer review) is the author/funder, who has granted bioRxiv a license to display the preprint in perpetuity. It is made available under aCC-BY-NC 4.0 International license.

within the dataset and across individuals, we chose to fit our model to the mean EPSC amplitudes rather than individual responses. This approach may overlook sample-specific variations and does not easily allow for statistical analyses between conditions (47). Finally, our model considers synaptic dynamics in a highly simplified and isolated context. For example, we do not incorporate lateral and feedback inhibition from LNs in the antennal lobe that targets OSNs and PNs (48, 49) and may thus influence transmission dynamics.

Outlook. Future studies can build on our framework by i) comparing the examined Unc13A dominated synapse to differently Unc13B tuned synapse types (25, 36), and ii) exploring how the distinct roles of Unc13 isoforms in shaping synaptic transmission extend to sensory processing and behavior in large-scale neural network simulations, highlighting the documented functional significance of Unc13 isoform-specific transmission dynamics in *D. melanogaster* (22).

Materials and Methods

Experimental data. The experimental data were obtained from (25). A single *in vivo* recording was performed per animal. In each PN, EPSC peak amplitudes were extracted for all stimulus pulses.

Model. Our minimal spiking neural network was implemented using Brian2. The model included a SpikeGeneratorGroup(), which mimicked the stimulation protocol from the experimental dataset, and a synapse with either the original or modified variant of the TMM connected to a postsynaptic neuron.

Parameter optimization. To optimize the model, we conducted a grid search to determine for which parameter set the TMM and mTMM could capture the experimental synaptic dynamics for each single recording optimally. For parameters X and U, we selected a uniformly spaced grid, whereas for A, τ_f, and τ_d we used an exponential grid to efficiently sample a broader range, each with a grid size of 10. For each parameter set we calculated the root mean square error (RMSE) between simulated EPSC amplitudes y_i and experimental EPSC amplitudes $\hat{y}_i$ across 40 stimulations as

$$\mathrm{RMSE}(y, \hat{y}) = \sqrt{\frac{\sum_{i=0}^{N-1} w_i (y_i - \hat{y}_i)^2}{N}}$$

where a weighted error was used, with weights w_i proportional to the experimental peak value in order to proportionally emphasize high peak values observed after the frequency change from 10 to 50 Hz.

To ensure comparability of the model performance for the TMM and the mTMM considering the fact that the latter has one additional parameter, we applied the Akaike Information Criterion (AIC)

$$\mathrm{AIC} = 2k - 2\log(L)$$

where L is the model likelihood and k is the number of free model parameters. Lower AIC values indicate a model that better fits the data while penalizing excess complexity.

Bayesian inference. For parameter tuning and comparison of the KD conditions, we used Bayesian optimization (33). Due to the limited sample sizes in the KD experiments (n=7 in Unc13A KD, n=5 in Unc13B KD), we used the mean postsynaptic EPSC amplitudes. We assumed uniform prior distributions for the parameters X, U, τ_f, τ_d. We assumed Gaussian noise, with mean μ equal to the average amplitude per stimulus pulse. Due to limited sample size, the standard deviation was estimated visually, leading to a selection of $\sigma = 10\,pA$. Sampling employed the Differential Evolution Metropolis variant, DEMetropolisZ (50), with a burn-in of 2500 samples, followed by 7500 samples across four chains. The optimal parameter set for each condition was selected based on the maximum log-likelihood.

All data analysis and parameter fitting were performed in Python 3. The programming code is accessible at: https://github.com/nawrotlab/Unc13-STP-Model.

bioRxiv preprint doi: https://doi.org/10.1101/2025.06.18.660326; this version posted June 19, 2025. The copyright holder for this preprint (which was not certified by peer review) is the author/funder, who has granted bioRxiv a license to display the preprint in perpetuity. It is made available under aCC-BY-NC 4.0 International license.

ACKNOWLEDGMENTS. We thank Katherine Eyring and Katherine Nagel for providing us with the electrophysiological data set as analyzed in (25). Funding was received from the German Research Foundation (DFG) through the priority program "Evolutionary Optimization of Neuronal Processing" (DFG-SPP 2205, ID 430592330 to M.P.N.), the Collaborative Research Center "Motor Control in Health and Disease" (DFG-SFB 1451, Project A06, ID 431549029 to M.P.N.), and the Research Unit "Structure, Plasticity and Behavioral Function of the Drosophila Mushroom Body" (DFG-FOR 2705, ID 365082554 to S.S. and M.P.N.).

bioRxiv preprint doi: https://doi.org/10.1101/2025.06.18.660326; this version posted June 19, 2025. The copyright holder for this preprint (which was not certified by peer review) is the author/funder, who has granted bioRxiv a license to display the preprint in perpetuity. It is made available under aCC-BY-NC 4.0 International license.

1. H Markram, Y Wang, M Tsodyks, Differential signaling via the same axon of neocortical pyramidal neurons. *Proc. Natl. Acad. Sci. United States Am.* **95**, 5323–5328 (1998).
2. C Rosenmund, et al., Differential control of vesicle priming and short-term plasticity by Munc13 isoforms. *Neuron* **33**, 411–424 (2002).
3. H Kazama, RI Wilson, Homeostatic Matching and Nonlinear Amplification at Identified Central Synapses. *Neuron* **58**, 401–413 (2008).
4. A Asopa, US Bhalla, A computational view of short-term plasticity and its implications for E-I balance. *Curr. Opin. Neurobiol.* **81**, 102729 (2023).
5. H Markram, M Tsodyks, Redistribution of synaptic efficacy between neocortical pyramidal neurons. *Nature* **382**, 807–810 (1996).
6. LF Abbott, WG Regehr, Synaptic computation. *Nature* **431**, 796–803 (2004).
7. G Mongillo, O Barak, M Tsodyks, Synaptic theory of working memory. *Science* **319**, 1543–1546 (2008).
8. G Deco, ET Rolls, R Romo, Synaptic dynamics and decision making. *Proc. Natl. Acad. Sci. United States Am.* **107**, 7545–7549 (2010).
9. H Motanis, MJ Seay, DV Buonomano, Short-term synaptic plasticity as a mechanism for sensory timing. *Trends Neurosci.* **41**, 701–711 (2018).
10. ES Fortune, GJ Rose, Short-term synaptic plasticity as a temporal filter. *Trends Neurosci.* **24**, 381–385 (2001).
11. JP Pfister, P Dayan, M Lengyel, Synapses with short-term plasticity are optimal estimators of presynaptic membrane potentials. *Nat. Neurosci.* **13**, 1271–1275 (2010).
12. R Rosenbaum, J Rubin, B Doiron, Short term synaptic depression imposes a frequency dependent filter on synaptic information transfer. *PLoS Comput. Biol.* **8**, e1002557 (2012).
13. M Díaz-Quesada, FJ Martini, G Ferrati, I Bureau, M Maravall, Diverse thalamocortical short-term plasticity elicited by ongoing stimulation. *J. Neurosci.* **34**, 515–526 (2014).
14. LF Abbott, JA Varela, K Sen, SB Nelson, Synaptic depression and cortical gain control. *Science* **275**, 220–224 (1997).
15. JS Rothman, L Cathala, V Steuber, RA Silver, Synaptic depression enables neuronal gain control. *Nature* **457**, 1015–1018 (2009).
16. Z Deng, S Oosterboer, W Wei, Short-term plasticity and context-dependent circuit function: Insights from retinal circuitry. *Sci. Adv.* **10**, eadp5229 (2024).
17. Y Katori, et al., Representational switching by dynamical reorganization of attractor structure in a network model of the prefrontal cortex. *PLoS Comput. Biol.* **7**, e1002266 (2011).
18. T Wang, et al., A phenomenological synapse model for asynchronous neurotransmitter release. *Front. Comput. Neurosci.* **10**, 153 (2016).
19. Y Mi, M Katkov, M Tsodyks, Synaptic correlates of working memory capacity. *Neuron* **93**, 323–330 (2017).
20. M Pals, TC Stewart, EG Akyürek, JP Borst, A functional spiking-neuron model of activity-silent working memory in humans based on calcium-mediated short-term synaptic plasticity. *PLoS Comput. Biol.* **16**, e1007936 (2020).
21. JS Dittman, Unc13: a multifunctional synaptic marvel. *Curr. Opin. Neurobiol.* **57**, 17–25 (2019).
22. C Piao, SJ Sigrist, (M)unc13s in active zone diversity: A Drosophila perspective. *Front. Synaptic Neurosci.* **13**, 798204 (2022).
23. TC Südhof, The presynaptic active zone. *Neuron* **75**, 11–25 (2012).
24. MA Böhme, et al., Active zone scaffolds differentially accumulate Unc13 isoforms to tune Ca2+ channel-vesicle coupling. *Nat. Neurosci.* **19**, 1311–1320 (2016).
25. A Fulterer, et al., Active zone scaffold protein ratios tune functional diversity across brain synapses. *Cell Reports* **23**, 1259–1274 (2018).
26. MA Böhme, AT Grasskamp, AM Walter, Regulation of synaptic release-site Ca2+ channel coupling as a mechanism to control release probability and short-term plasticity. *FEBS Lett.* **592**, 3516–3531 (2018).
27. N Brose, K Hofmann, Y Hata, TC Sudhof, Mammalian homologues of Caenorhabditis elegans unc-13 gene define novel family of C2-domain proteins. *J. Biol. Chem.* **270**, 25273–25280 (1995).
28. MV Tsodyks, H Markram, The neural code between neocortical pyramidal neurons depends on neurotransmitter release probability. *Proc. Natl. Acad. Sci. United States Am.* **94**, 719–723 (1997).
29. O Barak, M Tsodyks, Persistent activity in neural networks with dynamic synapses. *PLoS Comput. Biol.* **3**, e35 (2007).
30. JM Cortes, et al., Short-term synaptic plasticity in the deterministic Tsodyks-Markram model leads to unpredictable network dynamics. *Proc. Natl. Acad. Sci. United States Am.* **110**, 16610–16615 (2013).
31. L Tauffer, A Kumar, Short-term synaptic plasticity makes neurons sensitive to the distribution of presynaptic population firing rates. *eNeuro* **8** (2021).
32. KI Nagel, EJ Hong, RI Wilson, Synaptic and circuit mechanisms promoting broadband transmission of olfactory stimulus dynamics. *Nat. Neurosci.* **18**, 56–65 (2015).
33. RP Costa, PJ Sjostrom, MC van Rossum, Probabilistic inference of short-term synaptic plasticity in neocortical microcircuits. *Front. Comput. Neurosci.* **7** (2013).
34. L Pothmann, et al., Altered dynamics of canonical feedback inhibition predicts increased burst transmission in chronic epilepsy. *J. Neurosci.* **39**, 8998–9012 (2019).
35. A Pooryasin, et al., Unc13A and Unc13B contribute to the decoding of distinct sensory information in Drosophila. *Nat. Commun.* **12** (2021).
36. HS Kim, JM Jeanne, Divergent short-term plasticity creates parallel pathways for computation and behavior in an olfactory circuit (2024) Preprint on bioRxiv. https://doi.org/10.1101/2024.04.29.591740.
37. J Das, et al., The pre-synaptic Munc13-1 binds alcohol and modulates alcohol self-administration in Drosophila. *J. Neurochem.* **126**, 715–726 (2013).
38. J Woitkuhn, et al., The Unc13A isoform is important for phasic release and olfactory memory formation at mushroom body synapses. *J. Neurogenetics* **34**, 106–114 (2020).
39. O Turrel, N Ramesh, MJF Escher, A Pooryasin, SJ Sigrist, Transient active zone remodeling in the Drosophila mushroom body supports memory. *Curr. Biol.* **32**, 4900–4913.e4 (2022).
40. MA Böhme, et al., Rapid active zone remodeling consolidates presynaptic potentiation. *Nat. Commun.* **10**, 1085 (2019).
41. S Hallermann, et al., Bassoon speeds vesicle reloading at a central excitatory synapse. *Neuron* **68**, 710–723 (2010).
42. S Hallermann, M Heckmann, RJ Kittel, Mechanisms of short-term plasticity at neuromuscular active zones of Drosophila. *HFSP J.* **4**, 72–84 (2010).
43. N Ehmann, et al., Quantitative super-resolution imaging of Bruchpilot distinguishes active zone states. *Nat. Commun.* **5** (2014).
44. KH Lin, H Taschenberger, E Neher, A sequential two-step priming scheme reproduces diversity in synaptic strength and short-term plasticity. *Proc. Natl. Acad. Sci.* **119**, e2207987119 (2022).
45. I Weichard, et al., Fully-primed slowly-recovering vesicles mediate presynaptic ltp at neocortical neurons. *Proc. Natl. Acad. Sci.* **120**, e2305460120 (2023).
46. JR Kobbersmed, et al., Rapid regulation of vesicle priming explains synaptic facilitation despite heterogeneous vesicle:ca^{2+} channel distances. *eLife* **9**, e51032 (2020).
47. MA Churgin, et al., A neural correlate of individual odor preference in Drosophila. *eLife* **12**, RP90511 (2025).
48. YH Chou, et al., Diversity and wiring variability of olfactory local interneurons in the Drosophila antennal lobe. *Nat. Neurosci.* **13**, 439–449 (2010).
49. P Schlegel, et al., Information flow, cell types and stereotypy in a full olfactory connectome. *eLife* **10**, e66018 (2021).
50. CJF ter Braak, JA Vrugt, Differential evolution Markov Chain with snooker updater and fewer chains. *Stat. Comput.* **18**, 435–446 (2008).

Chapter 2 – Appendix

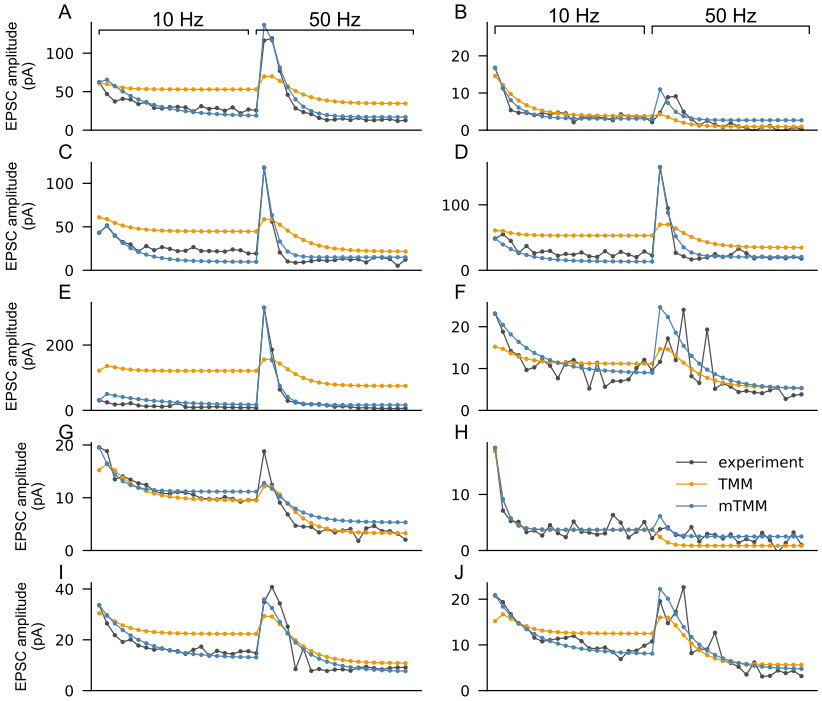

A1. Grid search resolved for each cell. While the averaged fits of the TMM and mTMM models are presented in Figure 1, A1 shows the individually best-fitting parameter sets obtained through grid search for each recorded cell. Notably, synaptic transmission at OSN–PN synapses is not uniform across cells. Some cells (**A, C, D,** and **E**) exhibit strong and prominent paired-pulse facilitation during the onset of the 50 Hz stimulation, whereas others show markedly less paired-pulse facilitation (**B, G, I,** and **J**), or none at all (**F** and **H**). The mTMM model outperforms the TMM especially in capturing the paired-pulse facilitation dynamics. The variability between cells aligns with a recent study showing that OSN–PN synapses differ in their levels of Bruchpilot, which is critical for active zone organization and the localization of Unc13A (1). These molecular differences correlate with variations in postsynaptic calcium responses and contribute to shaping individual behavioral outcomes in flies. Future studies with larger sample sizes could help to further dissect synapse variability in functional properties.

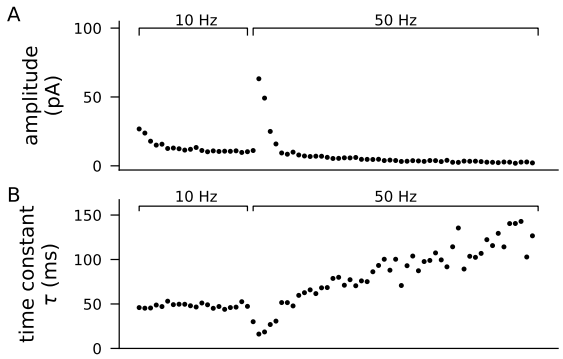

A2. Time constants of EPSCs during 10 Hz and 50 Hz stimulation. (A) Mean EPSC amplitudes across pulses during 10 Hz and 50 Hz stimulation. Amplitudes were calculated by first averaging current traces across trials and then measuring the peak amplitude relative to baseline for each stimulus pulse. **(B)** Corresponding time constants (τ) estimated from the decay phase of each EPSC, using the time difference between peak and the local minimum divided by the natural logarithm of their amplitude ratio. During the 10 Hz stimulation, τ remains relatively constant. In contrast, at the onset of the 50 Hz stimulation, τ drops sharply and then gradually increases over the course of the high-frequency stimulation. Notably, the estimation of τ becomes less reliable toward later pulses as EPSC amplitudes decrease and signal-to-noise ratio declines. The biphasic behavior of τ during the 50 Hz stimultation may reflect distinct contributions of Unc13A- and Unc13B-mediated release. The rapid Unc13A-driven release dominates early in the 50 Hz train and may correspond to faster time constants, while slower Unc13B-dependent transmission, characterized by delayed vesicle release, might underlie the progressive increase in τ. This interpretation is consistent with previous findings at the OSN–PN synapse that pharmacologically distinguished fast and slow release components with distinct kinetics (2).

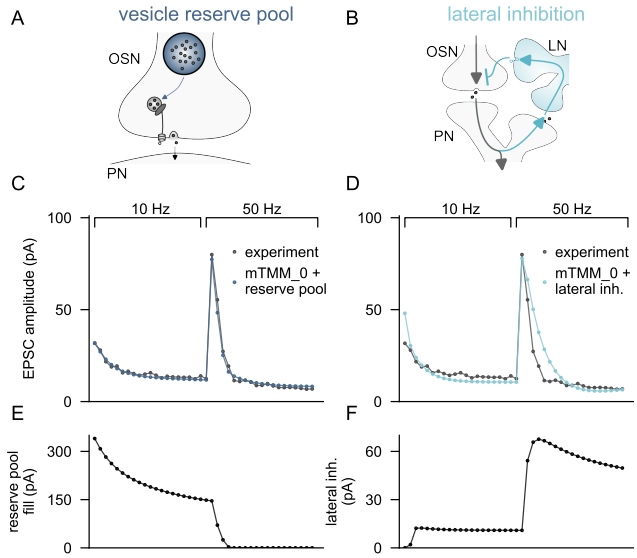

A3. Alternative modeling approaches. Alternatively to the implementation of the mTMM presented in the main text (eqns. 2a-2c), we implemented another modified version of the TMM, which does not the include X as an exponent, but rather defines the increase in the depression defining parameter x as the product of X and x^- according to

$$\frac{dx}{dt} = \frac{1-x}{\tau_d} - X * x^- \delta(t - t_{sp})$$

While this version of the TMM effectively replicates the experimental data at 10 Hz stimulations and during frequency modulations, it does not adequately capture the decrease in EPSC amplitudes during prolonged 50 Hz stimulations. To address this limitation, we propose two hypothetical mechanisms that could extend the transmission dynamics at this synapse type. We developed two model extensions, incorporating either of the two mechanisms.

(A) One potential extension involves implementing a vesicle reserve pool in our synapse model, following the proposal by (3). This concept suggests that a readily releasable vesicle pool is replenished by a larger reserve pool. The reserve pool refills at a slower time constant, leading to depletion and thus decrease in EPSC amplitudes during prolonged stimulation. We implemented a vesicle reserve pool as

$$\frac{dR}{dt} = \frac{R_0 - R}{\tau_r}$$

where R $(0 \leq \ R \leq \ R_0)$ is the current pool size, R_0 is the maximal pool capacity and τ_r is the pool's refill time constant. For each spike, the amplitude I was then computed as

$$I_S = A * u * x * 100 * \left(\frac{1}{1 + 4 * \exp(-R * 0.02)} \right)$$

where R modulates the EPSC amplitude via a transfer function. While vesicles are present in the reserve pool, peak amplitude remains unaffected; however, as the reserve depletes, I decreases. The pool R is updated upon every spike according to

$$R = R - I_S$$

(B) An alternative potential extension involves implemention of a simplified form of presynaptic inhibition, with lateral inhibition via local interneurons (LNs). Previous studies indicate that OSN–PN transmission dynamics are shaped not only by direct connections but also by indirect pathways involving LNs that presynaptically inhibit OSN synaptic terminals with slower transmission dynamics (2). Additionally, LN terminals have shown to exhibit higher expression of the Unc13B component, which shapes synaptic transmission towards slow and facilitating dynamics (4). LNs in the antennal lobe are highly specialized and diverse in their firing behavior (5, 6). Here, we only incorporated a simplified version of this lateral inhibition by modeling a second current I_2 that was calculated in the same manner as I, but with a differently tuned parameter set, which was then subtracted from I.

(C,D) By fitting the two extended model versions to the experimental data, we demonstrate that both effectively enhance model performance during prolonged 50 Hz frequency stimulations. Specifically, the model incorporating the vesicle reserve pool (RMSE = 2.52) demonstrates superior performance compared to the presynaptic inhibition model (RMSE = 8.13). However, we hypothesize that both mechanisms likely contribute synergistically to shaping synaptic transmission dynamics.

(E) Filling dynamics of the vesicle reserve pool. **(F)** Inhibitory current representing presynaptic lateral inhibition.

1. MA Churgin, et al., A neural correlate of individual odor preference in Drosophila. *eLife* **12**, RP90511 (2025).
2. KI Nagel, EJ Hong, RI Wilson, Synaptic and circuit mechanisms promoting broadband transmission of olfactory stimulus dynamics. *Nat. Neurosci.* **18**, 56–65 (2015).
3. S Hallermann, M Heckmann, RJ Kittel, Mechanisms of short-term plasticity at neuromuscular active zones of Drosophila. *HFSP J.* **4**, 72–84 (2010).
4. A Fulterer, et al., Active zone scaffold protein ratios tune functional diversity across brain synapses. *Cell Reports* **23**, 1259–1274 (2018).
5. YH Chou, et al., Diversity and wiring variability of olfactory local interneurons in the Drosophila antennal lobe. *Nat. Neurosci.* **13**, 439–449 (2010).
6. P Schlegel, et al., Information flow, cell types and stereotypy in a full olfactory connectome. *eLife* **10**, e66018 (2021).

Chapter 3

Discussion

3.1 Balancing Abstraction and Biological Detail in Computational Modeling

Computational modeling is a valuable tool for gaining insight into brain function. It offers a framework for formalizing brain structure and function, simulating mechanisms, testing hypotheses, and predicting neural dynamics. Modeling approaches can vary widely in their level of abstraction, depending on the research questions being addressed. This thesis presents four modeling approaches that span different abstraction levels, from circuit-level rate models to detailed synapse-level simulations (Figure 1.2). In Chapter 2.1, we examine learning paradigms at the circuit level to reproduce learning-related changes in firing rates. For this purpose, trial-based rate models, in which synaptic weights are adjusted between trials, are suitable. In Chapter 2.2, the implementation of a spiking model is preferred to investigate the role of lateralization in sensory processing, where precise spike timing plays a functional role. In Chapter 2.3, we focus on STP, and to simulate time-dependent changes in synaptic efficacy, we employ a dynamic synapse model.

While this thesis refers to abstraction primarily in terms of model granularity, the presented models also span another dimension, which is the modeling paradigm, ranging from mechanistic to phenomenological approaches. For example, while Chapter 2.1 uses mechanistic learning models grounded in established circuit motifs and synaptic plasticity rules, Chapter 2.3 explores short-term plasticity using a phenomenological synapse model that captures functional outcomes rather than underlying molecular mechanisms. To ensure that model predictions are informative and generalizable, it is crucial to balance biological detail and abstraction, depending on the purpose of the model. Abstract models can isolate specific mechanisms and offer conceptual clarity, but at the risk of oversimplifying the system under study. In contrast, increasing biological detail by integrating cellular and synaptic mechanisms into circuit models can improve plausibility and allow comparison to experimental data, but at the cost of increased complexity and reduced interpretability. In the following, I will discuss several modeling decisions from the perspectives of biological scale, computational cost, and biological realism.

3.1.1 Point versus Compartmental Neuron Models

All neuronal network models presented in this thesis are based on point neuron implementations. Although point neurons exhibit a high level of abstraction, they are widely used in computational neuroscience and beyond, and have proven highly useful models for neuronal circuits. Their main advantage is computational efficiency: they require fewer resources than morphologically detailed neuron models

and avoid the need to estimate a large number of often biophysical parameters. Despite their simplicity, point neurons can capture key dynamical features of neural activity, such as spiking behavior, adaptation, and synaptic integration (Herz et al., 2006). However, specific hypotheses require spatial structure within neurons, for instance, to model dendritic computations, compartmentalized input processing, or the effects of passive cable properties (London and Häusser, 2005). Recent work has increasingly provided valuable information on how dendritic organization and processing contribute to neural computation (Kirchner and Gjorgjieva, 2022). Studies carried out on mammalian systems have shown that single cortical neurons can perform complex computations within their apical dendrites, effectively functioning as microcircuits (Gidon et al., 2020; Larkum et al., 2022). While some models approximate dendritic computations using single point neurons, most modeling approaches use reduced or detailed compartmental models, separating dendrite and axon, or simulating full spatial morphology, respectively (Li et al., 2019; Herz et al., 2006; Poirazi and Papoutsi, 2020). Integrating dendritic mechanisms into artificial and deep neural network architectures drastically enhances their computational power, enabling functions such as deep convolutional processing, backpropagation, and more robust, precise, and efficient learning (Sacramento et al., 2018; Beniaguev et al., 2021; Chavlis and Poirazi, 2021; Chavlis and Poirazi, 2025).

Compartmentalization within neuronal branches plays an especially interesting role when axonal and dendritic domains are not clearly segregated. This is often the case in invertebrates, where many neurons possess a single neurite that either branches into dendritic and axonal regions or remains fully unsegregated (Strausfeld, 1976; Burrows, 1996). For example, widely branching LNs in the AL lacking clear axon–dendrite distinction have been implicated in mediating odor-evoked neural oscillations (Schlegel et al., 2021; Tanaka et al., 2009). Moreover, the absence of axonal myelination allows direct axo-axonal synapses, such as between OSNs in the AL (Schlegel et al., 2021; Manoim-Wolkovitz et al., 2025, see also Chapter 2.2, Figure 1B). These morphological characteristics, together with the non-spiking graded transmission in several neuron types, as observed for LNs in the AL and other brain regions, highlight the potential relevance of compartmentalized models beyond neuron-to-neuron communication (Wolf and Büschges, 1995; Joesch et al., 2008; Husch et al., 2009a; Husch et al., 2009b; Tabuchi et al., 2015; Schenk and Gaudry, 2023). In Chapter 2.2, we employ a spiking neural network with simplified LIF point neurons to study AL dynamics. While suitable for probing important aspects of interneuronal connectivity, we discuss potential benefits of extending the model to additionally explore spatio-temporal patterns of dendritic computation in compartmentalized LNs.

A pioneering example of compartmental modeling in the *Drosophila* olfactory pathway was presented by Gouwens and Wilson (2009), in which one DM1 PN (which is part of our AL analysis and model in Chapter 2.2) was modeled using detailed morphological and electrophysiological data. In this study, compartmentalization allowed for complex analysis of electrophysiological properties and signal propagation in this PN (Gouwens and Wilson, 2009; Tuthill, 2009). A more recent study by Liu et al. (2022) further extended this by creating a fully compartmentalized, connectome-based model of LH neurons integrating PN input. By comparing simulations with electrophysiological recordings (Jeanne et al., 2018), their findings showed that the density of the synapse strongly predicts the magnitude of the postsynaptic response. Furthermore, they could show that the location of the

postsynaptic site (axon versus dendrite) significantly influenced responses, while the distance from the synapse to the soma did not (Liu et al., 2022; Ganguly and Litwin-Kumar, 2022). Thus, the authors supported the usage of two-compartment models, where input and output are segregated.

However, in some neurons, synapses show distinct spatial patterns along dendritic trees, making full compartmentalization potentially relevant. One compelling use case is the modeling of synapses that neurons form with themselves, so-called autapses (Van Der Loos and Glaser, 1972). Autapses are a common phenomenon in the fly brain, including olfactory and visual circuits (Takemura et al., 2015; Gruber et al., 2023), but also occur in mammalian systems (Van Der Loos and Glaser, 1972; Lübke et al., 1996; Bacci et al., 2003). Previous computational studies have implemented autaptic activity using point neurons to study their role in firing regularity (Guo et al., 2016). However, recent investigations highlighting the peculiar spatial separation of autapse pre- and postsynaptic sites along dendritic arbors demand further investigation in more detailed models. A study by Gruber et al. (2023) demonstrated that the DL5 PN in the AL forms autaptic loops from the basal to the distal dendrite branches (Figure 3.1A). This specific neuron is also included in the analysis and modeling of odor mixture processing (Chapter 2.2). Here, we extend our modeling approach by building a spiking compartmentalized model of the DL5 PN, incorporating dendro-dendritic autapses as localized voltage-conductance couplings (Figure 3.1B). For this model, another EM dataset is used, since not all connectome datasets consider autaptic wiring in their analysis (Scheffer et al., 2020; Gruber et al., 2023). When we expose our model to a biologically realistic dynamic odor environment with short stimulus pulses (Murlis et al., 1992; Rapp and Nawrot, 2020), we observe that autapses may locally burst incoming signals into distant dendritic compartments in a temporally defined amplification window. Thus, they

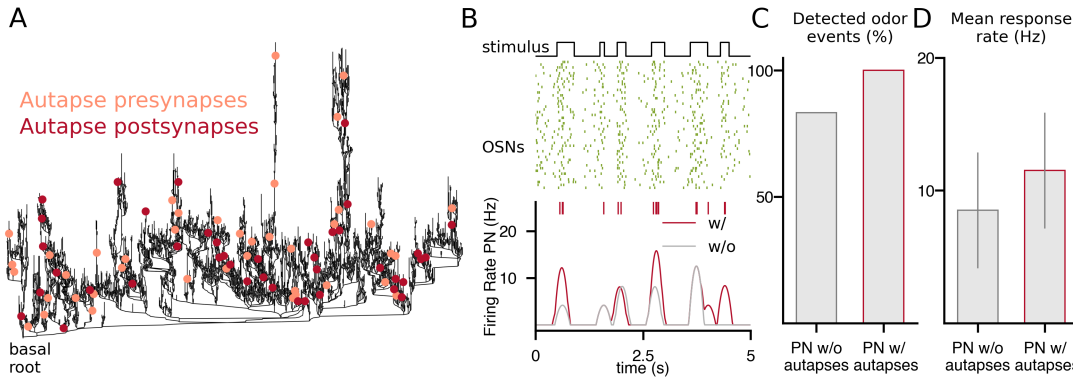

FIGURE 3.1: Functional interpretation of uPN autapses in a compartmentalized spiking model. (A) The uPN innervating the DL5 glomerulus forms chemical autapses (a synapse from a neuron onto itself). These autapses are distributed throughout the entire dendritic branches of the PN. The pre-autaptic sites basal to the dendritic root project to the more distal post-autaptic sites. (B) Rapid on-off stimulus dynamics (top, black) simulates navigation flight and results in temporally patterned OSN population response (green). The single uPN of DL5 is simulated as full-scale multi-compartment model based on EM reconstruction of dendrite and pre- and postsynaptic locations of dendro-dendritic autapses. It shows distinct spiking during stimulus encounters (red). Model with (w/) in comparison to the identical model without (w/o) uPN autapses shows (C) superior performance in stimulus detection and (D) increased odor response rate in the uPN. (Springer, Gruber, Rybak and Nawrot, *unpublished*).

may improve the detectability of transient odor events and accentuate responses to discrete and short-lived sensory events (Figure 3.1C-D). In the future, it would be interesting to further investigate this hypothesis, for example, by shuffling autapse pre- and postsynaptic localizations along the dendritic tree.

In the three examples of compartment models of the *Drosophila* olfactory pathway described above, as well as in other studies, full compartmentalization has been applied at the level of individual neurons (Gouwens and Wilson, 2009; Liu et al., 2022; Tobin et al., 2017, Figure 3.1). Scaling this approach to entire neuronal circuits would substantially increase both parameter complexity and computational load. Nonetheless, ongoing research efforts, such as the reconstruction of neocortical microcircuits in the Blue Brain Project or recent attempts to model the *Drosophila* brain using a compartmentalized HH model, provide an outlook of how compartmental modeling could be further extended (Markram et al., 2015; Higuchi et al., 2022) . Crucial for these efforts will be the availability of databases containing (i) detailed 3D morphological and physiological neuron models (McDougal et al., 2017; Gouwens et al., 2018), and (ii) tools to integrate structural electron microscopy and functional light microscopy data (Clements et al., 2024). Further, the implementation of such research efforts is largely facilitated through the availability of large-scale connectomic datasets that provide not only synaptic connectivity but also detailed 3D morphologies of neurons across an entire brain.

3.1.2 Benefits and Limitations of Connectome-Constrained Models

After the release of the first complete electron microscopy (EM)-based connectome reconstruction of *C. elegans* by White et al. (1986), the field of microscale structural connectomics has undergone rapid developments. During recent years, scientific breakthroughs have been further accelerated with technical advances in microscopy, such as the development of multi-beam SEM that allows faster data recording and advances in AI-accelerated automated image segmentation (Eberle and Zeidler, 2018; Schneider-Mizell et al., 2016; Januszewski et al., 2018; Buhmann et al., 2021). *Drosophila* as a model organism has played a key role in this research field (Schlegel et al., 2017), with connectomes of parts of the *Drosophila* brain, such as centers of olfaction (Bates et al., 2020), vision (Takemura et al., 2013; Nern et al., 2025), learning (Takemura et al., 2017; Eichler et al., 2017; Li et al., 2020), navigation (Turner-Evans et al., 2020; Hulse et al., 2021) being published over the past few years. The reconstruction of a complete hemisphere of the *Drosophila* brain with full segmentation, annotation, and public accessibility via user interface in 2020 has been heavily used by the fly community for analysis and modeling ever since (Scheffer et al., 2020; Plaza et al., 2022). The most comprehensive brain map of the entire *Drosophila* brain to date has been published for the larva by Winding et al. (2023) and for the adult fly and by Dorkenwald et al. (2024). In addition, the central brain connectome has been complemented by the ventral nerve cord connectome (Takemura et al., 2024; Azevedo et al., 2024; Stürner et al., 2025). For higher species, just recently the biggest up-to-date connectome of the mouse visual cortex has been published, allowing comparison between different species (Loomba et al., 2022; Bae et al., 2025).

Having access to detailed structural data that contain wiring diagrams at synaptic resolution offers major advantages in the construction of comprehensive and biologically realistic circuit models of the brain. In this thesis, we leverage connectomic data at multiple levels to inform and constrain our models. In Chapter 2.1.2,

we investigate the neuronal circuitry underlying second-order conditioning in the MB and examine the hemibrain connectome for missing pieces of information in a previously proposed circuit model (Scheffer et al., 2020). Our circuit model hypothesized an indirect connection between two MBONs via a third neuron. Using a systematic screening of the connectome, we identified three candidate MBONs that potentially mediate this functional link. Thereupon, one of the three candidate neurons could be validated to play a functional role in higher-order learning through behavioral experiments, further supported by our extended computational model. In Chapter 2.2, we made more extensive use of the hemibrain data set to analyze the AL circuitry and construct a fully connectome-constrained spiking network model. This approach aimed to link structural connectivity with functional data on odor mixture processing. However, we found that for our specific research question, connectomic data alone could not fully explain the observed functional dynamics, highlighting some of the limitations of connectomics.

While connectomics provides highly precise structural maps of the brain, it misses out on other critical dimensions of neural function and complexity. To achieve a comprehensive understanding of brain function, it is essential to integrate complementary methodologies alongside connectomics (Scheffer and Meinertzhagen, 2021). These missing aspects concern biochemistry, biophysics, cellular and synaptic physiology, as well as biological variability (see also the Discussion in Chapter 2.2). Another major limitation of current connectomic approaches is their lack of temporal resolution, since connectomes are static snapshots that cannot capture the dynamic, short- or long-term structural changes occurring in the brain. For example, current connectomic datasets do not allow for investigation or comparison of learning-dependent changes in the MB, which would be highly informative for studying the different learning paradigms explored in Chapter 2.1. However, recent research efforts suggest promising directions to bridge this gap. In particular, a recent preprint by Grasso et al. (2025) maps synaptic weight distributions in EM data to synaptic plasticity and learning. According to the Hebbian rule stating that the synaptic strength between two neurons increases with their co-activation, the suggest that synaptic plasticity may be reflected in systematic changes in the size of pre- and postsynaptic densities. Such advances may open the door to identifying plasticity sites and memory engrams even within static connectomic data.

3.1.3 Parameters and Computational Cost in Neural Networks

Inclusion of more biological details, such as including connectome or morphological data in a model, generally requires an increasing number of assumptions and parameter estimates, as many relevant factors, such as the biophysical properties of neurons, are not fully known. Some large-scale simulations of the whole *Drosophila* brain have demonstrated that it is possible to produce meaningful predictions even without parameter tuning (Shiu et al., 2024). However, setting model parameters arbitrarily comes at the risk of unknown or soft parameters dominating the output, which can undermine the interpretability and explanatory power of a model.

In Chapters 2.2 and 2.3 of this thesis, we employ grid or Bayesian searches to fit a small set of biophysical model parameters, for example synaptic time constants, that influence model dynamics directly, obtaining both point estimates and posterior likelihoods (Costa et al., 2013). In these two examples, exhaustive search remains feasible at this scale, due to the small number of free parameters, short simulated

time windows, and limited sample size in the experimental data. However, in the alternative synapse model variants as proposed in the Appendix of Chapter 2.3, the number of parameters already doubles, leading to an exponential increase in the number of parameter combinations and consequently to longer tuning times. Here, the process of tuning model parameters to match experimental data with Bayesian or brute-force search methods can become computationally expensive and time-consuming.

For large-scale networks, such as rate-coded or spiking models with dense synaptic connectivity, one normally decouples optimization layers: stochastic gradient descent (or variants such as Adam) efficiently updates millions of differentiable weight parameters, while separate hyper-parameter sweeps explore a much smaller external search space. In spiking models, however, these supervised learning algorithms pose additional challenges due to the non-differentiability of spikes. Here, recent advances inspired by neuromorphic computing have addressed this problem by employing surrogate gradient methods, such as Superspike (Zenke and Ganguli, 2018), or even exact gradient techniques like EventProp (Wunderlich and Pehle, 2021). These approaches restore differentiability and thus allow gradient-based optimization to coexist with classical hyper-parameter tuning, enabling efficient training of large spiking models.

Beyond parameter tuning, computational scalability plays a critical role in neural network simulations. The overall computational cost depends significantly on factors such as the size of the network in terms of number of neurons and layers, the degree of synaptic density, the duration of the simulation, and the modeling framework employed, and remains a matter of ongoing controversial debate (Valadez-Godínez et al., 2020). Scaling up one dimension of a model may require reducing complexity in others to keep computations tractable. There are different methods to reduce the computational cost of model simulations. In this thesis, we include parallelization and event-based simulation schemes in spiking models, which are particularly efficient in sparsely active networks. Furthermore, GPU-enhanced neural network simulators have been proven to be useful in reducing the computational demands of large-scale models, especially during extensive parameter searches (Yavuz et al., 2016; Knight and Nowotny, 2021; Schmitt et al., 2023).

3.2 Different Levels of Neural Plasticity

Neural systems exhibit plasticity across a broad range of temporal scales, from milliseconds to multiple days and beyond. In this thesis, we model both short-term plasticity (STP) on the order of milliseconds to seconds (Chapter 2.3) and long-term changes over minutes to hours or days (Chapter 2.1). In Chapter 2.3, we focus on modeling STP, which is a universal mechanism to rapidly modulate synaptic strength via presynaptic or postsynaptic mechanisms (Zucker and Regehr, 2002; Barroso-Flores et al., 2017). STP has been shown to play a crucial role in a broad range of functional aspects, including temporal filtering, gain control, working memory, and decision making (Goldman-Rakic, 1995; Abbott et al., 1997; Fortune and Rose, 2001; Deco et al., 2010; Deng and Klyachko, 2011). We investigate STP in the insect AL, which exhibits a particularly interesting interplay of neural adaptation, short-term depression (STD), and short-term facilitation (STF) at different sites (De Bruyne et al., 2001; Warren and Kloppenburg, 2014; Wilson, 2013; Kazama and

Wilson, 2008; Nagel and Wilson, 2016; Fulterer et al., 2018). However, STP is a general feature in *Drosophila* synaptic transmission and is also observed at peripheral sites such as the neuromuscular junction (Hallermann et al., 2010).

In contrast, Chapter 2.1 addresses long-term plasticity mechanisms, including long-term potentiation and depression that drive associative learning and memory processes. With the circuit models presented, we explore dopamine-mediated associative olfactory learning in the MB of *Drosophila*, which stores olfactory as well as visual memories (Heisenberg, 2003; Aso et al., 2009; Vogt et al., 2014; Owald and Waddell, 2015). In addition to the mushroom body, other brain regions like the central complex support distinct forms of learning and memory (Ofstad et al., 2011; Liu et al., 2006). In the following, we will discuss these modeling approaches in more detail, bring them into context, and explore their role in dynamic processes such as sensory adaptation, learning, and memory.

3.2.1 Linking Active Zone Composition to Plasticity and Behavior

In Chapter 2.3, we present a modified version of the well-established TM model to simulate STP in *Drosophila*, focusing on the isoforms of the Unc13 protein at presynaptic active zones. We chose a phenomenological modeling approach to realistically capture Unc13A and Unc13B dominated transmission in a lightweight synapse model. In contrast, other modeling efforts have employed synaptic function in more detailed and mechanistic models, incorporating calcium dynamics and vesicle release (Neher, 2015; Neher and Brose, 2018). These mechanistic models can be beneficial when aiming to explore specifically the interplay between different vesicle pools and their release dynamics.

In the future, phenomenological and mechanistic models could be extended by implementing the interplay of multiple active zone proteins and their roles in collectively shaping dynamical processes in more detail. For instance, Bruchpilot (Brp) and Syd-1 have been shown to differentially position Unc13A and Unc13B, respectively (Kittel et al., 2006; Wentzel et al., 2013; Fulterer et al., 2018). Moreover, a recently identified active zone protein named Blobby has been shown to regulate active zone assembly, scaffold organization, and release probability (Lützkendorf et al., 2025). Considering such molecular components beyond Unc13 in computational models would enable the investigation of how different synaptic protein families orchestrate vesicle release and STP. Importantly, the functional role of active zone proteins extends beyond short temporal scales and single-cell processes, contributing to circuit-level phenomena such as innate behavior, learning, and memory formation. At the level of the AL, Unc13A and Unc13B in PNs differently influence innate behavioral responses towards food odors, with Unc13A broadly attenuating behavior and Unc13B shifting behavioral valence towards attraction. At the MB level, the knockdown of Brp, Unc13A, or Blobby causes memory deficits (Knapek et al., 2011; Woitkuhn et al., 2020; Lützkendorf et al., 2025). Incorporating biologically realistic synapse models into circuit-level frameworks would allow for exploration of how short- and long-term plasticity might interact mechanistically. Further, implementation of specific protein manipulations into computational models would allow testing of hypotheses on how changes in active zone composition affect both synaptic dynamics and behavior. Overall, expanding models of synaptic transmission could provide a bridge between molecular synapse machinery and circuit-level computations.

3.2.2 Measuring Learned Behavior in Computational Models

In computational models of the brain, learning and memory are typically captured by long-lasting modifications of synaptic weights. Many models of associative learning in the fly MB are inspired by classical conditioning paradigms and implement learning based on the concept of Rescorla and Wagner (1972), which formalizes the idea that learning is driven by a prediction error, the mismatch between expected and actual outcomes (Horiuchi, 2019; Zhao et al., 2021; Jiang and Litwin-Kumar, 2021; Bennett et al., 2021; Jürgensen et al., 2024a).

In the two MB models presented in Chapter 2.1, prediction error drives synaptic plasticity at the connections between KCs and MBONs. As is common in MB modeling studies, we quantify learning using proxy measures that infer behavioral tendencies from MBON activity. Specifically, we interpret the learned valence of an odor as the change in MBON activation that it evokes. In the extinction model (Chapter 2.1.1), we compute the *Preference Index* based on the difference in activation between an approach-mediating MBON and another avoidance-mediating MBON. In the second-order conditioning model (Chapter 2.1.2), we derive a *Preference Index* by comparing odor-evoked activity for the avoidance-mediating MBON for the conditioned stimuli (CS1 or CS2) versus the non-conditioned stimulus (CS-). Thus, our proxies capture key functional aspects of learned behavior at the population level. Using this proxy is supported by numerous experimental studies showing that MBONs encode odor valence and learning, and steer behavioral decisions (Zhang et al., 2007; Aso et al., 2014a; Owald and Waddell, 2015; Hancock et al., 2022; Arican et al., 2023; Webb, 2024).

However, both models omit downstream motor circuits, which limits the ability to simulate the full sensorimotor transformation and embodied behavior directly. Further, other factors, such as individuality, integration of other influences such as internal states, and modeling of the full descending motor output pathway cannot be considered (Sayin et al., 2018; Tsai and Chou, 2022; Suárez-Grimalt et al., 2024; Stürner et al., 2025). Other studies have tackled this challenge by implementing models of insect locomotion and chemotaxis, and extending these to robotic systems (Helgadóttir et al., 2013; Davies et al., 2015; Webb, 2020; Sakagiannis et al., 2025b). An important future direction would be to extend MB learning models, such as the ones presented in Chapter 2.1, by integrating them with locomotion models (Feldotto et al., 2022; Jesusanmi et al., 2024; Lochner et al., 2024; Sakagiannis et al., 2025a). This would enable the direct simulation of learned behavior as motor output.

3.2.3 Opposing Learning Principles in Extinction and Second-Order Learning

In this thesis, we present two network rate models of the fly olfactory pathway, investigating different forms of associative learning and memory in *Drosophila*. Both models follow a mechanistic framework and are developed based on experimental investigations. In Chapter 2.1.1, we investigate extinction learning, in Chapter 2.1.2, we formalize second-order conditioning in a computational rate model. Even though the two learning concepts are theoretically incompatible, it can be shown that both principles are supported by same brain circuits. Both learning paradigms start with a classical conditioning, where an unconditioned stimulus is presented with a reinforcer, which leads to the association of the two, eliciting a learned

behavior in the conditioned stimulus. In a next step, there are two different conditioning paradigms for extinction and second-order learning. In the extinction learning paradigm, the previously learned stimulus is now a signal to form a parallel memory trace in order to modify the memory. In the second-order conditioning paradigm, the previously learned stimulus is serving as a signal to form a second memory trace towards another stimulus, while the original memory is preserved. The learning circuits involved in memory formation are similar, but not identical, with learning happens at the KC-MBON synapses and MBONs feedbacking onto dopaminergic neurons, which in turn functioning as neuromodulators mediating the learning signals (Felsenberg et al., 2017; Felsenberg et al., 2018; König et al., 2019; Yamada et al., 2023). Both phenomena have been formalized in computational models, but rarely within the same model (Jiang and Litwin-Kumar, 2021; Bennett et al., 2021; Yamada et al., 2023; Jürgensen et al., 2024b; Jürgensen et al., 2024a).

Why does the first trial during second-order conditioning does not lead to memory extinction? Potentially, both mechanisms are active, but the second-order memory is stronger than the extinction signal. It may be possible that the novelty of the CS2 presented during the new pairing during second-order conditioning may engage neuromodulators to gate or suppress the formation of active forgetting mechanisms that would normally occur during memory extinction. Another possible explanation could be that with the introduction of the new stimulus to the training session, the context is treated as a new distinct episode and thus functionally separates from the original associated memory trace. In future investigations, it would be interesting to further explore these opposing paradigms together in the same model circuitry. In addition, this would open up the possibility of further incorporating more aspects and principles of learning and unlearning, such as passive forgetting, conditioned or latent inhibition, trace conditioning, or reversal learning (Dwijesha et al., 2024).

3.3 Comparative Insights and Generalizability of *Drosophila*

Drosophila is a powerful model organism that offers numerous advantages for studying brain function (see also Chapter 1.2). In the past decades, *Drosophila* has become one of the most widely used models in neuroscience, taking a leading role in invertebrate science, similar to the mouse model in vertebrate science. However, discussions about diversity of animal models in biomedical science, criticizing the heavy reliance on single species such as mice, may be transferred to *Drosophila* as well (Keifer and Summers, 2016; Yartsev, 2017; Manger et al., 2008). Given the dominant role of *Drosophila* among insect models, it is important to avoid overgeneralizing its findings on neural principles to other organisms. For this reason, comparative neuroscience plays an essential role in providing a framework for distinguishing universal principles of neural computation from species-specific specializations of evolutionary optimization. In the following sections, I will compare similarities and differences between *Drosophila* and other arthropods, mostly insects, as well as vertebrate species.

3.3.1 Comparison to Other Arthropods

Among *Drosophila* and other arthropod species, there are many indications for conserved circuit principles as well as for evolutionary specializations shaped by ecological demands (Hansson and Stensmyr, 2011). Arthropod species inhabit highly different environments, from aquatic to terrestrial to aerial niches, and can follow either generalist or specialist evolutionary strategies. These specific idiosyncrasies lead to differences in sensory processing requirements and brain organization. The broad anatomical structure of the olfactory pathway is roughly similar between *Drosophila* and other arthropod species, with OSN signaling to the AL with its glomerular organization, to higher brain centers (Hansson and Anton, 2000; Zhao and McBride, 2020). However, there are substantial numerical differences among species, with *Drosophila* representing an exceptionally compact olfactory system at the lower end of the spectrum (Table 3.1).

TABLE 3.1: Comparison of olfactory system components across different arthropod species. Approximate neuron numbers are given per antenna or brain hemisphere. Numbers are obtained from the following studies: *Drosophila melanogaster*: Stocker (2001), Chou et al. (2010), Schlegel et al. (2021), Grabe et al. (2015), Bates et al. (2020), and Hallem and Carlson (2004); *Aedes aegypti*: McIver (1978), Ignell et al. (2005), and Thomas et al. (2025) *Panulirus argus*: Beltz et al. (2003), Grünert and Ache (1988), Schmidt and Ache (1996), and Harzsch and Krieger (2018); *Locusta migratoria*: Laurent (1996), Leitch and Laurent (1996), Anton et al. (2002), and Bicker and Stern (2020); *Apis mellifera*: Esslen and Kaissling (1976), Robertson and Wanner (2006), Galizia and Rössler (2010), and Paoli and Galizia (2021).

	Aesthetascs / Sensillae	OSNs	AL Glomeruli	PNs	LNs
Drosophila melanogaster	530	1.2k	55	300	200
Aedes aegypti	900	1.9k	65	?	?
Panulirus argus	1.2k	420k	1.3k	200k	100k
Locusta migratoria	4.7k	100k	1-2k	800	300
Apis mellifera	5k	60k	160	900	4k

The dense innveration within the AL of *Drosophila* exemplifies the high degree of connectivity found in insect brains, a characteristic observed observed across multiple species (Gascuel and Masson, 1991; Anton and Homberg, 1999; Fuscà and Kloppenburg, 2021a). In *Drosophila*, each AL glomerulus is typically packed with synapses from numerous OSNs, LNs and one or few PNs (Figure 3.2A-B). These synapses are typically part of polyadic clusters, in which a single presynaptic site contacts multiple postsynaptic sites (Figure 3.2C). This observation aligns with previous studies in flies (Meinertzhagen and O'Neil, 1991; Rybak et al., 2016) and other insect species such as cockroaches (Malun, 1991), honey bees (Gascuel and Masson, 1991) and locusts (Watson and Schürmann, 2002), indicating that polyadic synapses are a conserved feature in invertebrates. However, polyadic synapse formations with up to 20 postsynaptic partners, as observed in *Drosophila* (Figure 3.2D), may reflect a specialized adaptation for dense packing and energetically efficient signaling in the heavily miniaturized brain of the fruit fly (Rybak et al., 2016; Harzsch and

Krieger, 2018).

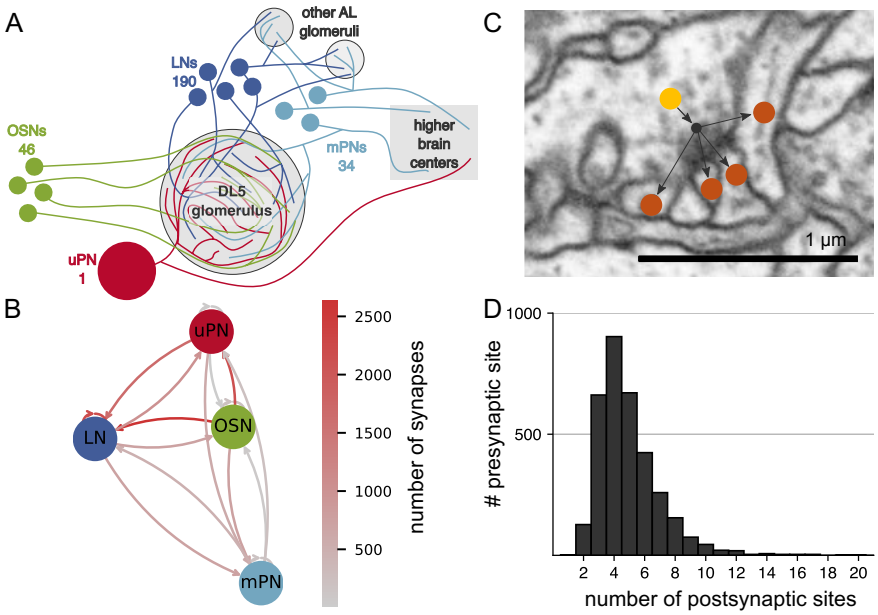

FIGURE 3.2: Statistical analysis of the connectome of the DL5 PN in *Drosophila*. (A) The DL5 is a glomerulus within the fly antennal lobe, which is innervated by a single uPN and broadly tuned towards aversive odors. For full dendritic tree and autaptic innervation of this neuron, see Figure 3.1A. OSN = Olfactory Sensory Neuron, uPN / mPN = uni / multiglomerular Projection Neuron, LN = Local Interneuron, AL = Antennal Lobe (B) Directed graph representation of neuron types and no. of connections based on the data set in Gruber et al. (2023). (C) Most synapses in the DL5 are part of polyadic structures, meaning that several postsynaptic sites (orange) share the same presynaptic partner (yellow). (D) Numerical distribution of postsynaptic sites per presynaptic site in DL5 glomerulus. In most of the polyadic groups, one presynaptic site targets four postsynaptic sites, also known as tetrads, but the maximal number goes up to 20 (Adapted from: Springer, Gruber, Rybak, Nawrot, *unpublished*).

Apart from the general organization, there seem to be different strategies among species of how odors are structurally encoded within the AL. *Drosophila* OSNs expressing one of ~50 receptors converge onto only one matching glomerulus in an organized manner, although recent studies have reported some degree of co-innervation (Hallem and Carlson, 2004; Couto et al., 2005; Task et al., 2022). This coding logic, which is similar in other species such as *Apis mellifera* (the honey bee), is also referred to as "canonical coding" (Paoli and Galizia, 2021). At the glomerular level, odors are then represented either as combinatorial codes, which involve activation patterns across multiple glomeruli for general odor processing, or as labeled lines, characterized by the exclusive activation of a single glomerulus. Labeled-line representations are particularly crucial for processing ecologically significant odors, such as toxins or pheromones (Haverkamp et al., 2018). However, this one-receptor-to-one-OSN-to-one-glomerulus organization as observed in the fruit fly does not appear to be a general principle among insects. For instance, *Aedes aegypti* (the mosquito) follows a non-canonical structure with more than twice as many receptor types than glomeruli, and co-expression of multiple receptor types in a single OSN (Herre et al., 2022; Thomas et al., 2025). *Locusta migratoria* (the locust) instead has many more glomeruli than receptor types, with glomeruli organized in a ring-like structure (Jiang et al., 2024). A non-canonical circuit design is suggested

to be a more general principle among arthropods, as it extends to other arthropod subclades such as crustaceans (e.g. *Panulirus argus*), which show a distributed representation of odor identity in compartmentalized glomeruli (Harzsch and Krieger, 2018).

Why do different arthropod species exhibit such divergent evolutionary strategies in odor coding? A conceptual comparison of odor representations in a fully distributed versus a fully canonical olfactory circuit is shown in Figure 3.3, representing two extremes of the strategies proposed, for instance, in crustaceans and *Drosophila*. To evaluate functional consequences of these architectures, we simulate odor processing in two simplified network models with identical numbers of neurons and synapses but differing in their connectivity logic. In the canonical model, each receptor type is assigned to a specific OSN population, which in turn projects exclusively to one glomerulus. In contrast, the distributed model randomized both OR-to-OSN expression and OSN-to-glomerulus connectivity (Figure 3.3A). When both networks are presented with two odor profiles, both are then processed through each network. Despite the same input profiles, the distributed network yields more overlapping glomerular representations than the canonical network, as measured by cosine similarity between the odor-evoked glomerular activation patterns (Figure 3.3B). Randomizing the connectivity might potentially increase representational similarity and reduce odor discriminability at the glomerular level.

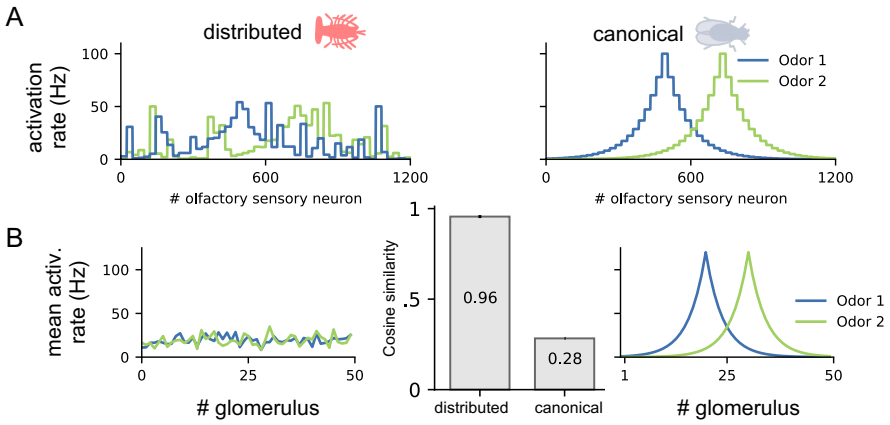

FIGURE 3.3: Comparison of odor representations in canonical versus distributed olfactory network architectures. (A) Activation pattern of OSNs for two odors (blue and green) in distributed and canonical circuit. The odor profiles are constructed using Laplacian-shaped tuning curves over receptor space. In the canonical model, receptor expression and OSN-to-glomerulus connectivity follow a structured 1:1 organization. In the distributed model, both receptor-to-OSN assignment and OSN-to-glomerulus mapping were randomized. (B) Odor-evoked activation patterns at the glomerular level are obtained by projecting receptor responses through the respective network architectures. Resulting population code in PNs is highly similar for randomized OSN-PN connectivity but separates odors well in the 1:1 organization.

A recent preprint uses computational modeling to explore the potential benefits of the non-canonical olfactory organization in *Aedes aegypti*. They find that distributed architectures may be better suited for robust odor detection in complex or noisy environments, where relevant odor cues are strongly correlated (Lienkaemper et al., 2025). In contrast, canonical architectures, such as those observed in *Drosophila* or the honeybee, may facilitate fine odor discrimination by decorrelating inputs in

cleaner, high-dimensional odor spaces. The choice between these circuit designs may thus reflect species-specific ecological niches and represent distinct evolutionary optimizations for balancing sensitivity and specificity in olfactory processing.

The MB is a highly conserved structure across insects, combining divergent input, sparse coding, and modulation by neuromodulatory signals that support memory formation (Strausfeld et al., 1998; Strausfeld et al., 2009; Jortner et al., 2007; Groh and Rössler, 2011; Anton and Rössler, 2021). However, the MB is not universally present across all arthropods, as for example crustaceans possess hemiellipsoid bodies, which serve as equivalent centers for associative learning and memory (Strausfeld et al., 2020). Across insect species, MB size is suggested to correlate in part with cognitive demands, suggesting evolutionary adaptation to ecological or behavioral complexity (Groh and Rössler, 2011; Couto et al., 2023; Farnworth et al., 2024). *Drosophila* exhibits advanced learning capabilities beyond classical conditioning, as illustrated by the two examples in Chapter 2.1 of this thesis and numerous other studies (Dwijesha et al., 2024). Nevertheless, certain complex learning behaviors, such as spatial navigation, numerical cognition, or elaborate social learning, are preferably studied in other insect species, such as honey bees or ants (Gould, 1996; Skorupski et al., 2018; Rapp et al., 2020; Dong et al., 2023; Collett et al., 2025).

In summary, while *Drosophila* shares key neural architectures and coding strategies with other arthropods, some features may reflect evolutionary specializations rather than general principles. Future comparative research, including both experimental and computational approaches, will be crucial to identify conserved versus lineage-specific mechanisms. In particular, the availability of connectome data from additional arthropod species will provide valuable context for interpreting *Drosophila* models in a broader evolutionary framework.

3.3.2 Comparison to Mammals

Despite the large evolutionary distance between the fruit fly and higher evolved species, such as mammals, the skills required for survival and reproduction, such as vision, olfaction, taste, navigation, learning, and locomotion are largely overlapping. Thus, we can ask how similar the structures that serve these functions are. Here, we will focus on comparing insects and mammals with respect to principles of odor coding and olfactory learning, since it is the focus of this thesis (Fulton et al., 2024). However, other studies have reviewed comparative approaches in other areas of the brain, such as comparing visual (Tanaka and Portugues, 2025) or navigational (Basu and Nagel, 2024) systems between invertebrates and vertebrates.

Similar to the AL as the first important computation hub in the insect olfactory pathway processing incoming signals from the antennae and maxillary palps, the olfactory bulb in mammalians processes incoming signals from the olfactory epithelium (Shepherd et al., 2004; Chen and Shepherd, 2005). Both the AL and the olfactory bulb are organized in a glomerular structure, with mitral and tufted cells as the equivalents to PNs (Fulton et al., 2024). In Chapter 2.2 of this thesis, we focus on LN innervation patterns and their functional role in odor mixture processing within the *Drosophila* AL. Interestingly, the vertebrate olfactory bulb exhibits a comparable LN organization, including periglomerular and granule cells, which form a similarly diverse set of LNs (Burton, 2017). As in the *Drosophila* AL, the

excitation-inhibition balance appears to be comparable, with more inhibitory than excitatory LNs (Shepherd et al., 2007). Further, LNs are suggested to also vary in their innervation patterns, with either isotropic (insect: broad) or anisotropic, directed (insect: patchy) patterns (Murthy, 2011; Egger and Kuner, 2021). These shared structural features extend to shared functional features in lateral interactions, such as gain control or stimulus discrimination (Abraham et al., 2010; Kato et al., 2013). Similarly to the investigations in *Drosophila*, odor mixture suppression in the mouse has been linked to neuronal crosstalk as well (Saraiva et al., 2016; Qiu et al., 2021), and future computational and experimental investigations may explore the mechanisms behind odor mixture suppression in vertebrates in more detail.

Beyond early processing, higher-order associative centers also show intriguing parallels. The insect mushroom body can be compared to several mammalian brain structures, which show structural or functional similarities in different aspects (Campbell and Turner, 2010). Developmental comparisons suggest a deep evolutionary relationship between mushroom bodies and the vertebrate pallium with a conserved molecular brain topology (Tomer et al., 2010). The first analogy that can be drawn with the MB is the piriform cortex, which is the mammalian cortical region processing olfactory stimuli (Fulton et al., 2024). The piriform cortex receives direct input from the olfactory bulb via mitral and tufted cells to superficial pyramidal and semilunar cells in the piriform cortex. Similarly to MB, the piriform cortex exhibits high recurrence and is involved in associative coding. Another region in the mammalian brain that has similarities with the MB is the hippocampus. This association is particularly drawn because of their feedback circuit organization and their structural synaptic plasticity underlying learning and memory (Hourcade et al., 2010). Further, many orthologue genes involved in learning and memory in the MB have orthologue genes in the hippocampus (Wolff and Strausfeld, 2016). Due to parallels in circuit architecture, the cerebellum has been proposed as a third functionally analogous structure to the MB (Farris, 2011; Modi et al., 2020). Cerebellar granule cells and *Drosophila* KCs both exhibit highly divergent input and convergent output pathways, and both utilize sparse coding supported by inhibitory circuits (Litwin-Kumar et al., 2017). Although the MB lacks the stereotyped laminar organization of the cerebellum, they may both serve similar functional roles in pattern separation, allowing fine discrimination of sensory or motor representations.

Of course, mammalian cognitive and learning capacities by far exceed those of *Drosophila*. However, they share the core principles of associative learning, with dopamine playing a key role as modulator in mediating reward prediction (Dayan, 2009; Schultz, 2016). Learning paradigms, such as extinction and second-order learning, which we explored in *Drosophila* in Chapter 2.1 can also be observed in rodents and humans (Pavlov, 1927; Dudai, 2004). In the case of extinction learning, studies in mammals suggest that a similar underlying mechanism, with the original memory not being erased, but rather complemented with the formation of a second, parallel memory trace which opposes the original memory (Bouton, 2017). Taken together, these comparisons reveal that despite different evolutionary paths, arthropods and mammals follow similar circuit principles to solve comparable computational challenges in olfactory processing and learning.

3.4 Outlook: Towards Integrative Brain Models Across Abstraction Levels

In this thesis, we implemented and analyzed computational models of olfactory processing and learning in *Drosophila*. At the sensory level, we formalized how different isoforms of a synaptic protein shape transmission dynamics. We further analyzed and modeled circuit motifs involved in integrating opposing sensory signals. At the level of learning and memory, we explored core principles of associative learning as well as two distinct modulations of learned information. The presented modeling approaches span four complementary axes: (i) biological scales, ranging from molecular mechanisms to circuit-level computations; (ii) computational abstraction levels, covering both rate-based and spiking models; (iii) processing stages, from early sensory circuits to memory-related structures; and (iv) temporal scales, from STP on the millisecond scale to long-lasting changes underlying memory formation. While each of these models provides individual insights, a promising future direction is to further integrate these scales and levels of abstraction. This integration would contribute to a more comprehensive understanding of how the brain processes and adapts to sensory information. In the following, we outline a conceptual bottom-up pathway through the different levels of abstraction, proposing how the presented modular building blocks might be combined into unified models.

In a first step, detailed molecular models can be embedded into circuit-level frameworks to study their effects on network function. As a practical example, the synapse model for STP (Chapter 2.3) could be incorporated into the AL model (Chapter 2.2). This would allow investigation of how Unc13 isoform-dependent STP shapes network dynamics during sensory information integration (Piao and Sigrist, 2022). Building upon this, biologically realistic whole-cell models could be introduced. This applies for both a realistic structural representation, as in compartmentalized models (Chapter 3.1.1), as well as functionally realistic representation, as in spiking models with ion dynamics, as proposed in the Blue Brain Project (Markram et al., 2015). Recent findings suggest that incorporating non-neuronal cell types, such as glia, into circuit models may contribute to a more comprehensive understanding of brain function as well (De Backer and Grunwald Kadow, 2022; Basu et al., 2024; Alberini, 2025; Battini et al., 2025). At the circuit level, combining multiple behavioral motifs into shared network architectures would allow exploration of their interactions. For instance, extinction (Chapter 2.1.1) and second-order learning (Chapter 2.1.2) could be integrated to investigate their functional interplay, as discussed in Chapter 3.2.4. Similarly, connecting individual brain regions, such as linking the AL model (Chapter 2.2) with mushroom body (MB) models (Chapter 2.1), would enable analysis of feedforward and feedback interactions, for example between the AL and the MB (Hu et al., 2010). Furthermore, extending MB models to descending pathways could improve behaviorally grounded modeling in learning contexts.

Integration across multiple brain regions could ultimately lead to more realistic models of entire nervous systems, as pursued in recent whole-brain modeling efforts in *Drosophila* (Huang et al., 2019; Shiu et al., 2024). While promising, such comprehensive modeling remains limited by incomplete functional data, even in model organisms like *Drosophila*, and will be incomparably more challenging in vertebrates (Wang and Aimone, 2024). With increasingly detailed brain models, integration of

models beyond the nervous system into whole-body simulations becomes highly interesting. Recent research endeavors demonstrate how neural models can be embedded into simulations of biomechanics, locomotion, and behavior (Sakagiannis et al., 2025a; Wang-Chen et al., 2024). These systems also yield the potential to incorporate environmental feedback and internal state representations, enabling models to perform sensorimotor transformations in closed-loop settings. Stitching together the building blocks across molecular, cellular and circuit levels might ultimately lead to creating highly realistic and comprehensive models of brain function in naturalistic contexts.

Bibliography

Abbott, L. F (1999). Lapicque's introduction of the integrate-and-fire model neuron (1907). *Brain Research Bulletin* 50.5-6, 303–304.

Abbott, L. F. and Regehr, W. G. (2004). Synaptic computation. *Nature* 431.October, 796–803.

Abbott, L. F., Varela, J. A., Sen, K., and Nelson, S. B. (1997). Synaptic Depression and Cortical Gain Control. *Science* 275.5297, 221–224.

Abraham, N. M., Egger, V., Shimshek, D. R., Renden, R., Fukunaga, I., Sprengel, R., Seeburg, P. H., Klugmann, M., Margrie, T. W., Schaefer, A. T., and Kuner, T. (2010). Synaptic Inhibition in the Olfactory Bulb Accelerates Odor Discrimination in Mice. *Neuron* 65.3, 399–411.

Aceves-Piña, E. O. and Quinn, W. G. (1979). Learning in Normal and Mutant Drosophila Larvae. *Science* 206.4414, 93–96.

Adams, M. D. et al. (2000). The genome sequence of Drosophila melanogaster. *Science* 287.5461, 2185–2195.

Aimon, S., Katsuki, T., Jia, T., Grosenick, L., Broxton, M., Deisseroth, K., Sejnowski, T. J., and Greenspan, R. J. (2019). Fast near-whole–brain imaging in adult Drosophila during responses to stimuli and behavior. *PLOS Biology* 17.2, e2006732–.

Alberini, C. M. (2025). Not just neurons: The diverse cellular landscape of learning and memory. *Neuron* 113.11, 1664–1679.

Anton, S. and Homberg, U. (1999). Antennal Lobe Structure. In: *Insect Olfaction*. Ed. by B. S. Hansson. Berlin, Heidelberg: Springer, 97–124. ISBN: 978-3-662-07911-9.

Anton, S., Ignell, R., and Hansson, B. S. (2002). Developmental changes in the structure and function of the central olfactory system in gregarious and solitary desert locusts. *Microscopy Research and Technique* 56.4, 281–291.

Anton, S. and Rössler, W. (2021). Plasticity and modulation of olfactory circuits in insects. *Cell and Tissue Research* 383.1, 149–164.

Arican, C., Schmitt, F. J., Rössler, W., Strube-Bloss, M. F., and Nawrot, M. P. (2023). The mushroom body output encodes behavioral decision during sensory-motor transformation. *Current Biology* 33.19, 4217–4224.e4.

Aso, Y., Grübel, K., Busch, S., Friedrich, A. B., Siwanowicz, I., and Tanimoto, H. (2009). The mushroom body of adult Drosophila characterized by GAL4 drivers. *Journal of Neurogenetics* 23.1-2, 156–172.

Aso, Y., Hattori, D., Yu, Y., Johnston, R. M., Iyer, N. A., Ngo, T. T., Dionne, H., Abbott, L. F., Axel, R., Tanimoto, H., and Rubin, G. M. (2014a). The neuronal architecture of the mushroom body provides a logic for associative learning. *eLife* 3, e04577.

Aso, Y., Sitaraman, D., Ichinose, T., Kaun, K. R., Vogt, K., Belliart-Guérin, G., Plaçais, P. Y., Robie, A. A., Yamagata, N., Schnaitmann, C., Rowell, W. J., Johnston, R. M., Ngo, T. T., Chen, N., Korff, W., Nitabach, M. N., Heberlein, U., Preat, T., Branson, K. M., Tanimoto, H., and Rubin, G. M. (2014b). Mushroom body output neurons encode valence and guide memory-based action selection in Drosophila. *eLife* 3.3, e04580.

Atoki, A. V., Aja, P. M., Shinkafi, T. S., Ondari, E. N., Adeniyi, A. I., Fasogbon, I. V., Dangana, R. S., Shehu, U. U., and Akin-Adewumi, A. (2025). Exploring the versatility of Drosophila melanogaster as a model organism in biomedical research: a comprehensive review. *Fly* 19.1, 2420453.

Azevedo, A., Lesser, E., Phelps, J. S., Mark, B., Elabbady, L., Kuroda, S., Sustar, A., Moussa, A., Khandelwal, A., Dallmann, C. J., Agrawal, S., Lee, S.-Y. J., Pratt, B., Cook, A., Skutt-Kakaria, K., Gerhard, S., Lu, R., Kemnitz, N., Lee, K., Halageri, A., Castro, M., Ih, D., Gager, J., Tammam, M., Dorkenwald, S., Collman, F., Schneider-Mizell, C., Brittain, D., Jordan, C. S., Dickinson, M., Pacureanu, A., Seung, H. S., Macrina, T., Lee, W.-C. A., and Tuthill, J. C. (2024). Connectomic reconstruction of a female Drosophila ventral nerve cord. *Nature* 631.8020, 360–368.

Azevedo, F. A. C., Carvalho, L. R. B., Grinberg, L. T., Farfel, J. M., Ferretti, R. E. L., Leite, R. E. P., Filho, W. J., Lent, R., and Herculano-Houzel, S. (2009). Equal numbers of neuronal and nonneuronal cells make the human brain an isometrically scaled-up primate brain. *Journal of Comparative Neurology* 513.5, 532–541.

Bacci, A., Huguenard, J. R., and Prince, D. A. (2003). Functional autaptic neurotransmission in fast-spiking interneurons: A novel form of feedback inhibition in the neocortex. *Journal of Neuroscience* 23.3, 859–866.

Bae, J. A., Baptiste, M., Baptiste, M. R., Bishop, C. A., Bodor, A. L., Brittain, D., Brooks, V., Buchanan, J., Bumbarger, D. J., Castro, M. A., Celii, B., Cobos, E., Collman, F., Costa, N. M. da, Danskin, B., Dorkenwald, S., Elabbady, L., Fahey, P. G., Fliss, T., Froudarakis, E., Gager, J., Gamlin, C., Gray-Roncal, W., Halageri, A., Hebditch, J., Jia, Z., Joyce, E., Ellis-Joyce, J., Jordan, C., Kapner, D., Kemnitz, N., Kinn, S., Kitchell, L. M., Koolman, S., Kuehner, K., Lee, K., Li, K., Lu, R., Macrina, T., Mahalingam, G., Matelsky, J., McReynolds, S., Miranda, E., Mitchell, E., Mondal, S. S., Moore, M., Mu, S., Muhammad, T., Nehoran, B., Neace, E., Ogedengbe, O., Papadopoulos, C., Papadopoulos, S., Patel, S., Vega, G. J. Y. P., Pitkow, X., Popovych, S., Ramos, A., Reid, R. C., Reimer, J., Rivlin, P. K., Rose, V., Sauter, Z. M., Schneider-Mizell, C. M., Seung, H. S., Silverman, B., Silversmith, W., Sterling, A., Sinz, F. H., Smith, C. L., Swanstrom, R., Suckow, S., Takeno, M., Tan, Z. H., Tolias, A. S., Torres, R., Turner, N. L., Walker, E. Y., Wang, T., Wanner, A., Wester, B. A., Williams, G., Williams, S., Willie, K., Willie, R., Wong, W., Wu, J., Xu, C., Yang, R., Yatsenko, D., Ye, F., Yin, W., Young, R., Yu, S.-c., Xenes, D., Zhang, C., and The MICrONS Consortium (2025). Functional connectomics spanning multiple areas of mouse visual cortex. *Nature* 640.8058, 435–447.

Barroso-Flores, J., Herrera-Valdez, M. A., Galarraga, E., and Bargas, J. (2017). Models of Short-Term Synaptic Plasticity. In: *The Plastic Brain*. Ed. by R. von Bernhardi, J. Eugenín, and K. J. Muller. Cham: Springer International Publishing, 41–57. ISBN: 978-3-319-62817-2.

Barth-Maron, A., D'Alessandro, I., and Wilson, R. I. (2023). Interactions between specialized gain control mechanisms in olfactory processing. *Current Biology* 33.23, 5109–5120.e7.

Basu, J. and Nagel, K. (2024). Neural circuits for goal-directed navigation across species. *Trends in Neurosciences* 47.11, 904–917.

Basu, R., Preat, T., and Plaçais, P.-Y. (2024). Glial metabolism versatility regulates mushroom body–driven behavioral output in Drosophila. *Learning & Memory* 31.5, a053823.

Bates, A. S., Schlegel, P., Roberts, R. J., Drummond, N., Tamimi, I. F., Turnbull, R., Zhao, X., Marin, E. C., Popovici, P. D., Dhawan, S., Jamasb, A., Javier, A., Serratosa Capdevila, L., Li, F., Rubin, G. M., Waddell, S., Bock, D. D., Costa, M., and

Jefferis, G. S. (2020). Complete Connectomic Reconstruction of Olfactory Projection Neurons in the Fly Brain. *Current Biology* 30.16, 3183–3199.

Battesti, M., Moreno, C., Joly, D., and Mery, F. (2012). Spread of Social Information and Dynamics of Social Transmission within Drosophila Groups. *Current Biology* 22.4, 309–313.

Battini, S., Cantarutti, N., Kotsalos, C., Roussel, Y., Cattabiani, A., Arnaudon, A., Favreau, C., Antonel, S., Markram, H., and Keller, D. (2025). Modeling of Blood Flow Dynamics in Rat Somatosensory Cortex. *Biomedicines* 13.1, 72.

Bekolay, T., Bergstra, J., Hunsberger, E., DeWolf, T., Stewart, T. C., Rasmussen, D., Choo, X., Voelker, A., and Eliasmith, C. (2014). Nengo: a Python tool for building large-scale functional brain models. *Frontiers in Neuroinformatics* 7, 48.

Bellen, H. J., Tong, C., and Tsuda, H. (2010). 100 years of Drosophila research and its impact on vertebrate neuroscience: a History Lesson for the Future. *Nature Reviews Neuroscience* 11, 514–522.

Bellen, H. and Yamamoto, S. (2015). Morgan's Legacy: Fruit Flies and the Functional Annotation of Conserved Genes. *Cell* 163.1, 12–14.

Beltz, B. S., Kordas, K., Lee, M. M., Long, J. B., Benton, J. L., and Sandeman, D. C. (2003). Ecological, evolutionary, and functional correlates of sensilla number and glomerular density in the olfactory system of decapod crustaceans. *Journal of Comparative Neurology* 455.2, 260–269.

Beniaguev, D., Segev, I., and London, M. (2021). Single cortical neurons as deep artificial neural networks. *Neuron* 109.17, 2727–2739.e3.

Bennett, J. E., Philippides, A., and Nowotny, T. (2021). Learning with reinforcement prediction errors in a model of the Drosophila mushroom body. *Nature Communications* 12.1, 2569.

Benton, R. (2022). Drosophila olfaction: past, present and future. *Proceedings of the Royal Society B: Biological Sciences* 289.1989, 20222054.

Bicker, G. and Stern, M. (2020). Structural and Functional Plasticity in the Regenerating Olfactory System of the Migratory Locust. *Frontiers in Physiology* 11.

Blohm, G., Kording, K. P., and Schrater, P. R. (2020). A How-to-Model Guide for Neuroscience. *eNeuro* 7.1.

Bouton, M. E. (2017). Extinction: Behavioral Mechanisms and Their Implications. Vol. 1. Elsevier. ISBN: 978-0-12-805291-4.

Bower, J. M. and Beeman, D. (1998). The Book of GENESIS. 2nd ed. New York, NY: Springer. ISBN: 978-0-387-94938-3 978-1-4612-1634-6.

Brand, A. H. and Perrimon, N. (1993). Targeted gene expression as a means of altering cell fates and generating dominant phenotypes. *Development* 118.2, 401–415.

Brunel, N. and Rossum, M. C. W. van (2007). Lapicque's 1907 paper: from frogs to integrate-and-fire. *Biological Cybernetics* 97.5, 337–339.

Buhmann, J., Sheridan, A., Malin-Mayor, C., Schlegel, P., Gerhard, S., Kazimiers, T., Krause, R., Nguyen, T. M., Heinrich, L., Lee, W.-C. A., Wilson, R., Saalfeld, S., Jefferis, G. S. X. E., Bock, D. D., Turaga, S. C., Cook, M., and Funke, J. (2021). Automatic detection of synaptic partners in a whole-brain Drosophila electron microscopy data set. *Nature Methods* 18.7, 771–774.

Burkitt, A. N. (2006). A Review of the Integrate-and-fire Neuron Model: I. Homogeneous Synaptic Input. *Biological Cybernetics* 95.1, 1–19.

Burrows, M. (1996). Components of the nervous system. In: *The Neurobiology of an Insect Brain*. Ed. by M. Burrows. Oxford University Press, 0. ISBN: 978-0-19-852344-4.

Burton, S. D. (2017). Inhibitory circuits of the mammalian main olfactory bulb. *Journal of Neurophysiology* 118.4, 2034–2051.

Campbell, R. A. A. and Turner, G. C. (2010). The mushroom body. *Current Biology* 20.1, R11–R12.

Casas-Tintó, S. (2024). Drosophila as a Model for Human Disease: Insights into Rare and Ultra-Rare Diseases. *Insects* 15.11, 870.

Chavlis, S. and Poirazi, P. (2021). Drawing inspiration from biological dendrites to empower artificial neural networks. *Current Opinion in Neurobiology*. Computational Neuroscience 70, 1–10.

Chavlis, S. and Poirazi, P. (2025). Dendrites endow artificial neural networks with accurate, robust and parameter-efficient learning. *Nature Communications* 16.1, 943.

Chen, W. R. and Shepherd, G. M. (2005). The olfactory glomerulus: A cortical module with specific functions. *Journal of Neurocytology* 34.3, 353–360.

Chou, Y. H., Spletter, M. L., Yaksi, E., Leong, J. C., Wilson, R. I., and Luo, L. (2010). Diversity and wiring variability of olfactory local interneurons in the Drosophila antennal lobe. *Nature Neuroscience* 13.4, 439–449.

Clemens, J. and Murthy, M. (2017). The Use of Computational Modeling to Link Sensory Processing with Behavior in Drosophila. In: *Decoding Neural Circuit Structure and Function: Cellular Dissection Using Genetic Model Organisms*. Ed. by A. Çelik and M. F. Wernet. Cham: Springer International Publishing, 241–260. ISBN: 978-3-319-57363-2.

Clements, J., Goina, C., Hubbard, P. M., Kawase, T., Olbris, D. J., Otsuna, H., Svirskas, R., and Rokicki, K. (2024). NeuronBridge: an intuitive web application for neuronal morphology search across large data sets. *BMC Bioinformatics* 25.1, 114.

Cognigni, P., Felsenberg, J., and Waddell, S. (2018). Do the right thing: neural network mechanisms of memory formation, expression and update in Drosophila. *Current Opinion in Neurobiology* 49, 51–58.

Collett, T., Graham, P., and Heinze, S. (2025). The neuroethology of ant navigation. *Current Biology* 35.3, R110–R124.

Costa, R. P., Jesper Sjöström, P., and Rossum, M. C. van (2013). Probabilistic inference of short-term synaptic plasticity in neocortical microcircuits. *Frontiers in Computational Neuroscience* MAY.

Couto, A., Alenius, M., and Dickson, B. J. (2005). Molecular, Anatomical, and Functional Organization of the Drosophila Olfactory System. *Current Biology* 15.17, 1535–1547.

Couto, A., Young, F. J., Atzeni, D., Marty, S., Melo-Flórez, L., Hebberecht, L., Monllor, M., Neal, C., Cicconardi, F., McMillan, W. O., and Montgomery, S. H. (2023). Rapid expansion and visual specialisation of learning and memory centres in the brains of Heliconiini butterflies. *Nature Communications* 14.1, 4024.

Das Chakraborty, S. and Sachse, S. (2021). Olfactory processing in the lateral horn of Drosophila. *Cell and Tissue Research* 383, 113–123.

Davies, A., Louis, M., and Webb, B. (2015). A Model of Drosophila Larva Chemotaxis. *PLOS Computational Biology* 11.11, e1004606.

Davis, R. L. (2005). Olfactory Memory Formation in Drosophila: From Molecular to Systems Neuroscience. *Annual Review of Neuroscience* 28, 275–302.

Davis, R. L. (2023). Learning and memory using Drosophila melanogaster: a focus on advances made in the fifth decade of research. *Genetics* 224.4, iyad085.

Dayan, P. (2009). Dopamine, Reinforcement Learning, and Addiction. *Pharmacopsychiatry* 42.S 1, S56–S65.

Dayan, P. and Abbott, L. F. (2001). Theoretical Neuroscience. MIT Press. ISBN: 978-0-262-04199-7.

De Backer, J.-F. and Grunwald Kadow, I. C. (2022). A role for glia in cellular and systemic metabolism: insights from the fly. *Current Opinion in Insect Science* 53, 100947.

De Bruyne, M., Foster, K., and Carlson, J. R. (2001). Odor coding in the Drosophila antenna. *Neuron* 30.2, 537–552.

Deco, G., Rolls, E. T., and Romo, R. (2010). Synaptic dynamics and decision making. *Proceedings of the National Academy of Sciences* 107.16, 7545–7549.

Deng, P.-Y. and Klyachko, V. A. (2011). The diverse functions of short-term plasticity components in synaptic computations. *Communicative & Integrative Biology* 4.5, 543–548.

Dhiman, G., Viriyasitavat, W., and Nagar, A. K. (2023). Editorial: Machine and deep-learning for computational neuroscience. *Frontiers in Computational Neuroscience* 17.

Dickson, W. B., Straw, A. D., and Dickinson, M. H. (2008). Integrative Model of Drosophila Flight. *AIAA Journal* 46.9, 2150–2164.

Dolan, M.-J., Belliart-Guérin, G., Bates, A. S., Frechter, S., Lampin-Saint-Amaux, A., Aso, Y., Roberts, R. J., Schlegel, P., Wong, A., Hammad, A., Bock, D., Rubin, G. M., Preat, T., Plaçais, P.-Y., and Jefferis, G. S. (2018). Communication from Learned to Innate Olfactory Processing Centers Is Required for Memory Retrieval in Drosophila. *Neuron* 100.3, 651–668.e8.

Dong, S., Lin, T., Nieh, J. C., and Tan, K. (2023). Social signal learning of the waggle dance in honey bees. *Science* 379.6636, 1015–1018.

Dorkenwald, S. et al. (2024). Neuronal wiring diagram of an adult brain. *Nature* 634.8032, 124–138.

Dudai, Y. (2004). The neurobiology of consolidations, or, how stable is the engram? *Annual Review of Psychology* 55, 51–86.

Dwijesha, A. S., Eswaran, A., Berry, J. A., and Phan, A. (2024). Diverse memory paradigms in Drosophila reveal diverse neural mechanisms. *Learning & Memory* 31.5, a053810.

D'Angelo, E., Solinas, S., Garrido, J., Casellato, C., Pedrocchi, A., Mapelli, J., Gandolfi, D., and Prestori, F. (2013). Realistic modeling of neurons and networks: towards brain simulation. *Functional Neurology* 28.3, 153 –166.

Eberle, A. L. and Zeidler, D. (2018). Multi-Beam Scanning Electron Microscopy for High-Throughput Imaging in Connectomics Research. *Frontiers in Neuroanatomy* 12.

Egger, V. and Kuner, T. (2021). Olfactory bulb granule cells: specialized to link coactive glomerular columns for percept generation and discrimination of odors. *Cell and Tissue Research* 383.1, 495–506.

Eichler, K., Li, F., Litwin-Kumar, A., Park, Y., Andrade, I., Schneider-Mizell, C. M., Saumweber, T., Huser, A., Eschbach, C., Gerber, B., Fetter, R. D., Truman, J. W., Priebe, C. E., Abbott, L. F., Thum, A. S., Zlatic, M., and Cardona, A. (2017). The complete connectome of a learning and memory centre in an insect brain. *Nature* 548.7666, 175–182.

Esslen, J. and Kaissling, K.-E. (1976). Zahl und Verteilung antennaler Sensillen bei der Honigbiene (Apis mellifera L.) *Zoomorphologie* 83, 227–251.

Faghihi, F., Moustafa, A. A., Heinrich, R., and Wörgötter, F. (2017). A computational model of conditioning inspired by Drosophila olfactory system. *Neural Networks* 87, 96–108.

Farnworth, M. S., Loupasaki, T., Couto, A., and Montgomery, S. H. (2024). Mosaic evolution of a learning and memory circuit in Heliconiini butterflies. *Current Biology* 34.22, 5252–5262.e5.

Farris, S. M. (2011). Are mushroom bodies cerebellum-like structures? *Arthropod Structure & Development*. Evolution of the Arthropod Nervous System: Part 2 40.4, 368–379.

Feldotto, B., Morin, F. O., and Knoll, A. (2022). The Neurorobotics Platform Robot Designer: Modeling Morphologies for Embodied Learning Experiments. *Frontiers in Neurorobotics* 16.

Felsenberg, J., Barnstedt, O., Cognigni, P., Lin, S., and Waddell, S. (2017). Re-evaluation of learned information in Drosophila. *Nature* 544.7649, 240–244.

Felsenberg, J., Jacob, P. F., Walker, T., Barnstedt, O., Edmondson-Stait, A. J., Pleijzier, M. W., Otto, N., Schlegel, P., Sharifi, N., Perisse, E., Smith, C. S., Lauritzen, J. S., Costa, M., Jefferis, G. S., Bock, D. D., and Waddell, S. (2018). Integration of Parallel Opposing Memories Underlies Memory Extinction. *Cell* 175.3, 709–722.e15.

Ferrante, M., Blackwell, K. T., Migliore, M., and Ascoli, G. A. (2008). Computational Models of Neuronal Biophysics and the Characterization of Potential Neuropharmacological Targets. *Current Medicinal Chemistry* 15.24, 2456–2471.

Fiala, A. and Kaun, K. R. (2024). What do the mushroom bodies do for the insect brain? Twenty-five years of progress. *Learning & Memory* 31.5, a053827.

Fortune, E. S. and Rose, G. J. (2001). Short-term synaptic plasticity as a temporal filter. *Trends in Neurosciences* 24.7, 381–385.

Frechter, S., Bates, A. S., Tootoonian, S., Dolan, M.-J., Manton, J., Jamasb, A. R., Kohl, J., Bock, D., and Jefferis, G. (2019). Functional and anatomical specificity in a higher olfactory centre. *eLife* 8, e44590.

Fulterer, A., Andlauer, T. F., Ender, A., Maglione, M., Eyring, K., Woitkuhn, J., Lehmann, M., Matkovic-Rachid, T., Geiger, J. R., Walter, A. M., Nagel, K. I., and Sigrist, S. J. (2018). Active Zone Scaffold Protein Ratios Tune Functional Diversity across Brain Synapses. *Cell Reports* 23.5, 1259–1274.

Fulton, K. A., Zimmerman, D., Samuel, A., Vogt, K., and Datta, S. R. (2024). Common principles for odour coding across vertebrates and invertebrates. *Nature Reviews Neuroscience* 25.7, 453–472.

Fuscà, D. and Kloppenburg, P. (2021a). Odor processing in the cockroach antennal lobe—the network components. *Cell and Tissue Research* 383.1, 59–73.

Fuscà, D. and Kloppenburg, P. (2021b). Task-specific roles of local interneurons for inter- and intraglomerular signaling in the insect antennal lobe. *eLife* 10, e65217.

Galizia, C. G. and Rössler, W. (2010). Parallel Olfactory Systems in Insects: Anatomy and Function. *Annual Review of Entomology* 55.Volume 55, 2010, 399–420.

Ganguly, I. and Litwin-Kumar, A. (2022). Connectomics: Relating synaptic connectivity to physiology. *Current Biology* 32.3, R118–R120.

Gascuel, J. and Masson, C. (1991). A quantitative ultrastructural study of the honeybee antennal lobe. *Tissue and Cell* 23.3, 341–355.

Gerber, B. and Stocker, R. F. (2007). The Drosophila Larva as a Model for Studying Chemosensation and Chemosensory Learning: A Review. *Chemical Senses* 32.1, 65–89.

Gerstner, W. and Kistler, W. (2012). Spiking Neuron Models. Cambridge University Press.

Gewaltig, M.-O. and Diesmann, M. (2007). NEST (NEural Simulation Tool). *Scholarpedia* 2.4, 1430.

Gidon, A., Zolnik, T. A., Fidzinski, P., Bolduan, F., Papoutsi, A., Poirazi, P., Holtkamp, M., Vida, I., and Larkum, M. E. (2020). Dendritic action potentials and computation in human layer 2/3 cortical neurons. *Science* 367.6473, 83–87.

Goldman-Rakic, P. S (1995). Cellular basis of working memory. *Neuron* 14.3, 477–485.

Goodman, D. F. M. and Brette, R. (2008). Brian: a simulator for spiking neural networks in Python. *Frontiers in Neuroinformatics* 2, 5.

Gould, J. L. (1996). Specializations in honey bee learning. In: *Neuroethological studies of cognitive and perceptual processes*. Boulder, CO, US: Westview Press, 11–30. ISBN: 978-0-8133-2654-2 978-0-8133-2655-9.

Gouwens, N. W., Berg, J., Feng, D., Sorensen, S. A., Zeng, H., Hawrylycz, M. J., Koch, C., and Arkhipov, A. (2018). Systematic generation of biophysically detailed models for diverse cortical neuron types. *Nature Communications* 9.1, 710.

Gouwens, N. W. and Wilson, R. I. (2009). Signal propagation in Drosophila central neurons. *Journal of Neuroscience* 29.19, 6239–6249.

Grabe, V., Baschwitz, A., Dweck, H. K., Lavista-Llanos, S., Hansson, B. S., and Sachse, S. (2016). Elucidating the Neuronal Architecture of Olfactory Glomeruli in the Drosophila Antennal Lobe. *Cell Reports* 16.12, 3401–3413.

Grabe, V., Strutz, A., Baschwitz, A., Hansson, B. S., and Sachse, S. (2015). Digital in vivo 3D atlas of the antennal lobe of Drosophila melanogaster. *Journal of Comparative Neurology* 523.3, 530–544.

Grasso, E., Corteze, M., and Schmidt, H. (2025). Connectomic traces of Hebbian plasticity in the entorhinal-hippocampal system. *bioRxiv* 10.1101/2025.04.07.647631.

Groh, C. and Rössler, W. (2011). Comparison of microglomerular structures in the mushroom body calyx of neopteran insects. *Arthropod Structure & Development*. Evolution of the Arthropod Nervous System: Part 2 40.4, 358–367.

Gruber, L., Cantera, R., Pleijzier, M. W., Steinert, M., Pertsch, T., Hansson, B. S., and Rybak, J. (2023). The unique synaptic circuitry of specialized olfactory glomeruli in Drosophila melanogaster. *eLife* 12, RP88824.

Grünert, U. and Ache, B. W. (1988). Ultrastructure of the aesthetasc (olfactory) sensilla of the spiny lobster, Panulirus argus. *Cell and Tissue Research* 251.1, 95–103.

Guo, D., Wu, S., Chen, M., Perc, M., Zhang, Y., Ma, J., Cui, Y., Xu, P., Xia, Y., and Yao, D. (2016). Regulation of Irregular Neuronal Firing by Autaptic Transmission. *Scientific Reports* 6.February, 1–14.

Gupta, A., Faghihi, F., and Moustafa, A. A. (2018). Computational Models of Olfaction in Fruit Flies. In: *Computational Models of Brain and Behavior*. Ed. by A. A. Moustafa. Vol. 1, 199–213.

Hallem, E. A. and Carlson, J. R. (2004). The odor coding system of Drosophila. *Trends in Genetics* 20.9, 453–459.

Hallermann, S., Heckmann, M., and Kittel, R. J. (2010). Mechanisms of short-term plasticity at neuromuscular active zones of Drosophila. *HFSP Journal* 4.2, 72–84.

Hancock, C. E., Rostami, V., Rachad, E. Y., Deimel, S. H., Nawrot, M. P., and Fiala, A. (2022). Visualization of learning-induced synaptic plasticity in output neurons of the Drosophila mushroom body γ-lobe. *Scientific Reports* 12.1, 10421.

Hansson, B. S. and Anton, S. (2000). Function and Morphology of the Antennal Lobe: New Developments. *Annual Review of Entomology* 45, 203–231.

Hansson, B. S. and Stensmyr, M. C. (2011). Evolution of Insect Olfaction. *Neuron* 72.5, 698–711.

Harzsch, S. and Krieger, J. (2018). Crustacean olfactory systems: A comparative review and a crustacean perspective on olfaction in insects. *Progress in Neurobiology* 161, 23–60.

Haverkamp, A., Hansson, B. S., and Knaden, M. (2018). Combinatorial Codes and Labeled Lines: How Insects Use Olfactory Cues to Find and Judge Food, Mates, and Oviposition Sites in Complex Environments. *Frontiers in Physiology* 9.

Heisenberg, M. (2003). Mushroom body memoir: From maps to models. *Nature Reviews Neuroscience* 4.4, 266–275.

Helgadóttir, L. I., Haenicke, J., Landgraf, T., Rojas, R., and Nawrot, M. P. (2013). Conditioned behavior in a robot controlled by a spiking neural network. In: *2013 6th International IEEE/EMBS Conference on Neural Engineering (NER)*, 891–894.

Herculano-Houzel, S., Mota, B., and Lent, R. (2006). Cellular scaling rules for rodent brains. *Proceedings of the National Academy of Sciences* 103.32, 12138–12143.

Herre, M., Goldman, O. V., Lu, T.-C., Caballero-Vidal, G., Qi, Y., Gilbert, Z. N., Gong, Z., Morita, T., Rahiel, S., Ghaninia, M., Ignell, R., Matthews, B. J., Li, H., Vosshall, L. B., and Younger, M. A. (2022). Non-canonical odor coding in the mosquito. *Cell* 185.17, 3104–3123.e28.

Herz, A. V. M., Gollisch, T., Machens, C. K., and Jaeger, D. (2006). Modeling Single-Neuron Dynamics and Computations: A Balance of Detail and Abstraction. *Science* 314.5796, 80–85.

Higuchi, K., Kazawa, T., Sakai, B., Namiki, S., Haupt, S. S., and Kanzaki, R. (2022). High performance, large-scale multi-compartment Hodgkin-Huxley simulation of Drosophila's whole-brain neural circuit model. *bioRxiv* 10.1101/2022.11.01.512969.

Hines, M. L. and Carnevale, N. T. (1997). The NEURON Simulation Environment. *Neural Computation* 9.6, 1179–1209.

Hodgkin, A. L. and Huxley, A. F. (1952). A quantitative description of membrane current and its application to conduction and excitation in nerve. *The Journal of Physiology* 117.4, 500–544.

Horiuchi, J. (2019). Recurrent loops: Incorporating prediction error and semantic/episodic theories into Drosophila associative memory models. *Genes, Brain and Behavior*, 1–11.

Hourcade, B., Muenz, T. S., Sandoz, J.-C., Rössler, W., and Devaud, J.-M. (2010). Long-Term Memory Leads to Synaptic Reorganization in the Mushroom Bodies: A Memory Trace in the Insect Brain? *The Journal of Neuroscience* 30.18, 6461–6465.

Hu, A., Zhang, W., and Wang, Z. (2010). Functional feedback from mushroom bodies to antennal lobes in the Drosophila olfactory pathway. *Proceedings of the National Academy of Sciences* 107.22, 10262–10267.

Huang, Y.-C., Wang, C.-T., Su, T.-S., Kao, K.-W., Lin, Y.-J., Chuang, C.-C., Chiang, A.-S., and Lo, C.-C. (2019). A Single-Cell Level and Connectome-Derived Computational Model of the Drosophila Brain. *Frontiers in Neuroinformatics* 12, 99.

Hulse, B. K., Haberkern, H., Franconville, R., Turner-Evans, D., Takemura, S.-y., Wolff, T., Noorman, M., Dreher, M., Dan, C., Parekh, R., Hermundstad, A. M., Rubin, G. M., and Jayaraman, V. (2021). A connectome of the Drosophila central complex reveals network motifs suitable for flexible navigation and context-dependent action selection. *eLife* 10, e66039.

Husch, A., Paehler, M., Fusca, D., Paeger, L., and Kloppenburg, P. (2009a). Calcium Current Diversity in Physiologically Different Local Interneuron Types of the Antennal Lobe. *Journal of Neuroscience* 29.3, 716–726.

Husch, A., Paehler, M., Fusca, D., Paeger, L., and Kloppenburg, P. (2009b). Distinct Electrophysiological Properties in Subtypes of Nonspiking Olfactory Local Interneurons Correlate With Their Cell Type–Specific Ca2+ Current Profiles. *Journal of Neurophysiology* 102.5, 2834–2845.

Ignell, R., Dekker, T., Ghaninia, M., and Hansson, B. S. (2005). Neuronal architecture of the mosquito deutocerebrum. *Journal of Comparative Neurology* 493.2, 207–240.

Ito, K., Suzuki, K., Estes, P., Ramaswami, M., Yamamoto, D., and Strausfeld, N. J. (1998). The organization of extrinsic neurons and their implications in the functional roles of the mushroom bodies in Drosophila melanogaster Meigen. *Learning and Memory* 5.1-2, 52–77.

Izhikevich, E. (2003). Simple model of spiking neurons. *IEEE Transactions on Neural Networks* 14.6, 1569–1572.

Januszewski, M., Kornfeld, J., Li, P. H., Pope, A., Blakely, T., Lindsey, L., Maitin-Shepard, J., Tyka, M., Denk, W., and Jain, V. (2018). High-precision automated reconstruction of neurons with flood-filling networks. *Nature Methods* 15.8, 605–610.

Jeanne, J. M., Fişek, M., and Wilson, R. I. (2018). The Organization of Projections from Olfactory Glomeruli onto Higher-Order Neurons. *Neuron* 98.6, 1198–1213.e6.

Jeibmann, A. and Paulus, W. (2009). Drosophila melanogaster as a Model Organism of Brain Diseases. *International Journal of Molecular Sciences* 10.2, 407–440.

Jennings, B. H. (2011). Drosophila – a versatile model in biology & medicine. *Materials Today* 14.5, 190–195.

Jesusanmi, O. O., Amin, A. A., Domcsek, N., Knight, J. C., Philippides, A., Nowotny, T., and Graham, P. (2024). Investigating visual navigation using spiking neural network models of the insect mushroom bodies. *Frontiers in Physiology* 15.

Jiang, H., Hanna, E., Gatto, C. L., Page, T. L., Bhuva, B., and Broadie, K. (2016). A fully automated Drosophila olfactory classical conditioning and testing system for behavioral learning and memory assessment. *Journal of Neuroscience Methods* 261, 62–74.

Jiang, L. and Litwin-Kumar, A. (2021). Models of heterogeneous dopamine signaling in an insect learning and memory center. *PLoS Computational Biology* 17.8, e1009205.

Jiang, X., Dimitriou, E., Grabe, V., Sun, R., Chang, H., Zhang, Y., Gershenzon, J., Rybak, J., Hansson, B. S., and Sachse, S. (2024). Ring-shaped odor coding in the antennal lobe of migratory locusts. *Cell* 187.15, 3973–3991.e24.

Joesch, M., Plett, J., Borst, A., and Reiff, D. F. (2008). Response Properties of Motion-Sensitive Visual Interneurons in the Lobula Plate of *Drosophila melanogaster*. *Current Biology* 18.5, 368–374.

Jortner, R. A., Farivar, S. S., and Laurent, G. (2007). A Simple Connectivity Scheme for Sparse Coding in an Olfactory System. *Journal of Neuroscience* 27.7, 1659–1669.

Jürgensen, A.-M., Khalili, A., Chicca, E., Indiveri, G., and Nawrot, M. P. (2021). A neuromorphic model of olfactory processing and sparse coding in the Drosophila larva brain. *Neuromorphic Computing and Engineering* 1, 024008.

Jürgensen, A.-M., Sakagiannis, P., Schleyer, M., Gerber, B., and Nawrot, M. P. (2024a). Prediction error drives associative learning and conditioned behavior in a spiking model of Drosophila larva. *iScience* 27.1, 108640.

Jürgensen, A.-M., Schmitt, F. J., and Nawrot, M. P. (2024b). Minimal circuit motifs for second-order conditioning in the insect mushroom body. *Frontiers in Physiology* 14, 1326307.

Kandel, E. R. (1979). Small Systems of Neurons. *Scientific American* 241.3, 66–77.

Kao, K. W. and Lo, C. C. (2020). Short term depression, presynaptic inhibition and local neuron diversity play key functional roles in the insect antennal lobe. *Journal of Computational Neuroscience* 48.2, 213–227.

Kato, H. K., Gillet, S. N., Peters, A. J., Isaacson, J. S., and Komiyama, T. (2013). Parvalbumin-Expressing Interneurons Linearly Control Olfactory Bulb Output. *Neuron* 80.5, 1218–1231.

Kazama, H. (2015). Systems neuroscience in Drosophila: Conceptual and technical advantages. *Neuroscience* 296, 3–14.

Kazama, H. and Wilson, R. I. (2008). Homeostatic Matching and Nonlinear Amplification at Identified Central Synapses. *Neuron* 58.3, 401–413.

Keifer, J. and Summers, C. H. (2016). Putting the "Biology" Back into "Neurobiology": The Strength of Diversity in Animal Model Systems for Neuroscience Research. *Frontiers in Systems Neuroscience* 10, 69.

Kirchner, J. H. and Gjorgjieva, J. (2022). Emergence of synaptic organization and computation in dendrites. *Neuroforum* 28.1, 21–30.

Kitamoto, T. (2001). Conditional modification of behavior in Drosophila by targeted expression of a temperature-sensitive shibire allele in defined neurons. *Journal of Neurobiology* 47.2, 81–92.

Kittel, R. J., Wichmann, C., Rasse, T. M., Fouquet, W., Schmidt, M., Schmid, A., Wagh, D. A., Pawlu, C., Kellner, R. R., Willig, K. I., Hell, S. W., Buchner, E., Heckmann, M., and Sigrist, S. J. (2006). Bruchpilot Promotes Active Zone Assembly, Ca2+ Channel Clustering, and Vesicle Release. *Science* 312.5776, 1051–1054.

Knapek, S., Sigrist, S., and Tanimoto, H. (2011). Bruchpilot, A Synaptic Active Zone Protein for Anesthesia-Resistant Memory. *Journal of Neuroscience* 31.9, 3453–3458.

Knight, J. C. and Nowotny, T. (2021). Larger GPU-accelerated brain simulations with procedural connectivity. *Nature Computational Science* 1.2, 136–142.

König, C., Khalili, A., Niewalda, T., Gao, S., and Gerber, B. (2019). An optogenetic analogue of second-order reinforcement in Drosophila, 9–13.

Lacpique, L. (1907). Recherches quantitatives sur l'excitation électrique des nerfs traiteé comme une polarization. *Journal de Physiologie et de Pathologie Générale* 9, 620–635.

Larkum, M. E., Wu, J., Duverdin, S. A., and Gidon, A. (2022). The Guide to Dendritic Spikes of the Mammalian Cortex *In Vitro* and *In Vivo*. *Neuroscience* 489, 15–33.

Latshaw, J. S., Mazade, R. E., Petersen, M., Mustard, J. A., Sinakevitch, I., Wissler, L., Guo, X., Cook, C., Lei, H., Gadau, J., and Smith, B. (2023). Tyramine and its Amtyr1 receptor modulate attention in honey bees (Apis mellifera). *eLife* 12, e83348.

Laurent, G. (1996). Dynamical representation of odors by oscillating and evolving neural assemblies. *Trends in Neurosciences* 19.11, 489–496.

Lee, C. T., Bell, M., Bonilla-Quintana, M., and Rangamani, P. (2024). Biophysical Modeling of Synaptic Plasticity. *Annual Review of Biophysics* 53, 397–426.

Leitch, B. and Laurent, G. (1996). GABAergic synapses in the antennal lobe and mushroom body of the locust olfactory system. *Journal of Comparative Neurology* 372.4, 487–514.

Li, F., Lindsey, J., Marin, E. C., Otto, N., Dreher, M., Dempsey, G., Stark, I., Bates, A. S., Pleijzier, M. W., Schlegel, P., Nern, A., Takemura, S., Eckstein, N., Yang, T., Francis, A., Braun, A., Parekh, R., Costa, M., Scheffer, L., Aso, Y., Jefferis, G. S., Abbott, L. F., Litwin-Kumar, A., Waddell, S., and Rubin, G. M. (2020). The connectome of the adult drosophila mushroom body provides insights into function. *eLife* 9, e62576.

Li, S., Liu, N., Zhang, X., McLaughlin, D. W., Zhou, D., and Cai, D. (2019). Dendritic computations captured by an effective point neuron model. *Proceedings of the National Academy of Sciences* 116.30, 15244–15252.

Lienkaemper, C., Younger, M. A., and Ocker, G. K. (2025). When non-canonical olfaction is optimal. *bioRxiv* 10.1101/2025.02.27.640624.

Lin, H.-H., Lai, J. S.-Y., Chin, A.-L., Chen, Y.-C., and Chiang, A.-S. (2007). A Map of Olfactory Representation in the *Drosophila* Mushroom Body. *Cell* 128.6, 1205–1217.

Litwin-Kumar, A., Harris, K. D., Axel, R., Sompolinsky, H., and Abbott, L. F. (2017). Optimal Degrees of Synaptic Connectivity. *Neuron* 93.5, 1153–1164.e7.

Liu, G., Seiler, H., Wen, A., Zars, T., Ito, K., Wolf, R., Heisenberg, M., and Liu, L. (2006). Distinct memory traces for two visual features in the Drosophila brain. *Nature* 439.7076, 551–556.

Liu, T. X., Davoudian, P. A., Lizbinski, K. M., and Jeanne, J. M. (2022). Connectomic features underlying diverse synaptic connection strengths and subcellular computation. *Current Biology* 32.3, 559–569.e5.

Lochner, S., Honerkamp, D., Valada, A., and Straw, A. D. (2024). Reinforcement learning as a robotics-inspired framework for insect navigation: from spatial representations to neural implementation. *Frontiers in Computational Neuroscience* 18.

London, M. and Häusser, M. (2005). Dendritic computation. *Annual Review of Neuroscience* 28, 503–532.

Loomba, S., Straehle, J., Gangadharan, V., Heike, N., Khalifa, A., Motta, A., Ju, N., Sievers, M., Gempt, J., Meyer, H. S., and Helmstaedter, M. (2022). Connectomic comparison of mouse and human cortex. *Science* 377.6602, eabo0924.

Luan, H., Diao, F., Scott, R. L., and White, B. H. (2020). The Drosophila Split Gal4 System for Neural Circuit Mapping. *Frontiers in Neural Circuits* 14.

Luo, S. X., Axel, R., and Abbott, L. F. (2010). Generating sparse and selective third-order responses in the olfactory system of the fly. *Proceedings of the National Academy of Sciences* 107.23, 10713–10718.

Lübke, J., Markram, H., Frotscher, M., and Sakmann, B. (1996). Frequency and dendritic distribution of autapses established by layer 5 pyramidal neurons in the developing rat neocortex: Comparison with synaptic innervation of adjacent neurons of the same class. *Annals of Anatomy - Anatomischer Anzeiger* 178.4, 309.

Lützkendorf, J., Matkovic-Rachid, T., Liu, S., Götz, T., Gao, L., Turrel, O., Maglione, M., Grieger, M., Putignano, S., Ramesh, N., Ghelani, T., Neumann, A., Gimber, N., Schmoranzer, J., Stawrakakis, A., Brence, B., Baum, D., Ludwig, K., Heine, M., Mielke, T., Liu, F., Walter, A. M., Wahl, M. C., and Sigrist, S. J. (2025). Blobby is a synaptic active zone assembly protein required for memory in Drosophila. *Nature Communications* 16.1, 271.

Magee, J. C. and Grienberger, C. (2020). Synaptic Plasticity Forms and Functions. *Annual Review of Neuroscience* 43, 95–117.

Malun, D. (1991). Synaptic relationships between GABA-immunoreactive neurons and an identified uniglomerular projection neuron in the antennal lobe of Periplaneta americana: a double-labeling electron microscopic study. *Histochemistry* 96.3, 197–207.

Manger, P. R., Cort, J., Ebrahim, N., Goodman, A., Henning, J., Karolia, M., Rodrigues, S.-L., and Strkalj, G. (2008). Is 21st century neuroscience too focussed on the rat/mouse model of brain function and dysfunction? *Frontiers in Neuroanatomy* 2, 5.

Manoim-Wolkovitz, J. E., Camchy, T., Rozenfeld, E., Chang, H.-H., Lerner, H., Chou, Y.-H., Darshan, R., and Parnas, M. (2025). Nonlinear high-activity neuronal excitation enhances odor discrimination. *Current Biology* 35.7, 1521–1538.e5.

Marin, E. C., Jefferis, G. S. X. E., Komiyama, T., Zhu, H., and Luo, L. (2002). Representation of the Glomerular Olfactory Map in the Drosophila Brain. *Cell* 109.2, 243–255.

Markram, H., Muller, E., Ramaswamy, S., Reimann, M. W., Abdellah, M., Sanchez, C. A., Ailamaki, A., Alonso-Nanclares, L., Antille, N., Arsever, S., Kahou, G. A. A., Berger, T. K., Bilgili, A., Buncic, N., Chalimourda, A., Chindemi, G., Courcol, J.-D., Delalondre, F., Delattre, V., Druckmann, S., Dumusc, R., Dynes, J., Eilemann, S., Gal, E., Gevaert, M. E., Ghobril, J.-P., Gidon, A., Graham, J. W., Gupta, A., Haenel, V., Hay, E., Heinis, T., Hernando, J. B., Hines, M., Kanari, L., Keller, D., Kenyon, J., Khazen, G., Kim, Y., King, J. G., Kisvarday, Z., Kumbhar, P., Lasserre, S., Le Bé, J.-V., Magalhães, B. R. C., Merchán-Pérez, A., Meystre, J., Morrice, B. R., Muller, J., Muñoz-Céspedes, A., Muralidhar, S., Muthurasa, K., Nachbaur, D., Newton, T. H., Nolte, M., Ovcharenko, A., Palacios, J., Pastor, L., Perin, R., Ranjan, R., Riachi, I., Rodríguez, J.-R., Riquelme, J. L., Rössert, C., Sfyrakis, K., Shi, Y., Shillcock, J. C., Silberberg, G., Silva, R., Tauheed, F., Telefont, M., Toledo-Rodriguez, M., Tränkler, T., Van Geit, W., Díaz, J. V., Walker, R., Wang, Y., Zaninetta, S. M., DeFelipe, J., Hill, S. L., Segev, I., and Schürmann, F. (2015). Reconstruction and Simulation of Neocortical Microcircuitry. *Cell* 163.2, 456–492.

Martin, J. P., Beyerlein, A., Dacks, A. M., Reisenman, C. E., Riffell, J. A., Lei, H., and Hildebrand, J. G. (2011). The neurobiology of insect olfaction: Sensory processing in a comparative context. *Progress in Neurobiology* 95.3, 427–447.

McDougal, R. A., Morse, T. M., Carnevale, T., Marenco, L., Wang, R., Migliore, M., Miller, P. L., Shepherd, G. M., and Hines, M. L. (2017). Twenty years of ModelDB and beyond: building essential modeling tools for the future of neuroscience. *Journal of Computational Neuroscience* 42.1, 1–10.

McIver, S. (1978). Structure of sensilla trichodea of female *Aedes aegypti* with comments on innervation of antennal sensilla. *Journal of Insect Physiology* 24.5, 383–390.

Meinertzhagen, I. A. and O'Neil, S. D. (1991). Synaptic organization of columnar elements in the lamina of the wild type in Drosophila melanogaster. *Journal of Comparative Neurology* 305.2, 232–263.

Meissner, G. W., Vannan, A., Jeter, J., Close, K., DePasquale, G. M., Dorman, Z., Forster, K., Beringer, J. A., Gibney, T., Hausenfluck, J. H., He, Y., Henderson, K., Johnson, L., Johnston, R. M., Ihrke, G., Iyer, N. A., Lazarus, R., Lee, K., Li, H.-H., Liaw, H.-P., Melton, B., Miller, S., Motaher, R., Novak, A., Ogundeyi, O., Petruncio, A., Price, J., Protopapas, S., Tae, S., Taylor, J., Vorimo, R., Yarbrough, B., Zeng, K. X., Zugates, C. T., Dionne, H., Angstadt, C., Ashley, K., Cavallaro, A., Dang, T., Gonzalez III, G. A., Hibbard, K. L., Huang, C., Kao, J.-C., Laverty, T., Mercer, M., Perez, B., Pitts, S. R., Ruiz, D., Vallanadu, V., Zheng, G. Z., Goina, C., Otsuna, H., Rokicki, K., Svirskas, R. R., Cheong, H. S., Dolan, M.-J., Ehrhardt, E., Feng, K., Galfi, B. E., Goldammer, J., Huston, S. J., Hu, N., Ito, M., McKellar, C., Minegishi, R., Namiki, S., Nern, A., Schretter, C. E., Sterne, G. R., Venkatasubramanian, L., Wang, K., Wolff, T., Wu, M., George, R., Malkesman, O., Aso, Y., Card, G. M., Dickson, B. J., Korff, W., Ito, K., Truman, J. W., Zlatic, M., Rubin, G. M., and FlyLight Project Team (2025). A split-GAL4 driver line resource for Drosophila neuron types. *eLife* 13, RP98405.

Modi, M. N., Shuai, Y., and Turner, G. C. (2020). The Drosophila Mushroom Body: From Architecture to Algorithm in a Learning Circuit. *Annual Review of Neuroscience* 43, 465–484.

Mohamed, A. A., Retzke, T., Das Chakraborty, S., Fabian, B., Hansson, B. S., Knaden, M., and Sachse, S. (2019). Odor mixtures of opposing valence unveil interglomerular crosstalk in the Drosophila antennal lobe. *Nature Communications* 10.1, 1–17.

Murlis, J., Elkinton, J. S., and Carde, R. T. (1992). Odor plumes and how insects use them. *Annual Review of Entomology* 37.86, 505–532.

Murthy, V. N. (2011). Olfactory Maps in the Brain. *Annual Review of Neuroscience* 34.Volume 34, 2011, 233–258.

Nagel, K. I. and Wilson, R. I. (2016). Mechanisms underlying population response dynamics in inhibitory interneurons of the Drosophila antennal lobe. *Journal of Neuroscience* 36.15, 4325–4338.

Neckameyer, W. S. and Bhatt, P. (2016). Protocols to Study Behavior in Drosophila. In: *Drosophila: Methods and Protocols*. Ed. by C. Dahmann. New York, NY: Springer New York, 303–320. ISBN: 978-1-4939-6371-3.

Neher, E. (2015). Merits and Limitations of Vesicle Pool Models in View of Heterogeneous Populations of Synaptic Vesicles. *Neuron* 87.6, 1131–1142.

Neher, E. and Brose, N. (2018). Dynamically Primed Synaptic Vesicle States: Key to Understand Synaptic Short-Term Plasticity. *Neuron* 100.6, 1283–1291.

Nehrkorn, J., Tanimoto, H., Herz, A. V. M., and Yarali, A. (2015). A model for non-monotonic intensity coding. *Royal Society Open Science* 2.5, 150120.

Nern, A., Loesche, F., Takemura, S.-y., Burnett, L. E., Dreher, M., Gruntman, E., Hoeller, J., Huang, G. B., Januszewski, M., Klapoetke, N. C., Koskela, S., Longden, K. D., Lu, Z., Preibisch, S., Qiu, W., Rogers, E. M., Seenivasan, P., Zhao, A., Bogovic, J., Canino, B. S., Clements, J., Cook, M., Finley-May, S., Flynn, M. A., Hameed, I., Fragniere, A. M. C., Hayworth, K. J., Hopkins, G. P., Hubbard, P. M., Katz, W. T., Kovalyak, J., Lauchie, S. A., Leonard, M., Lohff, A., Maldonado, C. A., Mooney, C., Okeoma, N., Olbris, D. J., Ordish, C., Paterson, T., Phillips, E. M., Pietzsch, T., Salinas, J. R., Rivlin, P. K., Schlegel, P., Scott, A. L., Scuderi, L. A., Takemura, S., Talebi, I., Thomson, A., Trautman, E. T., Umayam, L., Walsh, C., Walsh, J. J., Xu, C. S., Yakal, E. A., Yang, T., Zhao, T., Funke, J., George, R., Hess, H. F., Jefferis, G. S. X. E., Knecht, C., Korff, W., Plaza, S. M., Romani, S., Saalfeld, S., Scheffer, L. K., Berg, S., Rubin, G. M., and Reiser, M. B. (2025). Connectome-driven neural inventory of a complete visual system. *Nature* 641.8065, 1225–1237.

Ofstad, T. A., Zuker, C. S., and Reiser, M. B. (2011). Visual place learning in Drosophila melanogaster. *Nature* 474.7350, 204–207.

Okray, Z., Jacob, P. F., Stern, C., Desmond, K., Otto, N., Talbot, C. B., Vargas-Gutierrez, P., and Waddell, S. (2023). Multisensory learning binds neurons into a cross-modal memory engram. *Nature* 617.7962, 777–784.

Olsen, S. R. and Wilson, R. I. (2008). Lateral presynaptic inhibition mediates gain control in an olfactory circuit. *Nature* 452.7190, 956–960.

Owald, D. and Waddell, S. (2015). Olfactory learning skews mushroom body output pathways to steer behavioral choice in Drosophila. *Current Opinion in Neurobiology* 35, 178–184.

Paoli, M. and Galizia, G. C. (2021). Olfactory coding in honeybees. *Cell and Tissue Research* 383.1, 35–58.

Pavlov, I. P. (1927). Conditioned Reflexes: An investigation of the physiological activity of the cerebral cortex. *London: Oxford University Press,*

Piao, C. and Sigrist, S. J. (2022). (M)Unc13s in Active Zone Diversity: A Drosophila Perspective. *Frontiers in Synaptic Neuroscience* 13.

Plaza, S. M., Clements, J., Dolafi, T., Umayam, L., Neubarth, N. N., Scheffer, L. K., and Berg, S. (2022). neuPrint: An open access tool for EM connectomics. *Frontiers in Neuroinformatics* 16, 896292.

Poirazi, P. and Papoutsi, A. (2020). Illuminating dendritic function with computational models. *Nature Reviews Neuroscience* 21.6, 303–321.

Qiu, Q., Wu, Y., Ma, L., and Yu, C. R. (2021). Encoding innately recognized odors via a generalized population code. *Current Biology* 31.9, 1813–1825.e4.

Rall, W. (1964). Theoretical Significance of Dendritic Trees for Neuronal Input-Output Relations. In: *Theoretical Significance of Dendritic Trees for Neuronal Input-Output Relations*. Ed. by R. F. Reiss. Palo Alto: Standford University Press, 73–97.

Rapp, H. and Nawrot, M. P. (2020). A spiking neural program for sensorimotor control during foraging in flying insects. *Proceedings of the National Academy of Sciences*, 202009821.

Rapp, H., Nawrot, M. P., and Stern, M. (2020). Numerical Cognition Based on Precise Counting with a Single Spiking Neuron. *iScience* 23.2, 100852.

Reiter, L. T., Potocki, L., Chien, S., Gribskov, M., and Bier, E. (2001). A systematic analysis of human disease-associated gene sequences in Drosophila melanogaster. *Genome Research* 11.6, 1114–1125.

Rescorla, R. A. and Wagner, A. R. (1972). A Theory of Pavlovian Conditioning: Variations in the Effectiveness of Reinforcement and Nonreinforcement. In: *Classical conditioning II: current research and theory*. Ed. by A. Black and W. Prokasy. New York, 64–99.

Riemensperger, T., Kittel, R. J., and Fiala, A. (2016). Optogenetics in Drosophila Neuroscience. In: *Optogenetics: Methods and Protocols*. Ed. by A. Kianianmomeni. New York, NY: Springer New York, 167–175. ISBN: 978-1-4939-3512-3.

Robertson, H. M. and Wanner, K. W. (2006). The chemoreceptor superfamily in the honey bee, Apis mellifera: Expansion of the odorant, but not gustatory, receptor family. *Genome Research* 16.11, 1395–1403.

Roemschied, F., Ahmed, O., Ireland, E., Calhoun, A., Choi, M., and Murthy, M. (2024). A novel framework for social learning in male Drosophila. In: *Computational and Systems Neuroscience (Cosyne)*, 255.

Rubin, G. M., Yandell, M. D., Wortman, J. R., Gabor, G. L., null, Nelson, C. R., Hariharan, I. K., Fortini, M. E., Li, P. W., Apweiler, R., Fleischmann, W., Cherry, J. M., Henikoff, S., Skupski, M. P., Misra, S., Ashburner, M., Birney, E., Boguski, M. S., Brody, T., Brokstein, P., Celniker, S. E., Chervitz, S. A., Coates, D., Cravchik, A., Gabrielian, A., Galle, R. F., Gelbart, W. M., George, R. A., Goldstein, L. S. B., Gong, F., Guan, P., Harris, N. L., Hay, B. A., Hoskins, R. A., Li, J., Li, Z., Hynes, R. O., Jones, S. J. M., Kuehl, P. M., Lemaitre, B., Littleton, J. T., Morrison, D. K., Mungall, C., O'Farrell, P. H., Pickeral, O. K., Shue, C., Vosshall, L. B., Zhang, J., Zhao, Q., Zheng, X. H., Zhong, F., Zhong, W., Gibbs, R., Venter, J. C., Adams, M. D., and Lewis, S. (2000). Comparative Genomics of the Eukaryotes. *Science* 287.5461, 2204–2215.

Rybak, J., Talarico, G., Ruiz, S., Arnold, C., Cantera, R., and Hansson, B. S. (2016). Synaptic circuitry of identified neurons in the antennal lobe of Drosophila melanogaster. *Journal of Comparative Neurology* 524.9, 1920–1956.

Sachse, S. and Galizia, C. G. (2002). Role of Inhibition for Temporal and Spatial Odor Representation in Olfactory Output Neurons: A Calcium Imaging Study. *Journal of Neurophysiology* 87.2, 1106–1117.

Sacramento, J., Ponte Costa, R., Bengio, Y., and Senn, W. (2018). Dendritic cortical microcircuits approximate the backpropagation algorithm. In: *Advances in Neural Information Processing Systems*. Vol. 31. Curran Associates, Inc.

Sakagiannis, P., Jürgensen, A.-M., and Nawrot, M. P. (2025a). A behavioral architecture for realistic simulations of Drosophila larva locomotion and foraging. *eLife* 14.

Sakagiannis, P., Rapp, H., Jovanic, T., and Nawrot, M. P. (2025). Larvaworld : A behavioral simulation and analysis platform for Drosophila larva. *bioRxiv* 10.1101/2025.06.15.659765.

Saraiva, L. R., Kondoh, K., Ye, X., Yoon, K.-h., Hernandez, M., and Buck, L. B. (2016). Combinatorial effects of odorants on mouse behavior. *Proceedings of the National Academy of Sciences* 113.23, E3300–E3306.

Sayin, S., Boehm, A. C., Kobler, J. M., De Backer, J.-F., and Grunwald Kadow, I. C. (2018). Internal State Dependent Odor Processing and Perception—The Role of Neuromodulation in the Fly Olfactory System. *Frontiers in Cellular Neuroscience* 12.

Scheffer, L. K. and Meinertzhagen, I. A. (2021). A connectome is not enough – what is still needed to understand the brain of Drosophila? *Journal of Experimental Biology* 224.21, jeb242740.

Scheffer, L. K. et al. (2020). A connectome and analysis of the adult Drosophila central brain. *eLife* 9, e57443.

Schenk, J. E. and Gaudry, Q. (2023). Nonspiking Interneurons in the Drosophila Antennal Lobe Exhibit Spatially Restricted Activity. *eNeuro* 10.1, ENEURO.0109–22.2022.

Schlegel, P., Bates, A. S., Stürner, T., Jagannathan, S. R., Drummond, N., Hsu, J., Capdevila, L. S., Javier, A., Marin, E. C., Barth-Maron, A., Tamimi, I. F., Li, F., Rubin, G. M., Plaza, S. M., Costa, M., and Jefferis, G. S. (2021). Information flow, cell types and stereotypy in a full olfactory connectome. *eLife* 10, e66018.

Schlegel, P., Costa, M., and Jefferis, G. S. (2017). Learning from connectomics on the fly. *Current Opinion in Insect Science*. Neuroscience * Pheromones 24, 96–105.

Schlegel, P., Yin, Y., Bates, A. S., Dorkenwald, S., Eichler, K., Brooks, P., Han, D. S., Gkantia, M., Santos, M. dos, Munnelly, E. J., Badalamente, G., Serratosa Capdevila, L., Sane, V. A., Fragniere, A. M. C., Kiassat, L., Pleijzier, M. W., Stürner, T., Tamimi, I. F. M., Dunne, C. R., Salgarella, I., Javier, A., Fang, S., Perlman, E., Kazimiers, T., Jagannathan, S. R., Matsliah, A., Sterling, A. R., Yu, S.-c., McKellar, C. E., Costa, M., Seung, H. S., Murthy, M., Hartenstein, V., Bock, D. D., and Jefferis, G. S. X. E. (2024). Whole-brain annotation and multi-connectome cell typing of Drosophila. *Nature* 634.8032, 139–152.

Schmidt, M. and Ache, B. W. (1996). Processing of antennular input in the brain of the spiny lobster, Panulirus argus. *Journal of Comparative Physiology A* 178.5, 605–628.

Schmitt, F. J., Rostami, V., and Nawrot, M. P. (2023). Efficient parameter calibration and real-time simulation of large-scale spiking neural networks with GeNN and NEST. *Frontiers in Neuroinformatics* 17.

Schneider-Mizell, C. M., Gerhard, S., Longair, M., Kazimiers, T., Li, F., Zwart, M. F., Champion, A., Midgley, F. M., Fetter, R. D., Saalfeld, S., and Cardona, A. (2016). Quantitative neuroanatomy for connectomics in Drosophila. *eLife* 5. Ed. by R. L. Calabrese, e12059.

Schultz, W. (2016). Dopamine reward prediction error coding. *Dialogues in Clinical Neuroscience* 1.18, 23–32.

Schwartz, E. L. (1990). Computational Neuroscience. Cambridge, MA, USA: MIT Press. ISBN: 0-262-19291-8.

Sejnowski, T. J., Koch, C., and Churchland, P. S. (1988). Computational Neuroscience. *Science* 241.4871, 1299–1306.

Seki, Y., Rybak, J., Wicher, D., Sachse, S., and Hansson, B. S. (2010). Physiological and morphological characterization of local interneurons in the Drosophila antennal lobe. *Journal of Neurophysiology* 104.2, 1007–1019.

Shepherd, G. M., Chen, W. R., and Greer, C. A. (2004). Olfactory Bulb. In: *The Synaptic Organization of the Brain*. Ed. by G. M. Shepherd. Oxford University Press, 165–216. ISBN: 978-0-19-515956-1.

Shepherd, G. M., Chen, W. R., Willhite, D., Migliore, M., and Greer, C. A. (2007). The olfactory granule cell: from classical enigma to central role in olfactory processing. *Brain Research Reviews* 55.2, 373–382.

Shiu, P. K., Sterne, G. R., Spiller, N., Franconville, R., Sandoval, A., Zhou, J., Simha, N., Kang, C. H., Yu, S., Kim, J. S., Dorkenwald, S., Matsliah, A., Schlegel, P., Yu, S.-c., McKellar, C. E., Sterling, A., Costa, M., Eichler, K., Bates, A. S., Eckstein, N., Funke, J., Jefferis, G. S. X. E., Murthy, M., Bidaye, S. S., Hampel, S., Seeds, A. M., and Scott, K. (2024). A Drosophila computational brain model reveals sensorimotor processing. *Nature* 634.8032, 210–219.

Simpson, J. H. and Looger, L. L. (2018). Functional Imaging and Optogenetics in Drosophila. *Genetics* 208.4, 1291–1309.

Skorupski, P., MaBouDi, H., Galpayage Dona, H. S., and Chittka, L. (2018). Counting insects. *Philosophical Transactions of the Royal Society B: Biological Sciences* 373.1740, 20160513.

Stocker, H. and Gallant, P. (2008). Getting Started: An Overview on Raising and Handling Drosophila. In: *Drosophila: Methods and Protocols*. Ed. by C. Dahmann. Totowa, NJ: Humana Press, 27–44. ISBN: 978-1-59745-583-1.

Stocker, R. F., Lienhard, M. C., Borst, A., and Fischbach, K. F. (1990). Neuronal architecture of the antennal lobe in Drosophila melanogaster. *Cell and Tissue Research* 262.1, 9–34.

Stocker, R. F. (2001). Drosophila as a focus in olfactory research: Mapping of olfactory sensilla by fine structure, odor specificity, odorant receptor expression, and central connectivity. *Microscopy Research and Technique* 55.5, 284–296.

Strausfeld, N. J., Hansen, L., Li, Y., Gomez, R. S., and Ito, K. (1998). Evolution, Discovery, and Interpretations of Arthropod Mushroom Bodies. *Learning & Memory* 5.1, 11–37.

Strausfeld, N. J., Sinakevitch, I., Brown, S. M., and Farris, S. M. (2009). Ground plan of the insect mushroom body: Functional and evolutionary implications. *Journal of Comparative Neurology* 513.3, 265–291.

Strausfeld, N. J., Wolff, G. H., and Sayre, M. E. (2020). Mushroom body evolution demonstrates homology and divergence across Pancrustacea. *eLife* 9. Ed. by T. E. Behrens, C. E. Carr, C. E. Carr, D. Osorio, and P. Katz, e52411.

Strausfeld, N. (1976). Atlas of an Insect Brain. Berlin, Heidelberg: Springer. ISBN: 978-3-642-66179-2.

Stürner, T., Brooks, P., Serratosa Capdevila, L., Morris, B. J., Javier, A., Fang, S., Gkantia, M., Cachero, S., Beckett, I. R., Marin, E. C., Schlegel, P., Champion, A. S., Moitra, I., Richards, A., Klemm, F., Kugel, L., Namiki, S., Cheong, H. S. J., Kovalyak, J., Tenshaw, E., Parekh, R., Phelps, J. S., Mark, B., Dorkenwald, S., Bates, A. S., Matsliah, A., Yu, S.-c., McKellar, C. E., Sterling, A., Seung, H. S., Murthy, M., Tuthill, J. C., Lee, W.-C. A., Card, G. M., Costa, M., Jefferis, G. S. X. E., and Eichler, K. (2025). Comparative connectomics of Drosophila descending and ascending neurons. *Nature*, 1–15.

Summerfield, C. and Miller, K. (2023). Computational and systems neuroscience: The next 20 years. *PLOS Biology* 21.9, e3002306.

Suárez-Grimalt, R., Kadow, I. C. G., and Scheunemann, L. (2024). An integrative sensor of body states: how the mushroom body modulates behavior depending on physiological context. *Learning & Memory* 31.5, a053918.

Tabone, C. J. and Belle, J. S. de (2014). Olfactory learning and memory assays. In: *Behavioral Genetics of the Fly (Drosophila Melanogaster)*. Ed. by J. Dubnau. Cambridge Handbooks in Behavioral Genetics. Cambridge: Cambridge University Press, 231–249. ISBN: 978-0-511-92058-5.

Tabuchi, M., Dong, L., Inoue, S., Namiki, S., Sakurai, T., Nakatani, K., and Kanzaki, R. (2015). Two types of local interneurons are distinguished by morphology, intrinsic membrane properties, and functional connectivity in the moth antennal lobe. *Journal of Neurophysiology* 114.5, 3002–3013.

Takemura, S.-y., Bharioke, A., Lu, Z., Nern, A., Vitaladevuni, S., Rivlin, P. K., Katz, W. T., Olbris, D. J., Plaza, S. M., Winston, P., Zhao, T., Horne, J. A., Fetter, R. D., Takemura, S., Blazek, K., Chang, L.-A., Ogundeyi, O., Saunders, M. A., Shapiro, V., Sigmund, C., Rubin, G. M., Scheffer, L. K., Meinertzhagen, I. A., and Chklovskii, D. B. (2013). A visual motion detection circuit suggested by Drosophila connectomics. *Nature* 500.7461, 175–181.

Takemura, S.-y., Hayworth, K. J., Huang, G. B., Januszewski, M., Lu, Z., Marin, E. C., Preibisch, S., Xu, C. S., Bogovic, J., Champion, A. S., Cheong, H. S., Costa, M., Eichler, K., Katz, W., Knecht, C., Li, F., Morris, B. J., Ordish, C., Rivlin, P. K., Schlegel, P., Shinomiya, K., Stürner, T., Zhao, T., Badalamente, G., Bailey, D., Brooks, P., Canino, B. S., Clements, J., Cook, M., Duclos, O., Dunne, C. R., Fairbanks, K., Fang, S., Finley-May, S., Francis, A., George, R., Gkantia, M., Harrington, K., Hopkins, G. P., Hsu, J., Hubbard, P. M., Javier, A., Kainmueller, D., Korff, W., Kovalyak, J., Krzemiński, D., Lauchie, S. A., Lohff, A., Maldonado, C., Manley, E. A., Mooney, C., Neace, E., Nichols, M., Ogundeyi, O., Okeoma, N., Paterson, T., Phillips, E., Phillips, E. M., Ribeiro, C., Ryan, S. M., Rymer, J. T., Scott, A. K., Scott, A. L., Shepherd, D., Shinomiya, A., Smith, C., Smith, N., Suleiman, A., Takemura, S., Talebi, I., Tamimi, I. F., Trautman, E. T., Umayam, L., Walsh, J. J., Yang, T., Rubin, G. M., Scheffer, L. K., Funke, J., Saalfeld, S., Hess, H. F., Plaza, S. M., Card, G. M., Jefferis, G. S., and Berg, S. (2024). A Connectome of the Male Drosophila Ventral Nerve Cord. *eLife* 13.

Takemura, S. Y., Xu, C. S., Lu, Z., Rivlin, P. K., Parag, T., Olbris, D. J., Plaza, S., Zhao, T., Katz, W. T., Umayam, L., Weaver, C., Hess, H. F., Horne, J. A., Nunez-Iglesias, J., Aniceto, R., Chang, L. A., Lauchie, S., Nasca, A., Ogundeyi, O., Sigmund, C., Takemura, S., Tran, J., Langille, C., Lacheur, K. L., McLin, S., Shinomiya, A., Chklovskii, D. B., Meinertzhagen, I. A., and Scheffer, L. K. (2015). Synaptic circuits and their variations within different columns in the visual system of Drosophila. *Proceedings of the National Academy of Sciences of the United States of America* 112.44, 13711–13716.

Takemura, S., Aso, Y., Hige, T., Wong, A., Lu, Z., Xu, C. S., Rivlin, P. K., Hess, H., Zhao, T., Parag, T., Berg, S., Huang, G., Katz, W., Olbris, D. J., Plaza, S., Umayam, L., Aniceto, R., Chang, L. A., Lauchie, S., Ogundeyi, O., Ordish, C., Shinomiya, A., Sigmund, C., Takemura, S., Tran, J., Turner, G. C., Rubin, G. M., and Scheffer, L. K. (2017). A connectome of a learning and memory center in the adult Drosophila brain. *eLife* 6, e26975.

Tanaka, N. K., Awasaki, T., Shimada, T., and Ito, K. (2004). Integration of Chemosensory Pathways in the Drosophila Second-Order Olfactory Centers. *Current Biology* 14.6, 449–457.

Tanaka, N. K., Endo, K., and Ito, K. (2012). Organization of antennal lobe-associated neurons in adult Drosophila melanogaster brain. *Journal of Comparative Neurology* 520.18, 4067–4130.

Tanaka, N. K., Ito, K., and Stopfer, M. (2009). Odor-Evoked Neural Oscillations in Drosophila Are Mediated by Widely Branching Interneurons. *Journal of Neuroscience* 29.26, 8595–8603.

Tanaka, N. K., Tanimoto, H., and Ito, K. (2008). Neuronal assemblies of the Drosophila mushroom body. *Journal of Comparative Neurology* 508.5, 711–755.

Tanaka, R. and Portugues, R. (2025). On analogies in vertebrate and insect visual systems. *Nature Reviews Neuroscience*, 1–20.

Task, D., Lin, C.-C., Vulpe, A., Afify, A., Ballou, S., Brbic, M., Schlegel, P., Raji, J., Jefferis, G. S., Li, H., Menuz, K., and Potter, C. J. (2022). Chemoreceptor co-expression in Drosophila melanogaster olfactory neurons. *eLife* 11, e72599.

Tempel, B. L., Bonini, N., Dawson, D. R., and Quinn, W. G. (1983). Reward learning in normal and mutant Drosophila. *Proceedings of the National Academy of Sciences of the United States of America* 80.5, 1482–1486.

Thiagarajan, D., Eberl, F., Veit, D., Hansson, B. S., Knaden, M., and Sachse, S. (2022). Aversive Bimodal Associations Differently Impact Visual and Olfactory Memory Performance in *Drosophila*. *iScience* 25.12, 105485.

Thomas, A., Roy, M., and Gupta, N. (2025). Olfactory coding in the mosquito antennal lobe: labeled lines or combinatorial code? *Current Opinion in Insect Science* 68, 101299.

Tikidji-Hamburyan, R. A., Narayana, V., Bozkus, Z., and El-Ghazawi, T. A. (2017). Software for Brain Network Simulations: A Comparative Study. *Frontiers in Neuroinformatics* 11.

Tobin, W. F., Wilson, R. I., and Lee, W. C. A. (2017). Wiring variations that enable and constrain neural computation in a sensory microcircuit. *eLife* 6, e24838.

Tomer, R., Denes, A. S., Tessmar-Raible, K., and Arendt, D. (2010). Profiling by Image Registration Reveals Common Origin of Annelid Mushroom Bodies and Vertebrate Pallium. *Cell* 142.5, 800–809.

Trappenberg, T. P., ed. (2009). Fundamentals of Computational Neuroscience. 2nd ed. Oxford University Press. ISBN: 978-0-19-956841-3.

Tsai, K.-T. and Chou, Y.-H. (2022). Drosophila as a Model to Explore Individuality. In: *Behavioral Neurogenetics*. Ed. by D. Yamamoto. Vol. 181. New York, NY: Humana, 223–255. ISBN: 978-1-0716-2321-3.

Tully, T. and Quinn, W. G. (1985). Classical conditioning and retention in normal and mutant Drosophila melanogaster. *Journal of Comparative Physiology A* 157.1, 263–277.

Turner-Evans, D. B., Jensen, K. T., Ali, S., Paterson, T., Sheridan, A., Ray, R. P., Wolff, T., Lauritzen, J. S., Rubin, G. M., Bock, D. D., and Jayaraman, V. (2020). The Neuroanatomical Ultrastructure and Function of a Biological Ring Attractor. *Neuron* 108.1, 145–163.e10.

Tuthill, J. C. (2009). Lessons from a Compartmental Model of a Drosophila Neuron. *Journal of Neuroscience* 29.39, 12033–12034.

Valadez-Godínez, S., Sossa, H., and Santiago-Montero, R. (2020). On the accuracy and computational cost of spiking neuron implementation. *Neural Networks* 122, 196–217.

Van Der Loos, H. and Glaser, E. M. (1972). Autapses in neocortex cerebri: synapses between a pyramidal cell's axon and its own dendrites. *Brain Research* 48, 355–360.

Verzelli, P., Tchumatchenko, T., and Kotaleski, J. H. (2024). Editorial overview: Computational neuroscience as a bridge between artificial intelligence, modeling and data. *Current Opinion in Neurobiology* 84, 102835.

Vitay, J., Dinkelbach, H., and Hamker, F. H. (2015). ANNarchy: a code generation approach to neural simulations on parallel hardware. *Frontiers in Neuroinformatics* 9, 19.

Vogt, K., Schnaitmann, C., Dylla, K. V., Knapek, S., Aso, Y., Rubin, G. M., and Tanimoto, H. (2014). Shared mushroom body circuits underlie visual and olfactory memories in Drosophila. *eLife* 3. Ed. by M. Ramaswami, e02395.

Vosshall, L. B. and Stocker, R. F. (2007). Molecular Architecture of Smell and Taste in Drosophila. *Annual Review of Neuroscience* 30.1, 505–533.

Wang, F. and Aimone, J. B. (2024). On the path toward brain-scale simulations. *Nature Computational Science* 4.12, 882–883.

Wang-Chen, S., Stimpfling, V. A., Lam, T. K. C., Özdil, P. G., Genoud, L., Hurtak, F., and Ramdya, P. (2024). NeuroMechFly v2: simulating embodied sensorimotor control in adult Drosophila. *Nature Methods* 21.12, 2353–2362.

Warren, B. and Kloppenburg, P. (2014). Rapid and slow chemical synaptic interactions of cholinergic projection neurons and GABAergic local interneurons in the insect antennal lobe. *Journal of Neuroscience* 34.39, 13039–13046.

Watanabe, H. and Tateishi, K. (2023). Parallel olfactory processing in a hemimetabolous insect. *Current Opinion in Insect Science* 59, 101097.

Watson, A. H. D. and Schürmann, F.-W. (2002). Synaptic structure, distribution, and circuitry in the central nervous system of the locust and related insects. *Microscopy Research and Technique* 56.3, 210–226.

Webb, B. (2020). Robots with insect brains. *Science* 368.6488, 244–245.

Webb, B. (2024). Beyond prediction error: 25 years of modeling the associations formed in the insect mushroom body. *Learning & Memory* 31.5, a053824.

Weber, D., Richter, V., Rohwedder, A., Großjohann, A., and Thum, A. S. (2023). Learning and Memory in Drosophila Larvae. *Cold Spring Harbor Protocols* 2023.3, pdb.top107863.

Wentzel, C., Sommer, J. E., Nair, R., Stiefvater, A., Sibarita, J.-B., and Scheiffele, P. (2013). mSYD1A, a Mammalian Synapse-Defective-1 Protein, Regulates Synaptogenic Signaling and Vesicle Docking. *Neuron* 78.6, 1012–1023.

Wessnitzer, J., Young, J. M., Armstrong, J. D., and Webb, B. (2012). A model of non-elemental olfactory learning in Drosophila. *Journal of Computational Neuroscience* 32.2, 197–212.

White, J. G., Southgate, E., Thomson, J. N., and Brenner, S. (1986). The structure of the nervous system of the nematode Caenorhabditis elegans. *Philosophical Transactions of the Royal Society of London. B, Biological Sciences* 314.1165, 1–340.

Wilson, R. I. (2013). Early olfactory processing in drosophila: Mechanisms and principles. *Annual Review of Neuroscience* 36, 217–241.

Wilson, R. I. and Laurent, G. (2005). Role of GABAergic Inhibition in Shaping Odor-Evoked Spatiotemporal Patterns in the Drosophila Antennal Lobe. *Journal of Neuroscience* 25.40, 9069–9079.

Winding, M., Pedigo, B. D., Barnes, C. L., Patsolic, H. G., Park, Y., Kazimiers, T., Fushiki, A., Andrade, I. V., Khandelwal, A., Valdes-Aleman, J., Li, F., Randel, N., Barsotti, E., Correia, A., Fetter, R. D., Hartenstein, V., Priebe, C. E., Vogelstein, J. T., Cardona, A., and Zlatic, M. (2023). The connectome of an insect brain. *Science* 379.6636, eadd9330.

Woitkuhn, J., Ender, A., Beuschel, C. B., Maglione, M., Matkovic-Rachid, T., Huang, S., Lehmann, M., Geiger, J. R., and Sigrist, S. J. (2020). The Unc13A isoform is important for phasic release and olfactory memory formation at mushroom body synapses. *Journal of Neurogenetics* 34.1, 106–114.

Wolf, H. and Büschges, A. (1995). Nonspiking local interneurons in insect leg motor control. II. Role of nonspiking local interneurons in the control of leg swing during walking. *Journal of Neurophysiology* 73.5, 1861–1875.

Wolff, G. H. and Strausfeld, N. J. (2016). Genealogical correspondence of a forebrain centre implies an executive brain in the protostome–deuterostome bilaterian ancestor. *Philosophical Transactions of the Royal Society B: Biological Sciences* 371.1685, 20150055.

Wong, A. M., Wang, J. W., and Axel, R. (2002). Spatial Representation of the Glomerular Map in the Drosophila Protocerebrum. *Cell* 109.2, 229–241.

Wunderlich, T. C. and Pehle, C. (2021). Event-based backpropagation can compute exact gradients for spiking neural networks. *Scientific Reports* 11.1, 12829.

Yadav, P., Shinde, P., and Singh, A. (2024). Brain rewiring during developmental transitions: A Comparative Analysis of Larva and Adult Drosophila melanogaster. *bioRxiv*, 2024.05.01.592061.

Yagi, R., Mabuchi, Y., Mizunami, M., and Tanaka, N. K. (2016). Convergence of multimodal sensory pathways to the mushroom body calyx in Drosophila melanogaster. *Scientific Reports* 6.1, 29481.

Yamada, D., Bushey, D., Li, F., Hibbard, K. L., Sammons, M., Funke, J., Litwin-Kumar, A., Hige, T., and Aso, Y. (2023). Hierarchical architecture of dopaminergic circuits enables second-order conditioning in Drosophila. *eLife* 12, e79042.

Yamazaki, K., Vo-Ho, V.-K., Bulsara, D., and Le, N. (2022). Spiking Neural Networks and Their Applications: A Review. *Brain Sciences* 12.7, 863.

Yartsev, M. M. (2017). The emperor's new wardrobe: Rebalancing diversity of animal models in neuroscience research. *Science* 358.6362, 466–469.

Yavuz, E., Turner, J., and Nowotny, T. (2016). GeNN: a code generation framework for accelerated brain simulations. *Scientific Reports* 6.1, 18854.

Zenke, F. and Ganguli, S. (2018). SuperSpike: Supervised Learning in Multilayer Spiking Neural Networks. *Neural Computation* 30.6, 1514–1541.

Zhang, K., Guo, J. Z., Peng, Y., Xi, W., and Guo, A. (2007). Dopamine-Mushroom Body Circuit Regulates Saliency-Based Decision-Making in Drosophila. *Science* 316.5833, 1901–1904.

Zhao, B., Sun, J., Zhang, X., Mo, H., Niu, Y., Li, Q., Wang, L., and Zhong, Y. (2019). Long-term memory is formed immediately without the need for protein synthesis-dependent consolidation in Drosophila. *Nature Communications* 10.1.

Zhao, C., Widmer, Y. F., Diegelmann, S., Petrovici, M. A., Sprecher, S. G., and Senn, W. (2021). Predictive olfactory learning in Drosophila. *Scientific Reports* 11.1, 1–17.

Zhao, Z. and McBride, C. S. (2020). Evolution of olfactory circuits in insects. *Journal of Comparative Physiology A* 206.3, 353–367.

Zheng, Z., Lauritzen, J. S., Perlman, E., Robinson, C. G., Nichols, M., Milkie, D., Torrens, O., Price, J., Fisher, C. B., Sharifi, N., Calle-Schuler, S. A., Kmecova, L., Ali, I. J., Karsh, B., Trautman, E. T., Bogovic, J. A., Hanslovsky, P., Jefferis, G. S., Kazhdan, M., Khairy, K., Saalfeld, S., Fetter, R. D., and Bock, D. D. (2018). A Complete Electron Microscopy Volume of the Brain of Adult Drosophila melanogaster. *Cell* 174.3, 730–743.e22.

Zucker, R. S. and Regehr, W. G. (2002). Short-term synaptic plasticity. *Annual Review of Physiology* 64, 355–405.

Żakowski, W. (2020). Animal Use in Neurobiological Research. *Neuroscience* 433, 1–10.

List of Contributions

Publications:

- **Springer M**, Nawrot MP (2021). A Mechanistic Model for Reward Prediction and Extinction Learning in the Fruit Fly. ***eNeuro*** 8:0549-20.2021
- Rachad EY, Deimel SH, Epple L, Gadgil YV, Jürgensen AM, **Springer M**, Lin CH, Nawrot MP, Lin S, Fiala A (2025). Functional dissection of a neuronal brain circuit mediating higher-order associative learning. ***Cell Reports*** 44, 115593

Preprints:

- **Springer M**, Sigrist SJ, Nawrot MP (2025). A model investigation of short-term synaptic plasticity tuned via Unc13 isoforms. ***bioRxiv*** 2025.06.18.660326

Other:

- **Springer M**, Bandyopadhyay P, Sachse S, Nawrot MP. A Connectome-Based Approach for Investigating Neural Circuits of Odor Mixture Processing. *in preparation*
- Franz HR, Scholz J, Thoener J, Schleyer M, Kobler O, **Springer M**, Gerber B, Fiala A, Widmann A. Induced developmental arrest of *Drosophila* larvae reveals capacity and limits of neuro-behavioral adaptation under excessive growth. *in preparation*